

UNIVERSITY OF CASSINO AND SOUTHERN LAZIO

**Department of Electrical and Information Engineering
"Maurizio Scarano"**

Master's Degree in
Telecommunications Engineering



**4G AND 5G CONTROL SIGNALS:
STABILITY ANALYSIS**

Candidate

Diego Tuzi
50435

Supervisor

Prof. Gianfranco Miele

Co-Supervisor

Prof. Domenico Capriglione
Prof. Marco Donald Migliore

Academic year 2019/2020

“We have two lives, and the second begins when we realize we only have one.”
- Confucios -

Acknowledgments

I would like to thank Professors Gianfranco Miele, Domenico Capriglione, Marco Donald Migliore and Gianni Cerro for received support and the availability during the thesis work.

I would like to thank Dario Scarano, Andrea Sacilotti and Marco Neri of Rohde & Schwarz Italy for the kindly grant of the Network Scanner used during the thesis work.

I would like to thank TATEL company for the kindly grant of the measurement point in Frosinone, measurement tools and for the flexibility on my working time during the thesis work.

Ringraziamenti

Per la produzione di questo lavoro di tesi, desidero ringraziare i professori Gianfranco Miele, Domenico Capriglione, Marco Donald Migliore e Gianni Cerro per il supporto ricevuto e la disponibilità dimostrata.

Ringrazio la Rohde & Schwarz Italia nelle persone di Dario Scarano, Andrea Sacilotti e Marco Neri per la gentile concessione in uso del Network Scanner essenziale nella produzione della parte sperimentale del presente lavoro di tesi.

Ringrazio la TATEL, per la disponibilità all'uso degli spazi sul punto di misura di Frosinone, l'utilizzo di materiale e strumentazione e la flessibilità sull'orario di lavoro durante il periodo di tesi.

Per essere dei punti di riferimento ed inesauribile fonte di affetto, ringrazio i miei genitori Filomena ed Antonino, mio fratello Claudio, mia sorella Maria Luisa, mio cognato Elio ed i miei nipoti Giulia, Beatrice, Domenico, Rocco e Chiara. Un pensiero a mia cognata Sandra che è sempre nei nostri cuori.

Ringrazio Sabrina per il continuo supporto, motivazione e comprensione per il raggiungimento di un obiettivo a lungo desiderato.

Ringrazio tutti i colleghi di lavoro conosciuti durante le precedenti ed attuali esperienze di lavoro.

A conclusione di un cammino iniziato insieme, in un luogo diverso ed in una vita diversa, ringrazio *“il gruppo numero quattro”* Alberto, Francesco e Roberto, costante fonte di ispirazione e di ammirazione.

Ringrazio tutto il gruppo del box Crossfit Sora dei coach Luciano e Vittorio, con con cui condivido grandi passioni, lo sport e le bistecche.

Ringrazio tutti gli amici che hanno reso e rendono la vita più felice. Tra gli altri non posso non menzionare, in ordine di apparizione, *“l'amico da una gita”* Cesare, *“I tacchini”* Davide, Ruggero e Serena, *“I coniugi”* Alessandro e Donatella, *“il direttore”* Massimo ed *“il numero uno”* Fulvio.

Un pensiero alla mia cara amica e *“cugi”* Chiara con cui avrei tanto voluto condividere un altro momento felice.

Abstract

At the awakening of the new 5G network, issues related to electromagnetic fields (EMFs) are becoming one of the key aspects. Introduction of new 5G emission sources, working in parallel with already existing 2G/3G/4G mobile technologies, are raising concerns about exceeding the admissible EMF exposure limits. Measurement techniques used to assess the compliance with EMF exposure limits are assuming a relevant role.

Among available Measurement Methods, the extrapolation to maximum power represents one of the most attractive measurement method. It enables to extrapolate the maximum possible output power emitted by a radio base station system (a time variant signal), measuring a time invariant component of the system (pilot, control or reference signal/channel). The stability of the reference signal in terms of measured power is extremely important to obtain a valid extrapolation. The stability analysis of the 5G control signals is the main goal of this document.

Firstly, this thesis work gives to the reader a complete framework to understand Limits, Measurement methods, 4G and 5G control signal, 4G standardized extrapolation methods and 5G most recent extrapolation proposals from the scientific community.

Secondly this thesis work presents the results of two measurement campaigns involving five active 5G DSS signals and five active 5G FR1 signals coming from the main four Italian provider.

Lastly this thesis work shows the results of the performed stability analysis on 5G control signals.

Table of Contents

Acknowledgments.....	iii
Ringraziamenti.....	iv
Abstract.....	v
Table of Contents.....	vi
1 EMF limits and measurements.....	1
1.1 Evolution of mobile cellular networks.....	1
1.2 EMF guidelines and exposure limits.....	5
1.3 EMF measurement methods.....	23
1.4 Conclusion.....	30
2 4G systems: Control signals and Extrapolation.....	31
2.1 4G overview.....	31
2.2 LTE E-UTRA technology review and control signals.....	32
2.3 LTE E-UTRA EMF extrapolation methods.....	39
2.4 Conclusion.....	44
3 5G systems: Control signals and Extrapolation.....	45
3.1 5G overview.....	45
3.2 5G NR technology review and control signals.....	49
3.3 5G NR EMF extrapolation proposals.....	62
3.4 Conclusion.....	86
4 5G NR and 4G LTE Coexistence.....	89
4.1 NSA mode and 4G/5G dual connectivity.....	89
4.2 Dynamic Spectrum Sharing.....	90
4.3 Conclusion.....	101
5 5G control signals: Stability analysis.....	102
5.1 Measurement devices.....	102
5.2 Measurement scenarios.....	107
5.3 Stability analysis.....	126
5.4 Conclusion.....	151
6 Conclusion and further development.....	155
Bibliography.....	I

1 EMF limits and measurements

“After a brief introduction about the evolution of mobile cellular networks from 1G to 5G, this chapter will address to radio frequency (RF) electromagnetic fields (EMF) limits and measurements.”

1.1 Evolution of mobile cellular networks

The last two decades have witnessed an extremely fast evolution of mobile cellular network technologies, from 1G to 4G, with 5G networks expected to be fully operational within the commonly expected time-frame (i.e. 2020-2025). Figure 1 graphically depicts the evolution of mobile wireless communication technology from 1G to 5G.

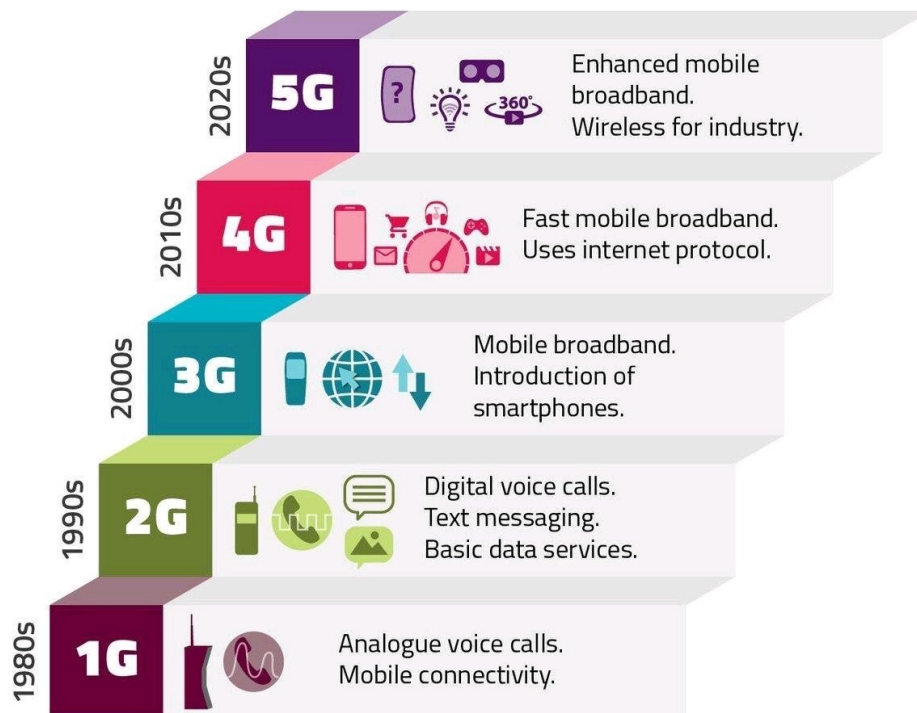


Figure 1: The evolution of mobile wireless communication technology: from 1G to 5G [1].

The initial basic voice-only calls featured by 1G mobile systems evolved into a multitude of different services with the subsequent generations, from simple text messaging and basic high-latency data exchange to high-quality video streaming and chatting services, to radically new services supported by 5G networks. Services evolution was enabled by several factors, including ever-rising supported bit rates, advances in air interface design, signal processing at physical layer, and MAC layer procedures, technological advances in mobile terminals manufacturing, evolution of mobile internet protocols, cloud computing, advanced networking control

paradigms. Second generation global system for mobile communications (GSM) cellular networks initially provided digital voice service at bit rate 9.6 kbps. General Packet Radio Service (GPRS) and ultimately Enhanced Data Rates for GSM Evolution (EDGE) data services were subsequently introduced, with bit rates of a few tens of kbps and up to 200 kbps, respectively. Push email was also introduced for the first time on Blackberry devices. These bit rates were largely increased in the next generations. The third generation UMTS offered up to 2 Mbps bit rate (often 364 kbps) initially, and then several tens of Mbps in downlink with High Speed Packet Access (HSPA). The fourth-generation Long Term Evolution (LTE) features up to 300 Mbps in downlink, with a target of 1 Gbps, and up to 50 Mbps in uplink. The fifth generation cellular networks are expected to significantly increase the bit rate, up to 20 Gbps. These bit rates, end-to-end latencies down to 1 ms, ultra-reliability (packet error rate 10^{-5} or less), and massive multiple access, will foster services such as enhanced mobile broadband, ultra-reliable and low-latency Internet of Things (IoT) and machine-type communication (MTC), e-health, augmented reality and tactile Internet, industrial control for the Industry 4.0, automated driving and flying.

Each generation of wireless cellular networks came with its own technical innovations, both on the network, air interface, and user terminal side.

Multiple access: Multiple access schemes were constantly enhanced, from single carrier per channel frequency division multiple access (FDMA), to frequency and time division multiple access (FDMA/TDMA), code division multiple access (CDMA), up to orthogonal frequency division multiple access (OFDMA) and non-orthogonal multiple access (NOMA), with a progressive explosion of the network capacity in terms of the number of users served at the same time with an adequate quality of service (QoS).

PHY layer enhancements: Fundamental innovations at the physical layer contributed to the above-reviewed ever-increasing bit rates. Among them multiple-input multiple-output (MIMO) is evolving into massive MIMO in 5G, as well as advanced channel coding schemes such as 3G/4G turbo codes and 5G New Radio traffic channel low-density parity-check (LDPC) codes and control channel polar codes.

Frequency bands: New frequency bands were exploited by each generation. First generation advanced mobile phone system (AMPS) and total access communication system (TACS) were operated in the 800 MHz and 900 MHz bands, respectively, while second generation GSM was initially operated in the 900 MHz band, and then also in the 1800 MHz and 1900 MHz (in North America) ones. Frequency bands around 2 GHz were for the first time used by UMTS networks, while a number of frequency bands are

available worldwide for LTE, based on regulatory aspects in different geographical areas (e.g., 450/800/900 MHz, 1800/2100 MHz, 2600 MHz in Europe). From a spectrum allocation viewpoint, the main breakthrough introduced by 5G is the use of licensed, shared, and unlicensed frequency bands in the mmWave band, above 24 GHz. The one around 60 GHz is of particular interest for indoor very-high data rate applications, wireless backhaul, and femtocell implementation.

Evolution of switching and networking: The 1G network was fully circuit based, resembling the traditional telephone network, a choice motivated by being voice calls the target service of the networks. In 2G and 3G systems data oriented services progressively became more important and a packet switched network dedicated to the transport of data was set aside the existing circuit switched network. From 4G the Evolved Packet Core (EPC) concept is adopted meaning that the transport network is based on packet switching only and that such packet switching is IP based. Therefore the transport technology of the mobile networks converges with the transport technology of the Internet. The EPC definition brings along another concept fundamental for the evolution to the 5G: the separation of the control and data plane. The technologies to control the transport of the user data are logically separated from the transport itself, which is essential to allow a separate evolution path to guarantee the required network scalability.

Network softwarization: The emergence of the cloud computing paradigm and of the related virtualization technologies brought forward a key innovation in the 5G. Complex networking functionalities, traditionally requiring dedicated hardware and management may be virtualized as pieces of software into the cloud. This is the Network Function Virtualization (NFV) paradigm, defined and standardized by the European Telecommunications Standards Institute (ETSI) in the recent years. Meanwhile Software Defined Networking (SDN) also emerged, a novel approach that allows a very effective separation of the network control and data plane, thus further extending the ideas behind the EPC. The OpenFlow protocol is the key component of SDN, supporting the implementation of a communication channel between the controller (the brain of the network) and the network nodes (that carry data). NFV exploits virtualization, cloud computing and SDN to define an architecture which supports the implementation of network services as subsets of software functionalities, with an unprecedented degree of flexibility and adaptation capabilities. Network programmability and split of control and data plane are key enabling technologies towards a full implementation of the 5G [2].

Mobile cellular networks need improvements because the amount of data exchanged by mobile users continue and will continue to increase, on one side due to the increasing number of non-human devices connected (including vehicles, UAVs, and autonomous systems), and to the enhanced quality 3D video / holographic type communication that will be used by humans. As of today (2021), more than one and half million Terabytes (i.e., 1 Exabyte = 10^{18} bytes) of data per day are exchanged over the mobile networks all over the world (see Figure 2).

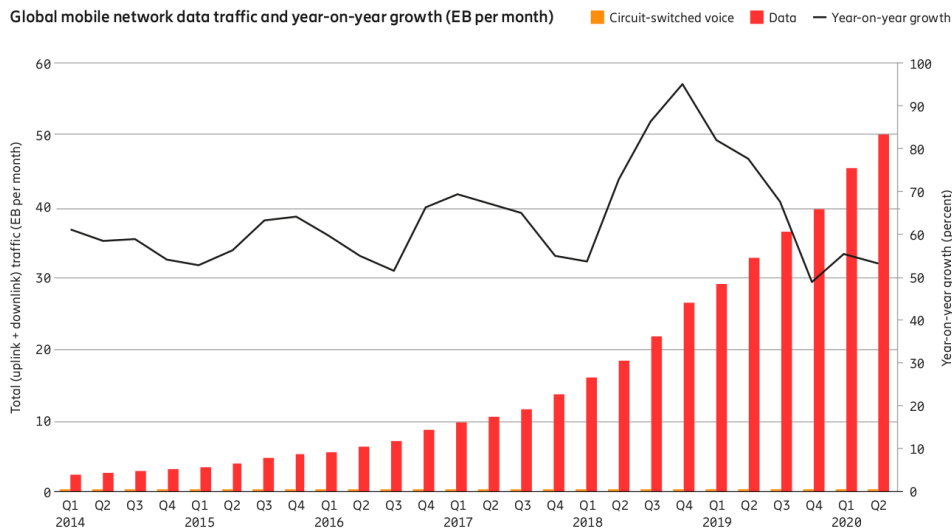


Figure 2: Global mobile network data traffic and year-on-year growth (EB per month) [3].

Although mobile traffic, mobile subscribers and in general demand of mobility continues to increase, preoccupation about radio frequency (RF) electromagnetic fields (EMF) is becoming high.

Introduction of new 5G emission sources, working in parallel with already existing 2G/3G/4G mobile technologies and other wireless sources, raises concerns about exceeding the admissible EMF exposure limits. In addition to the EMF exposure limits, public concern about the negative impact of radio frequencies on human health may be also an important factor affecting widespread implementation of the 5G infrastructure. Attention is particularly focused on higher frequencies, since millimeter-waves energy is mostly absorbed in human skin, and the mm-wave bands will be used to establish a dense structure of small pico-cells resulting in the installation of a large number of new radio transmitters. Consequently, some members of society are frightened that 5G will expose the population to new sources of dangerous radio frequency radiation. For these reasons, effective measurements of electromagnetic fields are essential for both, the deployment of 5G networks and their later operation. Proper measurement methodology will enable monitoring of the EMF intensity, allowing

government bodies as well as local communities to control whether EMF values are at a safe level [4].

1.2 EMF guidelines and exposure limits

A significant increase in interest in EMF occurred with the development of GSM mobile networks and the related installation of a large number of base stations emitting radio signals.

In the early 1990s, the World Health Organization (WHO) initiated research work on the biological effects of radio frequency waves. In 1998, associated with WHO the International Commission on Non-Ionizing Radiation Protection (ICNIRP) defined science-based guidelines for limiting exposure to electric, magnetic and electromagnetic fields. The ICNIRP guidelines form the basis for different recommendations on EMF exposure limits developed, among others, by WHO and International Telecommunications Union (ITU) and addressed to governments.

Whilst most countries have adopted these scientifically based RF-EMF guidelines, a small group of countries, regions or even cities within the same country, especially in Europe (e.g., Poland, Russia, Italy, Switzerland, the city of Paris and regions of Belgium), use limits that are 10 to 100 times lower. Limits below the guidelines are not limited to Europe; however, China and India, among others, have also adopted limits below guidelines. In addition, some countries (e.g., Poland and Italy) apply a very strict measurement methodology, resulting in even stricter RF-EMF requirements.

Because disparities in standards around the world have caused increasing public anxiety about exposure from the introduction of new technologies, WHO has commenced a process of harmonization of EMF standards worldwide.

The ICNIRP has just revised its ICNIRP 1998 “ICNIRP Guidelines for Limiting Exposure to Time-varying Electric, Magnetic and Electromagnetic Fields (up to 300 GHz)” [5]. Following an extensive public consultation process, the final ICNIRP guidelines were published in March 2020. In the following a review of ICNIRP guideline is presented, based on information from ICNIRP 2020 [6].

1.2.1 ICNIRP guidelines

The ICNIRP RF EMF guidelines protect against all potential adverse health effects relating to exposure to RF EMFs from wireless technologies. This includes potential differences in the effect of RF EMFs as a function of age,

health status, and depth of penetration, the effect of both acute and chronic exposures, and it includes all substantiated effects regardless of mechanism.

ICNIRP guidelines concerning radio-frequency are:

- ICNIRP guidelines 1998: for limiting exposure to time-varying electric, magnetic and electromagnetic fields (up to 300 GHz);
- ICNIRP guidelines 2010 (LF): for limiting exposure to time-varying electric and magnetic fields (1 Hz – 100 KHz);
- ICNIRP guidelines 2020 for limiting exposure to electromagnetic fields (100 KHz to 300 GHz).

ICNIRP guideline 2020 replaces the 100 kHz to 300 GHz part of the ICNIRP (1998) [5] radiofrequency guidelines, as well as the 100 kHz to 10 MHz part of the ICNIRP (2010) [7] low-frequency guidelines.

It is important to note that, in terms of the 5G exposure levels measured so far, the ICNIRP (1998) [5] guidelines would also provide protection for 5G technologies. However, as it is difficult to predict how new technologies will develop, ICNIRP (2020) [6] has made a number of changes to ensure that new technologies such as 5G will not be able to cause harm, regardless of our current expectations. These changes include the addition of whole body average restrictions for frequencies >6 GHz, restrictions for brief (<6 minutes) exposures for frequencies >6 GHz, and the reduction of the averaging area for frequencies >6 GHz.

The main objective of ICNIRP 2020 [6] is to establish guidelines for limiting exposure to EMFs that will provide a high level of protection for all people against substantiated adverse health effects from exposures to both short-term and long-term, continuous and discontinuous radiofrequency EMFs.

In order to set safe exposure levels, ICNIRP first decided whether there was evidence that radiofrequency EMFs impair health, and for each adverse effect that was substantiated, both the mechanism of interaction and the minimum exposure required to cause harm were determined (where available). This information was obtained primarily from major international reviews of the literature on radiofrequency EMFs and health:

- an in-depth review from the World Health Organization on radiofrequency EMF exposure and health that was released as a draft Technical Document (WHO 2014 [8], [6]);
- reports by the Scientific Committee on Emerging and Newly Identified Health Risks (SCENIHR 2015 [9], [6]);

- reports by the Swedish Radiation Safety Authority (SSM 2015 [10] [6], 2016 [11] [6], 2018 [12] [6]).

To complement those reports, ICNIRP also considered research published since cut-off date September 1st, 2019.

ICNIRP closely follows the RF EMF related scientific research and any new outcomes relevant to health will inform the evolution of the guidelines.

1.2.1.1 Principles for limiting RF exposure

ICNIRP guidelines specify quantitative EMF levels for personal exposure following process in Figure 3.

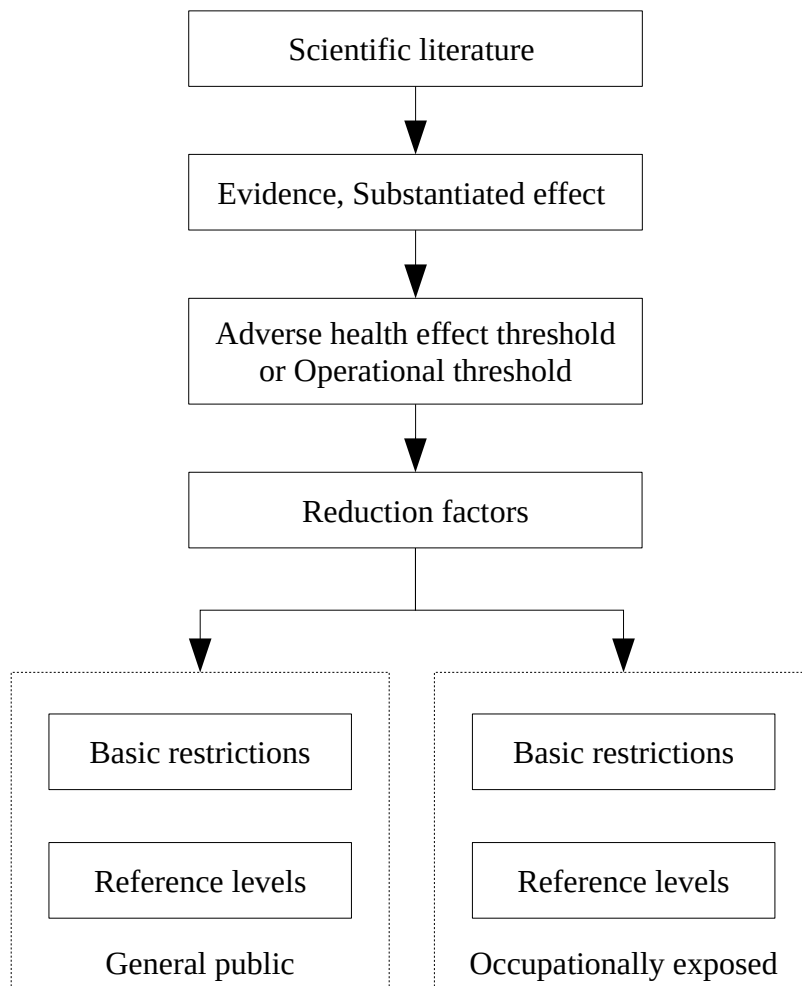


Figure 3: Determination process of EMF exposure levels.

To determine these levels, ICNIRP first identified published scientific literature concerning effects of radiofrequency EMF exposure on biological systems, and established which of these were both harmful to human health and scientifically substantiated. Within the guidelines, “evidence” will be used within this context, and “substantiated effect” used to describe reported

effects that satisfy this definition of evidence. For each substantiated effect, ICNIRP then identified the “adverse health effect threshold”, the lowest exposure level known to cause the health effect. These thresholds were derived to be strongly conservative for typical exposure situations and populations. Where no such threshold could be explicitly obtained from the radiofrequency health literature, ICNIRP set an “operational threshold”. Reduction factors were then applied to the resultant thresholds (or operational thresholds) to provide exposure restriction values.

These exposure restriction values are referred to as “basic restrictions”. They relate to physical quantities that are closely related to rf-induced adverse health effects. Some of these are physical quantities inside an exposed body, which cannot be easily measured, so quantities that are more easily evaluated, termed “reference levels”, have been derived from the basic restrictions to provide a more-practical means of demonstrating compliance with the guidelines. An exposure is taken to be compliant with the guidelines if it is shown to be below either the relevant basic restrictions or relevant reference levels.

The guidelines differentiate between occupationally exposed individuals and members of the general public. Occupationally-exposed individuals are defined as adults who are exposed under controlled conditions associated with their occupational duties, trained to be aware of potential radiofrequency EMF risks and to employ appropriate harm-mitigation measures. The general public is defined as individuals of all ages and of differing health statuses, which includes more vulnerable groups or individuals, and who may have no knowledge of or control over their exposure to EMFs. A pregnant woman is treated as a member of the general public.

ICNIRP adopts a conservative approach to each step in order to ensure that its limits would remain protective even if exceeded by a substantial margin. There is no evidence that additional precautionary measures will result in a benefit to the health of the population.

1.2.1.2 Scientific basis

When the field impacts upon material, it interacts with the atoms and molecules in that material. When a biological body is exposed to radiofrequency EMFs, some of the power is reflected away from the body, and some is absorbed by it. This results in complex patterns of electromagnetic fields inside the body that are heavily dependent on the EMF characteristics as well as the physical properties and dimensions of the body. The main component of the radiofrequency EMF that affects the body

is the electric field. Electric fields inside the body are referred to as induced electric fields (E_{ind} , measured in volt per meter V/m), and they can affect the body in different ways that are potentially relevant to health.

Firstly, the induced electric field in the body exerts a force on both polar molecules (mainly water molecules) and free moving charged particles such as electrons and ions. In both cases a portion of the EMF energy is converted to kinetic energy, forcing the polar molecules to rotate and charged particles to move as a current. As the polar molecules rotate and charged particles move, they typically interact with other polar molecules and charged particles, causing the kinetic energy to be converted to heat. This heat can adversely affect health in a range of ways.

Secondly, if the induced electric field is below about 10 MHz and strong enough, it can exert electrical forces that are sufficient to stimulate nerves, and if the induced electric field is strong and brief enough (as can be the case for pulsed low frequency EMFs), it can exert electrical forces that are sufficient to cause dielectric breakdown of biological membranes, as occurs during direct current (DC) electroporation.

From a health risk perspective, we are generally interested in how much EMF power is absorbed by biological tissues, as this is largely responsible for the heating effects described above. This is typically described as a function of a relevant dosimetric quantity.

For example, below about 6 GHz, where EMFs penetrate deep into tissue (and thus require depth to be considered), it is useful to describe this in terms of “specific energy absorption rate” (SAR), which is the power absorbed per unit mass ($\text{W}\cdot\text{kg}^{-1}$). Conversely, above 6 GHz, where EMFs are absorbed more superficially (making depth less relevant), it is useful to describe exposure in terms of the density of absorbed power over area ($\text{W}\cdot\text{m}^{-2}$), which we refer to as “absorbed power density” (S_{ab}). In such situations, specific energy absorption (SA, in $\text{J}\cdot\text{kg}^{-1}$) and absorbed energy density (U_{ab} , in $\text{J}\cdot\text{m}^{-2}$) are used, for EMFs below and above 6 GHz, respectively. SAR, S_{ab} , SA, U_{ab} , and E_{ind} are the quantities used in these guidelines to specify the basic restrictions.

As the quantities used to specify basic restrictions can be difficult to measure, quantities that are more easily evaluated are also specified, as reference levels. The reference level quantities relevant to these guidelines are incident electric field strength (E_{inc}) and incident magnetic field strength (H_{inc}), incident power density (S_{inc}), plane-wave equivalent incident power density (S_{eq}), incident energy density (U_{inc}), and plane-wave equivalent

incident energy density (U_{eq}), all measured outside the body, and electric current inside the body, I , described in units of ampere (A).

1.2.1.3 Biological effects and resultant thresholds

Radio-frequency EMFs can affect the body via three primary biological effects:

- nerve stimulation;
- changes in the permeability of membranes;
- temperature rise.

Nerve stimulation

Exposure to EMFs can induce electric fields within the body, which for frequencies up to 10 MHz can stimulate nerves.

The effect of this stimulation varies as a function of frequency, and it is typically reported as a “tingling” sensation for frequencies around 100 kHz. As frequency increases, heating effects predominate and the likelihood of nerve stimulation decreases; at 10 MHz the effect of the electric field is typically described as “warmth”. Nerve stimulation by induced electric fields is detailed in the ICNIRP low frequency guidelines (2010) [7].

Changes to permeability of cell membranes

When (low frequency) EMFs are pulsed, the power is distributed across a range of frequencies, which can include radiofrequency EMFs. If the pulse is sufficiently intense and brief, exposure to the resultant EMFs may cause cell membranes to become permeable, which in turn can lead to other cellular changes.

However, there is no evidence that the radiofrequency spectral component from an EMF pulse (without the low-frequency component) is sufficient to cause changes in the permeability of cell membranes.

The restrictions on nerve stimulation in the ICNIRP (2010) [7] guidelines (and used in ICNIRP 2020 [6]) are sufficient to ensure that permeability changes do not occur, so additional protection from the resultant radiofrequency EMFs is not necessary.

Temperature Rise

Radiofrequency EMFs can generate heat in the body and it is important that this heat is kept to a safe level. Although exposures (and resultant temperature rises) have occasionally been shown to cause severe harm, the literature lacks concomitant evidence of the lowest exposures required to

cause harm. For very low exposure levels (such as within the ICNIRP (1998) [5] basic restrictions) there is extensive evidence that the amount of heat generated is not sufficient to cause harm, but for exposure levels above those of the ICNIRP (1998) [5] basic restriction levels, there is limited research. It is important to note that guidelines restrict radiofrequency EMF exposure to limit temperature rise rather than absolute temperature, whereas health effects are primarily related to absolute temperature.

ICNIRP 2020 [6] guidelines differentiate between:

- Steady-state temperature rises: where temperature increases slowly, allowing time for heat to dissipate over a larger tissue mass and for thermoregulatory processes to counter temperature rise:
 - Body core temperature;
 - Local temperature: Type-1 and Type-2, Head and Torso, Limbs;
- Brief temperature rises (rapid): where there may not be sufficient time for heat to dissipate, which can result in larger temperature rises in small regions given the same absorbed radiofrequency energy.

Steady-state temperature rise – Body core temperature (100 KHz to 6 GHz)

Body core temperature refers to the temperature deep within the body, such as in the abdomen and brain, and varies substantially as a function of such factors as sex, age, time of day, work rate, environmental conditions and thermoregulation. Body core temperature rise due to radiofrequency EMFs that results in harm is only seen where temperature increases more than +1°C, with no clear evidence of a specific threshold for adverse health effects. Due to the limited literature available, ICNIRP has adopted a conservative temperature rise value as the operational adverse health effect threshold (the 1°C rise of ACGIH 2017 [13] [6]). It is important to note that significant physiological changes can occur when body core temperature increases by 1°C. Such changes are part of the body's normal thermoregulatory response (e.g., Van den Heuvel et al. 2017 [14] [6]), and thus do not in themselves represent an adverse health effect.

Recent theoretical modeling and generalization from experimental research across a range of species predicts that exposures resulting in a whole-body average SAR of approximately $6 \text{ W}\cdot\text{kg}^{-1}$, within the 100 kHz to 6 GHz range, over at least a 1-hour interval under thermoneutral conditions (28°C, naked, at rest), is required to induce a 1°C body core temperature rise in human adults. A higher SAR is required to reach this temperature rise in children due to their more-efficient heat dissipation (Hirata et al. 2013 [15] [6]).

However, given the limited measurement data available, ICNIRP has adopted a conservative position and uses $4 \text{ W}\cdot\text{kg}^{-1}$ averaged over 30 min as the radiofrequency EMF exposure level corresponding to a body core temperature rise of 1°C .

As a comparison, a human adult generates a total of approximately $1\cdot\text{W kg}^{-1}$ at rest (Weyand et al. 2009 [16] [6]), nearly $2 \text{ W}\cdot\text{kg}^{-1}$ standing, and $12 \text{ W}\cdot\text{kg}^{-1}$ running (Teunissen et al. 2007 [17],[6]).

Steady-state temperature rise – Body core temperature (6 GHz to 300 GHz)

As EMF frequency increases, exposure of the body and the resultant heating becomes more superficial, and above about 6 GHz this heating occurs predominantly within the skin. For example, 86% of the power at 6 and 300 GHz is absorbed within 8 and 0.2 mm of the surface respectively (Sasaki et al. 2017 [18] [6]).

Compared to heat in deep tissues, heat in superficial tissues is more easily removed from the body because it is easier for the thermal energy to transfer to the environment. This is why basic restrictions to protect against body core temperature rise have traditionally been limited to frequencies below 10 GHz (e.g., ICNIRP 1998 [5]).

ICNIRP is not aware of research that has assessed the effect of 6 to 300 GHz EMFs on body core temperature, nor of research that has demonstrated that it is harmful. However, as a conservative measure, ICNIRP uses the $4\cdot\text{kg}^{-1}$ corresponding to the operational adverse health effect threshold for frequencies up to 6 GHz, for the >6 to 300 GHz range also.

Steady-state temperature rise – Local temperature (Type-1, Type-2)

In addition to body core temperature, excessive localized heating can cause pain and thermal damage. There is an extensive literature showing that skin contact with temperatures below 42°C for extended periods will not cause pain or damage cells. However, there is also a substantial body of literature assessing thresholds for tissue damage which shows that damage can occur at tissue temperatures $>41\text{--}43^\circ\text{C}$, with damage likelihood and severity increasing as a function of time at such temperatures.

ICNIRP 2020 [6] guidelines treat radiofrequency EMF exposure that results in local temperatures of 41°C or greater as potentially harmful. As body temperature varies as a function of body region, ICNIRP treats exposure to different regions separately.

- “Type-1” tissue (all tissues in the upper arm, forearm, hand, thigh, leg, foot, pinna and the cornea, anterior chamber and iris of the eye,

epidermal, dermal, fat, muscle, and bone tissue); The normothermal temperature of Type 1 tissue is typically <33–36 °C;

- “Type-2” tissue (all tissues in the head, eye, abdomen, back, thorax, and pelvis, excluding those defined as Type-1 tissue); The normothermal temperature of Type-2 tissue is typically <38.5 °C.

These values were used to define operational thresholds for local heat-induced health effects; adopting 41 °C as potentially harmful, ICNIRP 2020 [6] guidelines take a conservative approach and treat radiofrequency EMF-induced temperature rises of 5°C and 2°C, within Type-1 and Type-2 tissue, respectively, as operational adverse health effect thresholds for local exposure.

Steady-state temperature rise – Local temperature (Head and Torso, Limbs)

It is difficult to set exposure restrictions as a function of the above tissue-type classification. ICNIRP thus defines two regions and sets separate exposure restrictions, where relevant, for these regions:

- “Head and Torso”, comprising the head, eye, pinna, abdomen, back, thorax and pelvis, which includes both Type-1 and Type-2 tissue; Exposure levels have been determined for each of these regions such that they do not result in temperature rises of more than 5°C and 2°C, in Type-1 and Type-2 tissue, respectively;
- “Limbs”, comprising the upper arm, forearm, hand, thigh; The operational adverse health effect threshold for the Limbs is always 5°C.

*Steady-state temperature rise – Local temperature (Head and Torso, Limbs)
(100 KHz to 6 GHz)*

Within the 100 kHz to 6 GHz EMF range, average SAR over 10g provides an appropriate measure of the radiofrequency EMF-induced steady-state temperature rise within tissue.

A SAR 10g of at least $20 \text{ W}\cdot\text{kg}^{-1}$ is required to exceed the operational adverse health effect thresholds in the Head and Torso, and $40 \text{ W}\cdot\text{kg}^{-1}$ in the Limbs, over an interval sufficient to produce a steady-state temperature (from a few minutes to 30 min). This time interval is operationalized as a 6-min average as it closely matches the thermal time constant for local exposure.

*Steady-state temperature rise – Local temperature (Head and Torso, Limbs)
(6 GHz to 300 GHz)*

Within the >6 to 300 GHz range, absorbed power density (S_{ab}) provides a measure of the power absorbed in tissue that closely approximates the superficial temperature rise. Recent thermal modeling and analytical solutions suggest that for EMF frequencies between 6 and 30 GHz, the exposure over a square averaging area of 4 cm^2 provides a good estimate of local maximum temperature rise.

ICNIRP uses a square averaging area of 4 cm^2 for >6 to 300 GHz as a practical protection specification. Moreover, from >30 to 300 GHz (where focal beam exposure can occur), an additional spatial average of 1 cm^2 is used to ensure that the operational adverse health effect thresholds are not exceeded over smaller regions.

As 6 minutes is an appropriate averaging interval and as an absorbed power density of approximately $200 \text{ W}\cdot\text{m}^{-2}$ is required to produce the Type-1 tissue operational adverse health effect threshold of a 5°C local temperature rise for frequencies of >6 to 300 GHz, ICNIRP has set the absorbed power density value for local heating, averaged over 6 min and a square 4 cm^2 region, at 200 W m^{-2} ; this will also restrict temperature rise in Type-2 tissue to below the operational adverse health effect threshold of 2°C . An additional specification of $400 \text{ W}\cdot\text{m}^{-2}$ has been set for spatial averages of square 1 cm^2 regions, for frequencies >30 GHz.

Rapid temperature rise

For some types of exposure, rapid temperature rise can result in “hot spots,” heterogeneous temperature distribution over tissue mass. To account for such heterogeneous temperature distributions, an adjustment to the steady-state exposure level is required. This can be achieved by specifying the maximum exposure level allowed, as a function of time, in order to restrict temperature rise to below the operational adverse health effect thresholds.

From 400 MHz to 6 GHz, ICNIRP specifies the restriction in terms of specific energy absorption (SA) of any 10g cubic mass, where SA is restricted to $7.2 [0.05+0.95(t/360)0.5] \text{ kJ kg}^{-1}$ for Head and Torso, and $14.4 [0.025+0.975(t/360)0.5] \text{ kJ kg}^{-1}$ for Limb exposure, where “t” is exposure interval in seconds.

Above 6 GHz, ICNIRP specifies the exposure level for both Head and Torso, and Limbs, in terms of absorbed energy density (U_{ab}) over any square averaging area of 4 cm^2 , such that U_{ab} is specified as $72[0.05+0.95(t/360)0.5] \text{ kJ m}^{-2}$, where “t” is the exposure interval in seconds (extension of Kodera et al. 2018 [19] [6]).

An additional exposure level for square 1 cm² averaging areas is applicable for EMFs with frequencies of >30 to 300 GHz to account for focused beam exposure and is given by $144[0.025+0.975(t/360)0.5]$ kJ m⁻².

1.2.1.4 Reduction factors

Reduction factors were then applied to the resultant thresholds (or operational thresholds) to provide exposure restriction values.

A reduction factor was applied to the thresholds to account for scientific uncertainty, as well as differences in thermal physiology across the population and variability in environmental conditions and physical activity levels.

	<i>Frequency Range</i>	<i>Occupational Exposure</i>	<i>General Public</i>
<i>Whole-body average SAR</i>	(100 kHz to 300 GHz)	10	50
<i>Local SAR Head and Torso</i>	(100 kHz to 6 GHz)	2	10
<i>Local SAR Limbs</i>	(100 kHz to 6 GHz)	2	10
<i>Local SA</i>	(400 MHz to 6 GHz)	2	10
<i>Local absorbed power density</i>	(>6 GHz to 300 GHz)	2	10
<i>Local absorbed energy density</i>	(>6 GHz to 300 GHz)	2	10

Table 1: Summary of reduction factors applied to resultant/operational thresholds to obtain "Basic Restrictions".

As previous reported, exposure restriction values are referred to as “Basic restrictions”. “Reference levels”, have been derived from the basic restrictions to provide a more-practical means of demonstrating compliance with the guidelines.

Basic restrictions and Reference Levels values are respectively reported in Table 2-4 and Table 5-9 of ICNIRP 2020 [6].

1.2.1.5 Guidelines comparison

Although ICNIRP 2020 [6] is the latest release of the Guidelines, EMF worldwide limits are based upon ICNIRP Guidelines 1998 [5]. In Figure 4, the general public whole-body E-field reference levels for the traditional and revised version of ICNIRP guidelines is presented. Exposure values in

the range of frequencies used by cellular systems are not changed. Furthermore E-field levels between 0.1 MHz to 20 MHz are higher for the updated version than previous releases.

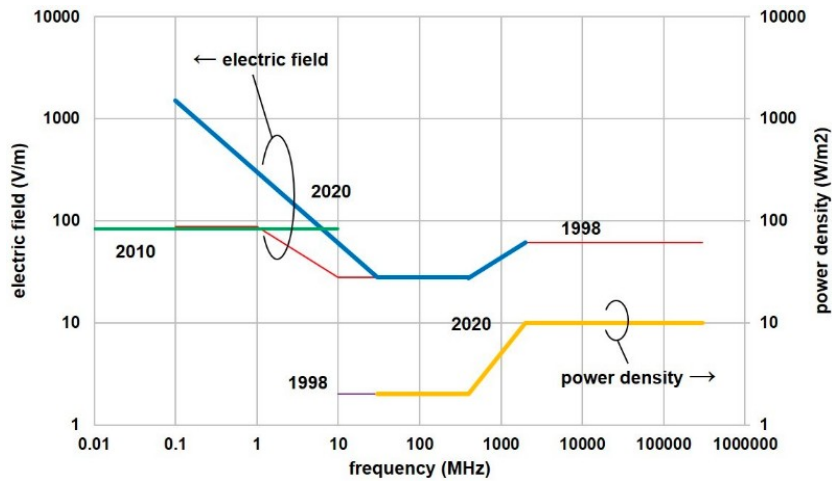


Figure 4: Whole body average reference levels for the general public for the ICNIRP 1998 (red), ICNIRP 2010 (green) and ICNIRP 2020 (blue), for the 100 kHz to 300 GHz frequency range. Note that the units of the two y-axes (i.e. electric field and power density) are independent of each other [20].

Also IEEE (Institute of Electrical and Electronics Engineers) develops a standard addressing exposure safety, namely IEEE Std C95.1. IEEE Std C95.1 2019 [21] is the last version of the document. It specifies exposure criteria and limits to protect against established adverse health effects in humans associated with exposure to electric, magnetic, and electromagnetic fields in the frequency range of 0 Hz to 300 GHz. In Figure 5, the Exposure Limits for General Public/Unrestricted Environments for the ICNIRP guideline and IEEE standard is presented, in which power-densities (S) above 30 MHz are identical.

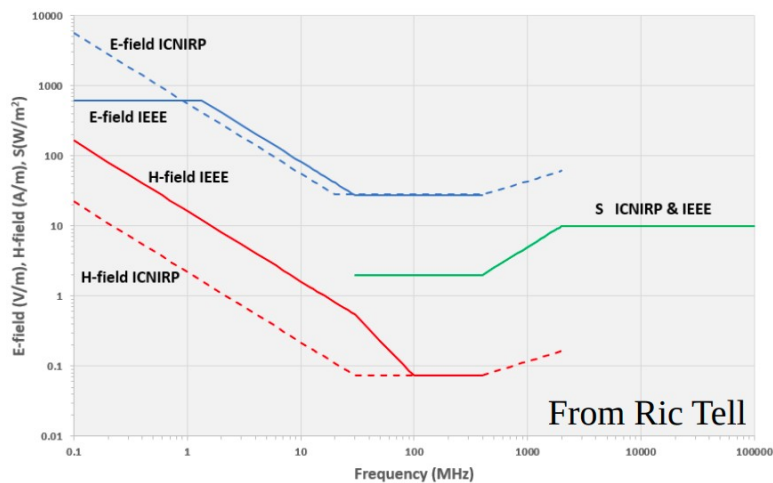


Figure 5: Comparison of Proposed ICNIRP and Proposed IEEE Exposure Limits for General Public/Unrestricted Environments [22].

It should be noted that international harmonization of standards and guidelines is highly desirable. Much effort has been devoted to doing this for the IEEE Std C95.1-2019 [21] standard and the current ICNIRP guidelines [23].

1.2.1.6 Criticisms on Guidelines

ICNIRP maintains strong collaboration ties with a number of international and national non-commercial organizations with interests in non-ionizing radiation protection. Those include the International Radiation Protection Association (IRPA), the World Health Organization (WHO), the International Labour Organization (ILO), the International Agency for Research on Cancer (IARC), the United Nations Environment Programme (UNEP), the International Telecommunications Union (ITU), the European Commission (EC), the International Electrotechnical Commission (IEC) and the North Atlantic Treaty Organisation (NATO). These entities are involved in the International EMF Project (EMF) from 1996 [24].

In this context, the World Health Organization (WHO), the Scientific Committee on Emerging and Newly Identified Health Risks (SCENIHR) of the European Union and the International Commission on Non-Ionizing Radiation Protection (ICNIRP) concluded that exposure related to wireless networks and their use does not lead to adverse effects for public health if it is below the limits recommended by the ICNIRP.

Research on possible human health effects of RF-EMF exposure to mmWave frequencies goes back many decades and is continuing. In terms of research specifically on the 5G frequency range, the EMF Portal database [25] lists approximately 350 studies on mmWave RF-EMF health related research. Extensive research on mmWave and health has been conducted on radar, microwave and military applications. Tissue heating remains the only recognised and substantiated hazard of exposure to mmWave frequencies based on scientific research to date [26].

However, despite much research and communication efforts to resolve it, there is still some public concern about the possible harmfulness of RF-EMFs from mobile communication equipment. In addition, there will be numerous new 5G base stations around the areas where people live and work, which may lead to additional public concern.

In contrast to Guidelines and the majority of the scientific community, Professor Rainer Nyberg and Professor Lennart Hardell wrote a moratorium on the roll-out of 5G called “The 5G Appeal” [27]. They state that the current ICNIRP/WHO guidelines for EMF are based on the obsolete hypothesis that “The critical effect of RF-EMF exposure relevant to human

health and safety is heating of exposed tissue.” They affirm there are many different kinds of illnesses and harms are caused without heating (“non-thermal effect”) at radiation levels well below ICNIRP guidelines. They also affirm the reason for the misleading guidelines is that “conflict of interest of ICNIRP members due to their relationships with telecommunications or electric companies undermine the impartiality that should govern the regulation of Public Exposure Standards for non-ionizing radiation” [28].

Their statements are primary based on human cancer epidemiology reports conducted by the Hardell’s workgroup [29] and animal carcinogenicity studies from National Toxicology Program ([30], [31]) and the other from the Ramazzini Institute [32].

It must be noted that ICNIRP analysed these studies with deeply dedicated reviews ([33], [34]). Furthermore ICNIRP 2020 appendix B [6] presents the summary of the research on biological and health effects of radiofrequency EMFs. ICNIRP concludes that “no effects of radiofrequency EMFs on the induction or development of cancer have been substantiated”.

1.2.2 Limits

The ICNIRP guidelines are accepted in many countries around the world, including most EU members. However, in some countries own legal regulations relating to the protection of human and the environment against the influence of EMF have been adopted. Table 2 presents the General Public exposure values adopted in different countries for two interesting centre frequencies.

<i>Country</i>	<i>Year</i>	<i>Radiofrequency Electric field (V/m) 900 MHz</i>	<i>Radiofrequency Electric field (V/m) 1800 MHz</i>
<i>Argentina</i>	<i>2017</i>	<i>41.25</i>	<i>58.36</i>
<i>Australia</i>	<i>2017</i>	<i>41.1</i>	<i>58.1</i>
<i>Austria</i>	<i>2017</i>	<i>41.25</i>	<i>58.34</i>
<i>Bahrain</i>	<i>2017</i>	<i>41</i>	<i>58</i>
<i>Brazil</i>	<i>2017</i>	<i>41.25</i>	<i>58.34</i>
<i>Bulgaria</i>	<i>2017</i>	<i>6.14</i>	<i>6.14</i>

Chapter 1 - EMF limits and measurements

Country	Year	Radiofrequency Electric field (V/m) 900 MHz	Radiofrequency Electric field (V/m) 1800 MHz
Canada	2017	32.1	40.07
Cyprus	2017	41	58
Finland	2017	41.4	58.55
France	2017	41	58
Germany	2017	41.25	58
Greece	2017	31.9/34.5	45.1/48.8
Iran (Islamic Republic of)	2017	41.25	58.34
Israel	2017	[13.0]	[18.0]
Italy	2017	6/20	6/20
Japan	2017	47.55	61.4
Malaysia	2017	41.25	58.34
Netherlands	2017	41.25	58.34
New Zealand	2017	41.25	58.34
Norway	2017	41.25	58.34
Peru	2017	41.25	58.34
Philippines	2017	41.25	58.34
Republic of Korea	2017	41.25	58.34
Saudi Arabia	2017	41.25	58.34
South Africa	2017	[41.0]	[58.0]
Sweden	2017	[41.25]	[58.33]

Country	Year	Radiofrequency Electric field (V/m) 900 MHz	Radiofrequency Electric field (V/m) 1800 MHz
Switzerland	2017	4/41.25	6/58.34
Tunisia	2017	41	58
Turkey	2017	3/10.23/41.0	3/14.5/58
United Kingdom of Great Britain and Northern Ireland	2017	[41.25]	[58.34]
United States of America	2017	47.6	61.4
Zambia	2017	41	58

Table 2: Exposure limits for radio-frequency fields (public) – Data by country – Last updated: 2017-05-31 [35].

1.2.2.1 European and Italian framework

The Council of the European Union (EU) has provided Recommendation 1999/519/EC of 12 July 1999 [36] that contains general-public reference levels of exposure, depending on the frequency range, that shall be considered as limit values. The reference levels are generally intended to be spatially averaged and refers to EMF values averaged over a period of six minutes in accordance with ICNIRP 1998 [5] recommendation.

Unperturbed RMS limit values for radio frequencies, defined by ICNIRP 1998 and included in the 1999/519/EC recommendation, are listed in Figure 6.

In Italy, a Framework Law No. 36/2001 on protection against electromagnetic fields was enforced in February 2001 [37]. Framework Law is followed by Dpcm 8 July 2003 published to Gazzetta Ufficiale n.199 [8] and n.200 in 28 August 2003. These regulations establish general rules and protection criteria that basically diverge from the UE Recommendation of July 1999, and from international guidelines.

The Italian regulations introduces so-called “exposure limits”, “attention values”, and “quality goals”.

“Exposure limits” means the emission value of an electric, magnetic and electromagnetic field, as assessed to protect human health from acute

effects, which shall never be exceeded, in case of the exposure of member of the general public and workers.

Frequency range	E-field strength (V/m)	H-field strength (A/m)	B-field (μT)	Equivalent plane wave power density S_{eq} (W/m ²)
0-1 Hz	—	$3,2 \times 10^4$	4×10^4	—
1-8 Hz	10 000	$3,2 \times 10^4/f^2$	$4 \times 10^4/f^2$	—
8-25 Hz	10 000	$4\,000/f$	$5\,000/f$	—
0,025-0,8 kHz	$250/f$	$4/f$	$5/f$	—
0,8-3 kHz	$250/f$	5	6,25	—
3-150 kHz	87	5	6,25	—
0,15-1 MHz	87	$0,73/f$	$0,92/f$	—
1-10 MHz	$87/f^{1/2}$	$0,73/f$	$0,92/f$	—
10-400 MHz	28	0,073	0,092	2
400-2 000 MHz	$1,375 f^{1/2}$	$0,0037 f^{1/2}$	$0,0046 f^{1/2}$	$f/200$
2-300 GHz	61	0,16	0,20	10

Figure 6: Reference levels for general public exposure to time-varying electric and magnetic fields (0 Hz to 300 GHz, unperturbed rms values) [5], [36].

“Attention values” means the emission value of an electric, magnetic and electromagnetic field which shall never be exceeded in children’s playgrounds, residential dwellings, school premises, and in areas where people are staying for 4 hours or more per day, as well as in outdoor annexes that may be used as residential environments, such as balconies, terraces, courtyards, but excluding roof pavings.

“Quality goals” means the emission value of an electric, magnetic and electromagnetic field to respect in order to progressively minimise exposure to electromagnetic fields, in highly frequented outdoor areas.

The Exposure limits, Attention values and Quality goals provided by Italian regulations are listed in Figure 7. The values shall be averaged over any six-minute period in an area equivalent to the vertical cross-section of the human body. After Decreto Legge 18 ottobre 2012, n. 179 was published, attention values a quality goals shall be averaged over any 24-hour period [39].

Adoption of policy to limit EMF exposure that relies on the exposure levels significantly lower than ICNIRP reference levels, as in Italy, has a negative influence on the cost of deployment and performance of 5G networks, and could hamper the process of their introduction and the development of 5G infrastructure. Stricter limits on EMF exposure may produce a high infrastructure density, which greatly escalates costs and complexity of the

5G network deployment and the inability to share an infrastructure (cell sites) with existing mobile technologies [4].

Table 1	Electric Field Strength (V/m)	Magnetic Field Strength (A/m)	Power Density (W/m ²)
Exposure limits			
0.1 < f = 3 MHz	60	0.20	-
3 < f = 3000 MHz	20	0.05	1
3 < f = 300 GHz	40	0.10	4

Table 2	Electric Field Strength (V/m)	Magnetic Field Strength (A/m)	Power Density (W/m ²)
Attention values			
0.1 MHz < f = 300 GHz	6	0.016	0.10 (3 MHz - 300 GHz)

Table 3	Electric Field Strength (V/m)	Magnetic Field Strength (A/m)	Power Density (W/m ²)
Quality goals			
0.1 MHz < f = 300 GHz	6	0.016	0.10 (3 MHz - 300 GHz)

Figure 7: Exposure limits, Attention values and Quality goals provided by Italian regulations [38].

Moreover Italian regulations could change soon. In April 2020, Italy’s Prime Minister Giuseppe Conte appointed Vittorio Colao, former Vodafone Group CEO, to lead a group of experts to outline a plan on how to restart the Italian economy after the coronavirus emergency. Colao and his taskforce presented a 121-page recovery plan to the Italian government [40]. The plan at point n.27 of 102 address the 5G network development. It specifies to increase Italian EMF exposure limits as provided by European recommendation and ICNIRP guidelines.

In addition to European and Italian regulations cited before, there are other documents based upon ICNIRP guidelines or IEEE standards specifically created for workers (or “occupationally exposed”). European Directive 2013/35/EU lays down minimum requirements for the protection of workers from risks to their health and safety arising, or likely to arise, from exposure to electromagnetic fields during their work [41]. Italian Government adopt European Directive 2013/35/EU with Decreto Legislativo 1° agosto 2016, n. 159 [42].

In Figure 8, action levels for exposure to electric and magnetic fields from 100 kHz to 300 GHz is presented, where occupational limits being generally five times higher than those for the general public.

Frequency range	Electric field strength ALs(E) [Vm ⁻¹] (RMS)	Magnetic flux density ALs(B) [μT] (RMS)	Power density ALs(S) [Wm ⁻²]
100 kHz ≤ f < 1 MHz	6,1 × 10 ²	2,0 × 10 ⁶ /f	—
1 ≤ f < 10 MHz	6,1 × 10 ⁸ /f	2,0 × 10 ⁶ /f	—
10 ≤ f < 400 MHz	61	0,2	—
400 MHz ≤ f < 2 GHz	3 × 10 ⁻³ f ^{1/2}	1,0 × 10 ⁻⁵ f ^{1/2}	—
2 ≤ f < 6 GHz	1,4 × 10 ²	4,5 × 10 ⁻¹	—
6 ≤ f ≤ 300 GHz	1,4 × 10 ²	4,5 × 10 ⁻¹	50

Figure 8: ALs for exposure to electric and magnetic fields from 100 kHz to 300 GHz [41], [42].

1.3 EMF measurement methods

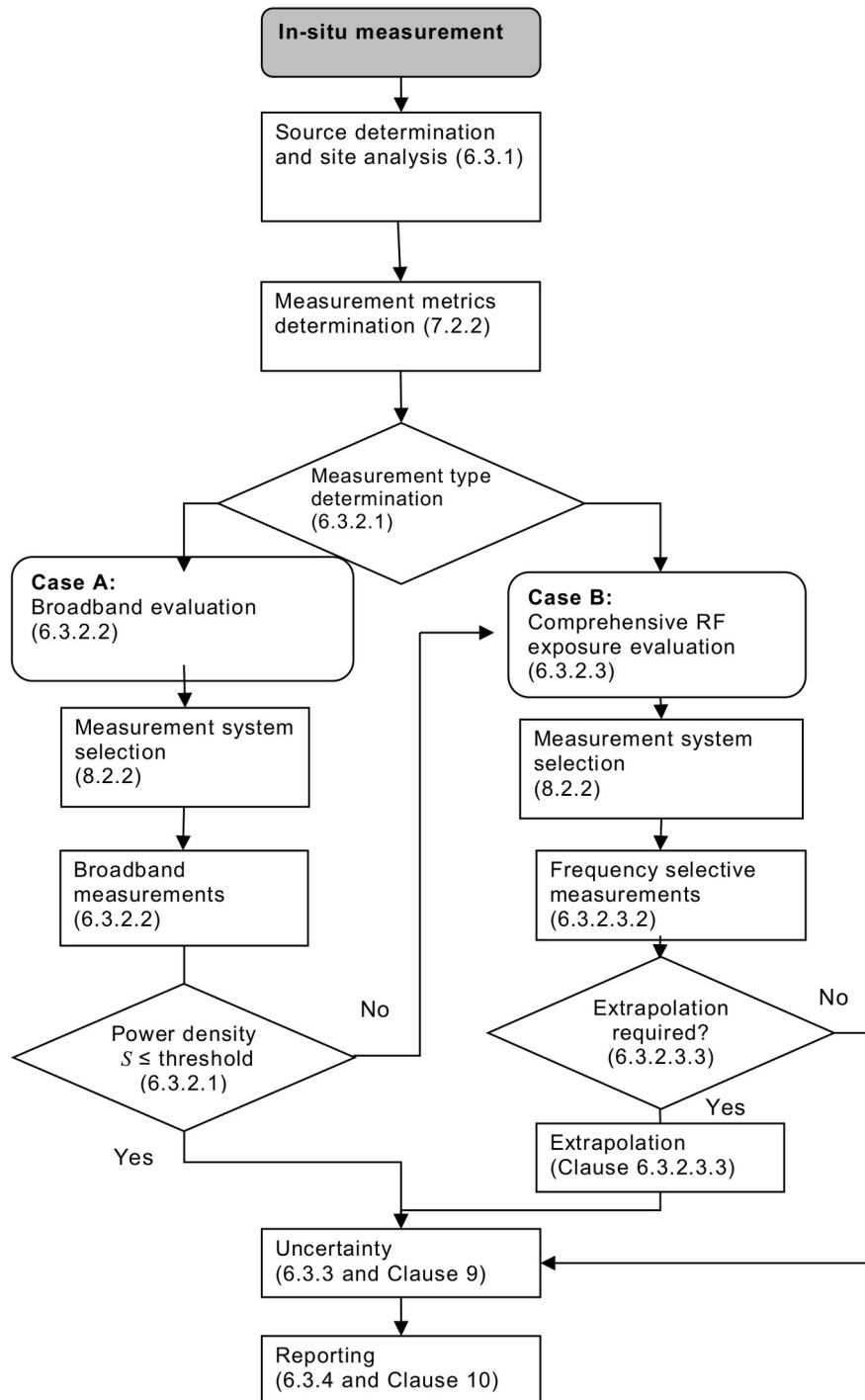
The evaluation of compliance with the permissible EMF exposure in the vicinity of a base station is achieved by measuring the levels of EMF produced by equipment installed on site, and then comparing the obtained results with appropriate reference levels constituting limit values.

Determination of RF field strength, power density and SAR in the vicinity of radiocommunication base stations for the purpose of evaluating human exposure is the scope of the International Standard IEC 62232:2017 [43]. This document addresses the evaluation of radiofrequency (RF) field strength, power density or specific absorption rate (SAR) levels in the vicinity of radiocommunication base stations (RBS), also called product or Equipment Under Test (EUT), intentionally radiating in the frequency range 110 MHz to 100 GHz, considering the impact of ambient sources on RF exposure at least in the 100 kHz to 300 GHz frequency range. This document specifies, among others, the RF exposure evaluation methods to be used for “in-situ RF exposure assessments”.

Checking the compliance of the measured RF exposure levels with the applicable exposure limits and regulations is the main goal of “in-situ RF measurement”.

The procedure described in Figure 9 shall be used to evaluate in-situ RF exposure assessment based on measurement methods, uncertainty, and reporting.

The process shall start by identifying all relevant fixed and permanently emitting RF source installations in the surrounding area. The measurement system(s) and the post processing shall cover the RF emissions from the product and all relevant ambient sources between at least 100 kHz and 300 GHz as determined by the site analysis.



IEC

Figure 9: Alternative routes to evaluate in-situ RF exposure [43].

Then, the measurement metrics applicable on the measurement area shall be determined according to the distance from the source antenna. The second step is to choose between two evaluation approaches, known as Case A and Case B as indicated in Figure 9. Case A provides a set of results covering all sources and frequencies at one measurement area. Case B provides separate

sets of field values for each source, frequency or frequency sub-band present in the measurement area. The choice of the measurement type depends on the objective of the in-situ evaluation. If the objective is to provide a global evaluation of RF exposure level from all sources together “as observed” then Broadband Measurements are enough. The evaluation shall start with Case A evaluation. However, if the power density assessment based on Case A is above applicable RF exposure limits (i.e. the threshold defined under Case A in Figure 13 is the applicable exposure limits) or if it is necessary or desired to investigate the contribution from each RF source, the Case A evaluation shall be complemented by a Case B evaluation.

Instead, If the objective is to provide a comprehensive evaluation of RF exposure i.e. investigating every contribution from RF sources using a frequency selective analysis, then Frequency Selective Measurement are required and a Case B evaluation shall be conducted. It is recommended that a Case B evaluation is preceded by a Case A evaluation.

For the case where the aim is to evaluate the maximum exposure conditions taking into account traffic and transmitted power variations, then the evaluation result data shall be extrapolated.

Although extrapolation is always possible, Extrapolation of broadband measurement results is not recommended. Such extrapolation can result in a vast overestimation depending on the characteristics of the probe and the characteristics of the EUT/ambient signals. Therefore frequency-selective measurements are recommended where accurate extrapolation is required.

Uncertainty analysis shall be performed. The target expanded uncertainty is 4 dB or below, which is considered industry best practice. The expanded uncertainty for RF exposure evaluation used in in-situ RF exposure assessment shall not exceed 6 dB.

Reporting shall be performed. The in-situ RF exposure evaluation or assessment report shall contain at least the most relevant informations, such as description of the measurement site, environmental conditions, time and date, measurement protocol used, probe(s) and measurement instrument(s) used, measurement results, if extrapolation is used, description of the extrapolation method, uncertainty analysis, etc..

Referring to measurements, International Standard IEC 62232:2017 defines three source regions according to distance from the source antenna: Source region I constitutes the reactive near-field; Source region II constitutes the radiating near-field; Source region III constitutes the far-field. Measurements are usually performed in the far field area. In this area the field has the character of a plane wave, the vectors of the electric field E and

the magnetic field H are perpendicular to each other, and the power density S is related to the electric field strength E by the free space impedance, according to the following mathematical formula.

$$S = \frac{E^2}{Z_0} = \frac{E^2}{120\pi} \quad (1)$$

The far field area boundary R is determined in (2) where D is the maximum antenna dimension, and λ is the wavelength corresponding to the appropriate frequency.

$$R > \frac{2D^2}{\lambda} \quad (2)$$

It must be noted that International Standards developed by IEC are not mandatory, their adoption is voluntary. Nevertheless they are often referenced in national laws or regulations around the world. For example, in Italy, IEC 62232:2017 is adopted from Italian Electrotechnical Committee (CEI) as CEI EN 62232:2018-03. From the knowledge of IEC 62232:2017, CEI develops further technical guidelines named CEI 211-7. DPCM 8 July 2003 published to Gazzetta Ufficiale n.199 orders “*Measurements and exposure assessment shall be made in accordance with the Standard CEI 211-7, and/or further relevant standards issued by CEI*” [38].

1.3.1 Broadband measurements

Broadband measurements give the sum of all signals over the frequency without distinguishing the contribution of different frequencies (whether from the EUT or from ambient sources).

Broadband measurement method enables determination of the RMS value of the electric field strength E and power density S in the vicinity of a base station. The measurements are usually performed in the far field area i.e. in the area where the field strength E and power density S are interrelated with each other by the equation (1) therefore to an unambiguous EMF determination, it is enough to determine the RMS value of the electric field strength E . Next, the power density S can be calculated. Typical measurement equipment consists of an electric field strength meter connected with broadband isotropic measuring antenna, i.e. a probe (see Figure 10). To evaluate the highest RF field strength or the RF field strength at discrete points in a region, perform a search using the handheld sweep method or tripod procedure to reduce influences of the surveyor’s body.

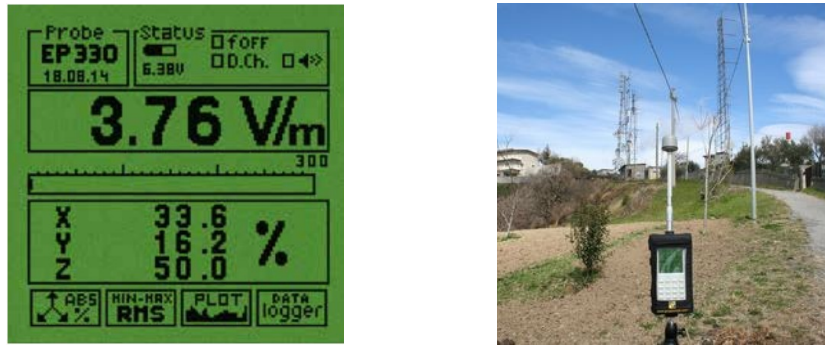


Figure 10: (a) Example of broadband meter display [44] - Example of E-field measurement using broadband meter, isotropic probe and tripod procedure [45].

The total broadband EMF measurement results of the E_{sum} and S_{sum} are in fact the sum of all components E_k and S_k from n signals received by the measurement antenna in the frequency range determined by its construction, according to (3) and (4).

$$E_{sum} = \sqrt{\sum_{k=1}^n E_k^2} \quad (3)$$

$$S_{sum} = \sum_{k=1}^n S_k^2 \quad (4)$$

If required, spatial averaging of the field can be performed. In the case of broadband EMF measurements, the identification of frequency components is not possible.

1.3.2 Frequency-selective measurements

The use of frequency-selective measurement equipment allows selective measurements in the frequency domain and enables determination of the EMF level in a precisely defined frequency range. This improves the situation regarding the identification of EMF frequency components and, as a result identification of, for example, a specific base station or a cell of a specific base station.

The RF field strength measurement shall consider contributions from all directions/polarizations. An isotropic antenna is best suited to this purpose but other antennas may be used. Single-axis (e.g. dipole) can be used to obtain the total RF field strength by positioning the probe in three orthogonal directions and summing the individual measured results. A directional measurement antenna or probe can be used to separate contributions from different directions. These contributions shall be summed to determine the total field strength. However, this value will be an overestimation of the true level.

Frequency-selective measurements could be done with several instruments. Basic spectrum analysers enable frequency discrimination but in case of frequency reuse system analysis it can't distinguish signals from different sources. In this case, spectrum analysers with technology specific decoding functions or vector spectrum analysers could be used. Figure 11 shows examples of measurement output using different frequency-selective instruments.

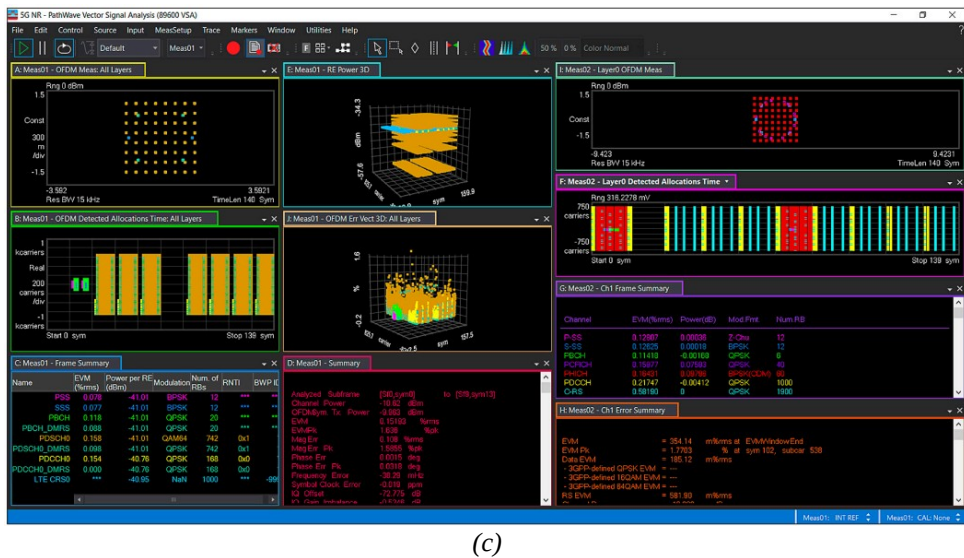
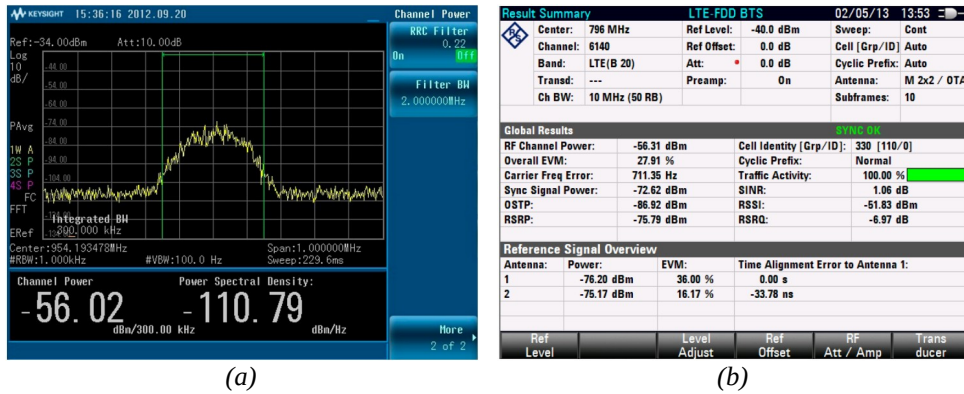


Figure 11: (a) Example of channel power measurement with basic spectrum analyser [46] – (b) Example of LTE measurement with basic spectrum analyser equipped with LTE decoding options [47] – (c) example of 5G NR complete signal analysis with a Vector Spectrum Analyser used with specific technology software [48].

1.3.3 Extrapolation to maximum RF field strength

Both broadband and frequency-selective measurements, reflect the level of EMF occurring in the vicinity of a base station during its normal operation. In fact, due to the momentary telecommunications traffic load carried by the base station, the EMF level changes over time.

For the case where the aim is to evaluate the maximum exposure conditions taking into account traffic and transmitted power variations, then the evaluation result data shall be extrapolated. To extrapolate time variant signals to the maximum possible output power conditions, a time invariant component of the signal (e.g. the pilot channel or control channel) shall be evaluated. This kind of approach is standardized for 2G, 3G, and 4G technologies as described in Annex F of IEC 62232:2017 [43], but is still under investigation for 5G technology.

It must be noted that in many cases extrapolation process can significantly overestimate the actual exposure.

Due to different access technique, adaptive power control and discontinuous transmission (DTX), the real maximum is well below the theoretical maximum. Mobile network management systems including the network manager provide counters representing the performance and operation of the system. Statistics can be generated for one single cell or multiple cell sites distributed over a very large geographical area. Example CDFs of the time-averaged transmitted power obtained from network-based measurements from a 3G network in India are shown in Figure 12 (a). Similar results from network-based measurements of a 2G/3G/4G network in Sweden are shown in Figure 12 (b).

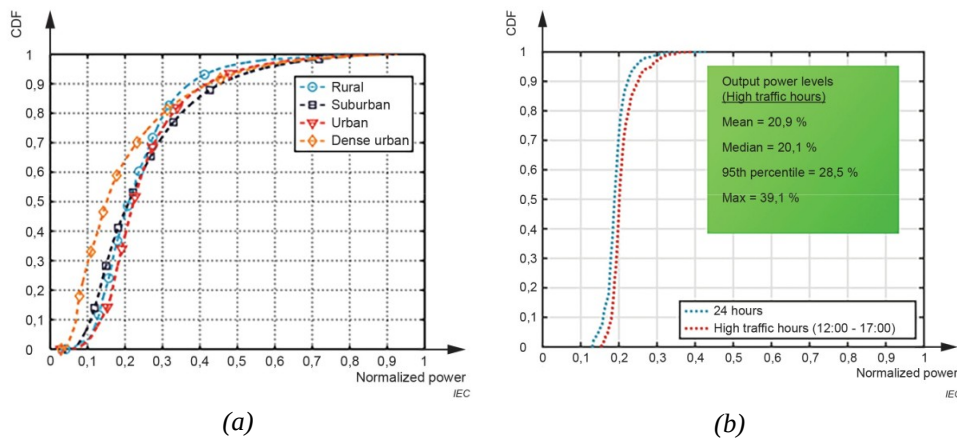


Figure 12: (a) Empirical CDFs of transmitted power (normalized) for different environments in 3G network in India [49], [50] – (b) Empirical CDFs of combined transmitted power (normalized) for a 2G/3G/4G network in Sweden [49], [51].

In addition to traffic variation, beamforming used in 5G technology involves additional variability in the determination of the power contributing to the actual maximum exposure. Base stations with mMIMO antennas produce a number of simultaneous narrow beams individually steered towards target devices in order to optimize the usage of radio resources by focusing radio energy to target users and reducing interference to other devices. This "beam-centric" behaviour of mMIMO systems differs from conventional

radio access technologies for which energy is constantly transmitted in a wide angular sector. The power reduction of a BS using mMIMO can be described by two factors: (i) the traffic variation and (ii) the time-averaged spatial distribution of transmitted power or EIRP.

In this context, IEC is working for the next edition of IEC 62232. It should consider defining methods for performing an RF exposure assessment of any type of BS using the actual maximum transmitted power or EIRP. The next standard should provide, among other, an enhanced methodology for EMF exposure assessment that defines the actual maximum power as the 95th percentile of the measured values instead of the theoretical maximum value (more details on chapter 13 of IEC TR 62669:2019 [49]).

1.4 Conclusion

This first chapter addressed to main concepts concerning radio frequency (RF) electromagnetic fields (EMF) limits and measurements. Next two chapters will deeply address to RF exposure assessment using extrapolation process of the LTE (4G) and 5G-NR signals. In case of 4G standardized procedures will be proposed. In case of 5G proposals from open scientific literature will be evaluated.

2 4G systems: Control signals and Extrapolation

“After 4G general aspects and a more detailed technical review on 4G access network, this chapter will address to 4G specific control signals and 4G EMF extrapolation process standardized by international and Italian regulations.”

2.1 4G overview

All mobile broadband systems are based on the ITU’s IMT standards. In January 2012, ITU defined IMT-Advanced [52]. A system that meets IMT-Advanced requirements is named a 4G wireless cellular technology.

From a practical point of view 4G is implemented by LTE standard. Moreover LTE standard became an effective 4G system only after the release of LTE-Advanced (see Figure 13).

Item	Subcategory	3GPP LTE (Release 8)	3GPP LTE-Advanced (Release 10)	ITU IMT-Advanced
Peak data rate	Downlink	300 Mbps	1 Gbps	1 Gbps low mobility, 100 Mbps high mobility
	Uplink	75 Mbps	500 Mbps	
Peak spectral efficiency (b/s/Hz)	Downlink	16.3 (4x4 MIMO)	30 (up to 8x8 MIMO)	15 (4x4 MIMO)
	Uplink	4.32 (64QAM SISO)	15 (up to 4x4 MIMO)	6.75 (2x4 MIMO)
Downlink cell spectral efficiency (b/s/Hz), 3 km/h, 500 m ISD	2x2 MIMO	1.69	2.4	2.6
	4.2 MIMO	1.87	2.6	
	4x4 MIMO	2.67	3.7	
Downlink cell-edge user spectral efficiency (b/s/Hz) 5 percentile, 10 users, 500 m ISD	2x2 MIMO	0.05	0.07	0.075
	4x2 MIMO	0.06	0.09	
	4x4 MIMO	0.08	0.12	

Figure 13: Performance targets for LTE, LTE Advanced and IMT-Advanced – Note: ISD stands for Inter-site distance [53].

Long Term Evolution (LTE) have been first time introduced in 3GPP Release 8 in 2008 [54], LTE Advanced was introduced in 3GPP Release 10 in 2011 [55], while LTE-Advanced Pro was introduced in 3GPP Release 13 in 2016 [56]. LTE enhancements are continuing along their distinctive development track, in parallel to 5G.

Today LTE is a mature technology and is widely deployed worldwide. Figure 14 shows 4G coverage map of Italy and of Cassino where green parts denotes a good signal coverage.

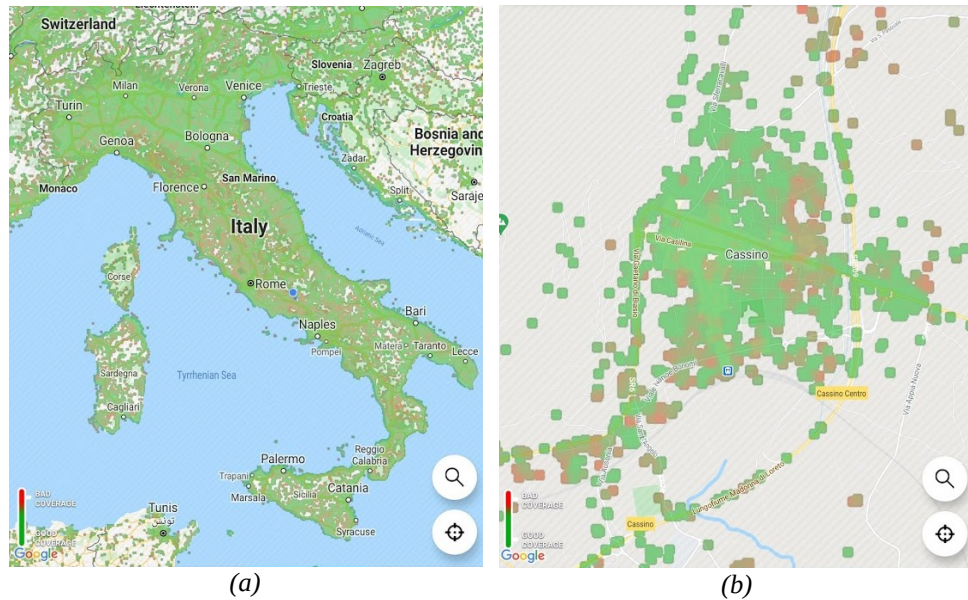


Figure 14: (a) OPENSIGNAL 4G coverage map of Italy from all operator, (b) OPENSIGNAL 4G coverage map of Cassino from all operator – Note: green means good signal and red means bad signal [57] (accessed at 28/10/2020).

For the purpose of RF-EMF measurement, a technical review of 4G is necessary. The following paragraph will introduce a technical review (mainly based on [58]) limited to the downlink part of Radio Access Network (RAN) of the LTE standard. LTE RAN is called E-UTRA.

2.2 LTE E-UTRA technology review and control signals

LTE main objectives are higher data rates, lower latency on the user plane and control plane and a packet-optimized radio access technology. Respect to previous generations of mobile broadband systems, LTE is based on new technical principles. LTE uses new multiple access schemes on the air interface: OFDMA (Orthogonal Frequency Division Multiple Access) in downlink and SC-FDMA (Single Carrier Frequency Division Multiple Access) in uplink. Furthermore, MIMO antenna schemes form an essential part of LTE. LTE includes an FDD (Frequency Division Duplex) mode of operation and a TDD (Time Division Duplex) mode of operation.

The downlink transmission scheme for E-UTRA FDD and TDD modes is based on conventional OFDM. In an OFDM system, the available spectrum is divided into multiple carriers, called subcarriers. Each of these subcarriers is independently modulated by a low rate data stream. OFDM has several

benefits including its robustness against multipath fading and its efficient receiver architecture.

Figure 15 shows a representation of an OFDM signal. In this figure, a signal with 5 MHz bandwidth is shown, but the principle is of course the same for the other E-UTRA bandwidths. Data symbols are independently modulated and transmitted over a high number of closely spaced orthogonal subcarriers. In E-UTRA, downlink modulation schemes QPSK and several QAM are available.

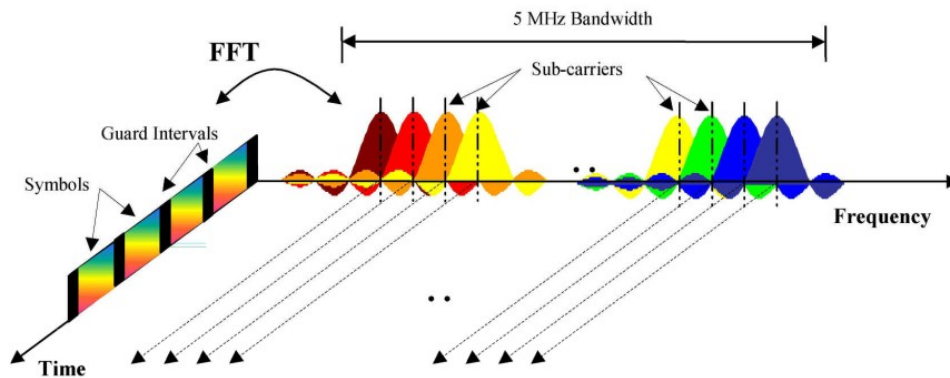


Figure 15: Frequency-time representation of an OFDM Signal [58], [59].

In contrast to an OFDM transmission scheme, OFDMA allows the access of multiple users on the available bandwidth. Each user is assigned a specific time-frequency resource. As a fundamental principle of E-UTRA, the data channels are shared channels, i.e. for each transmission time interval (TTI) of 1 ms, a new scheduling decision is taken regarding which users are assigned to which time/frequency resources during this TTI.

Two frame structure types are defined for E-UTRA: frame structure type 1 for FDD mode, and frame structure type 2 for TDD mode. The E-UTRA frame structures are defined in [60]. For the frame structure type 1, the 10 ms radio frame is divided into 20 equally sized slots of 0.5 ms. A subframe consists of two consecutive slots, so one radio frame contains ten subframes. This is illustrated in Figure 16.

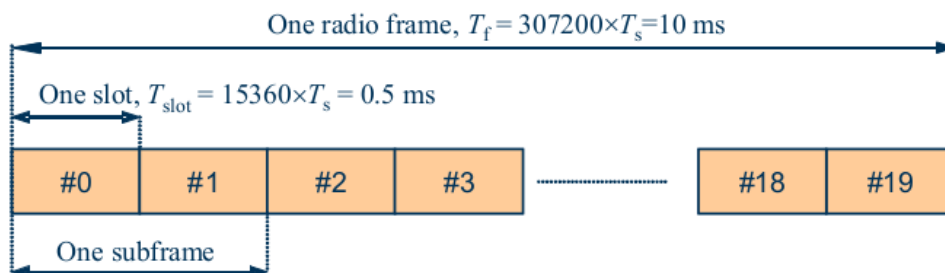


Figure 16: Frame structure type 1 [58], [60].

For the frame structure type 2, the 10 ms radio frame consists of two half-frames of length 5 ms each. Each half-frame is divided into five subframes of each 1 ms, as shown in Figure 17.

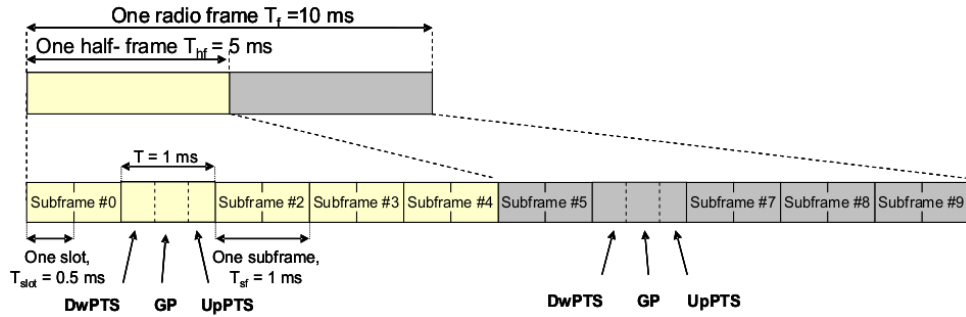


Figure 17: Frame structure type 2 (for 5 ms switch-point periodicity) [58], [60].

All subframes which are not special subframes are defined as two slots of length 0.5 ms in each subframe. The special subframes consist of the three fields DwPTS (Downlink Pilot Timeslot), GP (Guard Period), and UpPTS (Uplink Pilot Timeslot). Several uplink-downlink configurations with either different downlink-to-uplink switch-point periodicity are supported.

To obtain a two-dimensional definition of resources, the term resource grid was specified. Figure 18 shows the structure of the downlink resource grid for both FDD and TDD.

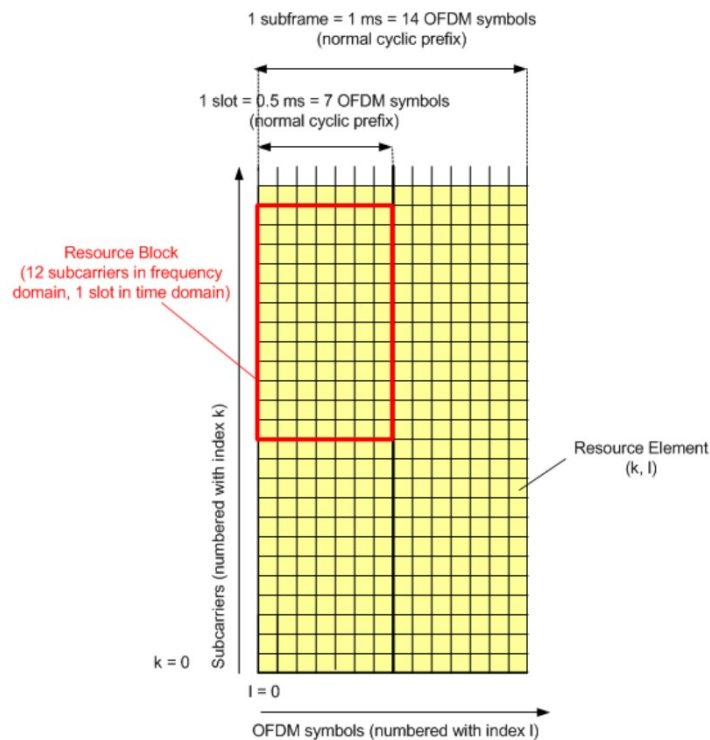


Figure 18: Downlink Resource grid [58], [60].

In the frequency domain, 12 subcarriers form one Resource Block (RB). With a subcarrier spacing of 15 kHz a RB occupies a bandwidth of 180 kHz. The number of resource blocks corresponds to the available transmission bandwidth ranging from 6 RBs (1.4 MHz) to 100 RBs (20 MHz).

The resource element, which is 1 subcarrier x 1 symbol, is the smallest discrete part of the frame and contains a single complex value representing data from a physical channel or signal.

To each OFDM symbol, a cyclic prefix (CP) is appended as guard time. One downlink slot consists of 6 or 7 OFDM symbols, depending on whether extended or normal cyclic prefix is configured, respectively.

Data is allocated to a device (User Equipment, UE) in terms of resource blocks, i.e. one UE can be allocated integer multiples of one resource block in the frequency domain. These resource blocks do not have to be adjacent to each other. In the time domain, the scheduling decision can be modified every transmission time interval of 1 ms. All scheduling decisions for downlink and uplink are done in the base station (enhanced NodeB, eNodeB or eNB). The scheduling algorithm has to take into account the radio link quality situation of different users, the overall interference situation, Quality of Service requirements, service priorities, etc. and is a vendor-specific implementation. Figure 20 shows an example for allocating downlink user data to different users (UE 1 – 6).

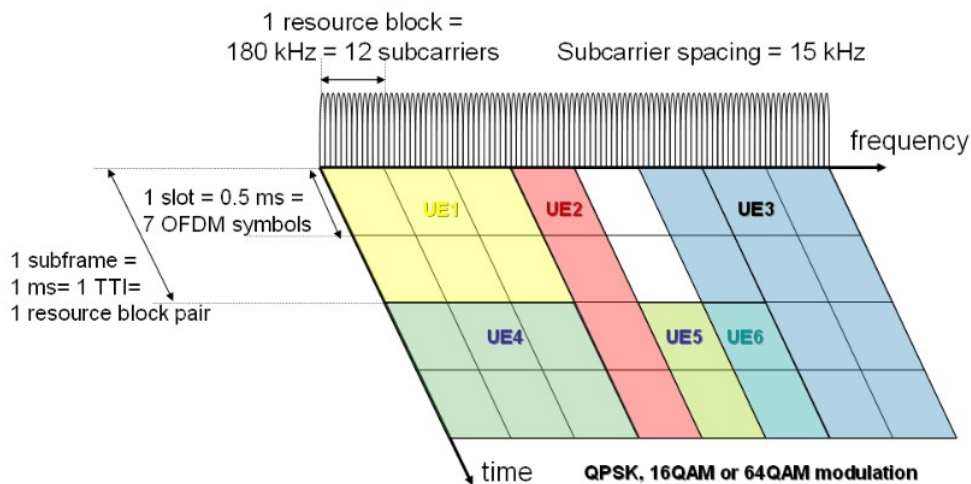


Figure 19: OFDMA time-frequency multiplexing (example for normal cyclic prefix) [58].

The data exchange is organized in physical channels. LTE downlink physical channel are: PDSCH, PDCCH, PCFICH, PHICH and PBCH.

The user data is carried on the Physical Downlink Shared Channel (PDSCH). The PDSCH is the only channel that can be QPSK, 16QAM, 64QAM modulated or higher QAM schemes in LTE-A and LTE-A-PRO.

The Physical Downlink Control Channel (PDCCH) serves a variety of purposes. Primarily, it is used to convey the scheduling decisions to individual UEs, i.e. scheduling assignments for downlink and uplink.

An additional Physical Control Format Indicator Channel (PCFICH) carried on specific resource elements in the first OFDM symbol of each subframe is used to indicate the number of OFDM symbols used for the PDCCH (1, 2, 3, or 4 symbols are possible).

Physical Hybrid ARQ Indicator channel (PHICH) is used to convey ACK/NACKs for the packets received in uplink.

Physical Broadcast Channel (PBCH) carries the Master Information Block. PBCH has an important role on EMF extrapolation.

Figure 20 shows a summary of downlink control channels, their purpose and the used modulation scheme.

Downlink Control channel	Purpose	Modulation scheme
Physical Downlink Control Channel (PDCCH)	Carries downlink control information (DCI), e.g. downlink or uplink scheduling assignments	QPSK
Physical Control Format Indicator Channel (PCFICH)	Indicates format of PDCCH (whether it occupies 1, 2, 3 or 4 symbols)	QPSK
Physical Hybrid ARQ Indicator Channel (PHICH)	Carries ACK/NACK for uplink data packets	BPSK
Physical Broadcast Channel (PBCH)	Carries Master Information Block	QPSK

Figure 20: Downlink control channels [58].

In addition to physical channels LTE provides physical signals. The most important is the downlink reference signal. The downlink reference signal structure is important for initial acquisition and cell search, coherent detection and demodulation at the UE and further basis for channel estimation and radio link quality measurements. Downlink reference signal provide further help to the device to distinguish between the different transmit antenna used at the eNodeB.

Figure 21 shows the mapping principle of the downlink reference signal structure for up to four transmit antennas. Specific pre-defined resource elements in the time-frequency domain are carrying the cell-specific reference signal sequence. In the frequency domain every six subcarrier carries a portion of the reference signal pattern, which repeats every fourth OFDM symbol.

The reference signal sequence is derived from a pseudo-random sequence and results in a QPSK type constellation. Frequency shifts are applied when

mapping the reference signal sequence to the subcarriers, means the mapping is cell-specific and distinguish the different cells.

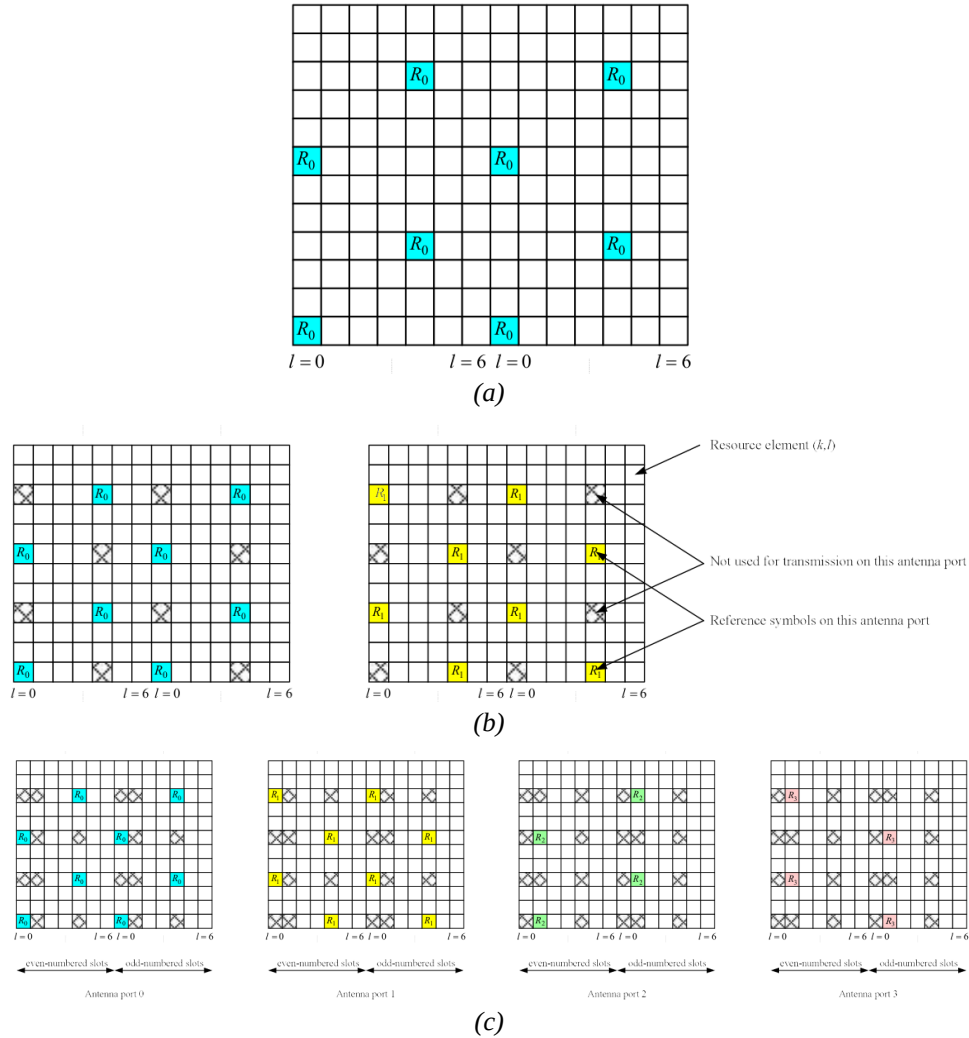


Figure 21: Downlink reference signal structure (normal cyclic prefix) [58], [60]: (a) One antenna port; (b) Two antenna ports; (c) Four antenna ports.

During cell search, different types of information need to be identified by the UE: symbol and radio frame timing, frequency, cell identification, overall transmission bandwidth, antenna configuration, and cyclic prefix length.

The first step of cell search in LTE is based on specific synchronization signals. LTE uses a hierarchical cell search scheme similar to WCDMA. Thus, a primary synchronization signal and a secondary synchronization signal are defined. The synchronization signals are transmitted twice per 10 ms on predefined slots. In the frequency domain, they are transmitted on 62 subcarriers within 72 reserved subcarriers around the unused DC subcarrier., see Figure 22 for FDD LTE mode and Figure 23 for TDD LTE mode.

Chapter 2 - 4G systems: Control signals and Extrapolation

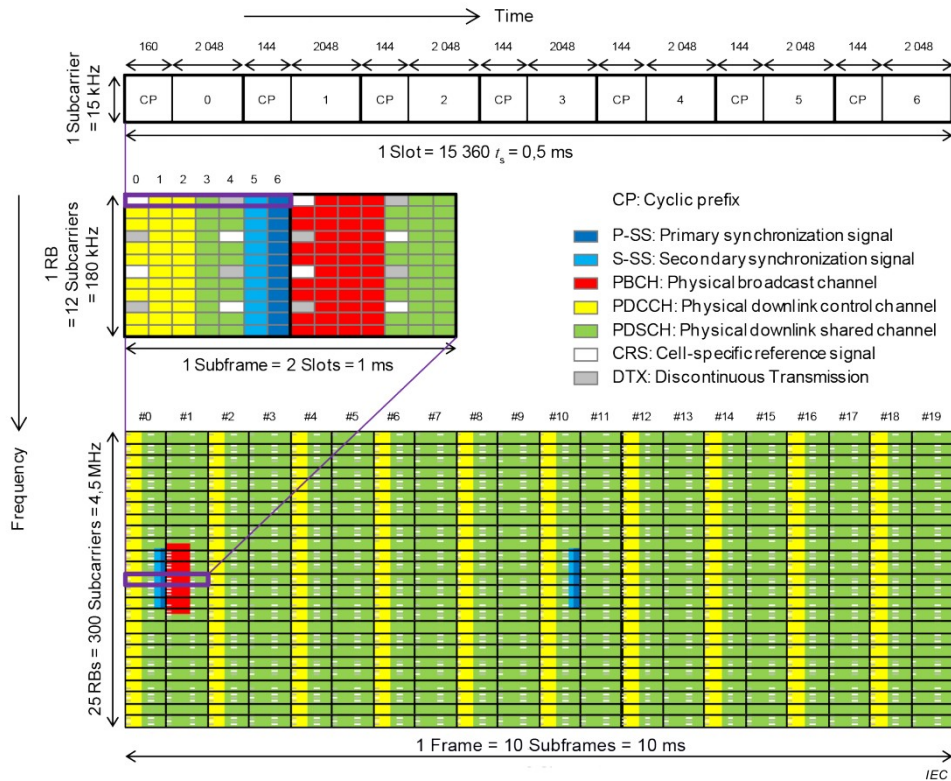


Figure 22: Frame structure of transmission signal for FDD LTE downlink [43].

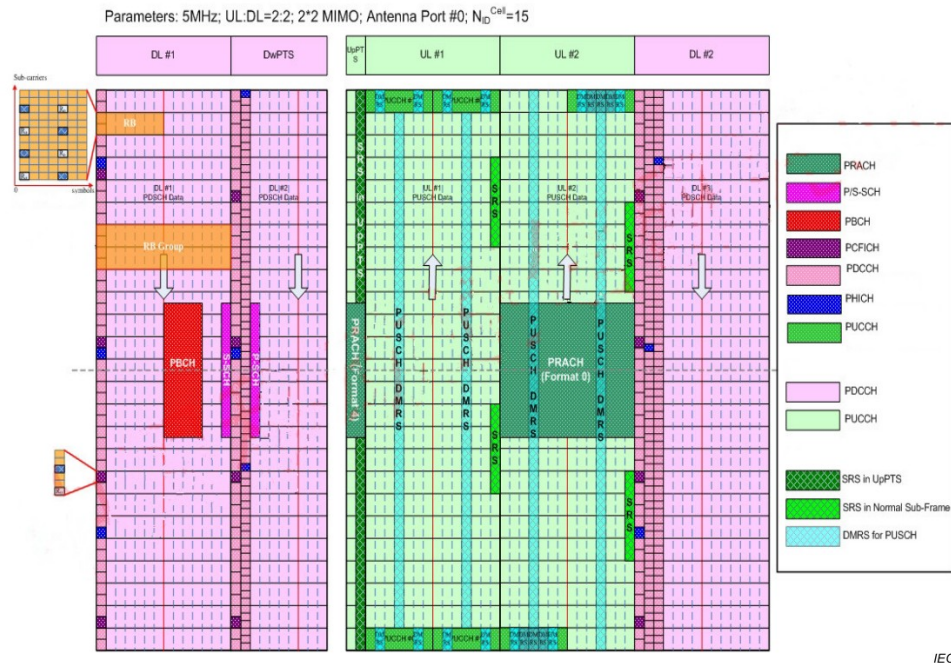


Figure 23: Frame structure of transmission signal for TDD LTE [43].

As additional help during cell search, the Physical Broadcast Channel (PBCH) is involved. It carries the Master Information Block (MIB). The MIB provides basic physical layer information, e.g. system bandwidth,

PHICH configuration, and system frame number. The number of used transmit antennas is provided indirectly using a specific CRC mask. The PBCH is transmitted on the first 4 OFDM in the second time slot of the first subframe on the 72 subcarriers centered around DC subcarrier. PBCH has 40 ms transmission time interval, means a device need to read four radio frames to get the whole content.

The reference signal (RS), the Primary Synchronization Signal (P-SS), the Secondary Synchronization Signal (S-SS), and the Physical Broadcast Channel (PBCH) are always on the air and they can be used as control signals in the extrapolation-based evaluation method, because the power levels are constant.

2.3 LTE E-UTRA EMF extrapolation methods

Evaluation methods based on extrapolation to assess the maximum exposure level from an LTE base station are provided by International Standard IEC 62232:2017 [43]. Italian guide CEI 211-7/E [61] is written from the knowledge of IEC 62232:2017 and IEC TR 62699:2019 [49].

In these documents, two extrapolation methods are presented. The first method uses an instrument with decoding capability (decoders). The second method considers to use a basic spectrum analyser. Both methods may be used, but in environments with strong selective fading or when evaluating each exposure level from multiple base stations accurately the method using a dedicated decoder is recommended.

To evaluate the exposure level for maximum traffic conditions by extrapolation, it is important that the transmitted power of the received signal or channel is not dependent on the amount of traffic. The reference signal (RS), the Primary Synchronization Signal (P-SS), the Secondary Synchronization Signal (S-SS), and the Physical Broadcast Channel (PBCH) can be used as the received signal in the extrapolation-based evaluation method, because the power levels are constant.

The RS is well suited for this because the locations of the LTE Reference Signals (RSs) are uniformly distributed over the occupied radio bandwidth to reduce effects of frequency selective fading. The RS represents the cell-specific reference signal (CRS), which is one type of reference signal.

2.3.1 LTE E-UTRA EMF extrapolation with decoders

In this method, the field strength corresponding to the RS of an LTE cell is measured. If multiple antennas are used for transmission by the same cell (MIMO), the RS should be determined for each antenna (or antenna port).

This type of measurement requires equipments with dedicated decoding functions, such as spectrum analyser with LTE decoder option or a more expensive vector signal analyser with LTE complete decoding capabilities.


The maximum electric field strength for FDD LTE signals is shown in (5) [61] and the maximum electric field strength for TDD LTE signals is shown in (6) [61].

$$E_{LTEmax} = \sqrt{\frac{n_{RS}}{BF}} \cdot \sqrt{\sum_n (E_{RS_ANTn})^2} \quad (V/m) \quad (5)$$

$$E_{LTEmax} = \sqrt{\frac{n_{RS}}{BF}} \cdot \sqrt{\sum_n (E_{RS_ANTn})^2} \cdot \sqrt{F_{TDC}} \quad (V/m) \quad (6)$$

E_{RS_ANTn} denotes the field level (V/m) of the RS from port n of the MIMO antenna and the sum is taken over all branches.

RS power per resource element measurement example is shown in Figure 24.

Result Summary		TD-LTE BTS		16/12/13 16:41	
	Center: 1.8 GHz	Ref Level: -20.0 dBm	Sweep: Cont		
	Channel: ---	Ref Offset: 0.0 dB	Cell [Grp/ID] Auto		
	Band: ---	Att: 0.0 dB	Cyclic Prefix: Auto		
	Transd: ---	Preamp: Off	Antenna: SISO / OTA		
	Ch BW: 10 MHz (50 RB)	UL/DL: Config 1	Subframes: 10		
Global Results			SYNC OK		
RF Channel Power:	-32.07 dBm	Cell Identity [Grp/ID]:	0 [0/0]		
Overall EVM:	62.29 %	Cyclic Prefix:	Normal		
Carrier Freq Error:	72.56 Hz	Traffic Activity:	100.00 % 		
Sync Signal Power:	-68.18 dBm	SINR:	-0.35 dB		
OSTEP:	-32.12 dBm	RSSI:	-32.20 dBm		
RSRP:	-63.03 dBm	RSRQ:	-13.84 dB		
		IQ Offset:	-57.59 dB		
Allocation Summary					
	Power:	EVM:		Power:	EVM:
Ref Signal:	-59.81 dBm	138.85 %	PSYNC:	-67.58 dBm	100.45 %
QPSK:	-59.77 dBm	54.42 %	SSYNC:	-68.87 dBm	104.06 %
16 QAM:	--- dBm	--- %	PBCH:	-63.09 dBm	72.26 %
64 QAM:	--- dBm	--- %	PCFICH:	-60.02 dBm	62.79 %
Result Display	Display Settings	Level Adjust	Antenna Settings	Signal Settings	Meas Settings

IEC

Figure 24: Reference signal (RS) measurement example from a spectrum analyser with LTE decoder option [43].

n_{RS} corresponds to the number of subcarriers for the system bandwidth of the target base station. The value of n_{RS} for each system bandwidth is shown in Figure 25, when all subcarriers are at the same power level.

Channel bandwidth (MHz)	Number of resource blocks	Transmission bandwidth (MHz)	N_{RS} (linear/dB)
1,4	6	1,08	72 / 18,57
3	15	2,7	180 / 22,55
5	25	4,5	300 / 24,77
10	50	9,0	600 / 27,78
15	75	13,5	900 / 29,54
20	100	18,0	1 200 / 30,79

Figure 25: Number of subcarriers function of channel bandwidths [43].

BF denotes the power boosting factor for the RS, this value may be obtained from the operator.

F_{TDC} denotes the fraction of the signal frame reserved for downlink transmission. The specific configuration ($C_{d/u}$, C_s) provides the value of F_{TDC} (see Figure 26) and may be obtained from the operator.

		downlink/uplink – $C_{d/u}$						
		0	1	2	3	4	5	6
subframe S – C_s	0	0.243	0.443	0.643	0.621	0.721	0.821	0.343
	1	0.329	0.529	0.729	0.664	0.764	0.864	0.429
	2	0.343	0.543	0.743	0.671	0.771	0.871	0.443
	3	0.357	0.557	0.757	0.679	0.779	0.879	0.457
	4	0.371	0.571	0.771	0.686	0.786	0.886	0.471
	5	0.243	0.443	0.643	0.621	0.721	0.821	0.343
	6	0.329	0.529	0.729	0.664	0.764	0.864	0.429
	7	0.343	0.543	0.743	0.671	0.771	0.871	0.443
	8	0.357	0.557	0.757	0.679	0.779	0.879	0.457
	9	0.286	0.486	0.686	0.643	0.743	0.843	0.386

Figure 26: F_{TDC} factor functions of Uplink/Downlink configuration and Subframes configuration [61].

As presented in [61], in the case of no a priori knowledge about the specific TDD scheme implemented by the signal under investigation, a direct determination of F_{TDC} can be carried out through a zero span measurement using a spectrum analyzer by means of the following procedure.

- Central frequency set to the LTE TDD central carrier.
- Sweep time set as a frame period (10 ms).
- RBW as large as signal bandwidth (maximum allowed by the spectrum analyser if RBW isn't larger as the signal bandwidth).
- A periodic trigger according to the frame period 10ms.
- Trace mode set to max-hold.

The acquired trace allows for an effective identification of the uplink slots, since the associated received power is several orders of magnitude lower than that related to downlink slots, if there aren't UE terminals near to measurement point.

2.3.2 LTE E-UTRA EMF extrapolation with basic SA

A basic spectrum analyser (SA) is less expensive and more commonly available compared with a dedicated LTE decoder. However, when using a basic SA, the powers of the Reference Signals cannot be accurately detected since they are transmitted on single resource elements spread in frequency and time.

To overcome this issue and to avoid requirements on access to prior knowledge regarding band occupation or service characteristics, the PBCH power can be measured. The PBCH is transmitted with the same characteristics regardless of the configuration or service bandwidth and spans a bandwidth of six RBs (approximately 1 MHz) over the centre frequency of the LTE signal.

Note that the signal from each LTE base station cannot be identified using this method due to frequency spectrum overlapping.

According to IEC 62232:2017 [43] the PBCH power should be measured using the following SA configuration.

- The centre frequency of the spectrum analyser should be equal to the centre frequency of the LTE signal.
- The frequency span should be set to zero (scope mode) in order to measure the received time signal for the downlink emission frequency.
- A resolution bandwidth (RBW) of 1 MHz should be set to integrate the signal over the PBCH spectral spread.
- The sweep time should be set equal to approximately the product of the number of display points of the SA and the symbol duration (approximately 70 μ s) in order to obtain an integration time close to the symbol duration of each pixel on the screen of the SA, e.g. a sweep time of approximately 70 ms for an SA with 1000 display points (or equivalent ratio for instruments with lower display resolution).
- The detector should be set to root-mean-square (r.m.s.).

- The trace type should be set to maximum hold using a minimum sweep time of 20 s.

In order to use the r.m.s. detector, the maximum power shall be effectively allocated to the PBCH channel.

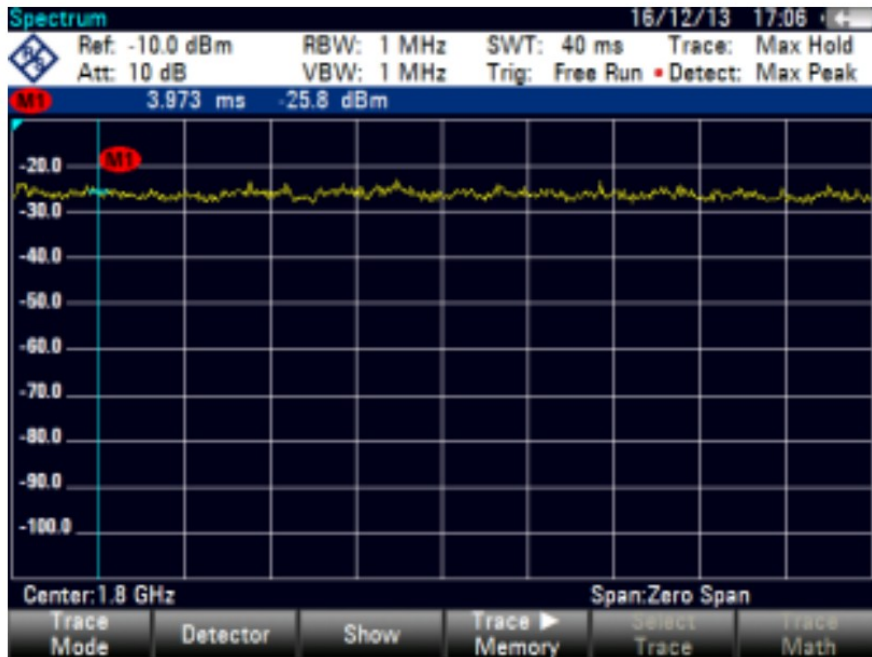
The maximum electric field strength for FDD LTE signals is shown in (7) [61] and the maximum electric field strength for TDD LTE signals is shown in (8) [61].

$$E_{LTEmax} = \sqrt{n_{PBCH}} \cdot E_{PBCH} \quad (V/m) \quad (7)$$

$$E_{LTEmax} = \sqrt{n_{PBCH}} \cdot E_{PBCH} \cdot \sqrt{F_{TDC}} \quad (V/m) \quad (8)$$

The electric field strength of the PBCH signal, E_{PBCH} , is determined from P_{PBCH} . The measured peak power, P_{PBCH} , corresponds to the received PBCH signal power over the bandwidth of six RBs (72 subcarriers).

Figure 27 shows measurement examples of PBCH power with spectrum analyser using zero span.



IEC

Figure 27: PBCH measurement example spectrum analyser using zero span mode [43].

n_{PBCH} denotes the ratio of the maximum transmission power to the transmission power corresponding to the PBCH over six RBs. It can be provided by the network operator or can be calculated theoretically according to (9) [43].

$$n_{PBCH} = \frac{n_{RS}}{72} \quad (9)$$

It must be recalled, that extrapolation method with basic SA does not allow the distinction of two different cells of the same operator/installation. Furthermore, since the spectrum analyser cannot distinguish uplink and downlink in a TDD transmission scheme, it is important to switch off every mobile phone in the vicinity of the measuring system. For these reasons extrapolation method with basic spectrum analyser gives an additional overestimation to the extrapolated maximum RF field.

2.4 Conclusion

This chapter has shown a technical review of LTE radio access network, called E-UTRA. Later, two extrapolation methods for the assessment the electric field emitted by a 4G signal source has presented according to IEC 62232:2017 and CEI 211-7/E. The basic principle of this assessment is to measure the power received from a constant radio frequency source, typically a pilot signal, and to apply a proper extrapolation factor. EMF extrapolation methods of 4G signals are based on the Reference Signal and the PBCH that are always on the air and have constant power. This kind of approach is also standardized for 2G, 3G technologies, but is still under investigation for 5G technology.

Main goal of the next chapter will be the presentation of several EMF extrapolation methods of 5G signals, taken from open scientific literature.

3 5G systems: Control signals and Extrapolation

“After 5G general aspects and a more detailed technical review on 5G access network, this chapter will address to 5G specific control signals and 5G EMF extrapolation proposals from open scientific literature.”

3.1 5G overview

All mobile broadband systems are based on the ITU’s IMT standards. In 2015, ITU defined its IMT Vision for 2020 and Beyond [62] for all upcoming services. A system meets IMT-2020 requirements is named a 5G wireless cellular technology (see Figure 28).

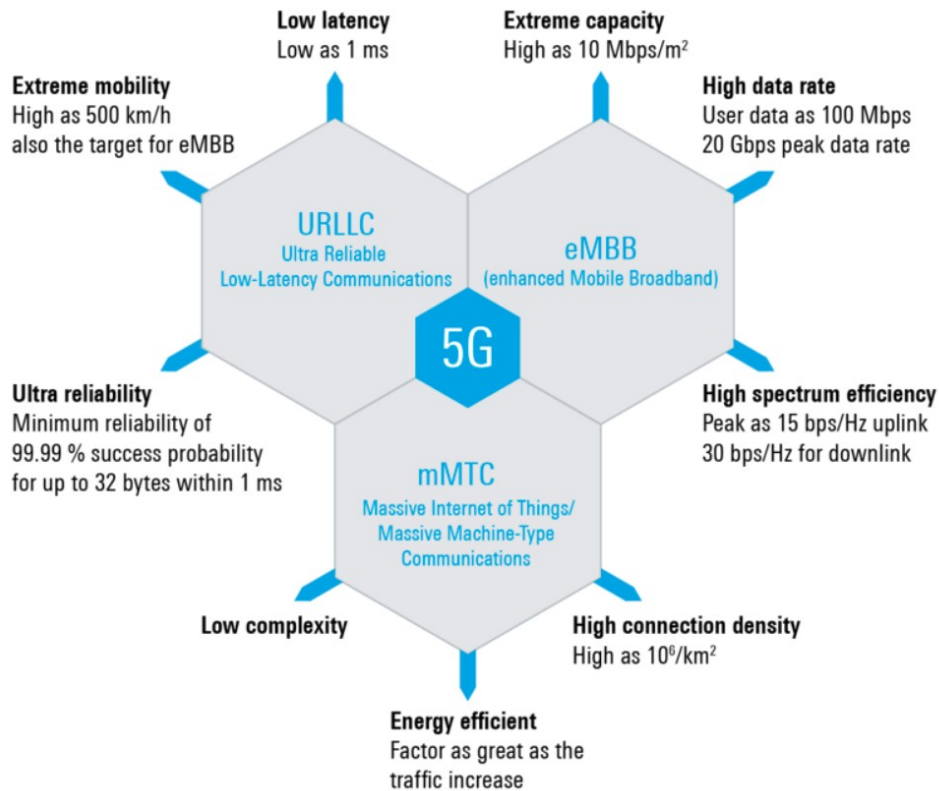


Figure 28: ITU Vision for IMT-2020 and Beyond [63].

5G intends to focus on the services provided to the users and the technologies required to fulfil the service requirements. The services within the 5G scope can be categorized into three main types:

- eMBB (enhanced mobile broadband): High data rate services shall be designed to cater to the ever-growing demand for faster and higher-volume data access. This concept is a direct successor to the high data rate services provided by LTE.

- mMTC (massive machine-type communications): Massive Internet of things (Massive IoT) shall be an extension of the current IoT services which includes probably almost every machine communicating with other machines. This approach shall open doors to major automation in every area of life.
- URLLC (ultra-reliable low-latency communications): Ultra-reliable low-latency services would involve new use cases in which small data exchanges can be realized to provide reliable and critical communications such as health monitoring.

The 5G system consists of the 5G core and the 5G access network as depicted in Figure 29 (a). Unlike previous mobile communication technologies, the core network for 5G is designed to work seamlessly with more than one access technology. The 5G access network (AN) could be built from a 3GPP defined AN and non-3GPP AN such as WLAN or wired broadband access as depicted in Figure 29 (b). Within the NG-RAN, a new cellular access technology known as “New Radio” (NR) is introduced together with E-UTRA, the access technology used for LTE.

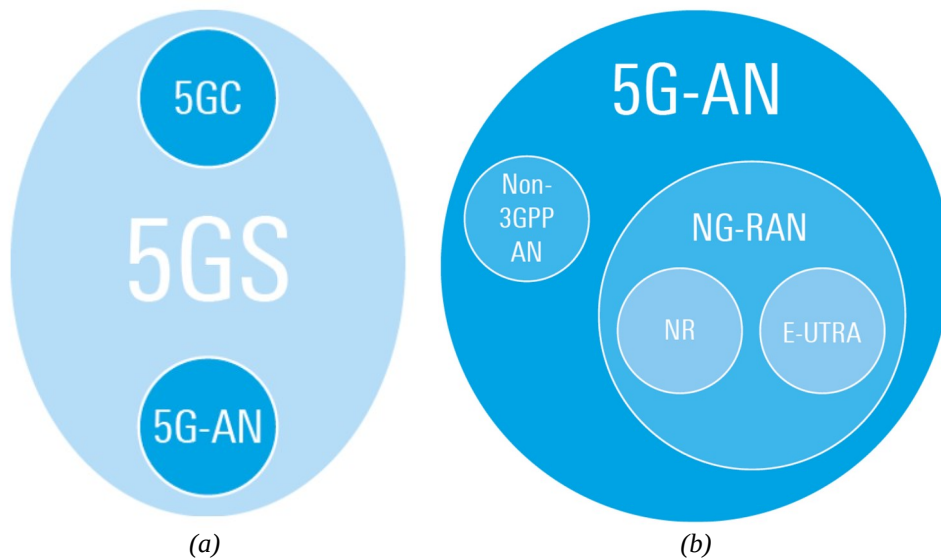


Figure 29: (a) 5G system (5GS), (b) 5G access network components [63].

The possibility of the same core network connecting with various access networks results in several connectivity scenarios. The UE can be connected over LTE (E-UTRA) or over NR to the new 5GC (standalone connectivity options). Moreover, connectivity involving the cellular technologies has further evolved with an option for the connection to pass via more than one access technology at the same time (non-standalone connectivity options), as depicted in Figure 30.

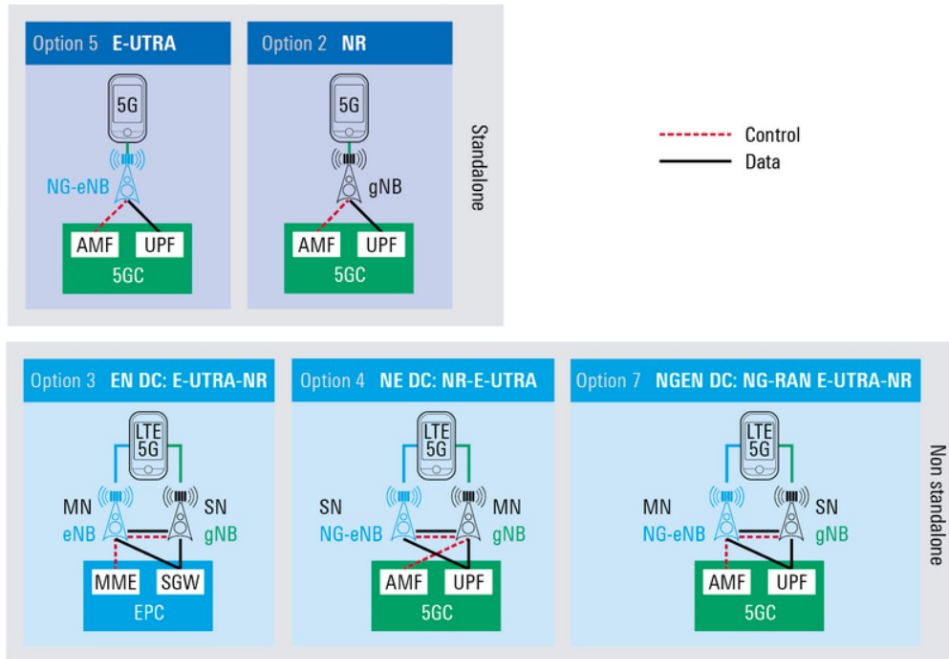


Figure 30: Connectivity options [63].

All 5G specifications are provided by 3GPP Releases. Release 15 ended in June 2019, often referred to informally as “5G Phase1”, is summarized in TR 21.915 [64]. Release 16 ended in July 2020, often referred to informally as “5G Phase1” is still in summarization with TR 21.916 expected for the end of the year. 5G system enhancements are still under development with Release 17 and Release 18.

Regarding 5G deployment, as 5G will need to coexist and interwork with 4G for many years to come, the vast majority of installations will be in non stand-alone mode (NSA) initially, as a way of reducing time to market and ensuring good coverage and mobility. The 5G standard for stand-alone (SA) mode will be following step. This mode, which requires a new (service-based) core network architecture, will enable deployments of 5G as an overlay to or independent of 4G coverage [65].

An “Assessment of 5G Deployment” released by ERT in September 2020 [66], reveals that Europe as a whole – and the largest individual nations – are behind global competitors in deploying 5G networks at this point of time. More than half of EU Member States have not yet launched 5G commercial services, whereas the first commercial services were available in South Korea and the US one year ago. The share of the subscriptions using 4G networks is around 70% in Europe in 2019, significantly lower than in the US, China and South Korea, where it reaches around 90%. The the 27 European Union countries (EU-27) have deployed around ten 5G base stations per million capita, whereas South Korea has rolled out around

1,500 base stations per million (by the end of 2019). The EU-27 has upgraded 1% of 4G base stations to 5G, whereas South Korea upgraded 98% (by the end of 2019).

According by European 5G Observatory [67], at the end of September 2020, 5G commercial services had been deployed in 18 (EU-27 plus the UK). In Italy, Vodafone and TIM launched 5G in some cities. Vodafone inked a network sharing 5G deal with TIM early 2019. Vodafone Italy launched its commercial 5G services in 5 cities on 6 June 2019 (Milan, Rome, Turin, Bologna and Naples). In Turin, the Vodafone network covers 80% of the city with 120 cell sites. The number of cities covered will increase up to 50 by the end of 2019 and to 100 by 2021. TIM launched its 5G service on June 24th, 2019 in parts of Rome and Turin, Naples followed in July 2019. As of 2020, 5G services were available in Bologna, Brescia, Florence, Genoa, Milan, Naples, Turin, and Rome.

Figure 31 shows the actual situation in Italy. Maps are taken from two of major platform aiming to quantify the internet user experience. Mobile network operators are starting the deployment in most populated cities of Italy, but actually the 5G coverage is very limited compared to 4G coverage.

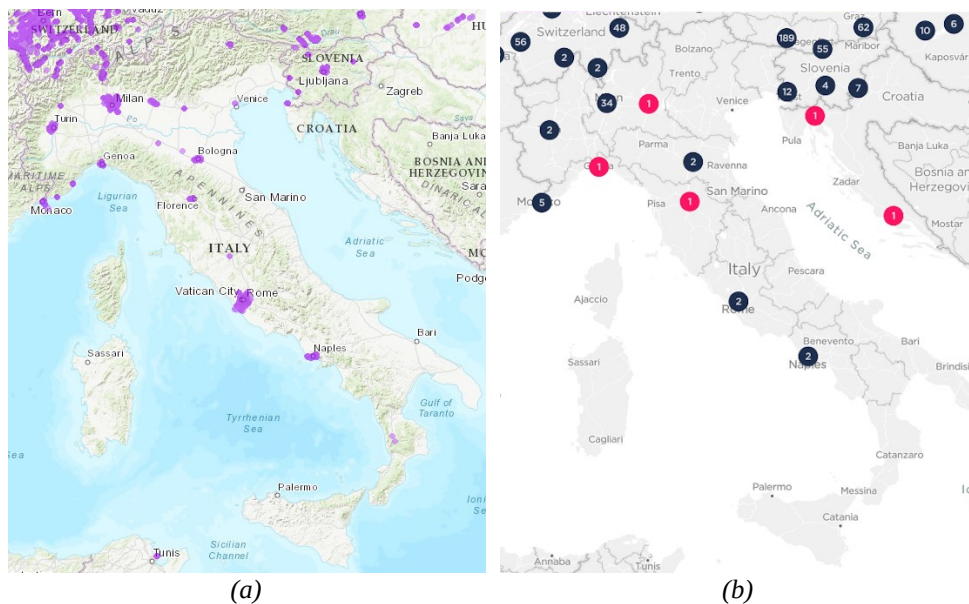


Figure 31: (a) Nperf 5G coverage map of Italy from all operator [68] (accessed at 05/11/2020) – (b) OOKLA 5G MAP of Italy from all operator [69] (accessed at 05/11/2020).

According to Ericsson Mobility Visualizer tool [70], looking ahead, in the first five years, 5G subscription uptake is expected to be significantly faster than that of LTE, following its launch back in 2009. By end of 2020, Ericsson forecasts a total of 190 million 5G subscriptions. By the end of

2025 Ericsson projects 2.8 billion 5G subscriptions worldwide (see Figure 32).

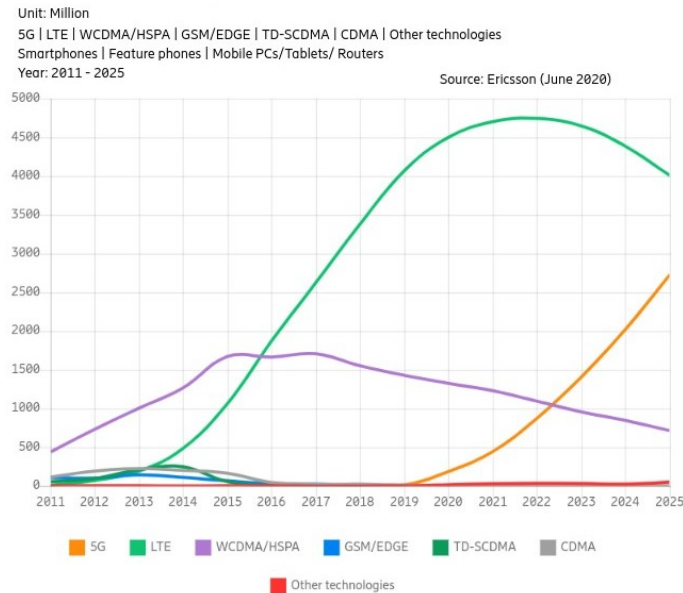


Figure 32: Mobile subscriptions data and forecast up to 2025 – Note: Chart realized using Ericsson Mobility Visualizer tool [70] (accessed at 05/11/2020).

After this brief overview, a more technical review of 5G is necessary for the purpose of RF-EMF measurement. The following paragraph will introduce a technical review (mainly based on [71] and [63]) focused to the downlink part of Access Network of the 5G system. “New Radio”, commonly referred as 5G NR, is the new access network technology introduced by 5G system.

3.2 5G NR technology review and control signals

To serve the three key NR scenarios eMBB, mMTC and URLLC, a flexible radio scheme is required. The essential NR technology components include new spectrum, high flexibility on the physical layer, multi connectivity, massive MIMO and beamforming.

3.2.1 New spectrum

5G NR deploys a much higher bandwidth (up to 400 MHz per carrier) compared with 4G. Due to spectrum allocation, high bandwidth is only available at higher absolute frequencies. Consequently, 5G NR is designed for deployment in two main frequency ranges, FR1 and FR2 (see Figure 33).

Frequency range designation	Corresponding frequency range
FR1	410 MHz – 7125 MHz
FR2	24250 MHz – 52600 MHz

Figure 33: Definition of frequency ranges, TS 38.104 Table 5.1-1 [72].

Figure 34 shows the primary spectrum that is intended for 5G NR deployment in different regions across the globe.

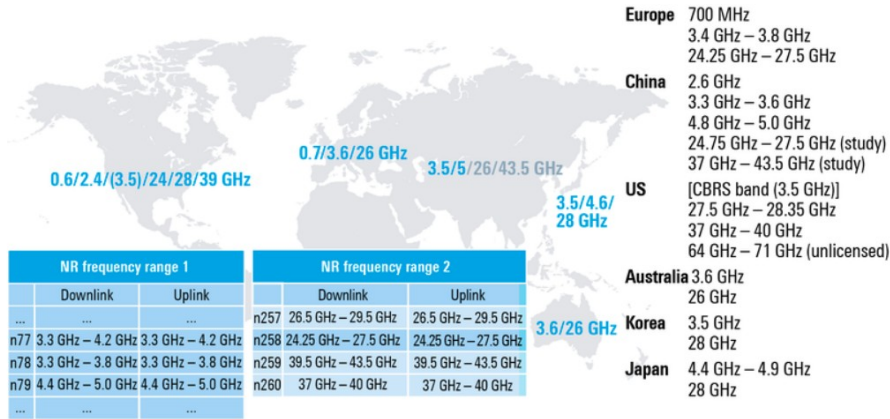


Figure 34: Main frequency bands and corresponding band numbers for the planned global 5G NR deployment [63].

3.2.2 Numerology and Bandwidth parts (BWP)

Although the waveform is still OFDMA-based as was the case in LTE, there are certain fundamental differences which enable the required flexibility. A key difference compared to existing OFDMA-based access schemes is the introduction of a so-called flexible numerology, i.e. the ability to use a number of different subcarrier spacings (SCS). In contrast to a fixed SCS of 15 kHz in LTE, 5G NR allows an SCS of 15 kHz, 30 kHz, 60 kHz, 120 kHz and 240 kHz (see Figure 35).

μ	$\Delta f = 2^\mu \cdot 15 [\text{kHz}]$	Cyclic prefix
0	15	Normal
1	30	Normal
2	60	Normal, Extended
3	120	Normal
4	240	Normal

Figure 35: Supported transmission numerologies, TS 38.211 Table 4.2-1 [71].

This leads to different symbol time durations since the SCS is inversely proportional to the symbol duration. Similarly, the number of symbols in a fixed time duration, e.g. the number of symbols within a 10 ms radio frame, is now variable. 5G NR numerology is based on CP-OFDMA, involving a kind of vertical orientation where one column represents one numerology

(Figure 36) consisting of the major parameters subcarrier spacing, symbol duration and cyclic prefix length.

5G NR flexibility is needed in the context of the key services eMBB, URLLC and mMTC in order to somehow shape the waveform to the QoS requirements of the application as well as to the circumstances dictated by the propagation scenario.

Subcarrier spacing (kHz)	15	30	60	120	240
Symbol duration (μs)	66.7	33.3	16.7	8.33	4.17
CP duration (μs)	4.7	2.3	1.2 (normal) 4.13 (extended)	0.59	0.29
Max. nominal bandwidth (MHz)	50	100	100 for FR1 200 for FR2	400	400
Max. FFT size	4096	4096	4096	4096	4096
Symbols per slot	14	14	14 12 (extended CP)	14	14
Slots per subframe	1	2	4	8	16
Slots per frame	10	20	40	80	160

Figure 36: 3GPP 5G NR numerology based on CP-OFDMA [63].

The nominal channel bandwidth per frequency band can be segmented into smaller subbands known as resource grids or bandwidth parts (BWP). A BWP applies one of the 5G NR numerologies. Following the QoS request from various application scenarios, a 5G NR scheduling scheme in a connection can now take advantage of these numerologies by dynamically applying the most suitable 5G NR numerology and thus providing the required physical layer flexibility.

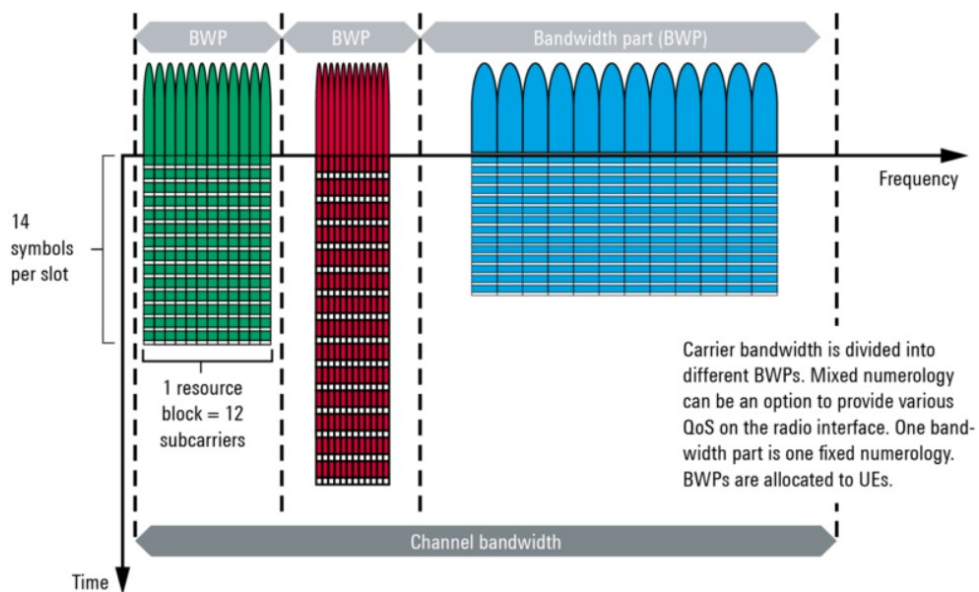


Figure 37: 5G NR numerologies used simultaneously via bandwidth parts [63].

3.2.3 Resource grid

The flexibility on the physical layer also requires a more general specification of the resource grid. For example, note that synchronization signals and data channels may use a different SCS. Furthermore, synchronization signals and broadcast signals are no longer placed in the center of the carrier. This requires the definition of a reference point for allocation of resources in the frequency domain.

5G NR uses physical resources in the time and frequency domain for resource allocation. To obtain a two-dimensional definition of resources, the term resource grid was specified like E-UTRA (see Figure 38). In the frequency domain, the term resource block was introduced to mean 12 consecutive subcarriers in the frequency domain. Note that this represents a difference compared to E-UTRA where a resource block was defined as 12 subcarriers in the frequency domain and 6 or 7 OFDM symbols, depending on the cyclic prefix length, in the time domain. Unlike E-UTRA, in 5G NR the term resource block is to be understood as a frequency domain indication only.

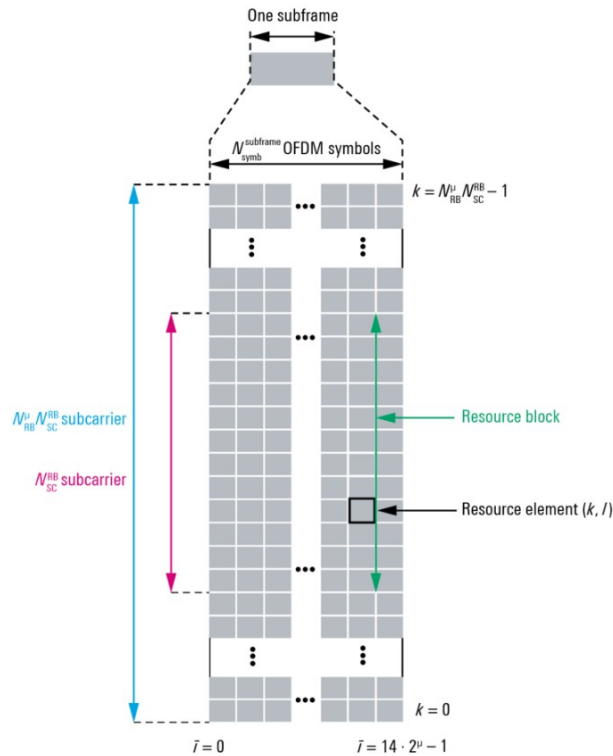


Figure 38: 5G NR resource block and resource elements [63].

Due to the increased flexibility and the introduction of OFDMA numerologies, TS 38.211 additionally defines the terms physical, common and virtual resource blocks. A common resource block (CRB) numbers the resource blocks starting from a reference point (Point A) for a fixed

numerology or SCS, respectively. This may be understood as a kind of orientation pointer in the frequency domain for frequency allocations. Note that the CRB is not used directly for spectrum allocation. The physical resource block (PRB) is related to the common resource block definition. Virtual resource blocks (VRB) allow mapping of virtual to physical resource blocks in a manner that is either frequency-contiguous-localized or distributed, i.e. frequency non-contiguous. A resource element is defined (like in EUTRAN) as a complex value mapped onto a physical resource indicated by a subcarrier number and OFDM symbol number.

3.2.4 Frame structure

The flexibility on the physical layer has also impact on frame structure. A major difference between NR and former standards is the flexibility of the frame structure. Certain service scenarios such as ultra-reliable low latency communications (URLLC) and transmission at mm-wave frequencies can require shorter slot or subframe structures in order to decrease the latency or enable faster UL and DL switching for immediate HARQ feedback. NR frames consist of a fixed frame length and subframe length, but with flexible allocations underneath. The radio frames have a length of 10 ms for both the DL and UL (TS 38.211, section 4.3). Each radio frame consists of ten subframes of 1 ms duration each. The first five and the last five subframes form a half-frame. There are {1, 2, 4, 8, 16} slots in a subframe and {12, 14} consecutive OFDM symbols in a slot. The number of slots per subframe depends on the 5G numerology or the SCS. The number of symbols per slot depends on the length of the cyclic prefix (CP). In 5G NR, two CP lengths are defined: a normal and an extended CP length. Figure 39 shows the frame structure and subframe structure.

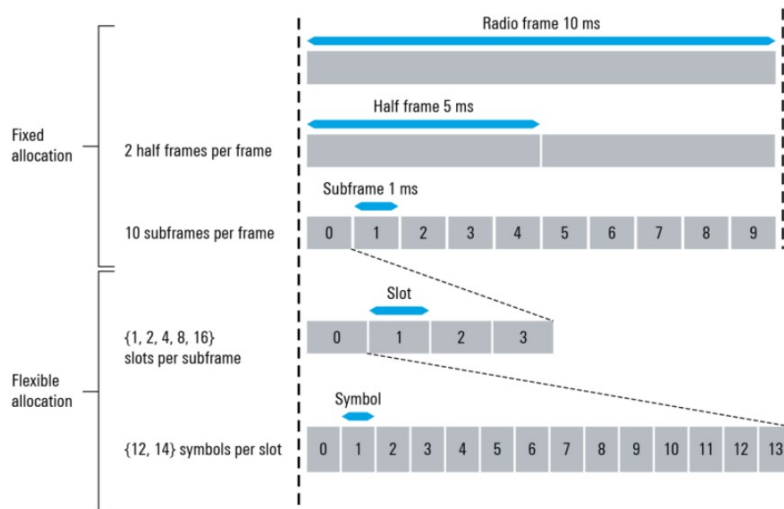


Figure 39: Frame structure in 5G NR (e.g. slot structure for SCS 60 kHz) [63].

3.2.5 Duplexing schemes

5G enables both FDD and TDD duplex schemes. Depending on the frequency bands, 5G NR supports various duplexing schemes such as FDD, static TDD, semi-static TDD and dynamic TDD in order to provide the highest possible flexibility.

Frequency division duplex (FDD) means that a carrier is designated as paired spectrum consisting of an uplink carrier and a downlink carrier. In FDD, the allocation of resources can be managed dynamically and assigned independently in either the uplink or downlink direction. As a drawback, the band definition requires a sort of guard band between UL and DL, and the receiver must be equipped with a duplex filter to suppress interference from the transmitter.

Time division duplex (TDD) means that only one carrier is used. It is divided into time slots that can be allocated either to the downlink or uplink. One advantage of TDD (as discussed in the literature) is that receiver complexity is reduced since a duplex filter is not needed. Moreover, the channel is considered to be reciprocal, thereby allowing improved implementation of channel estimation and link adaptation mechanisms. Especially for beamforming methods, channel reciprocity represents a major advantage. One drawback of TDD schemes, however, is related to a type of synchronization due to inter-cell interference and the need for a guard time between the transition from RX to TX to compensate for propagation delay.

In static TDD, this slot configuration is identical over the neighbor cells as well and it is kept static over a longer time period. Consequently, however, the cell has a sort of static allocation of downlink and uplink data rates.

Semi-static TDD (Figure 40) involves the introduction of more flexibility. Higher layer configuration parameters can be used in 5G NR to achieve cell-specific or even UE-specific UL/DL allocation parameterization. Thus, the slot configuration is flexible and can be changed from time to time while maintaining the focus on inter-cell interference aspects.

Dynamic TDD (Figure 41) is the most flexible concept for UL/DL configuration and is fully dynamic. This could be a use case for small cells or even standalone or isolated indoor cells with less overlapping coverage to neighbor cells and therefore less influence due to inter-cell interference. TS 38.213 ([73] Table 11.1.1-1) currently contains a table with 56 slot configurations for the case of normal CP length.

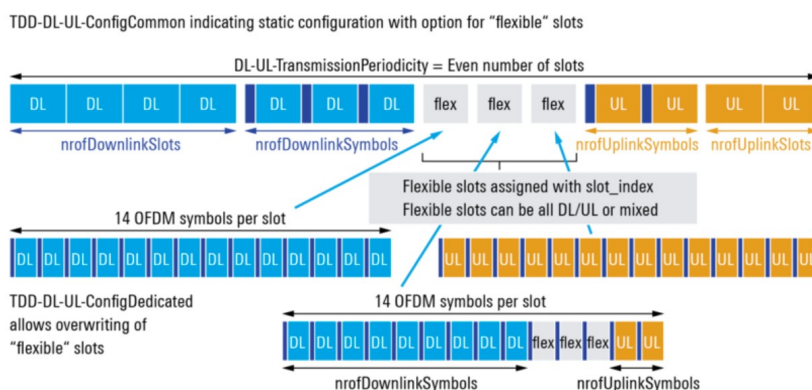


Figure 40: Semi-static UL-DL TDD configuration [63].

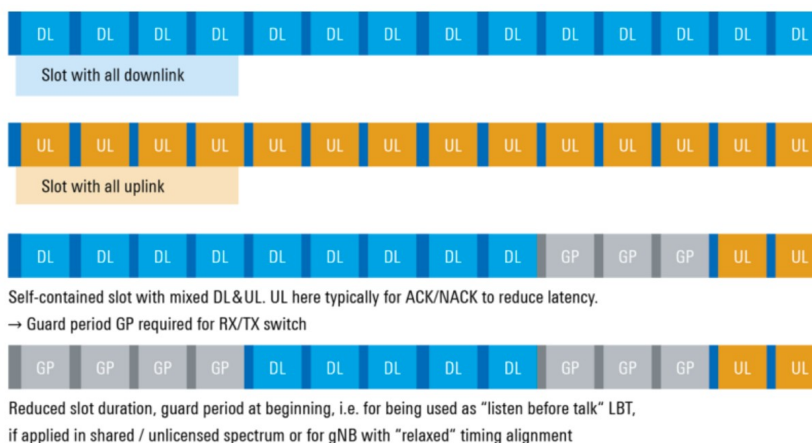


Figure 41: Dynamic UL-DL TDD slot configuration in 5G NR (abstract representation) [63].

3.2.6 Physical channels and signals

Physical channels are used to transport information over the radio channel and are characterized by their function as well as by RF aspects such as the modulation scheme, reference signal mapping, transmit power, coding, etc. There are physical channels that carry higher layer information as well as physical channels that are terminated in the physical layer. The nomenclature for the physical channels in 5G NR corresponds in a straightforward manner to the nomenclature in LTE.

The physical channels defined on the uplink are: Physical random access channel (PRACH), Physical uplink shared channel (PUSCH), Physical uplink control channel (PUCCH).

The physical channels defined on the downlink are: Physical downlink shared channel (PDSCH), Physical downlink control channel (PDCCH) and Physical broadcast channel (PBCH). These physical channels resemble

those from E-UTRA, and only the channels PHICH and PCFICH have been eliminated.

In addition to the physical channels, that provide services to higher layers, a number of additional physical signals are defined in 5G NR. They are used by the physical layer, but they do not carry information originating from the higher layers. The main purpose of the physical signals is related to synchronization aspects, channel estimation, tracking and beam identification for beamforming optimization, and channel status reporting.

The following UL physical signals are defined: Demodulation reference signals (DMRS) for PUSCH and PUCCH, Phase-tracking reference signals (PTRS) for PUSCH and Sounding reference signal (SRS).

For the DL, the following downlink physical signals are defined: Demodulation reference signals (DMRS) for PDSCH, PDCCH and PBCH, Phase-tracking reference signals (PTRS) for PDSCH, Channel-state information reference signal (CSI-RS), Tracking reference signals (TRS), Primary synchronization signal (PSS) and Secondary synchronization signal (SSS).

3.2.7 SS/PBCH block

Physical channel PBCH and physical signals DMRS for PBCH, PSS, SSS are defined together as SS/PBCH block (or SSB). The SSB can be considered as the only “always on air” signal that 5G NR provides and can therefore be detected even when no radio connection has been established such as in UE idle mode. In other words, the SSBs can be used for initial channel estimation or cell-specific channel status measurements.

The basic structure of an SS/PBCH block is illustrated in Figure 42.

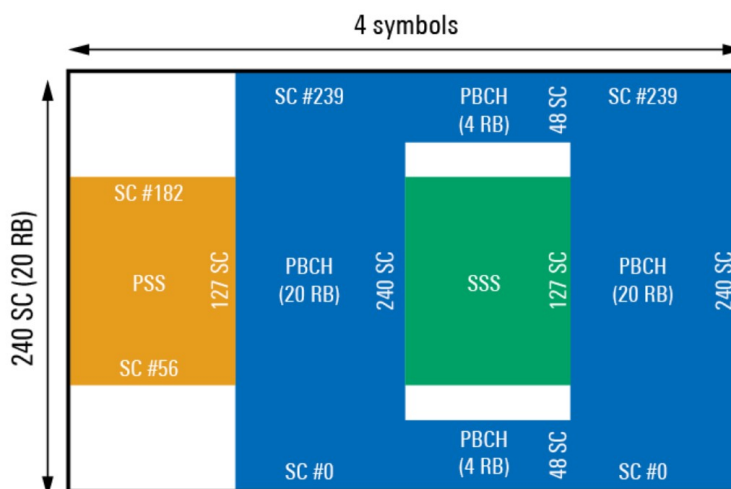


Figure 42: SS/PBCH block [63].

In the frequency domain, an SS/PBCH block consists of 240 contiguous subcarriers with the subcarriers numbered in increasing order from 0 to 239 within the SS/PBCH block.

In the time domain, an SS/PBCH block consists of 4 OFDM symbols, numbered in increasing order from 0 to 3 within the SS/PBCH block, where PSS, SSS, and PBCH with associated DMRS are mapped to symbols as given by Figure 43. The quantities k and l represent the frequency and time indices, respectively, within one SS/PBCH block.

Channel or signal	OFDM symbol number l relative to the start of an SS/PBCH block	Subcarrier number k relative to the start of an SS/PBCH block
PSS	0	56, 57, ..., 182
SSS	2	56, 57, ..., 182
Set to 0	0	0, 1, ..., 55, 183, 184, ..., 239
	2	48, 49, ..., 55, 183, 184, ..., 191
PBCH	1, 3	0, 1, ..., 239
	2	0, 1, ..., 47, 192, 193, ..., 239
DM-RS for PBCH	1, 3	$0 + v, 4 + v, 8 + v, \dots, 236 + v$
	2	$0 + v, 4 + v, 8 + v, \dots, 44 + v$ $192 + v, 196 + v, \dots, 236 + v$

Figure 43: Resources within an SS/PBCH block for PSS, SSS, PBCH and DMRS for PBCH [71] Table 7.4.3.1-1.

Note that the DMRS are different for different SS/PBCH blocks and thus allow individual power measurements per SS/PBCH block. Furthermore, the quantity v is given by $v = N_{ID}^{cell} \bmod 4$ and therefore depends on the cell ID.

In contrast to LTE where the PSS and SSS have a periodicity of 5 ms and PBCH of 10 ms, all signal components of the SSB are transmitted together, i.e. they all have the same periodicity. TS 38.213 [73] defines the appearance of these SS/PBCH blocks within 5ms (a half frame of the radio frame). SSBs are organized in burst sets, where a burst set is composed of one or more SSBs. The maximum number of SSBs per burst ($= L_{max}$) depends on the deployment frequency range and the applied subcarrier spacing (SCS) as shown in Figure 44. For higher frequencies, the number is significantly higher (max. 64) compared to the lower 1 GHz frequency range (max. 4). Each SS/PBCH block has an index with an increasing number from 0 to $L_{max}-1$. To provide greater flexibility for transmission of the SSB, the SS burst set periodicity can be set to 5 ms, 10 ms, 20 ms, 40 ms, 80 ms or 160 ms.

In LTE, the PSS/SSS and PBCH are always transmitted around the center frequency of the signal. In 5G NR, the SSB can be positioned anywhere within the transmission bandwidth of the signal but are subject to either a carrier raster or a so-called synchronization raster depending on the operation mode (NSA or SA).

	FR1	FR1	FR2
SC spacing	$f_c \leq 3 \text{ GHz}$ ($L_{\max} = 4$)	$f_c > 3 \text{ GHz}$ ($L_{\max} = 8$)	$f_c > 24.25 \text{ GHz}$ ($L_{\max} = 64$)
Case A (15 kHz)	2, 8, 16, 22	2, 8, 16, 22, 30, 38, 44, 50	N/A
Case B (30 kHz)	4, 8, 16, 20	4, 8, 16, 20, 32, 36, 44, 48	N/A
	FDD: $f_c \leq 3 \text{ GHz}$ ($L_{\max} = 4$) TDD: $f_c \leq 2.4 \text{ GHz}$ ($L_{\max} = 4$)	FDD: $f_c > 3 \text{ GHz}$ ($L_{\max} = 8$) TDD: $f_c > 2.4 \text{ GHz}$ ($L_{\max} = 8$)	
Case C (30 kHz)	2, 8, 16, 22	2, 8, 16, 22, 30, 38, 44, 50	N/A
Case D (120 kHz)	N/A	N/A	4, 8, 16, 20, ..., 508, 512, 520, 524
Case E (240 kHz)	N/A	N/A	8, 12, 16, 20, ..., 480, 484, 488, 492

Figure 44: L_{\max} and start symbol for the SS/PBCH block within a half frame [63].

3.2.8 Beamforming

Beamforming is a well-known and established antenna technology. Cellular networks such as LTE apply this technology to improve performance. Similarly, radar applications use beamforming to identify objects. Although it is not new, beamforming has a fundamentally different level of importance in 5G cellular communications compared to 4G. Especially to allow deployment of 5G in higher frequency ranges such as the cm-wave and mm-wave frequency spectrum, beamforming is necessary to achieve sufficient cell coverage, i.e. to compensate for the higher path loss at these frequencies.

The ability to dynamically manage beams (beam management) is equally important in fixed or mobile scenarios. For example, in a fixed wireless access (FWA) scenario, the customer premises equipment (CPE) in a household connects to an outdoor 5G base station. In this case, no mobility is involved and a beam sweeping procedure would identify the best beam to be used. In contrast, beamforming needs to be dynamic (steerable or switchable) when a moving car on a road is connected.

Beam management is realized with different operations known as:

- **Beam sweeping:** Using multiple beams at the base station to cover a geographic area and sweep through them at pre-specified intervals;
- **Beam measurement:** The UE provides measurement reports to the base station on a per beam basis;
- **Beam detection:** The UE identifies the best beam based on power measurements related to the configured thresholds;
- **Beam switching:** The UE switches between different beams to support mobility scenarios;

- Beam recovery: The UE is configured with basic information to recover a beam in case a connection is lost.

5G NR provides beamforming based on the specific design of the SS/PBCH blocks transmitted by the base station.

Figure 45 provides a basic illustration of how beamforming can be applied when 5G NR operates, for example, at 3.5 GHz with a SCS of 30 kHz (case B). In this case, the SS/PBCH blocks occupy a bandwidth of 7.2 MHz. Placement of the blocks within the carrier bandwidth is flexible and is configured by the network. In the example, out of a maximum of eight SS/PBCH blocks, only six are configured, thereby realizing six different beam directions.

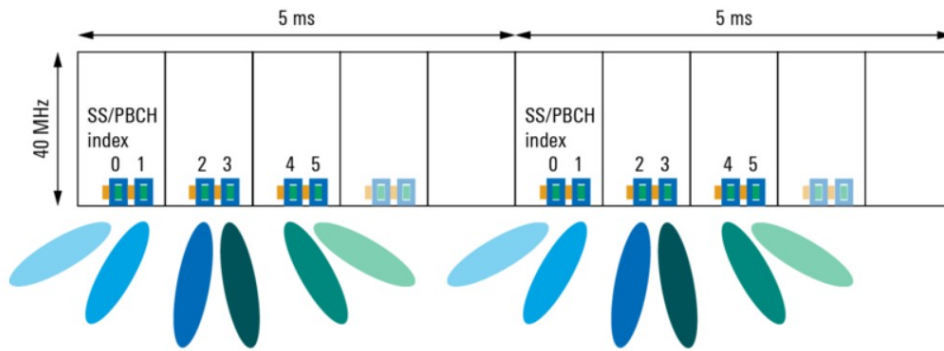


Figure 45: Example of a beamforming configuration (here $f_c = 3.5$ GHz, SCS = 30 kHz, Case B) [63].

Figure 46 provides a complex illustration of how beamforming can be applied to a 5G implementation operating in FR2 band.

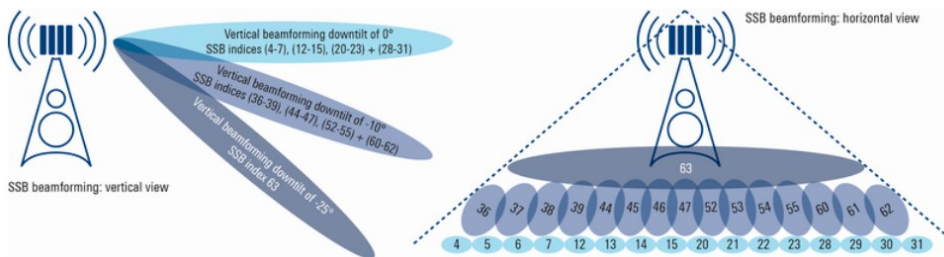


Figure 46: SSB beamforming in the horizontal and vertical directions (example of FR2 site) [63].

In the example, each sector is subdivided into different SSB beams. These SSB beams are vertically and horizontally oriented. Coverage in the vertical direction spans an elevation angle between 0° and -22.5° , which is achieved based on vertical beamforming mechanisms. Coverage of one cell in the horizontal direction spans an azimuth angle between -60° and $+60^\circ$, which is achieved based on horizontal beamforming mechanisms. In this example,

the cell coverage is based on 16 beams in the 0° vertical direction, 15 beams in the -10° vertical direction and 1 beam in the -25° vertical direction.

The base station broadcasts SS/PBCH at regular time intervals and over multiple beams (known as network beam sweeping).

When a UE wants to access the system, it begins by measuring several beam-based received synchronization signal blocks (SSB) identified by an SS-Index and selecting a specific beam based on the strongest received beam power.

3.2.9 Massive MIMO

The antenna technology that allows beamforming is called Massive MIMO. Multiple-input multiple-output (MIMO) antenna technology is a method for increasing the capacity of a radio link using multiple transmit antennas and multiple receive antennas. Due to multipath propagation and more importantly, decorrelated paths between the transmitter and receiver, multiple data streams can be sent over the same radio channel, thus increasing the peak data rate per user or the capacity of the cellular network.

If the number of applied antenna elements is significantly increased at the base station, for example, if 64 cross-polarized antennas are used, the network node becomes a massive MIMO base station.

The large number of antenna elements allows directional signal transmission and reception. To change the directionality of the array, a beamformer controls the phase and amplitude of the signal at each antenna element. The direction θ of the beam depends on the antenna spacing d , wavelength λ and phase shifts between antenna elements.

Analog, digital and hybrid beamforming schemes are known, whereas hybrid beamforming is most commonly used in 5G. Note that phase shifts on their own would be sufficient to achieve beam steering towards different directions. The ability to change the amplitude enables optimization of the side lobe suppression.

Figure 47 illustrates the principle of beam steering using phase and amplitude variations.

Even with the increased number of elements, the number of spatial layers is not increased. 5G NR supports eight layers on the downlink and four layers on the uplink (like LTE). However, the large number of elements allows the combination of beamforming with spatial multiplexing. More importantly, 3D or full-dimensional beamforming is enabled. Therefore, massive MIMO

antennas enable focused transmission and reception of signal energy in smaller regions of space.

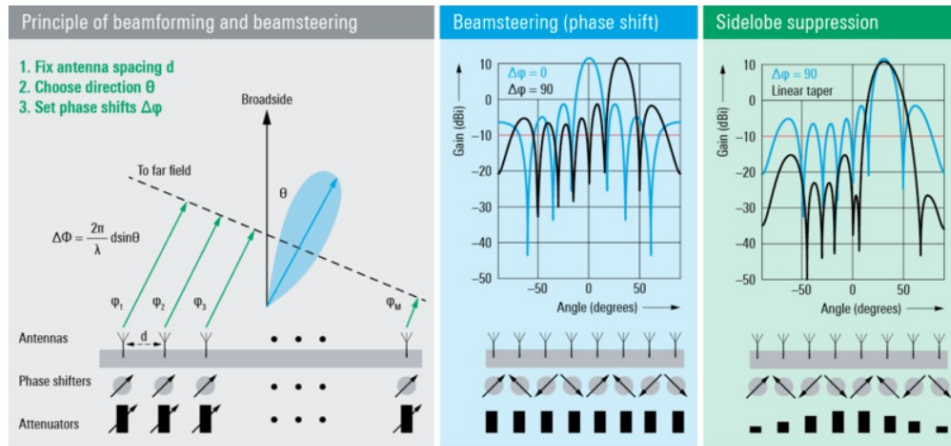


Figure 47: Principles of beamforming and beamsteering [63].

Massive MIMO brings about huge improvements in user throughput, capacity and energy efficiency, especially when combined with simultaneous scheduling of many users.

3.2.10 Identifying SSBs

LTE follows a bandwidth-centric approach. A UE only needs to scan the respective frequency band following the channel raster to find the carrier frequency of the signal. That was sufficient and allows the UE to identify the (LTE) PSS, (LTE) SSS and (LTE) PBCH since they were transmitted on six reserved resource blocks centered around the carrier frequency. In 5G NR, the SSB can be positioned anywhere within the transmission bandwidth. Therefore, the frequency position of the SSB within the downlink signal needs to be signaled to the UE.

In non-standalone (NSA) mode, where generally UE needs an LTE connection to obtain a 5G connection, the UE receives the exact frequency location of the synchronization signal blocks (SSB) via dedicated RRC signaling over the established LTE connection.

In standalone (SA) mode, the UE starts scanning the supported 5G NR frequency bands in the priority order, based on e.g. information stored on the USIM, for SSBs.

This information is signaled as the new radio absolute radio frequency channel number (NR-ARFCN), which can assume a value in the range 0 to 3 279 165. This range is dictated by the global frequency raster defined by 3GPP's working group RAN4 for 5G NR, covering frequencies from 0 to 100 GHz (Figure 48).

FR1, FR2	Frequency range	ΔF_{Global}	$F_{\text{REF-Offs}}$	$N_{\text{REF-Offs}}$	Range of N_{REF} (NR-ARFCN)
FR1: 450 MHz to 7.125 GHz	0 to 3000 MHz 3000 to 24 250 MHz	5 kHz 15 kHz	0 3000	0 600 000	0 to 599 999 600 000 to 2 016 666
FR2: 24.25 GHz to 52.6 GHz	24250 to 100 000 MHz	60 kHz	24 250.08 MHz	2 016 667	2 016 667 to 3 279 165

Figure 48: NR-ARFCN parameters for the global frequency raster [63] (obtained merging [74] Table 5.4.2.1-1 and [75] Table 5.4.2.1-1).

The global frequency raster defines a set of RF reference frequencies F_{REF} . The RF reference frequency is used in signalling to identify the position of RF channels, SS blocks and other elements.

5G NR provides a high granularity to position the signal in the frequency domain (so many F_{REF}). Second, the transmission periodicity of the SSBs is by default far less frequent than in LTE, ranging from 20ms to 160ms. During the initial access procedure, a UE assumes this to be 20 ms. This results in a longer scanning time due to the periodicity and higher granularity for placing a 5G NR carrier.

For this reason, an additional frequency raster has been defined by 3GPP's working group RAN4 as the global synchronization channel number(s) (GSCN). This raster is defined per deployment frequency range (first column in Figure 49) and further specified per frequency band, where, dependent on the utilized subcarrier spacing for the SSB, a different step size (1 or 2) is used.

Frequency range	SS block frequency position SS_{REF}	GSCN	Range of GSCN
0 to 3000 MHz	$N \cdot 1200 \text{ kHz} + M \cdot 50 \text{ kHz}$, $N = 1:2499, M \{1, 3, 5\}$	$3 \cdot N + (M - 3) / 2$	2 to 7498
3000 to 24250 MHz	$3000 \text{ MHz} + N \cdot 1.44 \text{ MHz}$ $N = 0:14756$	$7499 + N$	7499 to 22255
24250 to 100000 MHz	$24250.08 \text{ MHz} + N \cdot 17.28 \text{ MHz}$	$22256 + N$	22256 to 26639

Figure 49: GSCN parameters for the global frequency raster [63] (obtained merging [74] Table 5.4.3.1-1 and [75] Table 5.4.3.1-1).

The frequency position of the SS block is defined as SS_{REF} with corresponding number GSCN.

The relevant details are covered in TS 38.101-1 [74] and TS 38.101-2 [75].

3.3 5G NR EMF extrapolation proposals

As presented in previous chapters, measurement techniques used to assess the compliance with EMF exposure limits are object to international regulation, the main document is IEC 62232:2017 [43]. The basic principle of the assessment is to measure the power received from a constant radio

frequency source, typically a pilot signal, and to apply a proper extrapolation factor. This kind of approach is standardized for 2G, 3G, and 4G technologies, but is still under investigation for 5G technology.

Indeed, the use of flexible numerologies, advanced Time Division Duplexing (TDD) and beamforming, require the definition of new procedures and protocols for EMF measurement of 5G signals.

In the last few years, there have been a few publications discussing how to properly assess the exposure levels from 5G base stations. In the following paragraphs most relevant proposals will be presented.

3.3.1 5G NR EMF extrapolation “Proposal 1”

“Proposal 1” is taken from a work developed in three papers ([76], [77], and [78]) by a workgroup with ARPA Lazio, ARPA Piemonte, Vodafone Italia S.p.A., DIEI and ELEDIA@UniCAS Research Laboratory from University of Cassino and Southern Lazio and ICEmB from Genoa. In this proposal an extrapolation procedure for an accurate estimation of the instant maximum power received from a 5G source is proposed. The procedure is based on the choice of an effective pilot channel, whose received power is eligible to be the reference for the extrapolation technique. The extrapolation formula includes proper factors that take into account the effect of the TDD and of the sweep beam in the measured value of the 5G signal level.

As preliminary step, it is important to introduce the E_{5G}^{max} parameter. It represents the maximum field level [V/m] that can be reached in the measurement point. From a practical point of view, it is representative of a 5G base station transmitting at its maximum power and concentrating all its power in a single beam (single user) during an extensive amount of time (e.g., 6 minutes is one of the averaging times required by the ICNIRP guidelines [5]). From a practical point of view, it can be reached only if the scheduler gives all the available resources to a single user continuously for at least 6 minutes, leaving all the other users in stand by (i.e. causing at least a 6 minutes loss of data connections to all the other subscribers of the cell). This quantity, referring to an unrealistic condition, is used as a reference to estimated the EMF exposure in realistic conditions by proper scaling factor.

The maximum EMF level at a given location, E_{5G}^{max} , is estimated by the product of three factors as depicted in (10) [77] [78].

$$E_{5G}^{max} = \sqrt{N_{SC} F_{TDC}} E_{RE}^{max} \quad (10)$$

Where:

- N_{SC} is the total number of subcarriers of the NR carrier, i.e. twelve times the total number of Resource Blocks (N_{RB}) available for the signal;
- F_{TDC} is the deterministic scaling factor representing the duty cycle of the signal when TDD multiplexing strategy is used, i.e. the fraction of the signal frame reserved for downlink transmission;
- E_{RE}^{max} represents the maximum EMF level measured for a single Resource Element.

Regarding the evaluation of the third term, E_{RE}^{max} , the only NR signal that is always “on air” is the SS/PBCH block (or SSB). As a consequence of the beam sweeping, the received EMF level is different for each SSB, according to the relative orientation between the SSB beam and the receiver antenna (see Figure 50).

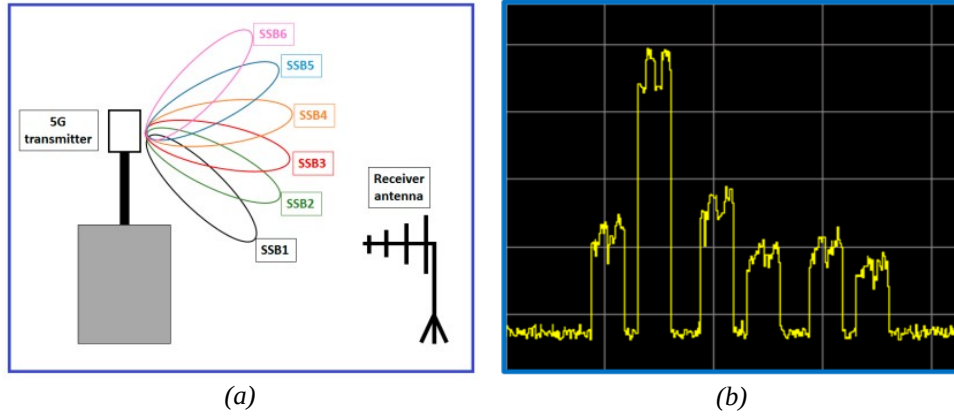


Figure 50: Beam sweeping synthesized by a 5G active antenna (a) and zero span measurement of the Synchronization Signal synthesized Blocks (SSBs) received power level (b), from [77].

The PBCH Demodulation Reference Signal (PBCH-DMRS) is proposed as pilot channel. The PBCH-DMRS signal is one of the main parameters in NR and is directly measurable with great accuracy using modern Vector Spectrum Analyzers (VSAs) with demodulation software or also by network scanners.

In particular E_{RE}^{max} can be obtained applying (11) [78].

$$E_{RE}^{max} = E_{RE,max}^{PBCH-DMRS} \sqrt{F_{beam}} \quad (11)$$

Where:

- $E_{RE,max}^{PBCH-DMRS}$ is the maximum received EMF level for the PBCH-DMRS per RE;
- F_{beam} is a parameter which takes into account the effect of the boost of the traffic beams with respect to maximum EMF level received from the pilot channel, due to the effect of beamforming and beamsweeping.

With reference to $E_{RE,max}^{PBCH-DMRS}$, it can be evaluated from the maximum PBCH-DMRS power related to the strongest SSB and from the knowledge of the Antenna Factor (AF) of the antenna used in the field measurements, the power losses α of the cable connecting the antenna and the input impedance Z_{in} of the instrument, as shown in (12) [78].

$$E_{RE,max}^{PBCH-DMRS} = \sqrt{\frac{P_{RE,max}^{PBCH-DMRS} Z_{in}}{\alpha}} AF \quad (12)$$

Some VSAs provide the detected PBCH-DMRS power for each SSB, allowing a direct evaluation $P_{RE,max}^{PBCH-DMRS}$. If only an average over the SSBs is available, it can be related to $P_{RE,max}^{PBCH-DMRS}$ by applying (13) [78].

$$P_{RE,max}^{PBCH-DMRS} = \frac{\langle P_{RE,max}^{PBCH-DMRS} \rangle}{R} \quad (13)$$

Where R is defined as the ratio between the average detected power of all the SSBs in a burst and the power of the strongest SSB in the burst, and accounts for the effect of the beamsweeping on the received EMF level of all the SSBs in a burst.

Equation (14) reports the maximum EMF level at a given location, wherein (11), (12) and (13) have been substituted in (10) [78].

$$E_{proposal1}^{5G,max} = E_{5G}^{max} = AF \sqrt{\frac{N_{SC} F_{TDC} F_{beam} Z_{in} \langle P_{RE,max}^{PBCH-DMRS} \rangle}{\alpha R}} \quad (14)$$

Some quantities in (14) require a more detailed explanation.

3.3.1.1 Number of subcarriers (N_{SC})

The total number of subcarriers N_{SC} is defined as $12 N_{RB}$, where N_{RB} represents the total number of Resource Blocks available for the signal. The value of N_{RB} depends on both the signal bandwidth and the subcarrier spacing, and is reported in Figure 51 and Figure 52.

SCS (kHz)	5 MHz	10 MHz	15 MHz	20 MHz	25 MHz	30 MHz	40 MHz	50 MHz	60 MHz	70 MHz	80 MHz	90 MHz	100 MHz
	N _{RB}	N _{RB}	N _{RB}	N _{RB}	N _{RB}	N _{RB}	N _{RB}	N _{RB}	N _{RB}	N _{RB}	N _{RB}	N _{RB}	N _{RB}
15	25	52	79	106	133	160	216	270	N/A	N/A	N/A	N/A	N/A
30	11	24	38	51	65	78	106	133	162	189	217	245	273
60	N/A	11	18	24	31	38	51	65	79	93	107	121	135

Figure 51: Transmission bandwidth configuration N_{RB} for FR1 ([72] Table 5.3.2-1).

SCS (kHz)	50 MHz	100 MHz	200 MHz	400 MHz
	N _{RB}	N _{RB}	N _{RB}	N _{RB}
60	66	132	264	N/A
120	32	66	132	264

Figure 52: Transmission bandwidth configuration N_{RB} for FR2 ([72] Table 5.3.2-2).

3.3.1.2 Time duty cycle factor F_{TDC}

The time duty cycle factor F_{TDC} is the fraction of the signal frame reserved for downlink transmission. In the case of no a priori knowledge about the specific TDD scheme implemented by the signal under investigation, a direct determination of F_{TDC} can be carried out through a zero span measurement using a scalar spectrum analyzer by means of the following procedure based on zero-span measurement.

- Central frequency set to the 5G central carrier;
- RBW as large as allowed by the spectrum analyzer (note that RBW should not be larger than the signal bandwidth, however);
- VBW was set to a value greater than RBW: this setting is not so important for a measurements aimed to determine time intervals, but in general this choice allows to avoid loss of energy contribution in a noise-like signal;
- sweep time set as a multiple of a frame period (10 ms);
- a periodic trigger according to the frame period (100 Hz);
- trace mode set to max-hold, in order to easily distinguish between downlink and uplink slots.

The acquired trace allows for an effective identification of the uplink slots, since the associated received power is several orders of magnitude lower than that related to downlink slots. Experimental evidence suggests an acquisition time of at least 10 sec per trace, in order to ensure the proper rising of downlink slots.

As an example of application on a true signal, the proposed procedure has been applied to the FR1 TDD signal. The measured data are plotted in Figure 53.

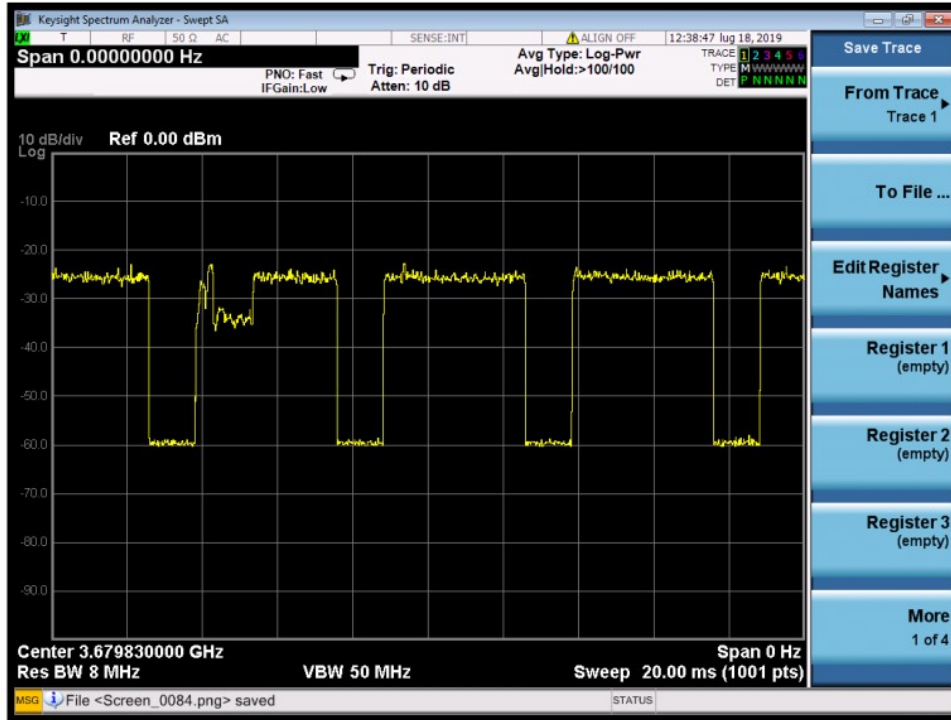


Figure 53: FRI-TDD case: Signal used for the estimation of the F_{TDC} factor [76].

Starting from these data, an estimated value for F_{TDC} can be obtained using the following formula [76].

$$F_{TDC} = \frac{N_{\text{downlink-pixel}}}{N_{\text{total-pixel}}} \quad (15)$$

Where $N_{\text{downlink-pixel}}$ is the number of pixels ‘on’ and $N_{\text{total-pixel}}$ is the total number of pixels provided by the analyzer. A pixel can be identified as ‘on’ if it exceeds a certain power threshold, used to distinguish between downlink and uplink symbols. Note that the receiver antenna must be placed at a proper distance from any user equipment, in order to not include the uplink transmission in the acquired spectrum.

3.3.1.3 PBCH-DMRS average power per resource element

Modern VSAs provide a reliable measurement of PBCH-DMRS power per RE, averaged over the SSBs in a burst, through demodulation analysis of the 5G signal. To ensure a correct demodulation of SSBs and, therefore, the reliability of PBCH-DMRS power measurement, a set of parameters defining the characteristics of the 5G signal under measurement must be provided to the instrument, such as:

- SSB numerology μ ;
- SSB frequency offset with respect to the signal center frequency;

- SSB pattern (Case A, B, C, D, E);
- SSB periodicity;
- The maximum number of SSBs allowed for the specific pattern (L_{max});
- TDD scheme.

This implies that the measurement session should be sustained by a preliminary survey aiming at acquiring all the mandatory information about the investigated signal. Some VSAs are equipped with automated detection routines which provide a reliable SSB demodulation, making the PBCH-DMRS power detection a quite easy task.

In Figure 54, an example of SS/PBCH power and frame summary given by the VSA is shown.

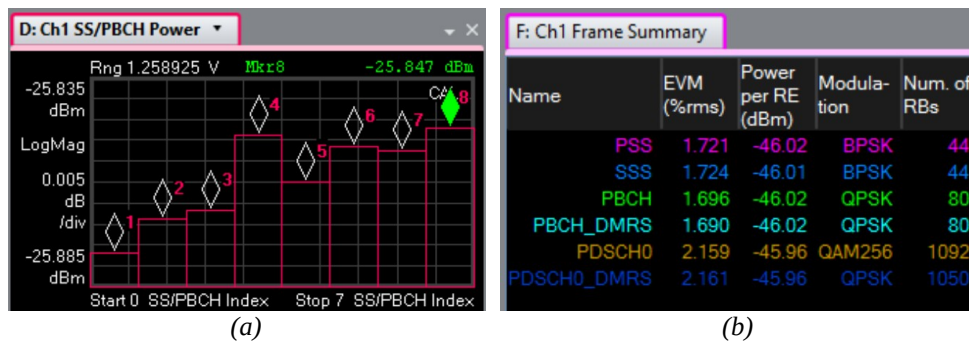


Figure 54: Measure of the data required to estimate the maximum power per RE using the VSA [76]; (a) Power of the SSBs; (b) A list of parameters including the PBCH-DMRS.

3.3.1.4 SSB power scale factor R

The power scale factor R is defined as the ratio between the average detected power of all the SSBs in a burst and the power of the strongest SSB in the burst. As shown in Figure 54(a) the VSA provides the received power for all the SSBs of a burst, allowing for an easy determination of R . Since the procedure relies on a demodulation analysis, the knowledge of all those parameters discussed in the previous section is still required.

Some VSAs provide the detected PBCH-DMRS power for each SSB instead of the averaged value. In this case, the user can directly use the PBCH-DMRS power related to the strongest SSB with no need to compute R factor.

3.3.1.5 Beamforming factor F_{beam}

The beamforming parameter F_{beam} takes into account the effect of a potential boost of the traffic beams with respect to maximum EMF level received

from the pilot channel, due to the effect of beamforming produced by the use of mMIMO antennas. To ensure a correct estimate of F_{beam} , the measurement should be carried out in conditions of maximum EMF exposure, i.e. with a traffic beamformed beam pointing towards the receiving antenna. This requirement can be obtained by placing an UE next to the receiving antenna, while exchanging data traffic with the 5G source under investigation.

F_{beam} can be measured with a zero span mode measurement using the following settings:

- center frequency set to the central frequency of the SSB;
- RBW smaller than 127 sub-carriers (e.g. 1 MHz);
- Also in this case, VBW was set to a value greater than RBW, even if the influence of this parameter is quite weak in the evaluation of a ratio between power levels;
- trace mode set to max-hold;
- detector set to peak;
- sweep time set to half-frame (5 ms);
- a periodic trigger according with the frame period (100 Hz);
- a fine-tuned trigger offset to ensure that both SSBs and traffic slots are visible on the acquired trace at the same time.

The ratio between the power of the highest traffic level and the power of the highest SSB represents F_{beam} factor. Since the power of the highest traffic level is quite variable within a single slot, the power value taken into account was the average of the values of the pixels in the zero span trace in each maximum load slot. It is understood that in the case of different numerologies used for traffic channels and SSB, a proper scaling factor depending on the numerologies must be introduced.

Figure 55 shows an example of F_{beam} evaluation. The SS Burst is visible on the left. The signalling data sent between the second and third SSB is clearly visible using max-hold trace function (yellow curve), while almost disappears using average trace function (blue curve). The value of F_{beam} is the difference between markers.

F_{beam} represents the critical points of the technique because its estimation requires to force the data beam toward the measurement position.

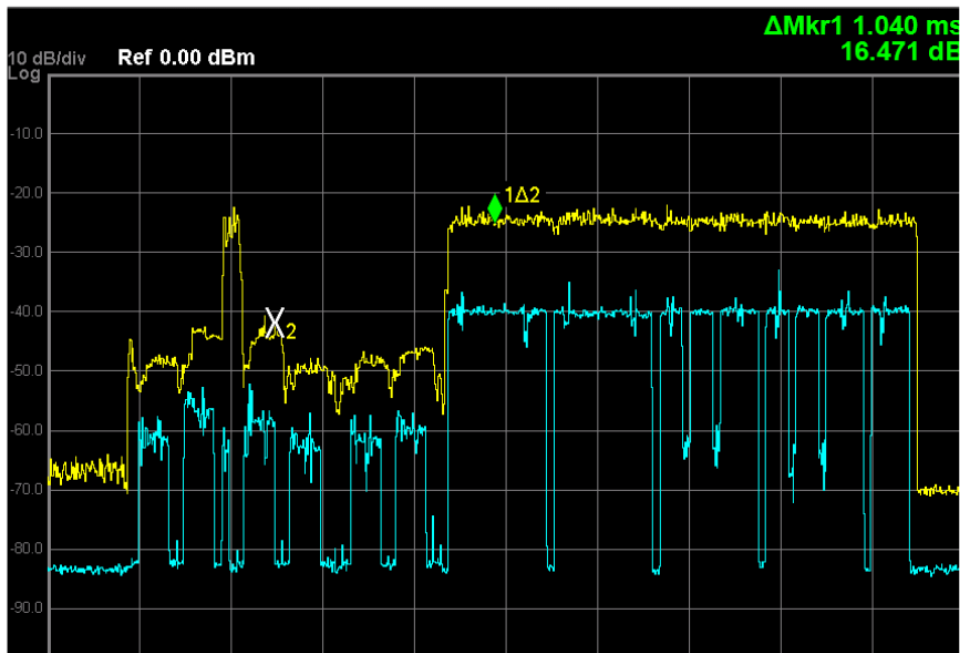


Figure 55: Zero span measurement of the signal in full-data conditions (1 MHz RBW); yellow: max-hold trace; blue: average value; the peak between the second SSB and the third SSB is a control signal [78].

In the example presented in [78] a customized phone, specifically modified to force downloading data using UDP protocol, has been used with excellent results. However, in practical applications the use of ‘on the shelf’ systems available on the market is preferable.

A first solution is to use a standard 5G phone to force data traffic toward the measurement position. In order to simulate this solution, a phone was used to download a 4K video. In spite of the relatively large amount of downloaded data, the number of REs per frame is modest and highly concentrated in frequency and time.

A different solution involves the use of receivers developed for testing of communication networks, that allows higher flexibility in download parameters. In the example presented in [78] a Rohde & Schwarz Qualipoc Android is used, successfully imposing a UDP download in the full bandwidth.

It is understood that in standard working conditions, i.e. in presence of a large number of users that compete for the network resources, the fraction of the available bandwidth assigned to a single user is not predictable since it is up to the scheduler. However, this second solution seems to be preferable, since it is reasonable to imagine that the scheduler tends to give more bandwidth to the UDP high data-rate receiver, allowing to decrease the measurement time.

3.3.1.6 Statistical factor F_{PR}

E_{5G}^{max} is a theoretical value that is not reached in any practical condition. The average amplitude of the field actually received in real conditions is generally significantly lower than E_{5G}^{max} . A more realistic field level, i.e. an “actual” maximum exposure level, requires to take into account an additional factor (F_{PR}) as indicated by the International Electromechanical Commission (IEC) [19]. Estimation of F_{PR} factor is extremely complex since the exposure of a user depends also on the activity of the other users.

As further observation, the proposed extrapolation formula (14) does not include the MU-MIMO case. The details of the MU-MIMO implementation depend on the vendors, and the effectiveness of any solution regarding this technology requires experimental test. In MU-MIMO the energy is shared among the UEs, which are sufficiently spatially separated. The maximum number of layers in case of MU-MIMO is 16, while the typical maximum number of layers for current mobile phones is 4, giving a large number of possible scenarios ranging from 16 different UEs using one layer each, to 4 UEs using 4 layers each. As a consequence, in MU-MIMO spatial multiplexing there is a large number of possible distributions of the energy among the UEs located in different positions, and forcing a communication in the measurement point does not assure the possibility to evaluate the maximum EMF level if there are other communication incurred.

A possible approach to MU-MIMO is to consider as ‘reference level’ the maximum field in the SU-MIMO condition, taking statistically into account the impact of MU-MIMO in an ‘extended’ version of the F_{PR} factor.

The choice of the factors that must be obtained by measurements, and the ones that must be included in the statistical F_{PR} factor is a further degree of freedom that must balance the complexity of field measurements and the accuracy of statistical approaches.

3.3.2 5G NR EMF extrapolation “Proposal 2”

“Proposal 2” is taken from a technical report developed by Swiss Federal Institute of Metrology METAS ([79]).

This proposal develops a method for measuring field levels of NR installations, in indoor and outdoor environments. The present proposal is restricted to the first frequency range (FR1) up to 6 GHz.

To assess the conformity of an installation with the legal requirements, a measurement of the electric field strength and additional calculations are needed. These two steps (measurement and calculations) make it possible to

determine the field strengths that are expected in the “*reference-operating mode*” which corresponds (in case of mobile telecommunication systems) to the operation at maximum “speech and data” traffic and at maximum transmission power.

In other words, the compliance assessment of a mobile phone base station includes a measurement of the electric field strength at a defined time as well as an extrapolation of the measured values to the reference-operating mode.

Two different measurements of the electric field strength are proposed:

- The code-selective measurement method (also reference method). It allows the compliance assessment of an installation with the installation limit value;
- The frequency selective measurement method (also approximate method). It does not allow the distinction of two different cells of the same operator/installation. Moreover, it suffers from overestimation of the extrapolated field strength of the reference-operating mode.

The measurement methods are based on the determination of the radiated field produced by the Secondary Synchronization Signal (SSS).

As seen in paragraph 3.2, the SSS is part of the SS/PBCH blocks which are distributed over a bandwidth of 3.6 MHz up to 7.2 MHz (for carrier frequency FR1 up to 6 GHz) within the NR downlink signal. The SSS occupies a bandwidth of 1.905 MHz or 3.810 MHz (127 resource elements). The SS/PBCH block is in general not centered with the downlink carrier frequency. Each SS/PBCH block occupies a set of four consecutive OFDM symbols. The SS/PBCH block contains the Demodulation Reference Signal (PBCH-DMRS). The PBCH-DMRS resource elements of the SS/PBCH block carry information on the cell identity number as well as on the SS/PBCH beam identity (SS/PBCH block index).

3.3.2.1 Code-selective measurement method

Measurement of the SSS, as well as decoding of the PBCH-DMRS signal, requires a code-selective field probe. A code-selective instrument could be a measuring receiver or a spectrum analyzer capable of decoding NR signals and of quantifying their power.

In a given location, the measurement is performed as follows: for each *NR cell i*, all measurable SS/PBCH blocks must be identified in terms of their *cell number i* and *SS/PBCH block index j* (obtained by demodulating the

PBCH-DMRS signal). Each SS/PBCH block with *index j* corresponds to an antenna beam. For each SS/PBCH block (identified by its *index j*), the $E_{i,j}^{SSS(RE)}$ per resource element of the SSS is measured. The electric field strengths $E_{i,j}^{SSS(RE)}$ of all SS/PBCH blocks within a half frame are then added quadratically to build a new value. The spatial maximum $E_{i,max}^{SSS(RE)}$ of this value has to be found within the measurement volume (16) [79].

$$E_{i,max}^{SSS(RE)} = \max \left(\sqrt{\sum_j (E_{i,j}^{SSS(RE)})^2} \right) \quad (16)$$

The spatial maximum is determined by scanning the receive antenna taking into account:

- Standing waves in the measurement volume;
- Polarization of the measuring antenna (receive antenna);
- Orientation (azimuth and elevation) of the measuring antenna;
- Minimum of 50 cm distance to walls, floor, ceiling, furniture and windows;
- Height above the floor between 0.5 m and 1.75 m.

For each *NR-cell i* of the base station, the measured value the electric field strength has to be extrapolated to the reference operating mode using the equation (17) [79].

$$E_{i,h} = E_{i,max}^{SSS(RE)} \cdot K_i(\phi_i, \theta_i) \quad (17)$$

Where $K_i(\phi_i, \theta_i)$ is the global extrapolation factor for *cell i*.

All NR cell-specific extrapolated electric field strength values are then summed together using the equation (18), where *n* is the number of cells of the base station respectively of the installation [79].

$$E_{proposal2-csm}^{5G,max} = E_h = \sqrt{\sum_{i=1}^n E_{i,h}^2} \quad (18)$$

3.3.2.2 Frequency selective measurement method

The frequency selective method is derived from the code selective measurement method, and it is also based on the measurements of the secondary synchronization signal (SSS). Frequency selective measurements of the synchronization signals require a spectrum analyzer with true RMS-detector, a minimum resolution bandwidth of the SSS bandwidth ($127 \cdot \Delta f$) and a maximum hold-function. Measurements are performed in “Zero Span” mode, and the sweep time must be chosen so that the measuring time for

one value is less than one-half of the duration of an SSS OFDM symbol. Depending on the used numerology (for FR1 band 15 kHz or 30 kHz), the duration of the OFDM symbol without prefix is $1/15 \text{ kHz} \cong 66 \mu\text{s}$ for 15 kHz numerology, and $1/30 \text{ kHz} \cong 33 \mu\text{s}$ for 30 kHz numerology. The spatial maximum of the synchronization signals have to be measured as mentioned in code-selective measurement method.

Regarding frequency selective method, the following aspects have to be considered:

- The center frequency of the measuring instrument has to be set to the center frequency of the SS/PBCH block, which does not in general match the center frequency of the downlink NR channel. The center frequency of the SSS must be given by the operator.
- Since the spectrum analyser cannot distinguish uplink and downlink in a TDD transmission scheme, it is important to switch off every mobile phone in the vicinity of the measuring system.

The value of the $E_{i,max}^{SSS(RE)}$ cannot be measured directly by a frequency selective measuring instrument, since it requires the quadratic addition of signals from different SS/PBCH beams. However, based on realistic estimations, equation 19 is used [79].

$$E_{i,max}^{SSS(RE)} \simeq E_{i,max}^{measured} \cdot \sqrt{\frac{1}{127}} \cdot K_i^{FSM} \quad (19)$$

Where:

- $E_{i,max}^{measured}$ Max & Hold value of the electric field strength measured over the whole measuring bandwidth (at least SSS bandwidth) set on the spectrum analyzer.
- $\sqrt{1/127}$ Reduction factor to obtain the field strength per resource element.
- K_i^{FSM} Frequency Selective Method (FSM) factor defined as $K_i^{FSM} = \sqrt{2}$ if the *cell i* has more than one SS/PBCH beam, and as $K_i^{FSM} = 1$ if the *cell i* has only one SS/PBCH beam. It takes into account the fact that the electric field produced by individual beams cannot be measured, and therefore cannot be added quadratically.

The measured value of the electric field strength has to be extrapolated to the reference operating mode as reported in (20) [79].

$$E_{proposat2-fsm}^{5G,max} = E_h = \left(E_{i,max}^{measured} \cdot \sqrt{\frac{1}{127}} \cdot K_i^{FSM} \right) \cdot \max_{i=1..n} K_i(\phi_i, \theta_i) \quad (20)$$

Where $K_i(\phi_i, \theta_i)$ is the global extrapolation factor for cell i .

3.3.2.3 Global extrapolation factor

$K_i(\phi_i, \theta_i)$ is the global extrapolation factor for cell i . The global factor depends on the azimuth ϕ_i and on the elevation θ_i and can be calculated by using the equation (21) [79].

$$K_i(\phi_i, \theta_i) = K_i^{SSS(RE)} \cdot K_i^{antenna}(\phi_i, \theta_i) \cdot K^{duplex} \cdot K_i^{stat} \quad (21)$$

Where:

- $K_i^{SSS(RE)}$ SSS extrapolation factor for cell i .
- $K_i^{antenna}(\phi_i, \theta_i)$ Antenna correction factor taking into account the difference between the antenna diagram of the SS/PBCH signal of cell i and the antenna diagram of the total signal in the maximum permitted operating condition. The antenna correction factor depends on the azimuth ϕ_i and on the elevation θ_i .
- ϕ_i Azimuth, defined as the horizontal angle in a spherical coordinate system, of the measurement location with respect to the transmit antenna of cell i .
- θ_i Elevation, defined as the vertical angle in a spherical coordinate system, of the measurement location with respect to the transmit antenna of cell i .
- K^{duplex} Duplex factor.
- K_i^{stat} Beam statistic factor for cell i .

3.3.2.3.1 Extrapolation factor for the SSS

For each cell i of the base station, an extrapolation factor $K_i^{SSS(RE)}$ is defined in the following way [79].

$$K_i^{SSS(RE)} = \sqrt{\frac{P_{i,permitted}}{P_i^{SSS(RE)}}} \quad (22)$$

The term $P_{i,permitted}$ is the maximum permitted effective radiated power (ERP) in W, without any reduction, taking into account the signal of all antenna ports of cell i : PSDCH, PBCH, and PDCCH.

The term $P_i^{SSS(RE)}$ is the Actual ERP per resource element (RE) of the SSS of the SS/PBCH block of cell i in watt. It corresponds to the maximum in all directions of the "summed SSS ERP radiation pattern" $P_i^{SSS(RE)}(\phi_i, \theta_i)$ and it is given by the equation (23) [79]. An example of a summed SSS ERP radiation pattern is shown in the right side of Figure 56.

$$P_i^{SSS(RE)} = \max_{\phi_i, \theta_i} P_i^{SSS(RE)}(\phi_i, \theta_i) \quad (23)$$

$P_i^{SSS(RE)}(\phi_i, \theta_i)$ is the "summed SSS ERP radiation pattern" obtained by summing the ERP radiated power per resource element of all SS/PBCH beams as defined by the following formula [79].

$$P_i^{SSS(RE)}(\phi_i, \theta_i) = \sum_j P_{i,j}^{SSS(RE)} \quad (24)$$

Where $P_{i,j}^{SSS(RE)}(\phi_i, \theta_i)$ represents the actual "effective radiated power" per resource element in W of the SSS of the SS/PBCH block of cell i and index j in the direction given by the azimuth ϕ_i and on the elevation θ_i .

The terms $P_{i,permitted}$ and $P_i^{SSS(RE)}$ are provided by the network operator.

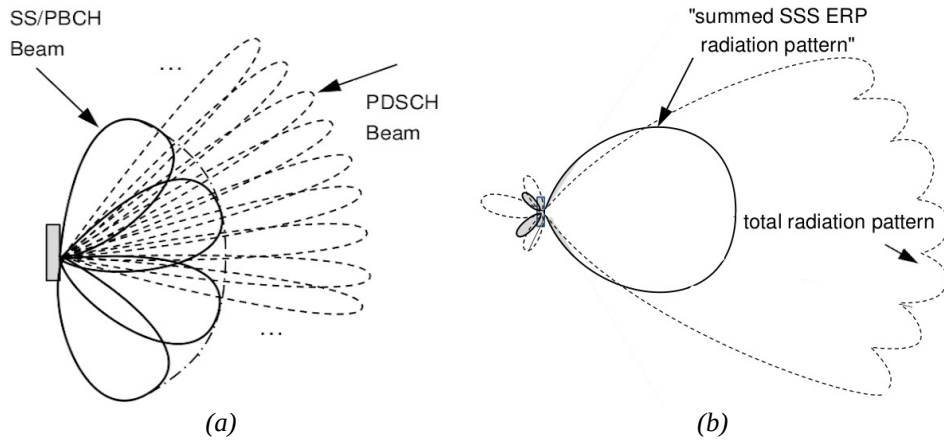


Figure 56: (a) A schematic representation (seen from above) of the horizontal radiation pattern of a NR-base station cell, where the PDSCH beams are not all represented; (b) A schematic representation (seen from above) of the horizontal summed and total radiation pattern of a NR-base station cell [79].

3.3.2.3.2 Antenna correction factor

Antenna correction factor taking into account the difference between the antenna diagram of the SS/PBCH signal of cell i and the antenna diagram of the total signal in the maximum permitted operating condition.

Before to define the antenna correction factor, it must be know the three following terms: $A_i^{SSS(RE)}(\phi_i, \theta_i)$, $A_i^{total}(\phi_i, \theta_i)$ and $K_{i,max}^{antenna}$.

The term $A_i^{SSS(RE)}(\phi_i, \theta_i)$ represents the attenuation of the "summed SSS ERP radiation pattern" of cell i in the direction given by the azimuth ϕ_i and by the elevation θ_i (25) [79]. This attenuation is defined as a "voltage ratio" (in contrast to a "power ratio") greater than 1.

$$A_i^{SSS(RE)}(\phi_i, \theta_i) = \sqrt{\frac{P_i^{SSS(RE)}}{P_i^{SSS(RE)}(\phi_i, \theta_i)}} \quad (25)$$

The term $A_i^{total}(\phi_i, \theta_i)$ represents the attenuation of the total signal radiation pattern of cell i in the direction given by the azimuth ϕ_i and by the elevation θ_i . The total radiation pattern corresponds to the envelope of all worst case radiation patterns in the permitted operation mode. This attenuation is defined as a "voltage ratio" (in contrast to a "power ratio") greater than 1.

The term $K_{i,max}^{antenna}$ represents the maximum value of the ratio $A_i^{SSS(RE)}(\phi_i, \theta_i)/A_i^{total}(\phi_i, \theta_i)$ where the maximum is taken on all directions for which the attenuation $A_i^{SSS(RE)}(\phi_i, \theta_i)$ of the SS/PBCH beam is less than 10 (26) [79].

$$K_{i,max}^{antenna} = \max_{\phi_i, \theta_i \mid A_i^{SSS(RE)}(\phi_i, \theta_i) < 10} A_i^{SSS(RE)}(\phi_i, \theta_i) / A_i^{total}(\phi_i, \theta_i) \quad (26)$$

For each cell i and for each azimuth ϕ_i and elevation θ_i , the corresponding extrapolation factors $K_i^{antenna}(\phi_i, \theta_i)$ are defined in the following formula [79].

$$K_i^{antenna}(\phi_i, \theta_i) = \begin{cases} 1 & \text{if } A_i^{SSS(RE)}(\phi_i, \theta_i) < 10 \\ & \text{and } A_i^{SSS(RE)}(\phi_i, \theta_i) \leq A_i^{total}(\phi_i, \theta_i) \\ A_i^{SSS(RE)}(\phi_i, \theta_i) / A_i^{total}(\phi_i, \theta_i) & \text{if } A_i^{SSS(RE)}(\phi_i, \theta_i) < 10 \\ & \text{and } A_i^{SSS(RE)}(\phi_i, \theta_i) > A_i^{total}(\phi_i, \theta_i) \\ K_{i,max}^{antenna} & \text{if } A_i^{SSS(RE)}(\phi_i, \theta_i) > 10 \end{cases} \quad (27)$$

The antenna correction factors $K_i^{antenna}(\phi_i, \theta_i)$ depend on the type of antenna and on the orientation of the antenna. These factors must be available, for example in a database or from the antenna manufacturer.

3.3.2.3.3 Duplex factor

The duplex factor K^{duplex} denotes the maximum ratio of the downlink transmission time in a time interval. It is defined as in the following [79].

$$K^{duplex} = \begin{cases} \sqrt{r_{DL}} & \text{for TDD} \\ 1 & \text{for TDD with unknown } r_{DL} \\ 1 & \text{for FDD} \end{cases} \quad (28)$$

The choice of $\sqrt{r_{DL}}$ is determined by the interpretation of the E-field limits as a quadratic time average of the electric field strength.

3.3.2.3.4 Beam statistic factor

For each NR-cell i of the base station, a statistical factor K_i^{stat} is defined to take into account the variability of the transmission direction and of the antenna pattern from adaptive antennas.

The definition of the statistical factor K_i^{stat} is still under study by METAS. For the moment, the following conservative value is considered $K_i^{stat} = 1$.

3.3.3 5G NR EMF extrapolation “Proposal 3”

“Proposal 3” is taken from a paper written by Helmut Keller of Narda Safety Test Solutions GmbH ([80]).

This proposal provides two methods for extrapolating to the theoretical maximum exposure based on SS/PBCH block measurements. The first method is based on a frequency selective measurement of the field strength of the SS/PBCH block, and the second method is based on a code selective measurement of the field strength of the Synchronization Signals (PSS and SSS).

3.3.3.1 Frequency selective extrapolation

The first precondition for this method is that resource elements outside the SS/PBCH blocks are never transmitted with a higher power and a higher antenna gain due to beamforming compared to the non-zero resource elements used in SS/PBCH blocks. The second precondition is that all non-zero resource elements used in SS/PBCH blocks are transmitted with a constant power and a constant antenna gain due to beam forming. It is not clear yet under which circumstances these two preconditions are met in real 5G NR systems.

If both preconditions are met, the maximum theoretical exposure can be calculated by using equation (29) [80].

$$E_{propos3-fsm}^{5G,max} = EI_{max} = \frac{E_{SSblock}^2}{E_{ref}^2} \times \frac{N_{SC}}{127} \times k_{TDD} \times k_{system} \quad (29)$$

The maximum field strength $E_{SSblock}$ is measured with a channel filter, which is 127 subcarriers broad and centered at the center frequency of the SSS and

PSS. The averaging time of the applied rms detector must be shorter than the length of four symbols to be able to settle within the length of an SS/PBCH block completely. On the other side, the averaging time should not be much shorter to attenuate short time-level fluctuations as much as possible.

The parameter E_{ref} is the reference level for the electric field strength at the center frequency of the SSS and PSS.

The parameter N_{SC} is the total number of subcarriers used in the associated 5G NR channel. $N_{SC} = 12 \times N_{RB}$ as already shown in 3.3.1.1 (Figure 51 and Figure 52).

The parameter k_{TDD} is the ratio of the maximum downlink time within a frame to the total frame length.

The parameter k_{system} is a parameter which is set to unity by default but might be different for special system settings.

Note that the power of SS/PBCH blocks from different cells, which coincide in frequency, can't be separated by this method. The extrapolation will extrapolate to the total exposure due to all received cells in this case.

3.3.3.2 SS demodulation-based extrapolation

The second method proposed by “Proposal 3” is called SS demodulation-based extrapolation. The basic idea behind it is that the received signal strength of PSS and SSS can be measured separately for each cell if a part of the cell search procedure is implemented in a measurement device. The advantages compared to the frequency selective method are that the first precondition of the frequency selective method is not necessary and that the exposure due to different cells can be separated. Note that the second precondition of the frequency selective method is also necessary. The maximum theoretical exposure can then be calculated applying (30) [80].

$$E_{proposal\ 3-ssdm}^{5G, max} = EI_{max} = \frac{E_{SSS}^2}{E_{ref}^2} \times \frac{N_{SC}}{127} \times k_{TDD} \times k_{system} \quad (30)$$

Using this method, one would implement the initial part of a cell search procedure in a measurement device and then identify the SS/PBCH blocks with the highest field strength E_{SSS} of the SSS.

3.3.3.3 k_{system} parameter

The parameter k_{system} is a parameter which is set to unity by default but might be different for special system settings. For example, it must be set to

0.5 if the resource elements of the SS/PBCH block are transmitted with twice the power of the other resource elements.

In the general case, k_{system} is a product of up to five factors reflecting five potentially relevant aspects of the system settings and the environment, which may affect SS and traffic load differently:

- The first aspect is the difference of the transmitted power per resource element;
- The second aspect is the gain difference of the used beams;
- The third aspect is the difference of the use of two polarization planes;
- The fourth is the difference of the combined envelope of the beams;
- The fifth aspect is the different influence of reflectors.

It will be difficult in practice to get precise values for all of these five factors, but probably some of them will be available from the network providers and some of them will be estimable.

3.3.4 5G NR EMF extrapolation “Proposal 4”

“Proposal 4” is taken from a paper developed by the Department of Information Technology of Ghent University and Ericsson ([81]).

This proposal provide a comprehensive and ready-to-use exposure assessment methodology for use with common spectrum analyser equipment to measure and calculate in-situ the theoretical maximum exposure from 5G NR base stations.

This proposal also comprises a number of steps that involve the identification of the Synchronization Signal Block, which is the only 5G NR component that is transmitted periodically and at constant power.

3.3.4.1 Theoretical maximum exposure

The exposure level at an evaluation point in line of sight (LOS) of a 5G NR base station will reach the maximal value when the traffic load is at its maximum (i.e., when the 5G NR frame is completely filled with downlink data) and all traffic is transmitted at the maximum possible gain G_{max} in the direction of the evaluation point. Then, to obtain the worst-case (theoretical maximum) exposure level E_{max} , the electric-field strength per RE of the dominant SSB beam ($E_{RE,SSB}$) is extrapolated based on the bandwidth of the channel and the radiation pattern of the traffic beam(s) (31) [81].

$$E_{proposal4}^{5G,max} = E_{max} = \sqrt{\alpha} \sqrt{12 N_{RB}} E_{RE,SSB} \quad (31)$$

The term N_{RB} is the number of resource blocks available over the 5G NR channel bandwidth, as already shown in 3.3.1.1 (Figure 51 and Figure 52).

While the term $\alpha = \frac{G_{max}}{G_{SSB}}$ is the ratio of G_{max} to the gain of the dominant SSB, G_{SSB} .

This ratio has to be derived based on the pattern of the base station product.

3.3.4.2 Assessment procedure

While 5G NR demodulation software can assist in locating the SSB, identifying its numerology, and measuring its power per RE, this proposal provides a procedure usable with a common spectrum analyzer (SA).

The proposed measurement methodology consists of four steps:

- Step 1 “Spectrum overview” — Overview measurement of the telecommunications frequency range to identify the RF signals that are present at the measurement location and in particular the 5G NR signal from the base station under test;
- Step 2 “Locating the SS burst” — An important step in the assessment of a 5G NR signal based on extrapolation of the SSB power, is the determination of the actual location of the SS burst. In this step, SS_{REF} as well as the numerology of the SSB(s) are identified;
- Step 3 “Obtaining the field level per RE of the SSB’ — Measurement of the electric-field strength per resource element of the dominant SSB, $E_{RE,SSB}$;
- Step 4 “Post-processing” — Extrapolation of $E_{RE,SSB}$ to the theoretical maximum exposure level E_{max} by using (31).

The SA settings provided by this proposal for each step of the measurement procedure can be found in Table 3. It is important to note that the mentioned settings may be specific to measurement equipment used by the authors of this proposal, but equivalent settings for other equipment can be used.

It must be noted that original procedure provided this proposal has five steps and Step 4 is indicate as Step 5 in the paper. Only the steps relevant to theoretical maximum exposure are presented in this section.

	<i>Step 1</i>	<i>Step 2</i>	<i>Step 3</i>
<i>SA mode</i>	Frequency	Frequency	Zero-span
<i>CF</i>	3350	CF or 5G channel	SS _{REF}
<i>Span [MHz]</i>	5300	100	0
<i>Detector</i>	peak	rms	rms
<i>RBW [MHz]</i>	0.3	1	1
<i>SWT [s]</i>	177	14.4x10 ³	x
<i>Number of sweep point</i>	17667	101	32001
<i>Sweep mode</i>	max-hold	actual	actual
<i>Measurement time [s]</i>	177	20	60

Table 3: Spectrum analyzer settings for sub-6 GHz 5G signals [81].

Referring to Table 3:

- CF = center frequency, RBW = resolution bandwidth, SWT = sweep time, SS_{REF} = CF of the SS/PBCH block, RBW_{SA} = maximum RBW of the SA, rms = root-mean-square;
- $x = 32001 \times \text{SSB symbol time}$, such that the measurement time per sample is equal to the SSB symbol time.

3.3.4.2.1 Settings for step 1

In the first step, a spectrum overview measurement is used to identify the RF signals present in the frequency range used by telecommunication signals (e.g., 700 MHz – 6 GHz). The proposed settings can be found in Table 3.

In order to distinguish between different telecommunication signals (2G–5G), the resolution bandwidth (RBW) is set to a value approximating the minimal bandwidth of the existing telecommunications signals, which is 200 kHz (used by 2G). By using a peak detector in combination with a long sweep time (SWT) and maximum-hold mode, and measuring until the display of the SA is relatively stable, all non-continuous but repetitive signals present at the measurement location are detected. The measurement time per sample is set equal to the duration of one 5G NR radio frame (i.e. 10 ms), by configuring the SWT accordingly.

Figure 57 show an example of Step 1.

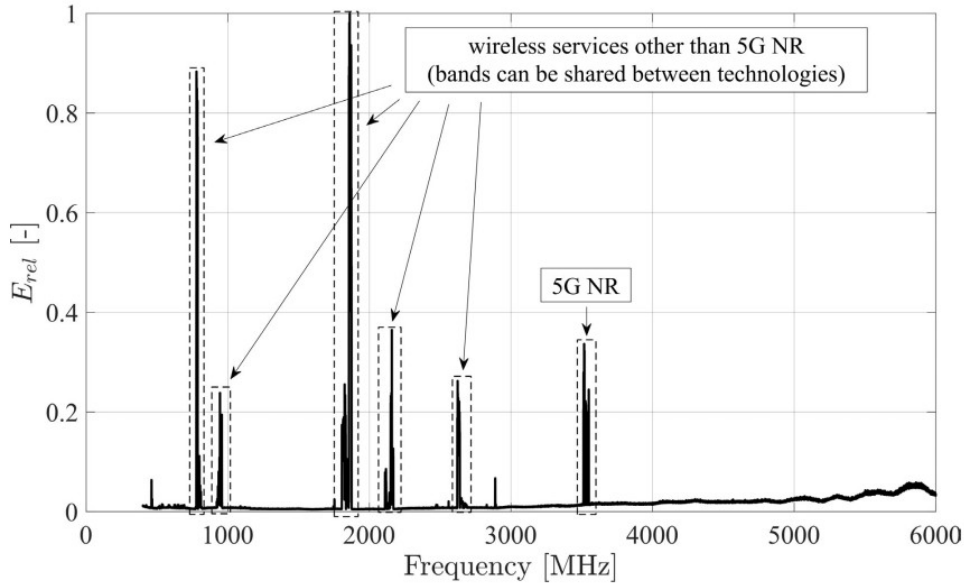


Figure 57: Example of Step 1 [81].

It is important to note that, with these settings, the measured power levels provide only an indication of the peak values (typically a large overestimate due to the effect of modulation) and no further conclusions can be made.

3.3.4.2.2 Settings for step 2

After 5G NR channel is identified, the frequency positions of their broadcast signals are located. If, at the location of assessment, SS_{REF} and the SSB numerology (which defines the BW of the SSB) were not provided by the operator and thus unknown, they can be determined using the following measurement (settings in Table 3).

As already shown in 3.2.10, as opposed to the constituting signal equivalents in LTE, in 5G NR the SSB is not fixed to the center frequency of the radio channel, but instead its position (denoted by SS_{REF}) is determined by the Global Synchronization Raster Channel (GSCN) value, which fixes it on a discrete raster.

The center frequency (CF) of the considered 5G NR channel is obtained from the previous step (or from operator information). The frequency span is set to 100 MHz, which is the largest BW for sub-6 GHz 5G NR signals, and the RBW to 1 MHz, as this is the widest possible setting for our measurement setup narrower than the minimum bandwidth of the SSB (i.e. 1.9 MHz for SCS 15 kHz). Furthermore, the measurement time per sample or sweep point is set to 143 μ s, which is the shortest duration of the SSB in case of sub-6 GHz 5G NR signals (SCS 30 kHz). In combination with 101 sweep points, this corresponds to an SWT of 14.4 ms. In the absence of traffic, which may be transmitted at a higher gain than the broadcast signals,

these settings result in the highest power levels when the SA sweeps the (exact) frequency and time range of an SSB, i.e., when within the measurement time per sample, exactly two (SCS 15 kHz) or four symbols (30 kHz) were transmitted at the same power.

Hence, by plotting the maximum power per frequency over all measurement traces, we are able to identify the SSB frequency range. With additional consideration about the possible frequencies provided by the GSCN, it is possible to find the exact location of SS_{REF} .

Figure 57 show an example of Step 2.

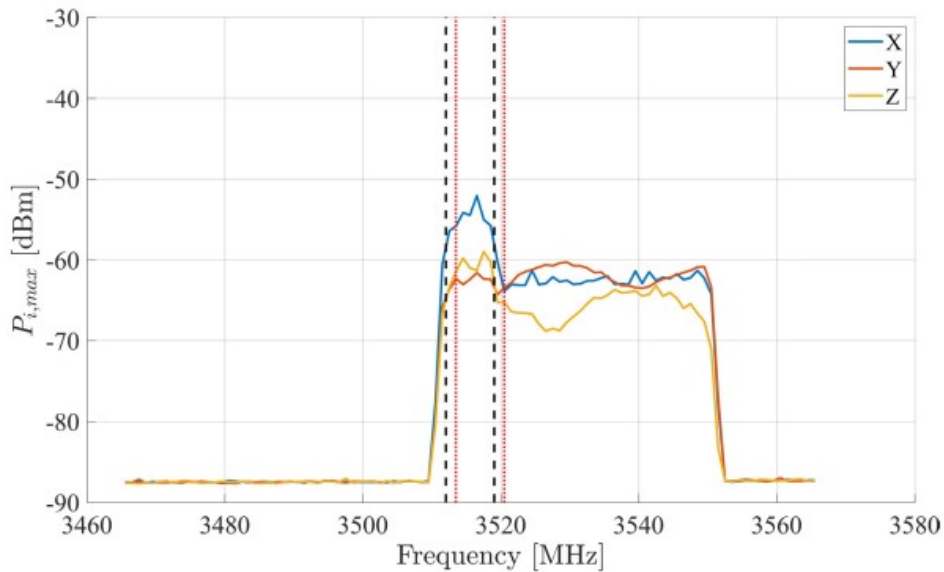


Figure 58: Example of Step 2 [81].

3.3.4.2.3 Settings for step 3

Thirdly, the power distribution of the REs that are part of the SSB is determined. As we are looking for a recurrent signal of a certain duration (which depends on the structure of the SS burst), aligning measurement samples in time should show us when the SS burst was transmitted. Then, we retain only those samples that were measured during the dominant SSB of the SS burst. The proposed settings for this measurement are previously reported in Table 3.

In order to continuously measure the power received in the SSB frequency range, a zero-span measurement is chosen, i.e., a measurement of the received power within a certain frequency band as a function of time, with SS_{REF} as CF and an RBW that is smaller than or equal to minimum BW of SS/PBCH block. To average out the variations in time (due to OFDM modulation) and in frequency, a measurement time per sample about equal to the symbol time of the SSB and an RBW of at least 1 MHz are proposed,

in combination with a root-mean-square (rms) detector (Table 3). Finally, to determine the power per RE (i.e. over a BW equal to the SCS), a deduction factor has to be applied to the resulting power measurements [81].

$$f_{BW} = 10 \log_{10}(RBW / SCS) \quad (32)$$

By plotting the measurement samples such that the x-axis holds two radio frames of 10 ms, or 560 symbols, and successive two-frame periods are stacked along the y-axis, while the color of the pixel indicates the power P received by the SA averaged (RMS detector) over the duration of one symbol, one can visualize the diversity and periodicity of the 5G NR signal components that are transmitted within the measured bandwidth (it is called a “waterfall reconstruction”).

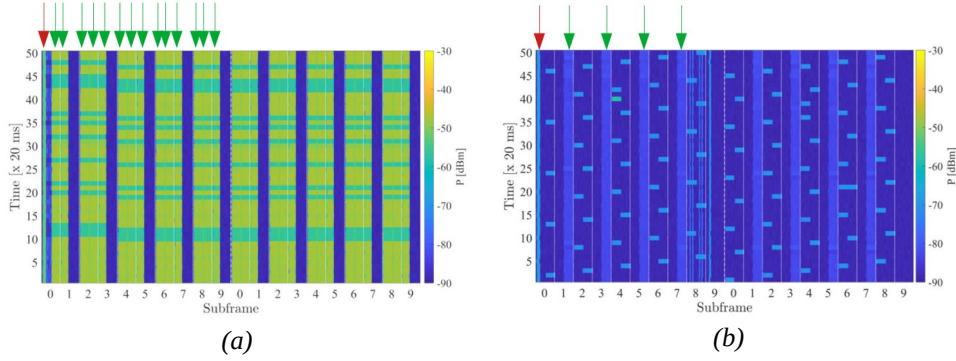


Figure 59: Example of "Waterfall reconstruction" plots of measurement traces of the X-component of the electric field [81]; (a) downlink session forced where red arrow indicates ssb slot and green arrows indicate downlink slots; (b) uplink session forced where red arrow indicates ssb slot and green arrows indicate uplink slots.

3.3.4.2.4 Post-processing for step 4

With the knowledge acquired from steps from 1 to 3 it is possible to calculate the theoretical maximum exposure level E_{max} by using (31).

Although not specified, also this proposal provide a factor that takes into account the possible use of TDD duplexing scheme. The allocation of downlink traffic is shown in Figure 59(a) roughly three out of every four slots (in fixed subframes) were allocated to downlink traffic. Figure 59(b) shows slots allocated to uplink traffic, essentially complementary to downlink traffic. From these results is easy to obtain the F_{TDD} factor.

Referring to $\alpha = G_{max} / G_{SSB}$, since it is possible to distinguish SSB signals from traffic signals in the measurements of Step 3 (Figure 59), it is possible to derive an approximation of the maximum gain difference between broadcast and traffic beams.

In Figure 60, the distributions of the SSB (orange) and the traffic samples (green) for the X -component of the electric field are compared. It is

interesting to note that SSB samples follow one Gaussian distribution while the traffic samples follow a mixture of three Gaussian distributions. These distributions correspond to different amounts of RBs (or REs) allocated to traffic signals within the part of the channel bandwidth demarcated by the configured RBW around SS_{REF} . By taking into account the difference in power between the SSB distribution and the dominant Gaussian of the traffic samples for all three components, a total difference in gain could be obtain. From this value is easy to obtain parameter α .

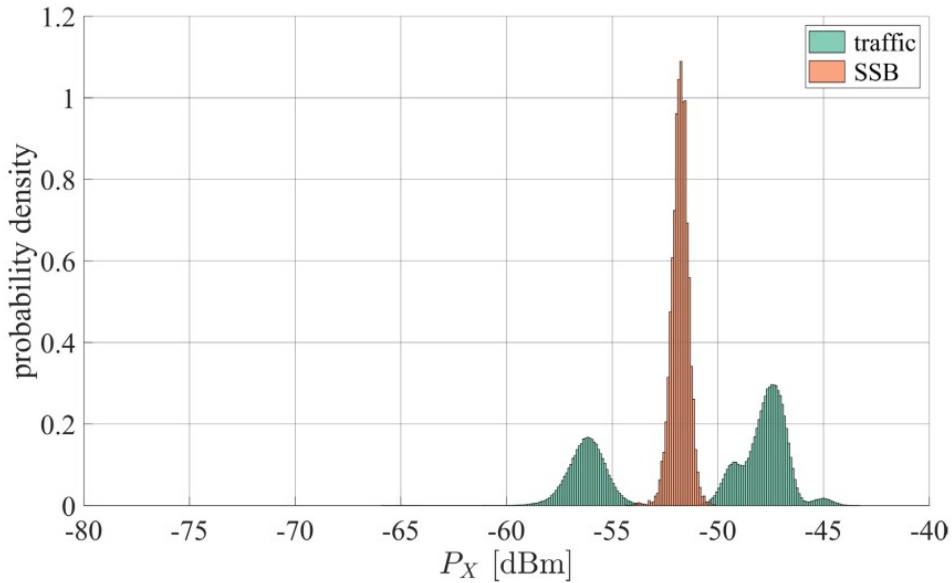


Figure 60: Example of histogram of the total power (of the X -component of the electric field) captured for SSB (in orange) and traffic signals (in green) [81].

3.4 Conclusion

After 5G general aspects and a more detailed technical review on 5G access network, this chapter addressed to 5G specific control signals and 5G EMF extrapolation proposals from open scientific literature. Four different proposals were presented. Although proposals give a different final formula, they have a common approach to the problem.

The common approach could be summarized in the following steps:

1. Measure one or more signals from SS/PBCH block (pilot signal) and obtain the maximum EMF level on resource element basis, or rather for a single subcarrier;
2. Identify a parameter representing the total number of subcarriers inside the bandwidth of the 5G NR signal under analysis;
3. Identify a parameter taking into account the possible use of TDD duplexing scheme;

4. Identify a parameter taking into account the boost of the traffic beams respect to maximum EMF level received from the pilot signal.

Referring to step 4, a possible way to estimate the parameter is by numerical simulation, as proposed by “Proposal 2”. Another way to estimate the parameter is by experimental measurement as proposed in other proposals. Although experimental measurements have the problem to force data traffic, numerical simulation alternative requires the complete knowledge of the antenna patterns and the environment.

Applying these previous steps, the proposals are able to extrapolate the theoretical maximum exposure level of the 5G NR signal in a specific measurement point.

Table 4 shows a summarization of the parameters used by Proposals presented in this chapter.

	<i>Proposal 1</i>	<i>Proposal 2</i>	<i>Proposal 3</i>	<i>Proposal 4</i>
<i>Measurement Type</i>	Decoder	Decoder	Decoder	Basic SA
		Basic SA	Basic SA	
<i>Measured value per RE</i>	PBCH-DMRS	SSS	SSS	SS/PBCH
		SSS	SS/PBCH	
<i>Total number of RE</i>	N_{SC}	$K_i^{SSS(RE)}$	N_{SC}	$12 \cdot N_{RB}$
<i>Downlink duty cycle</i>	F_{TDC}	K^{duplex}	k_{TDD}	F_{TDD}
<i>Differences between control signal and data signal beam</i>	F_{beam}	$K_i^{antenna}$	k_{system}	α

Table 4: Parameters summarization.

It must be noted that, the theoretical maximum exposure level obtained, gives the maximum field level in an ideal condition in which a single user is connected at the maximum power using all the resources for a continuous time interval that, considering the ICNIRP guidelines [5], must be not shorter than 6 minutes. In other words, theoretical maximum exposure level is a theoretical value that is not reached in any practical condition. The average amplitude of the field actually received in real conditions is generally significantly lower than the value obtain by formulas proposed by the four proposal presented.

For this reason, a more realistic field level, i.e. an “actual” maximum exposure level, requires to take into account an additional factor based on statistical considerations.

The four proposals presented in this chapter introduce an additional statistical factors as shown in Table 5, but these factors are only mentioned and addressed to future works.

	<i>Proposal 1</i>	<i>Proposal 2</i>	<i>Proposal 3</i>	<i>Proposal 4</i>
<i>Statistical factor (under development)</i>	F_{PR}	K_i^{stat}	k_{system}	<i>Spatial duty cycle</i>

Table 5: Additional statistical factor.

The estimation of this additional factor is extremely complex since the exposure of a user depends also on the activity of the other users.

Before to start with the chapters dedicated to experimental field testing, the next chapter will approach to “5G and 4G coexistence”. As shown in Figure 30, in first part of this chapter, there are several way to access to a 5G system with two major operating modes, the Non Stand-Alone (NSA) and Stand-Alone (SA) modes. In 5G NSA mode an UE can access to 5G resource only passing through an anchor to 4G system. The first implementations of 5G are and will be in NSA mode. To rapidly increase coverage of 5G, some operators may use an additionally feature. This feature is known as Dynamic Spectrum Sharing (DSS) and enables the transmission of 5G signals inside 4G spectrum.

4 5G NR and 4G LTE Coexistence

5G is not only poised to be the fastest cellular transition ever, but also the smoothest, thanks to innovations in the 5G standard that enable a phased evolution and tight interoperability with current 4G networks. Key 5G features that facilitate the transition from non-standalone (NSA) mode of operation include 4G/5G dual connectivity and Dynamic Spectrum Sharing (DSS).

4.1 NSA mode and 4G/5G dual connectivity

The NSA mode of operation introduced in 3GPP Release 15 [82] allows 5G deployments to utilize LTE core networks and base stations, while adding new 5G base stations. NSA allows mobile operators to introduce 5G and increase overall network capacity – thanks to the wider bandwidths in new bands in which 5G will be deployed, along with all the advanced radio techniques built into 5G – while relying on an anchor in the 4G radio access and core network.

All commercial 5G network rollouts are expected to use NSA mode with 5G New Radio (NR) deployed on either millimeter wave (mmWave) high bands or sub-6 GHz bands (2.5/2.6 GHz, 3.5/4.5 GHz or 600 MHz), while utilizing lower bands for the LTE anchor (<2.7 GHz). Instead of having to wait to launch 5G while an anchor 5G network is built, NSA allows 5G to be launched much sooner on top of a 4G anchor.

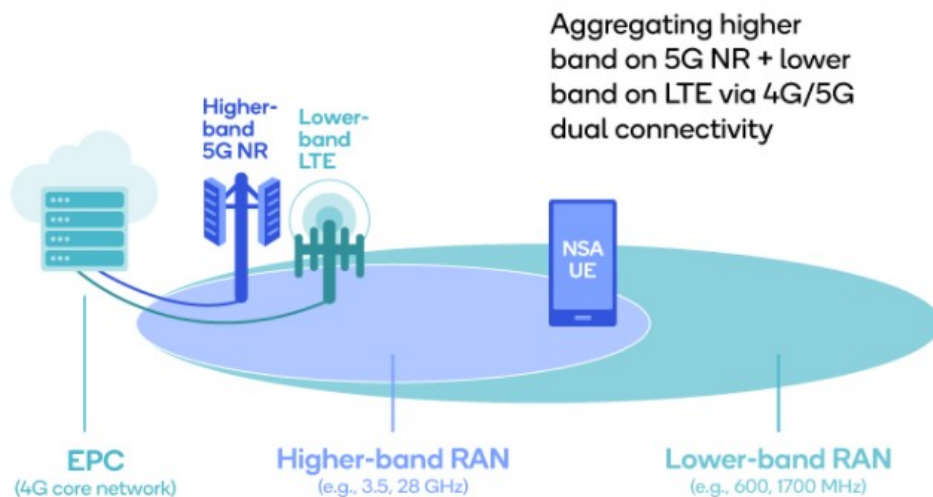


Figure 61: Non-standalone mode and 4G/5G dual connectivity scenario [83].

5G NSA mode utilizes dual connectivity with 4G and 5G radios, which allows devices to send and receive data using 4G and 5G simultaneously to independent sites as needed. In this scenario, the network is not just using a

4G anchor. It's carrying traffic over both 4G and 5G, each in its own spectrum, aggregating the content in the device. By using both 4G and 5G at once to carry data, users get much faster connectivity than if they were using only one or the other. In fact, results from real world deployments show that users are getting multi-gigabit speeds where this dual connectivity technique is deployed.

4.2 Dynamic Spectrum Sharing

A related issue in easing the transition to 5G is how to deploy 5G in spectrum currently used for 4G. In prior transitions from one G to another, this was done via “refarming.” If a spectrum band was used for 3G, before 4G could be deployed, the band had to be emptied of 3G users; it had to be refarmed. That process could take years, sometimes a decade or more — a very lengthy transition.

In 3GPP Release 15, a feature called 5G DSS, or Dynamic Spectrum Sharing, obviates the need for refarming, thereby greatly accelerating the 5G transition. In effect, 5G DSS turns virtually any band used with 4G LTE today into a band in which 5G can also be deployed immediately. This feature will typically be deployed in low sub-6 GHz frequencies, providing much better 5G coverage.

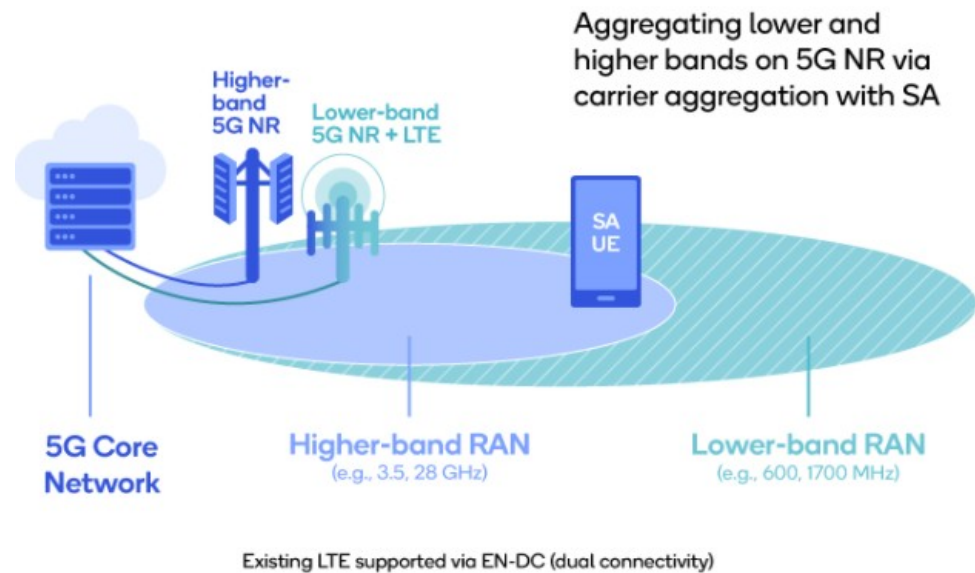


Figure 62: Dynamic Spectrum Sharing scenario [83].

The coverage benefits of DSS are a stepping stone to the introduction of 5G standalone (SA) mode of operation, which implements 5G end-to-end from core network to radio access, without the usage of an anchor 4G network.

The DSS concept is based on the flexible design of NR physical layer. It uses the idea that NR signals are transmitted over unused LTE resources. With LTE, all the channels are statically assigned in the time-frequency domain, whereas the NR physical layer is extremely flexible for reference signals, data and control channels, thus allowing dynamic configurations that will minimize a chance of collision between the two technologies.

One of the main concepts of DSS is that only 5G users are made aware of it, while the functionalities of the existing LTE devices remain unaffected (i.e. LTE protocols in connected or idle mode). Therefore, fitting the flexible physical layer design of NR around that of LTE is needed in order to deploy DSS on a shared spectrum.

4.2.1 DSS Deployment Options

NR offers a scalable and flexible physical layer design depicted by various numerologies. There are different subcarrier spacing (SCS) for data channels and synchronization channels based on the band assigned. This flexibility brings even more complexity because it overlays the NR signals over LTE, which requires very tight coordination between gNB and eNB in order to provide reliable synchronization in radio scheduling.

3GPP did not define one monolithic solution for spectrum sharing, but rather a set of tools. Some of them serve the exclusive purpose of operating NR and LTE on a common carrier. Other NR configurations, such as various PDCCH mappings or demodulation reference signal (DMRS) positions, are vital for spectrum sharing but are also used in other contexts.

There are three DSS Deployment Options:

- Option 1: DSS MBSFN-based;
- Option 2: DSS Mini-slot-based (non MBSFN-based);
- Option 3: DSS Rate-matching-based (non MBSFN-based).

Using one of the DSS options does not eliminate others. Despite each one has its own advantages and disadvantages, they all can find their proper application depending on particular configuration and they can be mixed to enable an optimal DSS solution.

4.2.1.1 DSS MBSFN-based

The main foundation of DSS is to schedule NR users in the LTE subframes while ensuring no respective impact on LTE users in terms of essential channels, such as reference signals used for synchronization and downlink measurements. LTE Cell Reference Signals (CRS) are typically the main

concept where DSS options are designated, as CRS have a fixed time-frequency resource assignment. The CRS resources layout can vary depending on the number of antenna ports. More CRS antenna ports leads to increased usage of Resource Elements (REs). CRS generates from 4.76% (1 antenna port) up to 14.29% (4 antenna ports) overhead in LTE resources.

As CRSs are the signals used for downlink measurements, avoiding possible collision with CRS is one of the foundations of the DSS options shown in figure 1. The other aspect of DSS design is to fit the 5G NR reference signals within the subframes in a way to avoid affecting NR downlink measurements and synchronization. For that, DSS considers the options shown in figure 1 to ensure NR reference signals such as Synchronization Signal Block (SSB) or Demodulation Reference Signal (DMRS) are placed in time-frequencies away from any collision with LTE signals.

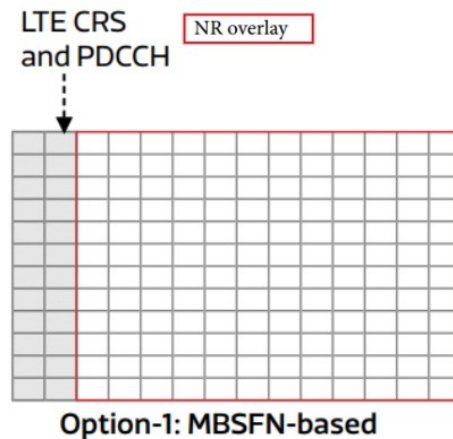


Figure 63: DSS Option-1: MBSFN-based [84].

MBSFN, option 1 in Figure 63, stands for Multi-Broadcast Single-Frequency Network and is used in LTE for point-to-multipoint transmission such as eMBMS (Evolved Multimedia Broadcast Multicast Services). The general idea of MBSFN is that specific subframes within an LTE frame reserve the last 12 OFDM symbols of such subframe to be free from other LTE channel transmission. These symbols were originally intended to be used for broadcast services and are “muted” for data transmission in other LTE UE. Now this idea has been adjusted for use in a DSS concept, so that these reserved symbols are used for NR signals instead of eMBMS.

Using MBSFN is completely transparent to legacy LTE-only devices from 3GPP Release 9 onwards, as such LTE UE knows that these subframes are used for other purposes. In this sense, this is the simplest way of deploying DSS. This method has disadvantages though. The main one is that if MBSFN subframes are used very frequently and it takes away resources from LTE users, heavily reducing LTE-only user throughput. Note that

option 1 shown in Figure 63 does not require LTE MBSFN Reference Signals to be used, because the MBSFN subframe is used to mute the subframe for DSS operation only, and LTE CRS shall only be transmitted in the non-MBSFN region (within the first two symbols) of the MBSFN subframe.

4.2.1.2 DSS Mini-slot-based (non MBSFN-based)

The other option illustrated in Figure 64 is dealing with non-MBSFN subframes that contain LTE reference signals. Option 2 is ‘mini-slot’ based; mini-slot scheduling is available in NR for URLLC applications that require extremely low latency. The symbols can be placed anywhere inside the NR slot. In respect to DSS, mini-slot operation just eliminates the usage of the symbols that contain LTE CRS and schedule only free ones for NR transmission.

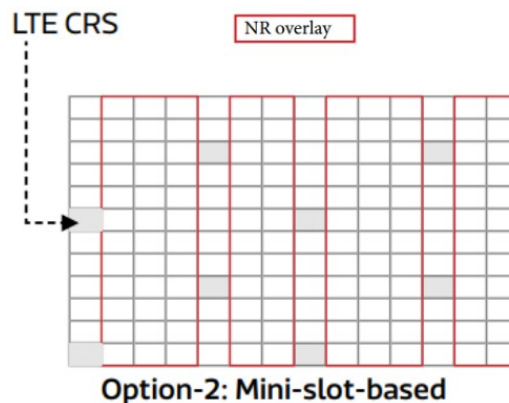


Figure 64: DSS Option 2: Mini-slot-based (non MBSFN-based) [84].

The basic limitation of this method comes from the concept itself. It is not very suitable for eMBB applications as too many resources are outside of NR scheduling. However it still can be utilized in some special cases like 30 kHz SSB insertion.

4.2.1.3 DSS Rate-matching-based (non MBSFN-based)

Option 3 is based on CRS rate matching in non-MBSFN subframes, and it is expected to be the one most commonly used for NR data channels. In this option, the UE performs puncturing of REs used by LTE CRS so that the NR scheduler knows which REs are not available for NR data scheduling on PDSCH. The implementation of this option can be either Resource Block (RB)-level when the whole RB containing LTE CRS is taken out of NR scheduling, or RE-level where NR PDSCH scheduling avoids particular REs only. The end result of this method is that the scheduler will reduce the

NR PDSCH transport block size as the number of REs available for scheduling become less in a slot.

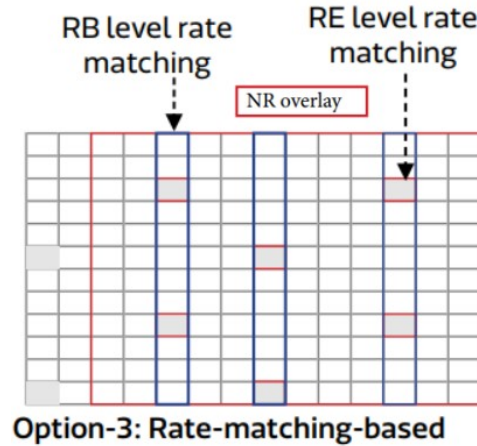


Figure 65: Option 3: DSS Rate-matching-based [84].

For better spectral efficiency, CRS RE-level rate-matching is preferred when compared to RB-level rate matching in NR PDCCH/PDSCH 15 kHz SCS. However for NR PDCCH/PDSCH at 30 kHz SCS, only RB-level rate matching is suitable because of the difference in numerologies with LTE. Another application for RB-level rate matching is to avoid collisions with the other LTE synchronization channels (PSS/SSS/PBCH).

4.2.1.4 Rate-matching “RE-level vs. RB-level”

Table 6 compares the available REs per RB in a slot, depending on the underlying LTE CRS configuration. As shown in Table 6, LTE CRS within an RB occupies four symbols (#0, 4, 7, 11) for one or two antenna ports and two additional symbols (#1, #8) for four CRS antenna ports.

LTE CRS Configuration	RE rate-matching	RB rate- matching
LTE 1 CRS port: 6 RE overhead in NR PDSCH region, or 3 symbols with RB Rate Matching	126 RE	96 RE
LTE 2 CRS port: 12 RE overhead in NR PDSCH region, or 3 symbols with RB Rate Matching	120 RE	96 RE
LTE 4 CRS port: 16 RE overhead in NR PDSCH region, or 4 symbols with RB Rate Matching	116 RE	84 RE

Table 6: RE-level vs. RB-level CRS Rate Matching [84].

Each CRS symbol consists of two subcarriers for each antenna port. However, since the first two symbols are occupied by LTE PDCCH, they are not considered for rate matching overhead of the NR PDSCH.

Then, the overall overhead generated by CRS is shown in Table 7.

<i>LTE CRS Configuration</i>	<i>CRS symbols [A]</i>	<i>Subcarriers [B]</i>	<i>CRS RE overhead [C=AxB]</i>
LTE CRS 1 port	3	2	6
LTE CRS 2 port	3	4	12
LTE CRS 4 port	4	4	16

Table 7: CRS overhead, in terms of Resource Elements, for different LTE CRS configuration [84].

As NR PDSCH scheduling can only occur after the second symbol in the slot where the third symbols is occupied for NR PDCCH (first two symbols are for LTE PDCCH), as a result, NR PDCSCH is scheduled with 11 symbols out of the total 14 symbols available in a slot. Then, $12 \text{ RE} * 11 \text{ Symbols}$ results in 132 RE available in a slot for NR PDSCH. In the case of one LTE CRS antenna port, the total available NR PDSCH REs available in a slot per one RB is $132-6 = 126 \text{ REs}$, $132-12 = 120 \text{ REs}$ with two CRS antenna ports, and $132-16 = 116 \text{ REs}$ with four CRS antenna ports. On the other hand, if the entire RB in a slot is being muted, 3 (one and two CRS ports) and 4 (otherwise) symbols will be rate matched, resulting in 12 RE per RB $*(11 \text{ symbols available for PDSCH} - 3 \text{ CRS symbols muted within NR slot}) = 96 \text{ REs}$ available for NR PDSCH with one or two CRS antenna ports, and 12 RE per RB $*(11 \text{ symbols available for PDSCH} - 4 \text{ CRS symbols muted within NR slot}) = 84 \text{ REs}$ available for NR PDSCH with four CRS antenna ports. This means that the transport block size for NR PDSCH will be higher in RE rate matching and hence better spectral efficiency.

4.2.2 Combining DSS Deployment Options

This section shows examples of NR transmissions inside LTE frame to demonstrate the importance of combining different DSS deployment options.

4.2.2.1 SS/PBCH transmission (MBSFN-based)

As shown in 3.2.7, SSB consists of synchronization signals (PSS and SSS) and a Physical Broadcast Channel (PBCH). For a half frame (5 msec) SSB transmission, the SSB contains 4 OFDM symbols in the time domain and 240 contiguous subcarriers (20 RBs) in the frequency domain. The subcarrier spacing (SCS) used for SSB is dependent on the frequency band. In case of FR1, it can be either 15 kHz or 30 kHz. In time domain, there is a number of options of SSB location depending on the band used and SCS. 3GPP TS 38.101-1 [74] contains pre-defined tables of starting symbol indices per band, marked as Case A, B or C in FR1.

SSB Subcarrier Spacing	$f \leq 3$ GHz	Band Example ($f \leq 3$ GHz) based on TS 38.101-1
Case A : 15 kHz	NR SSB Symbols within one LTE subframe = (2,3,4,5),(8,9,10,11)	FDD band n3, n5, or TDD band n41
Case B : 30 kHz	NR SSB Symbols within one LTE subframe = (4,5,6,7),(8,9,10,11),(16,17,18,19),(20,21,22,23)	FDD band n5
Case C : 30 kHz	NR SSB Symbols within one LTE subframe = (2,3,4,5),(8,9,10,11),(16,17,18,19),(22,23,24,25)	TDD band n41

Table 8: SSB Starting Symbol Indices for FR1 [84].

Table 8 illustrates SSB allocation in time domain for FR1 cases in a frequency range ≤ 3 GHz only, where DSS can be applied at the moment. In the frequency domain, up to four SSB beams can be transmitted in the FR1 range ≤ 3 GHz.

As discussed in previous section, DSS can be implemented in MBSFN or non-MBSFN options. The non-MBSFN can be easily used to allocate NR PDSCH channel used for data transmission. In this case rate matching can be used to avoid the REs occupied by LTE CRS. However, for NR SSB, puncturing the channel becomes impossible as it may affect the downlink measurements and synchronization. Therefore, SSB in a DSS cell must be transmitted in a way to totally avoids all symbols and subcarriers occupied by LTE CRS. Figure 66 shows the impact of SSB transmission inside a non-MBSFN subframe. The upper part of the figure depicts NR resource grid, while the lower part is the corresponding LTE non-MBSFN subframe.

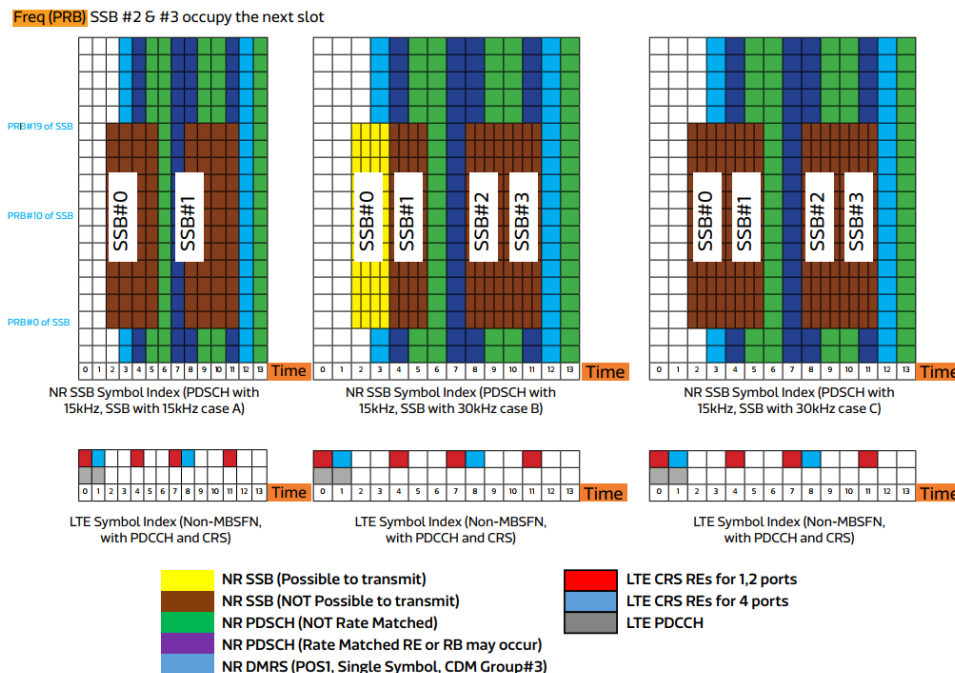


Figure 66: Impact of Spectrum Sharing on NR SSB Channel: Non-MBSFN [84].

In this example, it is always assumed that NR PDCCH/PDSCH SCS is 15 kHz to match the LTE subframe, which is expected to be the case used for the initial DSS implementation. With NR PDCCH/PDSCH SCS of 15 kHz, there is one NR slot per NR subframe and 10 NR slots per NR frame. Therefore, in this example, the terms “slot” and “subframe” are used interchangeably. This example assumes the channel configurations of 20 MHz bandwidth for DSS, unless mentioned otherwise. Starting with SSB 15 kHz Case A, the leftmost grid of Figure 66 shows both SSB beams that can be transmitted in one NR slot (i.e. one LTE subframe) colliding with LTE CRS. This makes such configuration totally not suitable for DSS, because once any SSB symbol collides with CRS it eliminates transmission of the whole SSB beam. The central grid in Figure 66 shows SSB 30 kHz Case B where all four beams can be transmitted in one slot because of wider SCS than the NR PDCCH/PDSCH 15 kHz SCS. One out of four SSB beams can be transmitted from gNB avoiding collision for SSB#0, yet other 3 bursts remain unavailable at least in LTE four antenna ports scenario. In this case NR mobility can be affected as we are left with one beam only. SSB 30 kHz Case C represented in the right side of Figure 66. Just like Case A, it has collisions with LTE CRS in all four SSB beams making its use impossible in LTE four CRS port scenario and limited to only one SSB beam in case LTE one or two CRS ports.

Different results can be achieved using an MBSFN subframe for SSB transmission and Figure 67 clearly shows why. Since MBSFN mutes the entire 12 symbols of the subframe, then SSBs do not have LTE CRS collision, and the impact on all SSB cases is minimal.

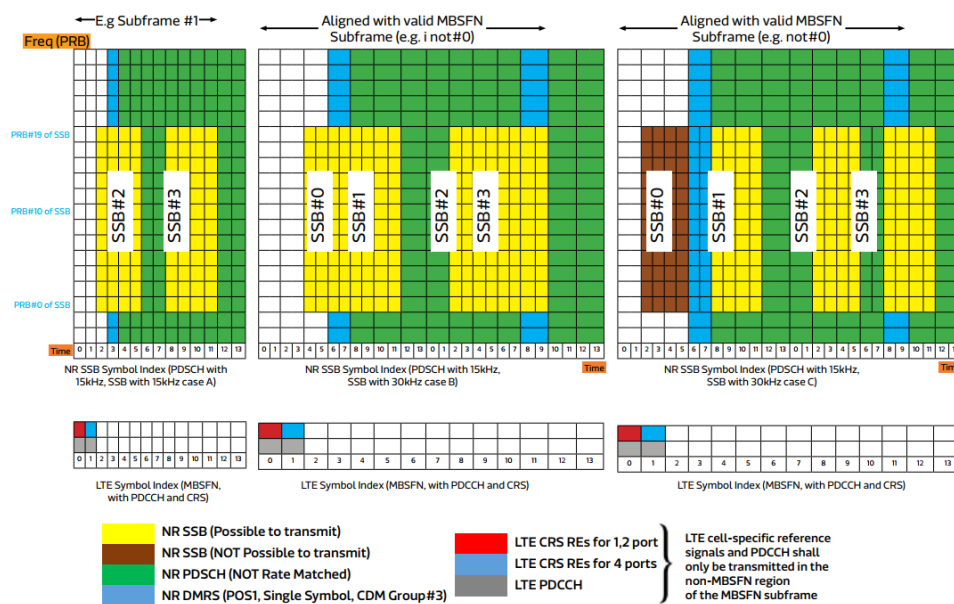


Figure 67: Impact of Spectrum Sharing on NR SSB Channel: MBSFN [84].

The only limitation for SSB Case C comes from LTE PDCCH and CRS transmitted in the first two symbols of the subframe which cause collision with SSB#0 making three SSBs available out of four. However, for MBSFN case, subframe alignment with NR SSB slots is essential.

4.2.2.2 NR Channels transmission (non MBSFN-based)

NR supports two types of PDSCH allocation. One of those is Type A and is a slot-based mapping. PDSCH time allocation can start from symbols (S) 0,1,2,3 and has a length (L) of 3 to 14 symbols. This mapping is commonly used for eMBB services. Another one is Type B or mini-slot based. PDSCH time allocation can start from any symbol in the slot but has length options limited to 2, 4 or 7 symbols in case of normal Cyclic Prefix. This one is a preferred type for URLLC services as it provides better latencies where data transmissions not restricted to slot boundaries. The current 5G deployment is typically using PDSCH mapping Type A. However for DSS deployment, PDSCH mapping Type B can be the only available option for some situations.

Considering the case of NR PDCCH/PDSCH transmission with 15 kHz SCS (slot does not carry any other reference signal than DMRS), Figure 68 shows NR channels transmission without and with DSS operation.

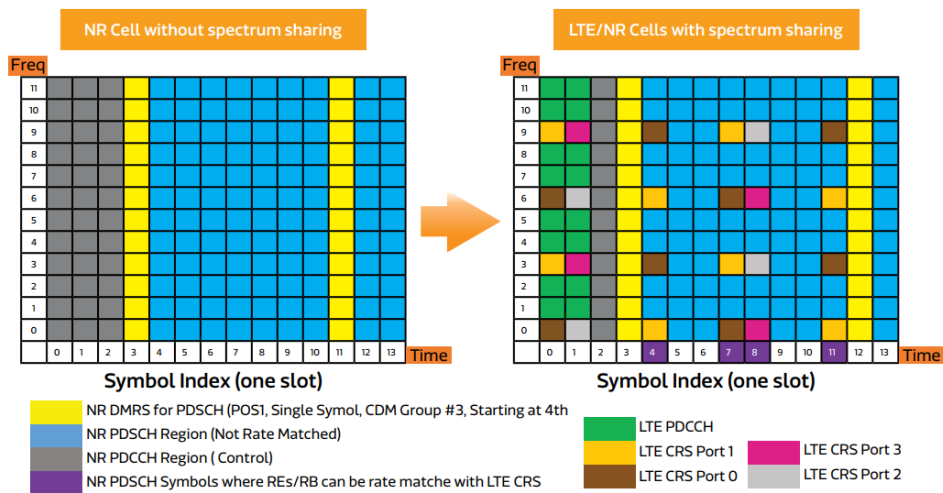


Figure 68: NR PDCCH/PDSCH SCS=15 kHz (without SSB) [84].

In the left side of this figure an example of dedicated NR carrier transmission is shown with 11 PDSCH symbols. The first 3 symbols are originally occupied with PDCCH, symbols 3 and 11 contain DMRS with a configuration that fully occupies all REs, and the rest 9 symbols are utilized by PDSCH. The right side of the figure has the same NR slot with spectrum sharing enabled in a cell. NR channels are rate matched around LTE-CRS. LTE in the given example is using four antenna port configuration. The first

2 symbols will be occupied by LTE PDCCH and there will be LTE CRS in the assigned positions as shown. This will take symbols #0 and #1 from NR use completely and will require special handling for slots #4, #7, #8 and #11. In particular Symbol #11 which was originally occupied by NR DMRS in case of DSS collides with LTE CRS. This is the main use case for Alternative DMRS Location feature. In case it is supported by the UE, NR DMRS will be moved to symbol #12.

4.2.3 Main UEs Features

The main design concepts of DSS on the network side are discussed in the previous section. From the UE side, DSS is completely transparent for LTE devices while NR devices require signalling capabilities.

The most important features are summarized in Table 9 and those essential for the initial deployment will be described in more details in this section. The table comes with a reference to 3GPP TS 38.822 containing Layer 1 Feature List Index and TS 38.331 RRC Field Names, if applicable. Not every DSS deployment option requires all of those features so suitability indication is also included.

Feature	Layer-1 Feature List Index (TS 38.822)	Short Explanation	Example of Field Name in RRC (TS 38.331)	DSS Option		
				1	2	3
LTE MBSFN subframe	LTE feature	Shared with LTE MBSFN subframes	mbsfn-Subframe ConfigList	0		
NR SSB with 30 kHz SCS	Based on band	For the applicable bands in FR1	subcarrierSpacing	0	0	
LTE CRS rate matching	5-28	RE-level rate matching. Allows transmission of NR PDSCH in non-MBSFN subframes	rateMatchingLTE-CRS			0
General rate matching pattern	5-26	RB-level rate matching. Allows PDSCH rate matching around LTE PSS/SSS and PBCH	rateMatching ResrcSetSemi-Static			0
NR PDCCH in symbol 2	3-1	Search Space Mapping for CORESET	monitoringSymbo WithinSlot	0	0	0
PDCCH monitoring on any up to 3 consecutive symbols	3-2	NR UE capability to mitigate DSS impact on PDCCH capacity	pdccchMonitoring SingleOccasion		0	0
PDSCH Mapping Type A (< 7 OFDM symbols)	5-6	Data channel mapping	pdsch-MappingTypeA	0	0	0
PDSCH Mapping Type B	5-6a		pdsch-MappingTypeB		0	
Alternative additional NR DMRS location	2-6b	For co-existence with LTE CRS	additionalMRS-DL-Alt			0
NR TRS in symbol 6 and 10	Mandatory for NR	Used to avoid collision with LTE CRS	Refer to table 11 in this paper	0	0	0
Flexible NR CSI-RS	Mandatory for NR			0	0	0
7.5 kHz UL shift	Mandatory for some NR bands	Enable the NR UL transmission with a 7.5 kHz shift to the LTE raster	frequencyShift7p5khz	0	0	0

Table 9: DSS Related UE Features Summary [84].

Among others, two main features are the Alternative DMRS Location and the 7.5 kHz UL shift.

4.2.3.1 Alternative DMRS Location

This feature (feature 2-6b) is designed to avoid collision of additional Demodulation Reference Symbol (DMRS) in case PDSCH mapping Type A when single-symbol DMRS is used. DMRS additional symbol located at index #11 will collide with LTE CRS as shown in Figure 69, causing higher PDSCH BLER especially in poor radio conditions. For this reason, the support of this feature is expected from all DSS enabled devices.

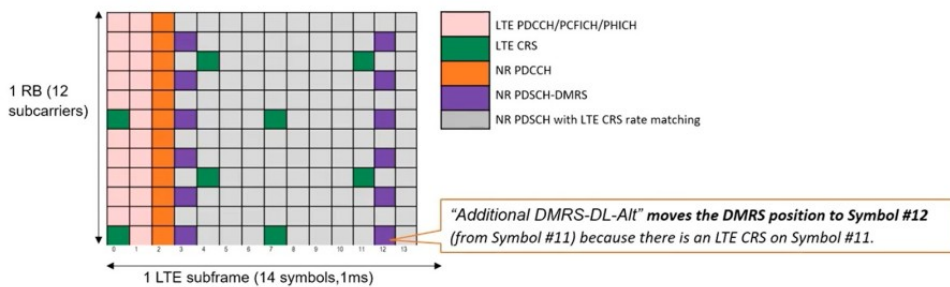


Figure 69: Alternative DMRS Location [85].

4.2.3.2 Half-subcarrier “7.5 kHz” UL shift

For the uplink, a half-subcarrier shift is a key consideration for DSS. The LTE uplink has a 7.5-kHz offset to avoid the use of the DC subcarrier, but not NR. The DC subcarrier is used for NR uplink transmission. The 7.5-kHz offset will break the orthogonality of LTE and NR. Adding a 7.5-kHz frequency shift for the uplink addresses this challenge, but NR UEs need to support it.

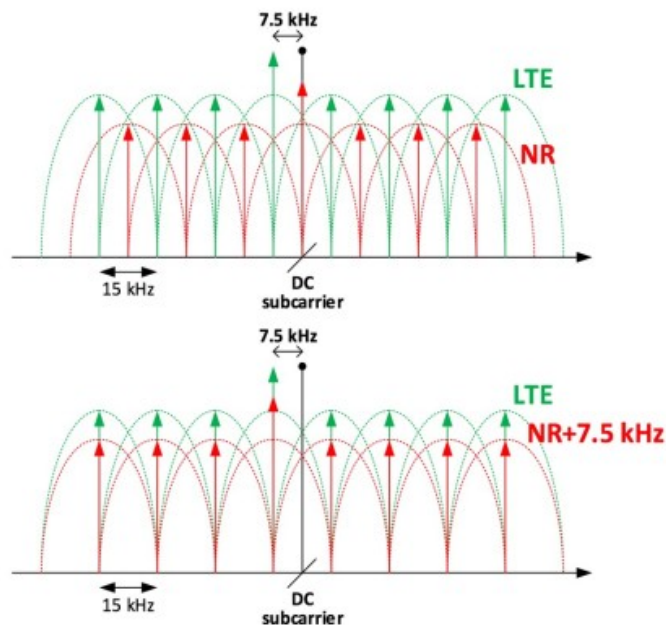


Figure 70: 7.5 kHz UL shift [85].

4.2.4 DSS performance

Although DSS provides the flexibility of spectrum usage for different radio technologies, it is obvious that the achievable maximum NR throughput will decrease due to overheads of LTE signals compared to NR cells deployed without DSS of the same bandwidth. DSS performance strictly depends on how DSS is implemented.

Mediatek whitepaper [84] makes several theoretical considerations on DSS performance. It reports a DSS throughput degradation ranging from 20% to 34% compared to 5G only transmission.

Keysight, inside a video course, did a lab test network using a DSS MBSFN-based solution [86]. It report a DSS throughput degradation up to 41% compared to 5G only and up to 21% compared to LTE only transmission.

4.3 Conclusion

In this chapter main characteristics of the DSS has been presented. It must be remarked that 3GPP did not define one monolithic solution for spectrum sharing, but rather a set of tools. The deployment options presented inside this chapter are examples. The actual implementation is vendor-specific.

At this point, with the knowledge acquired from the previous chapters, it is possible to introduce the last part of this document related to field testing.

5 5G control signals: Stability analysis

With the knowledge acquired from previous chapters, this one presents the experimental part of this thesis work. The main goal of this chapter is the stability analysis of 5G control signal performed with long-term measurements.

5.1 Measurement devices

The main devices used during the field tests are the following:

- Autonomous Mobile Network Scanner R&S TSMA6 with Mobile Network Testing software Romes 4;
- Receiving antennas.

In the following a brief description of the listed devices.

5.1.1 R&S TSMA6 with Mobile Network Testing software Romes 4

By gracious permission of Rohde & Schwarz Italia an Autonomous Mobile Network Scanner R&S®TSMA6 with Mobile Network Testing software Romes 4 was available for measurements.

The compact R&S®TSMA6 autonomous network scanner is an integrated solution for efficient field testing. It combines a multi-technology network scanner with a high-performance Intel CPU based PC to comply with the latest requirements for the state-of-the art mobile network testing. With its ultra-broadband frontend, the integrated scanner measures all supported technologies from 350 MHz to 6 GHz simultaneously [87]. The R&S®TSMA6 with battery pack available for measurement is show in Figure 71.



Figure 71: R&S®TSMA6 with battery pack [87].

Chapter 5 - 5G control signals: Stability analysis

The instrument available for measurement was a full-options device with complete support to all cellular systems from 2G to 5G and other wireless technologies.

For the purpose of this document only RF and 5G NR specifications are relevant. Table 10 reports main RF characteristics.

RF characteristics		
Frequency range		350 MHz to 6 GHz
Level measurement uncertainty	350 MHz to 3 GHz	< 1 dB
	3 GHz to 6 GHz	< 1.5 dB
Maximum operating measurement range input level		-10 dBm (nom.)
Maximum extended measurement range input level	in extended range mode: not 100% compliant with measured values	+10 dBm (nom.)
Maximum safe permissible input level		+20 dBm/10 V DC
Noise figure	900 MHz	5 dB (meas.)
	2100 MHz	5 dB (meas.)
	3500 MHz	6 dB (meas.)
	5100 MHz	7 dB (meas.)
Intermodulation-free dynamic range	900 MHz	-2 dB (meas.)
	2100 MHz	-2 dBm (meas.)
	3500 MHz	-9 dBm (meas.)
	5100 MHz	-14 dBm (meas.)
RF receive paths		1
VSWR (preselection on/off)	$350 \text{ MHz} \leq f \leq 1.6 \text{ GHz}$	< 2.7/2.0 (meas.)
	$1.6 \text{ GHz} \leq f \leq 2.45 \text{ GHz}$	< 2.6/1.7 (meas.)
	$2.45 \text{ GHz} \leq f \leq 3.6 \text{ GHz}$	< 3.0/2.3 (meas.)
	$3.6 \text{ GHz} \leq f \leq 6.0 \text{ GHz}$	< 3.4/2.6 (meas.)

Table 10: R&S®TSMA6 RF characteristics [87].

Table 11 reports main 5G NR characteristics of the device.

5G NR characteristics		
Frequency bands supported		FR1, sub6 GHz, FR2 (24 GHz to 30 GHz)
SSB subcarrier spacings supported		15 kHz, 30 kHz, 120 kHz, 240 kHz
SSB periodicities supported		5 ms, 10 ms, 20 ms, 40 ms, 80 ms, 160 ms
SSB sensitivity (single PCI)	SS-RSRP (10 ms periodicity, 30 kHz subcarrier spacing)	-150 dBm (meas.)
	SS-RSRP (40 ms periodicity, 30 kHz subcarrier spacing)	-142.5 dBm (meas.)
	SS-RSRP (5 ms periodicity, 15 kHz subcarrier spacing)	-156 dBm (meas.)
	SS-RSRP (20 ms periodicity, 15 kHz subcarrier spacing)	-149 dBm (meas.)
SSB index detection threshold (single PCI)	SS-RSRP (10 ms periodicity, 30 kHz subcarrier spacing)	-145 dBm (meas.)
	SS-RSRP (40 ms periodicity, 30 kHz subcarrier spacing)	-140 dBm (meas.)
	SS-RSRP (5 ms periodicity, 15 kHz subcarrier spacing)	-153 dBm (meas.)
	SS-RSRP (20 ms periodicity, 15 kHz subcarrier spacing)	-146 dBm (meas.)
	SS-RSRP (20 ms periodicity, 120 kHz subcarrier spacing)	-136 dBm (meas.)
	SS-RSRP (20 ms periodicity, 240 kHz subcarrier spacing)	-130 dBm (meas.)
SINR dynamic range	20 ms periodicity, 30 kHz subcarrier spacing	-19 dB to +40 dB
	20 ms periodicity, 240 kHz subcarrier spacing	-15 dB to +40 dB
Measurement speed (single PCI)	20 ms periodicity, 30 kHz subcarrier spacing	49 Hz (meas.)
	40 ms periodicity, 30 kHz subcarrier spacing	26 Hz (meas.)
	20 ms periodicity, 120 kHz subcarrier spacing	49 Hz (meas.)
	80 ms periodicity, 120 kHz subcarrier spacing	14 Hz (meas.)
Minimum MIB demodulation threshold	SS-RSRP	-144 dBm
	SS-SINR	-21 dB (meas.)
Minimum SIB demodulation threshold	SS-RSRP	-123 dBm
	SS-SINR	-5 dB (meas. relative to AWGN)
Time base accuracy (for time alignment measurements)	depending on quality of GNSS signal	5 ns to 30 ns (meas.)

Table 11: R&S TSMA6 5G NR characteristics [87].

In case of 5G FR2 deployments, an additional downconverter (R&S®TSME30DC) is needed to down-convert the cm-wave frequency to an intermediate frequency of 3 GHz.

The system runs Windows 10 OS with Mobile Network Testing software R&S®Romes 4 [88]. The software offers some innovative functions very useful in the measurements.

5.1.1.1 Automatic channel detection

The most useful function of the Scanner is the automatic channel detection (ACD). With only some clicks, to select the technologies and the 3gpp bands (or frequency interval) to be scanned, it is possible to show all signals on the air. Figure 72 shows the automatic channel detection status view obtained during measurement for LTE 3gpp band 20, 3, 1, 7 and 5G NR band n3. Thanks to this powerful function several 5G NR signals were discovered during measurements.

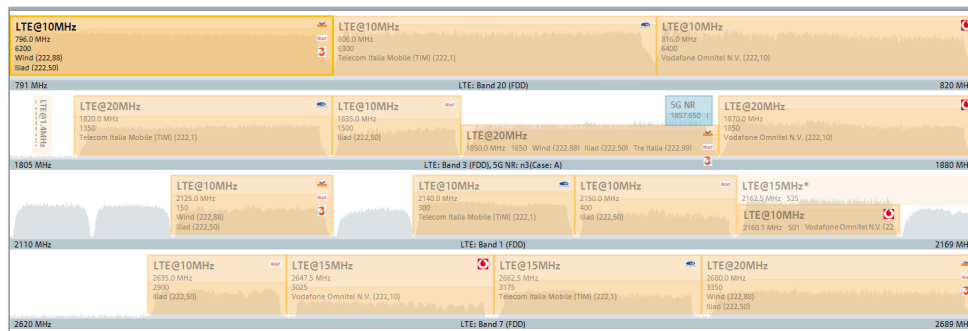


Figure 72: Screenshot of ACD status view during measurement.

5.1.1.2 5G NR Scanner views

The Scanner summarizes the available measurements in a technology window tab. Inside each tab there are several views. In the 5G Scanner tab, there are two main views, where measured and decoded data are reported. The other views are graphical representations of the same information. Figure 73 shows an example of 5G NR Scanner views.

The Scanner measures 5G NR synchronization signal blocks (SSB) and decodes the PBCH/MIB content of each detected SSB. Each SSB can be transmitted on different beams (depending on the network configuration), which can be decoded by the scanner. The 5G NR scanner, among others, can measure the Reference Signal power (RSRP), the Reference Signal quality (RSRQ) and signal to noise and interference (SINR) of synchronization signals. In particular:

- The power “SS-RSRP” is defined as the linear average over the power contributions of the resource elements that carry the Secondary Synchronization Signal (SS) [89];
- The signal to noise and interference “SS-SINR” is defined as the linear average over the power contributions of the Secondary Synchronization Signal (SS) divided by the linear average of interference and noise over the same signals [89];
- The quality (SS-RSRQ) is defined as the received quality of all resource elements of the Secondary Synchronization Signal (SS) [89].

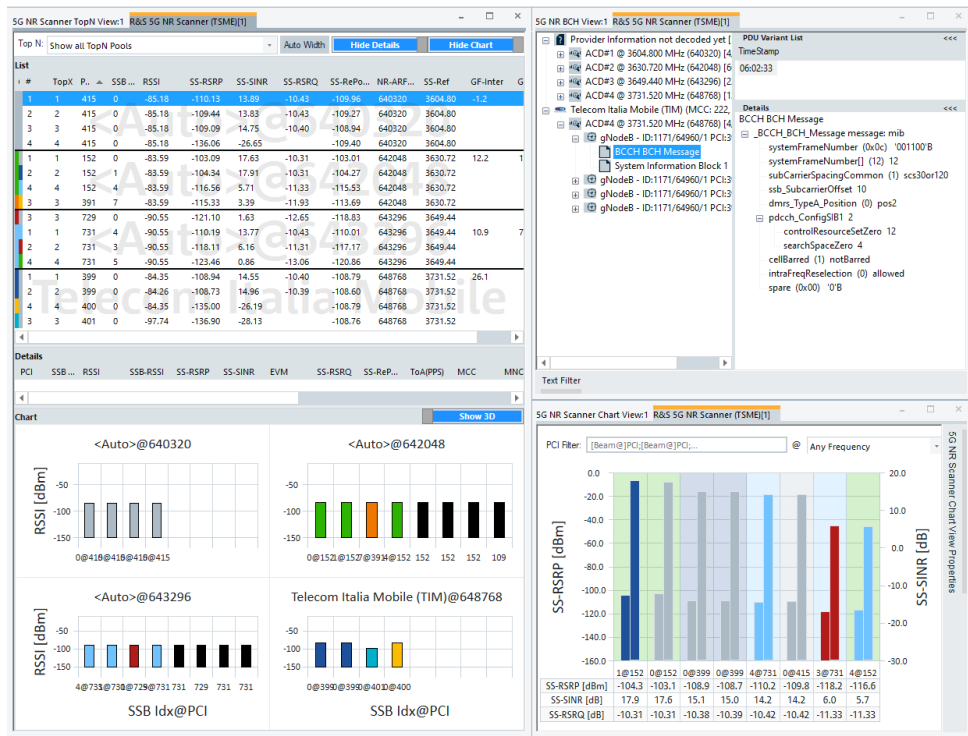


Figure 73: Screenshot of 5G scanner views during measurement.

It must be noted that the Scanner is a passive measurement device that do not require an active communications link between itself and the base station. It performs same measurements done in the end-user device and reported to the network during idle mode for cell reselection or in connected mode for handovers.

5.1.1.3 BTS position estimation

Another useful function of the scanner is the BTS position estimation. During a drive test, R&S®ROMES can use the measurement data and GPS data delivered by the R&S®TSMA6 to estimate the geographic position of the base stations. This calculation is fast and accurate. GSM, WCDMA,

LTE, 5G NR, CDMA2000®/1xEVDO and TETRA networks are supported in parallel. This unique feature enables users to quickly generate a base station list for export or graphic display [88].

Figure 74 shows the Romes Map Route Track view obtained during the measurements.

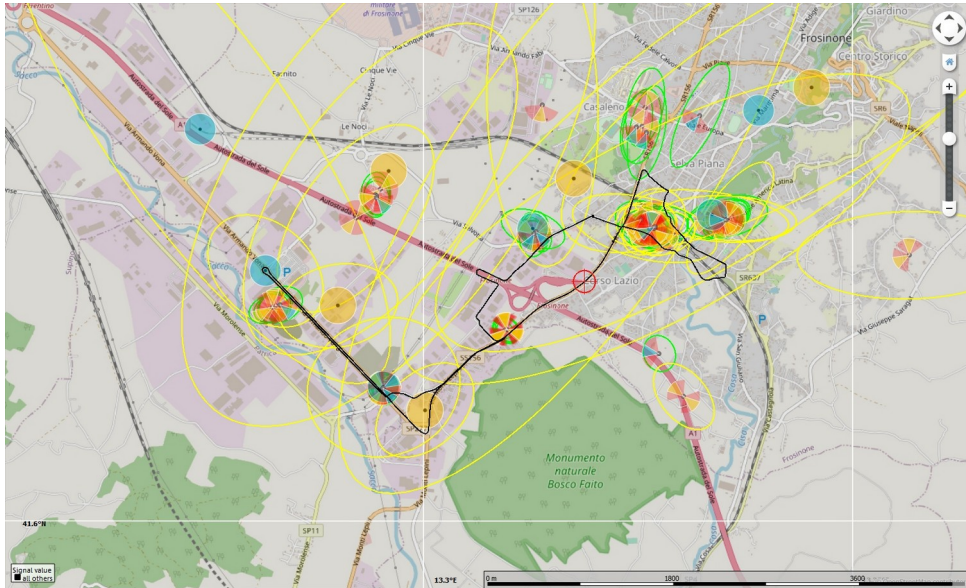


Figure 74: Screenshot of Navigation Tab, RomesMap Route Track view during measurement.

Thanks to this function, several 5G Base Stations location were identified during measurements.

5.1.1.4 Record, Replay, Export

All data acquired by scanner can be recorded in a measurement file. The measurement file can be managed with TMSA6 or any other Windows OS PC running ROMES (Replay ONLY). The measurement files can be replayed or used for exportations. Thanks to ASCII exportations the data can be elaborated with other tools like Matlab.

5.1.2 Receiving antennas

During measurements different RF antennas were used. The main characteristics are described in the following Table 12.




Description	Type	Peak Gain [dBi]	Picture
Single-port ultra-wideband antenna up to 6000 MHz	Omnidirectional	1-3	
PCTEL 278H, single-port ultra-wideband antenna up to 3800 MHz with magnetic mount	Omnidirectional	1-2	
Siretta Oscar 20A antenna quad band 2G/3G/4G and 5G	Omnidirectional	7-10	

Table 12: RF antennas description.

A GPS antenna is also used during measurements (Table 13).


Description	Picture
PCTEL 034H, High Performance Magnetic Mount GPS Antenna	

Table 13: GPS antenna description.

5.2 Measurement scenarios

Two field test were realized in two locations generalized as Site n.1 and Site n.2. For each site a Measurement Point (MP) and several Base Stations were identified.

Generally a Base Station has three cells. The Base Station cells are identified by their Physical Cell Identity (PCI). As shown in 3.2.7 and 3.2.8 for each 5G NR cell i , several SS/PBCH blocks (or SSB blocks) can be transmitted. In the following, the measured signals will be identified in terms of their PCI number i and SS/PBCH block index j .

It must be noted that for the following paragraphs provider's sensitive information won't reported. Providers will be identified by a colour.

5.2.1 Site n.1 scenario

5.2.1.1 Site n.1 localization

The main informations regarding Site n.1 measurement are reported in the following Table 14.

<i>Measurement point (MP)</i> <i>-Latitude, Longitude</i> <i>-Sea level</i>	41°29'17.35"N, 13°49'33.44"E 46 m
<i>Measurement Point (MP)</i> <i>Descriptions</i>	Cassino (FR) Via Gaetano di Biasio Room on Second floor of a building Faculty of Engineering University of Cassino
<i>Probe Antenna position</i> <i>Terrain elevation</i>	Indoor 10 m
<i>Start – End Date</i>	10/03/2021-22/03/2021
<i>Acquisition start – end</i> <i>date and time</i>	19/03/2021 00:00:00 21/03/2021 23:59:59

Table 14: Site n.1 measurement informations.

As reported in previous table, the measurement were realized from 10/03/2021 to 22/03/2021 but the recorded continuous dataset is limited from 19/03/2021 00:00:00 to 21/03/2021 23:59:59.

Figure 75 shows a picture of the measurement point for a clear identification.

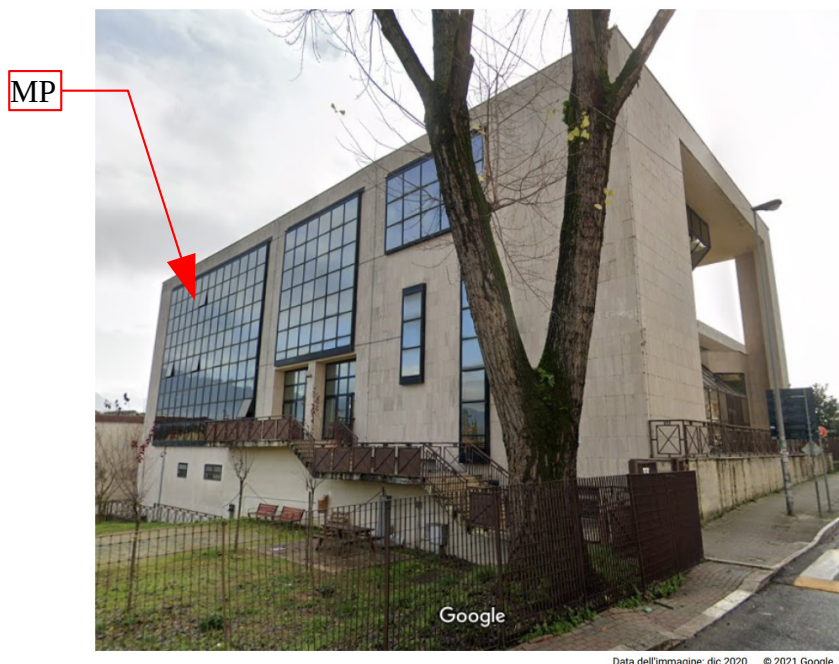


Figure 75: Site n.1 measurement point identification from Google Maps [90].

5.2.1.2 Site n.1 setup

The diagram of the measurement setup is shown in the following Figure 76. As shown the measurement chain was composed by the network scanner and an omnidirectional antenna.

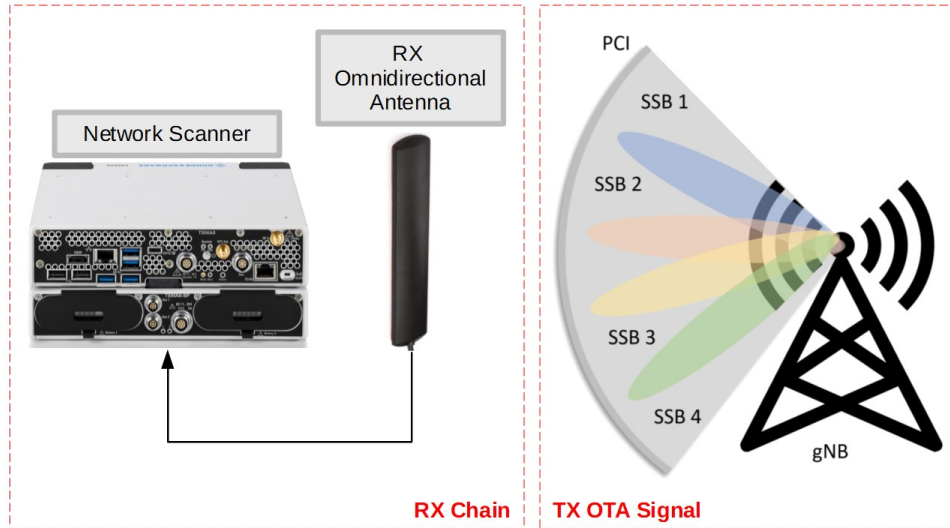
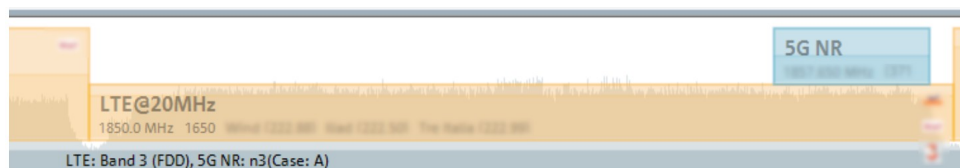


Figure 76: Site n.1 measurement setup diagram.

5.2.1.3 Site n.1 measured signals

Thanks to the automatic channel detection (ADC) function of the network scanner, running in the full frequency range of the instrument, several 5G signals were discovered in 3gpp band n3 (FDD 1800 MHz). These signals are 5G DSS transmitted inside LTE bandwidth. Figure 77 (a) shows a screenshot of the automatic channel detection of the Scanner, where the 5G signal were discovered inside LTE spectrum. Figure 77 (b) shows top ten most powerful PCI/SSB index detected from the scanner.



(a)

#	TopX	PCI	SSB Idx	RSSI	SS-RSRP	SS-SINR	SS-RSRQ	SS-RePower	NR-ARFCN	SS-Ref	GF-Inter	GF-Intra
1	1	61	2	-64.86	-83.63	10.47	-10.64	-83.25			7.8	
2	2	410	2	-64.86	-91.44	3.67	-12.03	-89.89				
3	3	177	2	-64.86	-95.80	-12.29	-22.81	-83.25				
4	4	97	2	-64.86	-96.20	1.39	-12.86	-93.84				
5	5	3	2	-64.86	-101.48	-8.36	-19.65	-92.52				
6	6	47	2	-64.86	-105.87	-13.55	-24.61	-92.13				
7	7	32	2	-64.40	-108.03	-13.61	-24.52	-94.24				
8	8	405	2	-63.93	-112.56	-29.19		-83.36				

(b)

Figure 77: (a) Screenshot of automatic channel detection, (b) screenshot of 5G NR scanner TopN view (provider's sensitive information blurred).

It is possible to assign these signals, without any doubt, to the “Orange Provider” from considerations on bandwidth assignment in LTE 3gpp band 3.

From the observation of the 5G NR and LTE signals, Orange Provider seems to use same PCI numbers for both technologies. From these assumption, thanks to informations collected by the service Cellmapper.net [91] and the Google Street View services, it was possible to identify the exact positions of the signals received. In particular the analysis was focused on the five most powerful PCI/SSB index control signal received from different base stations. Figure 78 shows the measurement point and the base stations involved on a map created with Google Earth Pro software [92] while Table 15 reports main information about five most powerful PCI/SSB index control signal received.

It is important to note that, as expected in 5G DSS implementation, the 5G signal is similar to LTE signal. The subcarrier spacing (SCS) used is 15 kHz as LTE and the total number of SS/PBCH block transmitted is one. A total number of SS/PBCH block equal to one means that the 5G signal can’t use the antenna beamforming, one of the most innovation introduced by 5G.



Figure 78: Site n.1 measurement map realized with Google Earth Pro software [92], thanks to informations collected by the service Cellmapper.net [91] and Google Maps [90].

<i>PCI</i>	<i>SSB index number</i>	<i>Total Number SSB blocks</i>	<i>Signal</i>	<i>Provider</i>	<i>5G NR 3gpp band</i>	<i>SCS [KHz]</i>
61	2	1	5G DSS	Orange	n3	15
410	2	1	5G DSS	Orange	n3	15
97	2	1	5G DSS	Orange	n3	15
3	2	1	5G DSS	Orange	n3	15
47	2	1	5G DSS	Orange	n3	15

Table 15: Five most powerful 5G DSS signals detected in Site n.1 measurement.

After the clear identifications of received signals, they were recorded for the stability analysis purpose.

The network scanner was set to acquire all data received from technology 5G NR 3gpp band n3 and technology 4G LTE 3gpp band 3.

5.2.1.3.1 Site n.1 line of sight characterization

To complete the Site n.1 scenario description, a characterization of the path between the measurement point and the measured signals is proposed. These informations will be useful during the stability analysis of the observed signals.

Figure 79, Figure 80, Figure 81, Figure 82 and Figure 83 respectively show the main information for the paths from measurement point to base station cells 61, 410, 97, 3 and 47. Information reported in the following figures are generated using Google Earth Pro software [92] and practice considerations. It must be reported that despite its useful tools, Google earth is designed for scientific precision and isn't intended to be used as a definitive data source [93].

Considering that the measurement point is inside a room, all paths from measurement point to involved base stations are obstructed at least by the wall of the same room. An exception can be made for the PCI 61 signal where only a window was placed inside the path. Nevertheless as shown in the following figures there are a lot of building inside the paths and the visibility can't be assured without dedicated surveys and without knowing the exact position of the transmitting antenna.

Referring to following figures:

- the field “*Signal [PCI/SSB index]*” indicates the measured signal PCI number i and SS/PBCH block index j ;

- the field “*Distance [m]*” indicates the air distance in meters between the measurement point and the base station;
- the field “*Azimuth to N [°]*” indicates the azimuth respect to north of the base station point considering the point of view of the measurement point;
- the field “*Elevation [+/- m]*” indicates the terrain elevation difference between measurement point and base station (positive value means that the base station is more elevated than the measurement point);
- the field “*Environment*” gives an indication propagation environment between the measurement point and the base station.

<i>Signal [PCI/SSB index]</i>	<i>Distance [m]</i>	<i>Azimuth to N [°]</i>	<i>Elevation [+/- m]</i>	<i>Environment</i>
61/2	607	344	+77	Sub-Urban

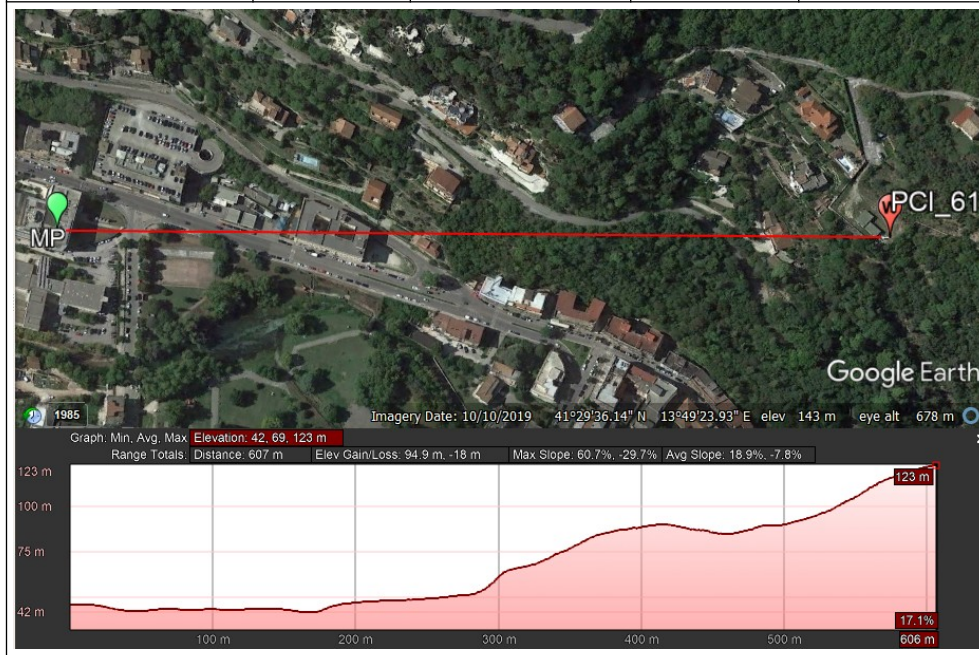


Figure 79: Google Earth [92] elevation profile from measurement point to base station cell PCI 61.

Chapter 5 - 5G control signals: Stability analysis

Signal [PCI/SSB index]	Distance [m]	Azimuth to N [°]	Elevation [+/- m]	Environment
410/2	1060	25	0	Urban



Figure 80: Google Earth [92] elevation profile from measurement point to base station cell PCI 410.

Signal [PCI/SSB index]	Distance [m]	Azimuth to N [°]	Elevation [+/- m]	Environment
97/2	809	89	-8	Urban

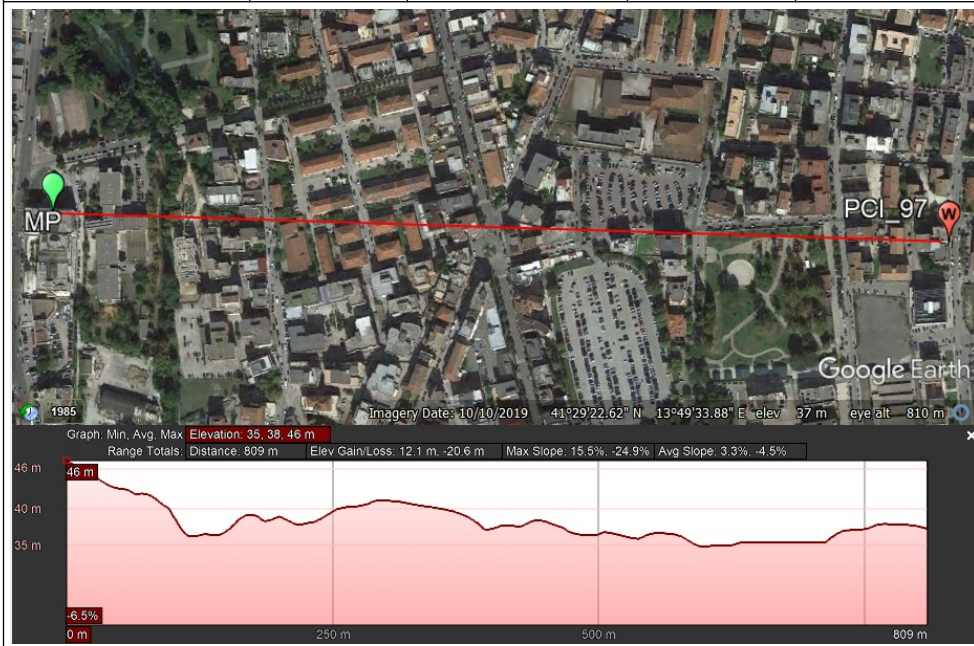


Figure 81: Google Earth [92] elevation profile from measurement point to base station cell PCI 97,

Chapter 5 - 5G control signals: Stability analysis

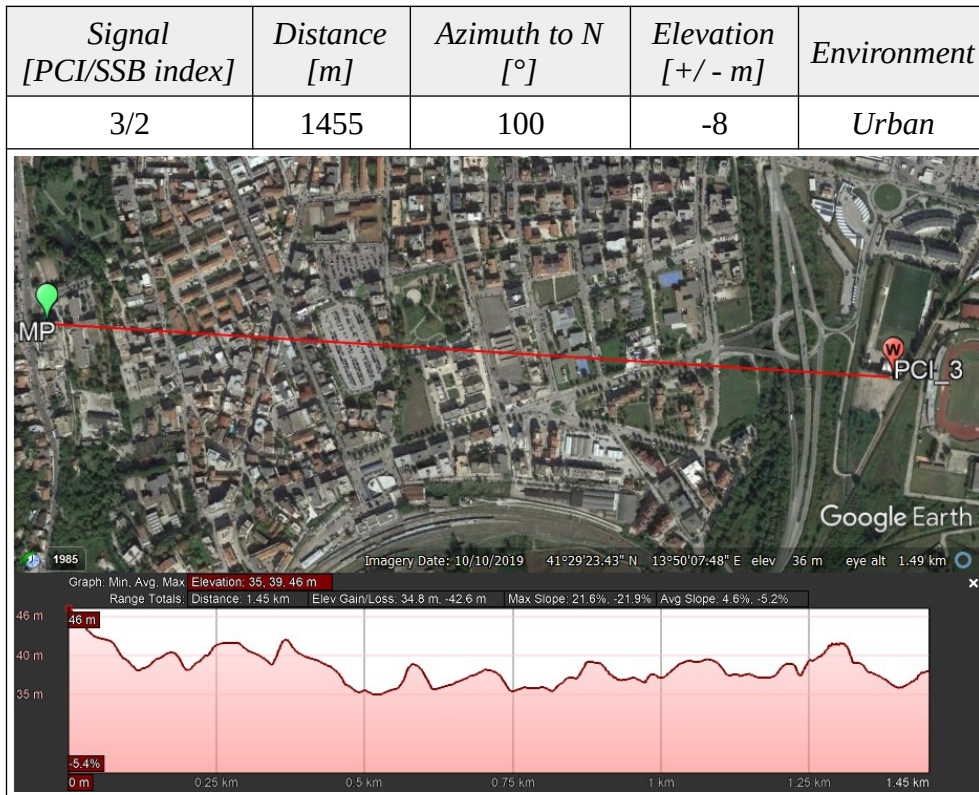


Figure 82: Google Earth [92] elevation profile from measurement point to base station cell PCI 3.

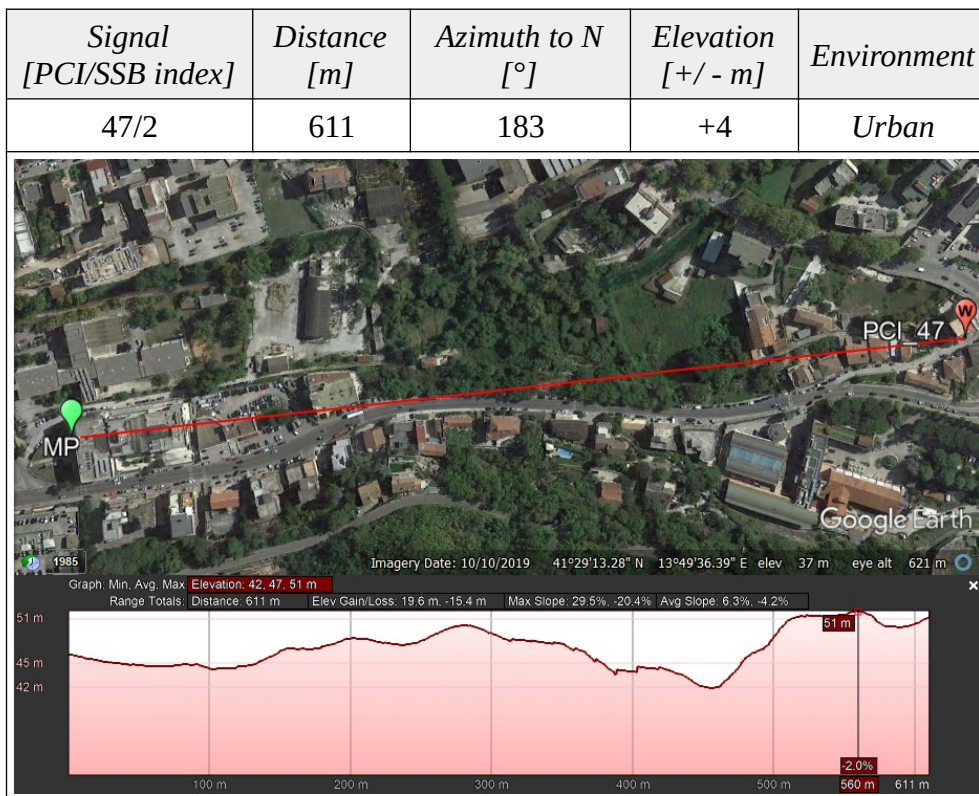


Figure 83: Google Earth [92] elevation profile from measurement point to base station cell PCI 47.

5.2.2 Site n.2 scenario

With Site n.1 scenario, 5G DSS signals were observed. Unfortunately, in the Cassino area there aren't any active 5G not-DSS base stations.

To find 5G signals, some surveys were realized in Frosinone. In the following the surveys results are presented.

5.2.2.1 Preliminary survey

5.2.2.1.1 Survey n.1

The survey n.1 was realized on 20/03/2021 near to a base station in Via Armando Vona in Frosinone. Surprisingly a 5G operating signal inside 3720-3800 MHz frequency interval was discovered. Figure 84 shows some pictures of the survey.

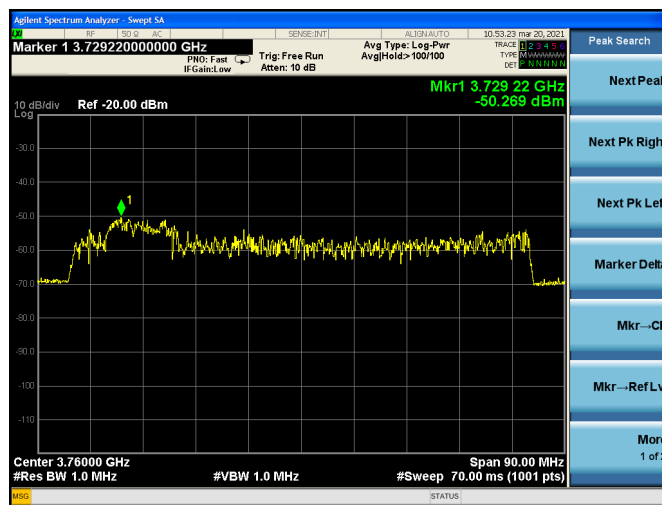
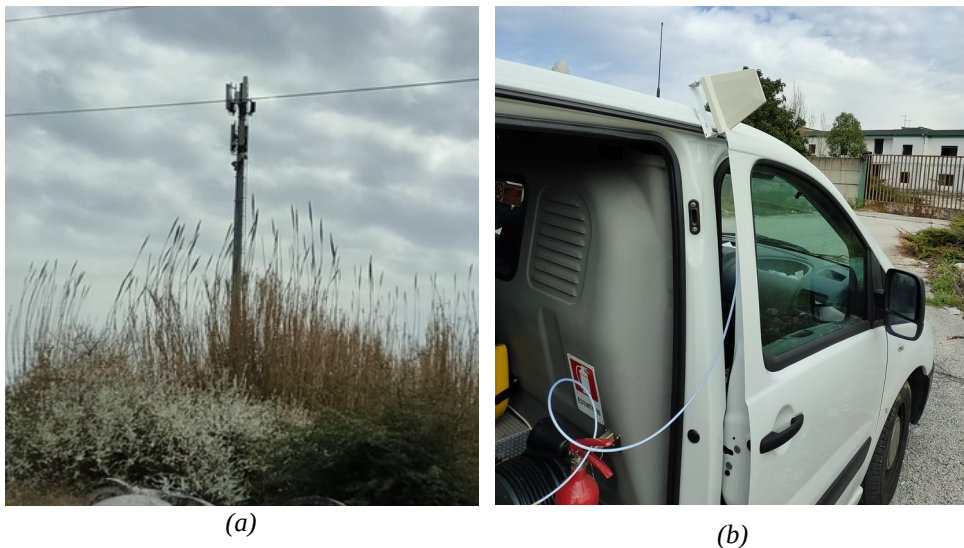


Figure 84: (a) Base station, (b) Receiving Antenna, (c) Spectrum Analyser result.

5.2.2.1.2 Survey n.2

The Survey n.2 was realized on 21/03/2021. The goal of Survey n.2 was to validate a candidate measurement point placed in the city centre of Frosinone.

Surprisingly, an other 5G operating signal inside 3620-3640 MHz frequency interval was clearly discovered. Figure 85 shows some pictures of the survey.

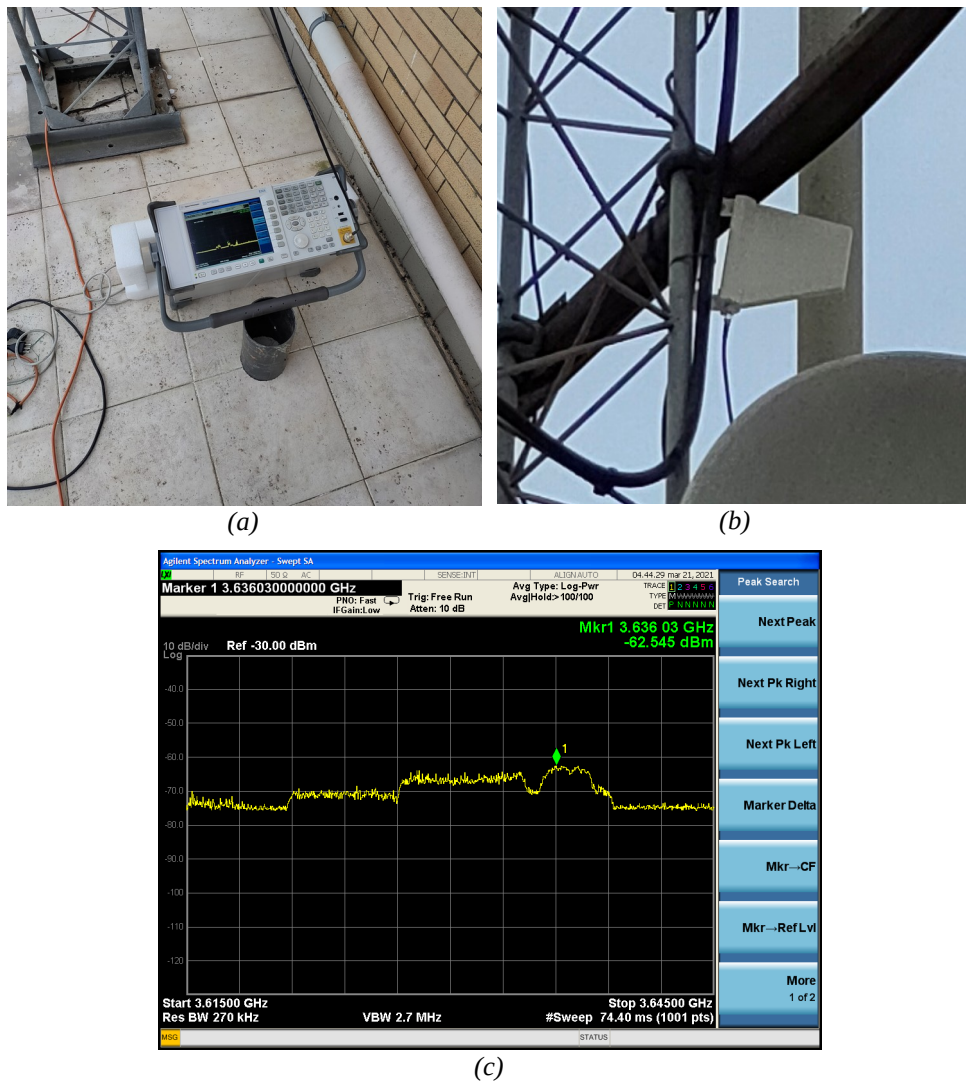


Figure 85: (a) Spectrum Analyser, (b) Receiving Antenna, (c) Spectrum Analyser result.

From results of this Survey at least two 5G signal could be detected. Thanks to these results, It was decided to use the last week of Network scanner availability to carry out a second measurement experiment, generalized in the following as Site n.2 measurement.

5.2.2.2 Site n.2 measurement localization

The main informations regarding Site n.2 measurement are reported in the following Table 16.

Measurement point (MP) -Latitude, Longitude -Sea Level	41°37'30.51"N, 13°19'20.78"E 160 m
Measurement Point (MP) Descriptions	Frosinone (FR) Via Dei Monti Lepini Roof of a six floor building
Probe Antenna position Terrain elevation	Outdoor 27 m
Start – End Date	22/03/2021-01/04/2021
Acquisition start – end date and time	29/03/2021 00:00:00 31/03/2021 23:59:59

Table 16: Site n.1 measurement informations.

As reported in previous table, the measurement were realized from 22/03/2021 to 01/04/2021 but the recorded continuous dataset is limited from 29/03/2021 00:00:00 to 31/03/2021 23:59:59.

Figure 86 shows a picture of the measurement point for a clear identification.



Figure 86: Site n.2 measurement point identification from Google Maps [90].

5.2.2.3 Site n.2 measurement setup

The diagram of the measurement setup is shown in the following Figure 87.

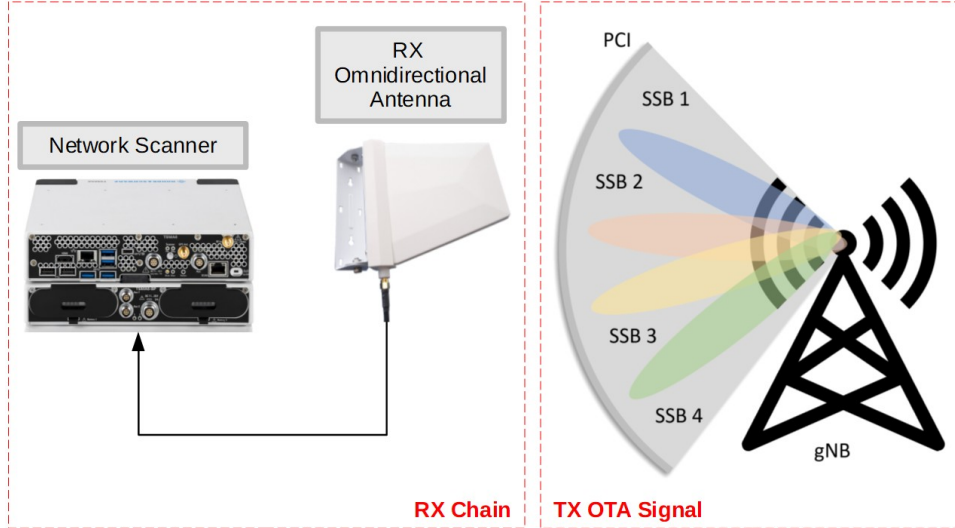


Figure 87: Site n.2 measurement setup diagram.

As shown the measurement chain was composed by the network scanner and an omnidirectional antenna.

Figure 88 shows the Site n.2 real measurement setup.

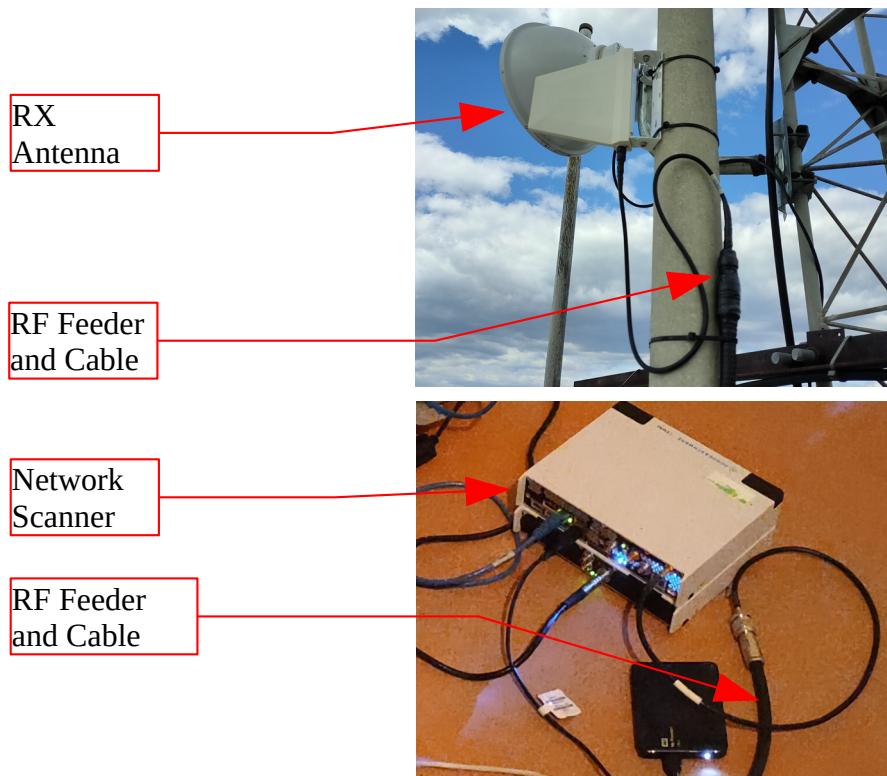


Figure 88: Site n.2 measurement setup pictures.

5.2.2.4 Site n.2 measured signals

Thanks to the automatic channel detection (ACD) function of the network scanner, running in the full frequency range of the instrument, four 5G blocks were discovered in 3gpp 5G band n78 (3300-3800 MHz from standard, only 3600-3800 MHz assigned to Mobile Service in Italy).

Figure 89 (a) shows a screenshot of the automatic channel detection of the Scanner. Figure 89 (b) shows top ten most powerful PCI/SSB index detected from the scanner.

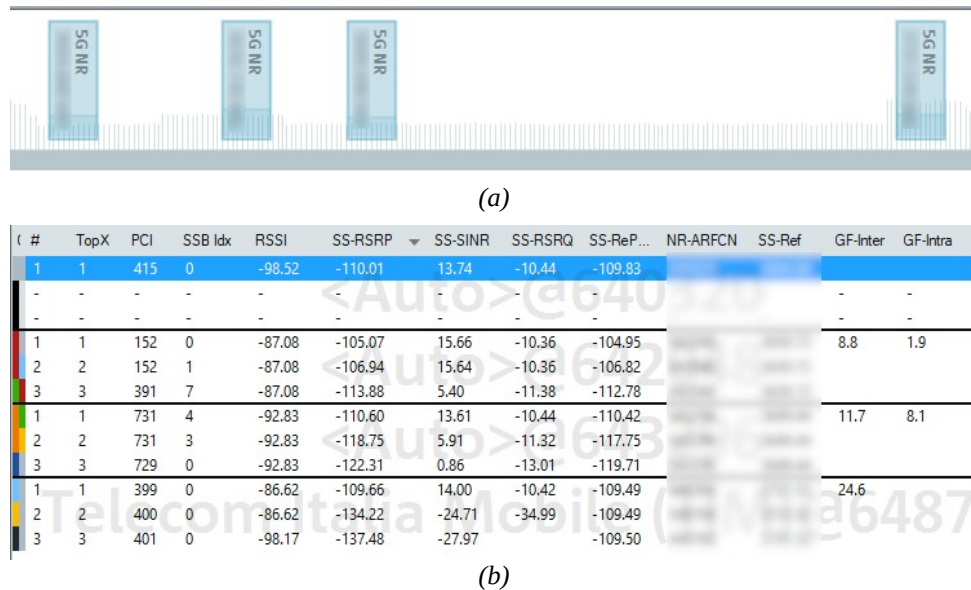


Figure 89: (a) Screenshot of automatic channel detection, (b) screenshot of 5G NR scanner TopN view.

It is possible to assign these signals, without any doubt, to respective provider from considerations on bandwidth assignment.

To localize the source of these signals the R&S BTS position estimation of the Network Scanner was used. A drive test was taken at the end of the measurement on 01/04/2021 to localize the base stations position. Figure 90 shows the setup used during the drive test.

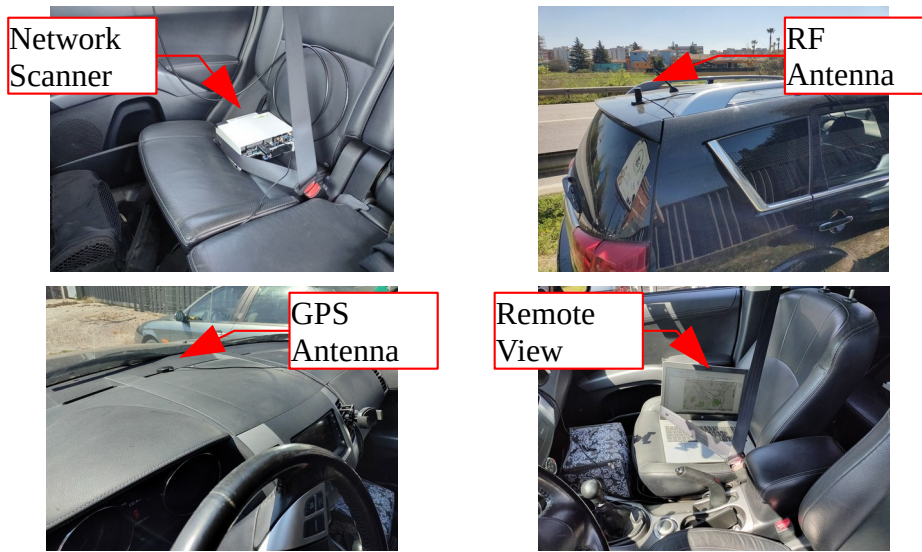


Figure 90: Drive test setup.

Figure 91 shows the of measurement point and the base stations involved on a map created with Google Earth Pro software [92].

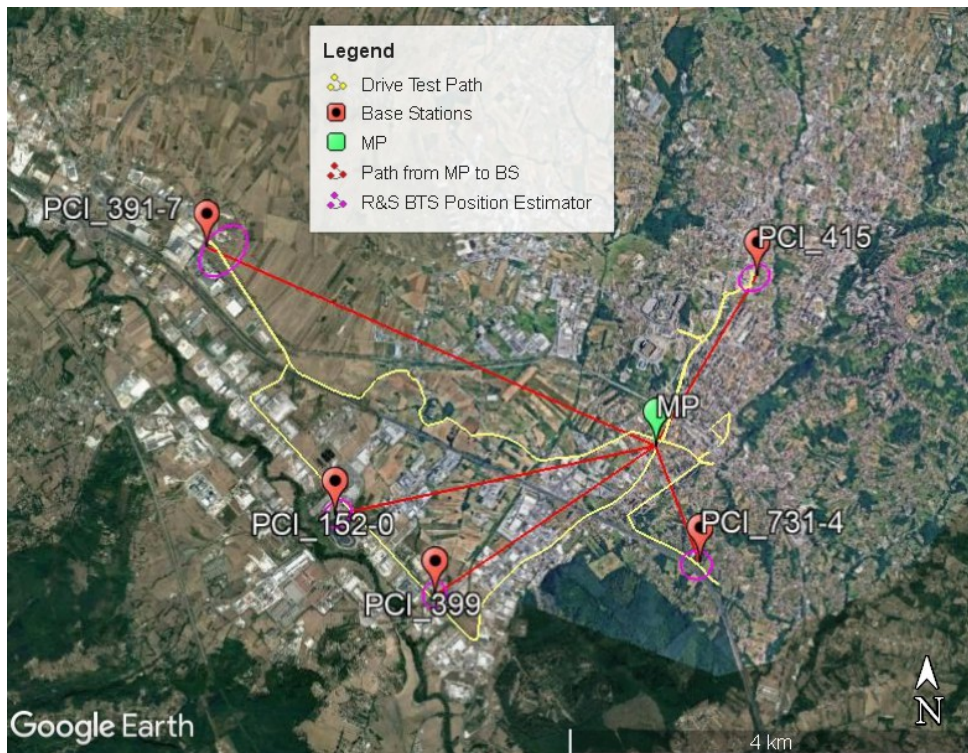


Figure 91: Site n.2 measurement map realized with Google Earth Pro software [92].

The analysis was focused on the five most powerful PCI/SSB index control signal received from different base stations. Table 17 reports main information about five most powerful PCI/SSB index control signal received.

<i>PCI</i>	<i>SSB index number</i>	<i>Total Number SSB blocks</i>	<i>Signal</i>	<i>Operator</i>	<i>5G NR 3gpp band</i>	<i>BW [MHz]</i>	<i>SCS [kHz]</i>
415	0	1	5G	Orange	n78	20	30
152	0	8	5G	Purple	n78	20	30
391	7	8	5G	Purple	n78	20	30
731	4	8	5G	Red	n78	20	30
399	0	1	5G	Blue	n78	80	30

Table 17: Five most powerful 5G control signals detected in Site n.2 measurement.

The 5G control signals from Orange and Blue providers have a total number of SS/PBCH block transmitted equals to one. A total number of SS/PBCH block equal to one means that the 5G base stations will not have the UE measurements to enable beamforming. The 5G control signals from from Purple and Red are using a total number of SS/PBCH block transmitted equals to eight which is the maximum number allowed in FR1 band. It is important to remark that field tests were conducted in an early stage of 5G deployment where 5G traffic was almost absent. Moreover, observed 5G installations could be operating in test mode.

After the clear identifications of received signals, they were recorded for the stability analysis purpose. The network scanner was set to acquire all data received from technology 5G NR 3gpp band n78.

5.2.2.4.1 Site n.2 Path characterization

To complete the Site n.2 scenario description, a characterization of the path between the measurement point and the measured signals is proposed. These informations will be useful during the stability analysis of the observed signals.

Figure 92, Figure 93, Figure 94, Figure 95 and Figure 96 respectively show some information for the paths from measurement point to base station cell 415, 152, 391, 731 and 399.

Considering that elevation respect to the ground of the measurement point is 27 meters and an estimate value of the transmitting tower height range from 25 to 30 meters, with a good probability there is visibility of the direct path from Measurement point and Base Stations. Nevertheless as shown in the following figures there are a lot of building inside the paths and the visibility can't be assured without dedicated surveys and without knowing the exact position of the transmitting antenna.

Information reported in the following figures are generated using Google Earth Pro software [92] and practice considerations. Google earth tools are not designed for scientific precision and aren't intended to be used as a definitive data source [93].

Previous figure report the main information for the paths from measurement point to measured signals.

Referring to previous figures:

- the field “*Signal [PCI/SSB index]*” indicates the measured signal PCI number i and SS/PBCH block index j ;
- the field “*Distance [m]*” indicates the air distance in meters between the measurement point and the base station;
- the field “*Azimuth to N [°]*” indicates the azimuth respect to north of the base station point considering the point of view of the measurement point;
- the field “*Elevation [+/- m]*” indicates the terrain elevation difference between measurement point and base station (positive value means that the base station is more elevated than the measurement point);
- the field “*Environment*” gives an indication propagation environment between the measurement point and the base station.

Chapter 5 - 5G control signals: Stability analysis

Signal [PCI/SSB index]	Distance [m]	Azimuth to N [°]	Elevation [+/- m]	Environment
415/0	2006	30	+31	Dense Urban

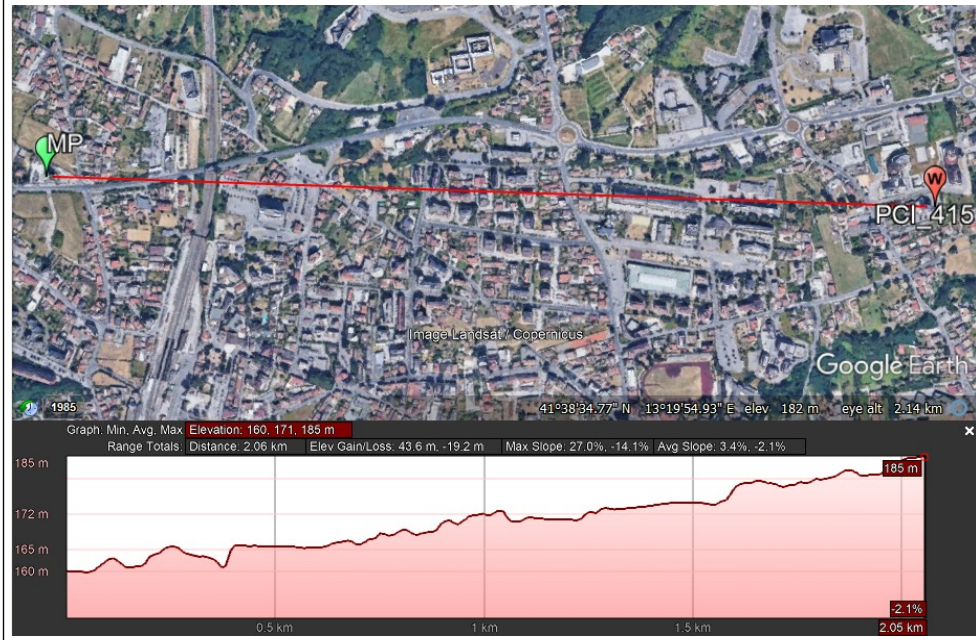


Figure 92: Google Earth [92] elevation profile from measurement point to base station cell PCI 415.

Signal [PCI/SSB index]	Distance [m]	Azimuth to N [°]	Elevation [+/- m]	Environment
152/0	3350	258	-20	Sub-Urban

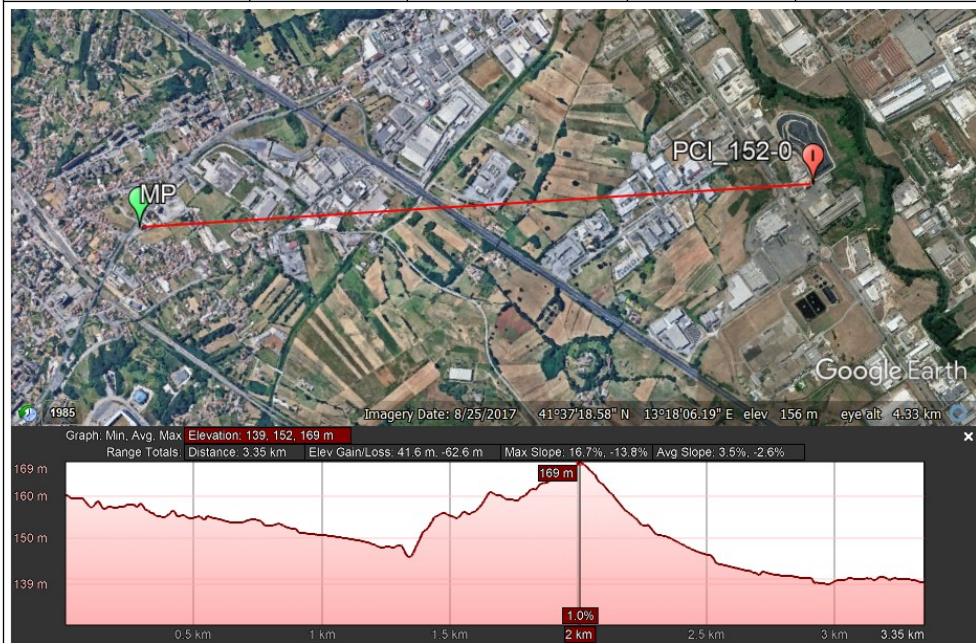


Figure 93: Google Earth [92] elevation profile from measurement point to base station cell PCI 152.

Chapter 5 - 5G control signals: Stability analysis

Signal [PCI/SSB index]	Distance [m]	Azimuth to N [°]	Elevation [+/- m]	Environment
391/7	5100	294	-1	Sub-Urban

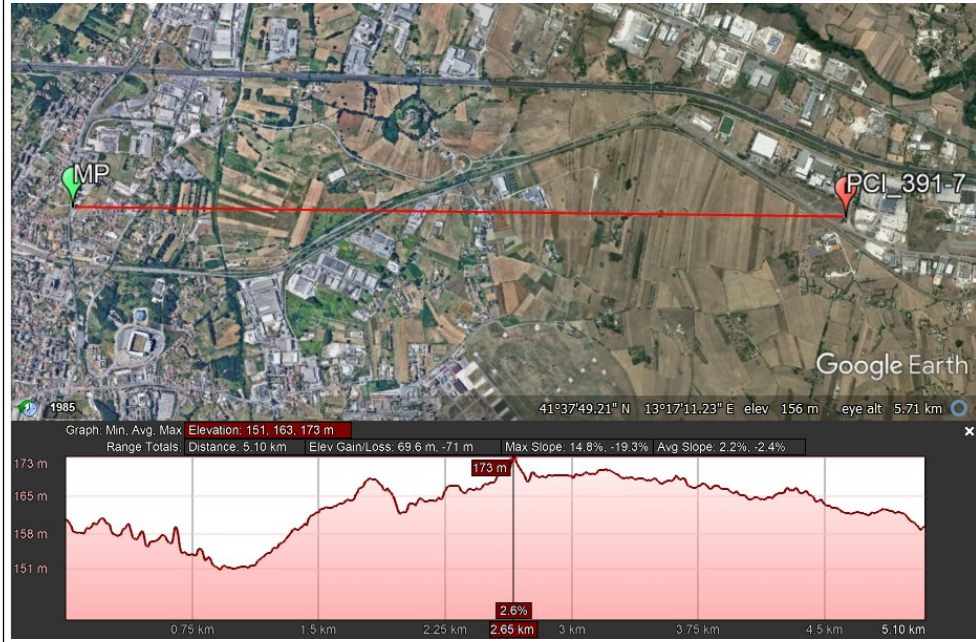


Figure 94: Google Earth [92] elevation profile from measurement point to base station cell PCI 391.

Signal [PCI/SSB index]	Distance [m]	Azimuth to N [°]	Elevation [+/- m]	Environment
731/4	1250	160	0	Urban



Figure 95: Google Earth [92] elevation profile from measurement point to base station cell PCI 731.

Chapter 5 - 5G control signals: Stability analysis

Signal [PCI/SSB index]	Distance [m]	Azimuth to N [°]	Elevation [+/- m]	Environment
399/0	2700	236	-20	Sub-Urban

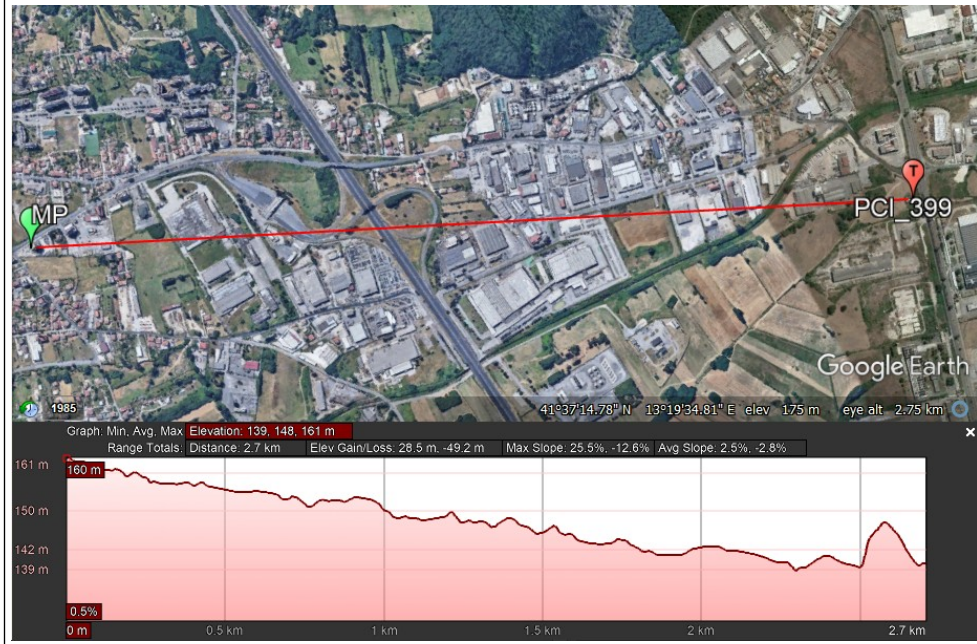


Figure 96: Google Earth [92] elevation profile from measurement point to base station cell PCI 47.

5.3 Stability analysis

This paragraph presents a first stability analysis based on long-term data acquisition from the Site n.1 and Site n.2.

The data were recorded with a sampling frequency of 1 Hz (one sample every one second). From recorded data SS-RSRP parameters were extracted.

Secondary Synchronization Reference Signal Received Power (SS-RSRP) is defined as the linear average over the power contributions of the resource elements that carry the Secondary Synchronization Signal (SS) [89] [94].

These values will be characterized several ways in terms of mean value and standard deviation. Before to apply the linear operators “mean” and “standard deviation” the following conversion were applied.

Measured value from Network Scanner
 $ssRSRP [dBm]$

$$ssRSRP [mW] = 10^{\frac{ssRSRP [dBm]}{10}}$$

$$x [mW] = ssRSRP [mW]$$

Linear mean value

$$\bar{x} = \frac{1}{N} \sum_i^N x_i$$

Linear standard deviation

$$\sigma_x = \sqrt{\frac{\sum_i^N (x_i - \bar{x})^2}{N - 1}}$$

Logarithmic mean value

$$\bar{x} [dBm] = 10 \cdot \log_{10}(\bar{x})$$

Logarithmic standard deviation

$$\sigma_x [dB] = 10 \cdot \log_{10}\left(\frac{\bar{x} + \sigma_x}{\bar{x}}\right)$$

Figure 97: Conversion from Logarithmic to Linear and from Linear to Logarithmic.

For convenience of notation the reference signals will be identified only by their PCI, without the explicit indication of the SSB index.

5.3.1 Site n.1

As shown in 5.2.1.1, Site n.1 measurement were carried out in Cassino, from 10/03/2021 to 22/03/2021 but the recorded continuous dataset is limited from 19/03/2021 00:00:00 to 21/03/2021 23:59:59. In this Scenario, the observed reference signals were coming from base stations owned by Orange Provider operating in 5G DSS technology.

5.3.1.1 Complete data analysis

The following Figure 98 shows the date and time trend of the five most powerful SS-RSRP from PCI of different base stations. All traces are reported in the same x and y axis to facilitate the comparison.

Because of different paths between measurement point and base stations, the traces show different power levels. As expected from the path characterization in 5.2.1.3.1, PCI 61 presents the maximum power level because it is the nearest and the most visible from the measurement point.

Despite power values, all traces trend seems to be very similar. This behaviour can be explained by that all observed signals were coming from the same Provider.

When no power was detected by the Network Scanner, an empty value is reported on the graphs.

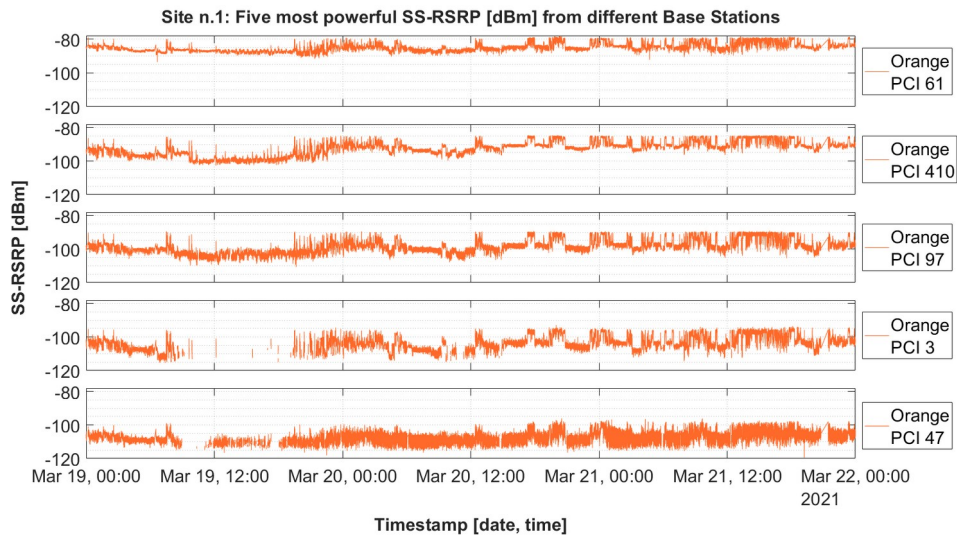


Figure 98: Site n.1 five most powerful SS-RSRP from different base stations versus date and time.

A first statistical characterization of the observed signals is reported in Table 18. Standard deviation values are more interesting than Mean values for the stability purpose.

<i>PCI</i>	<i>Provider</i>	<i>Mean [dBm]</i>	<i>Standard Deviation[dB]</i>
61	Orange	-84,4	2,2
410	Orange	-90,8	2,9
97	Orange	-96,7	3,2
3	Orange	-101,7	3,1
47	Orange	-106,2	2,5

Table 18: Site n.1 first statistical characterization of the reference signal from 5G DSS technology.

5.3.1.2 Daily data analysis

After the statistical characterization realized on all recorded data, a statistical characterization based on a daily subset of the recorded data is proposed.

Figure 99, Figure 100, Figure 101, Figure 102 and Figure 103 respectively show the statistical daily analysis conducted for the reference signals coming from PCI 61, 410, 97, 3 and 47.

Referring to the following figures, each figure is sub-divided into three rows. Each row represents a day. In each row there are two graphs. The rightmost graph represents the SS-RSRP power level versus time observed during the day as previous Figure 98. The leftmost graph represents a histogram of the power level observed during the day. In the x-axis of the histogram there are several power level bins, in the y-axis the counts of the occurrences of the respective power level bin. The histogram is an approximate representation of the distribution of numerical data.

All graphs are reported on the same x and y axis to facilitate the comparison between days of the same PCI and also between PCIs.

As observed in previous sub-paragraph, despite power levels, the signals trend is very similar.

Focusing on histograms, in the majority of cases, two distinct peaks (local maxima) appear on the graphs, evidencing a bimodal distribution.

Chapter 5 - 5G control signals: Stability analysis

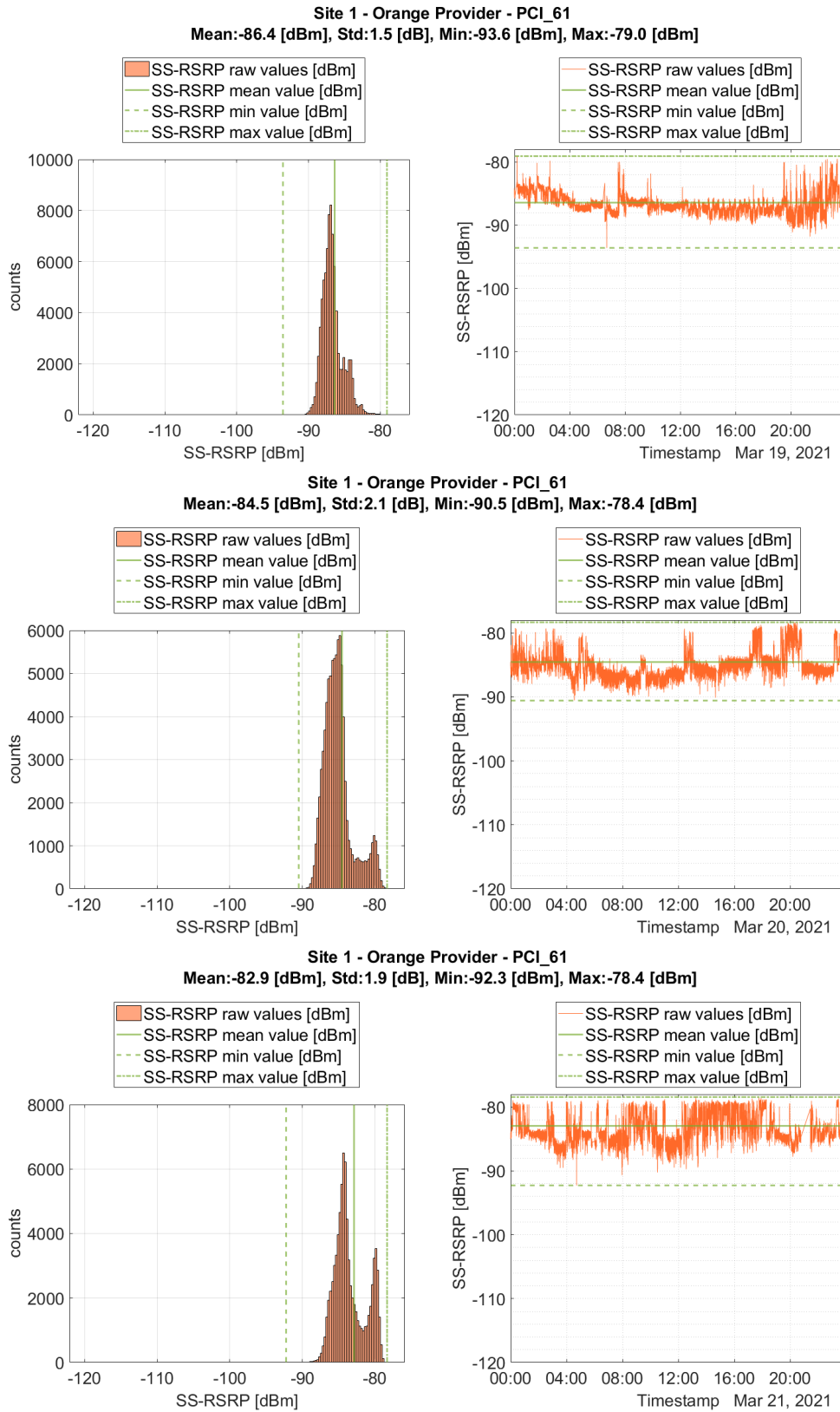


Figure 99: Site n.1 PCI 61 daily analysis.

Chapter 5 - 5G control signals: Stability analysis

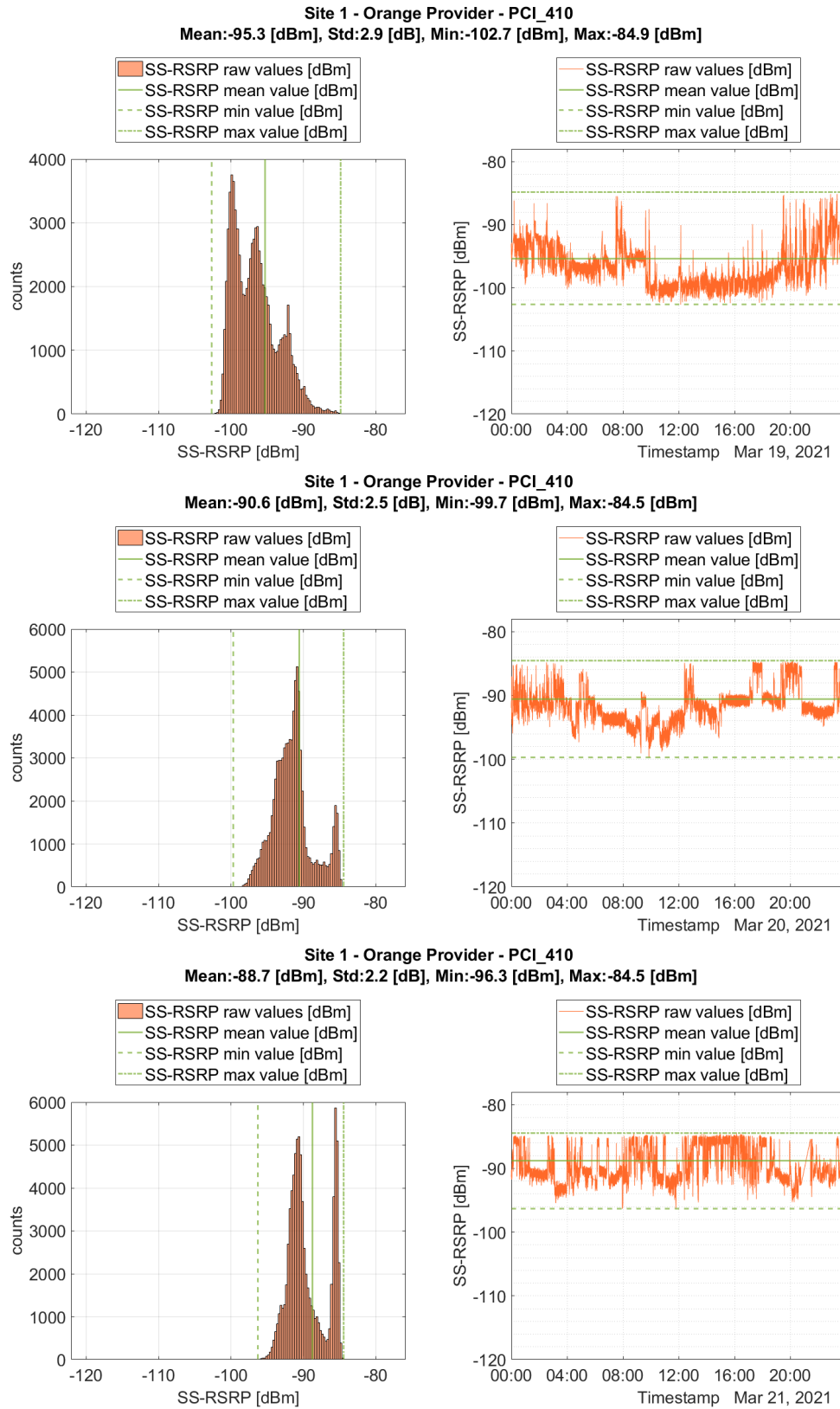


Figure 100: Site n.1 PCI 410 daily analysis.

Chapter 5 - 5G control signals: Stability analysis

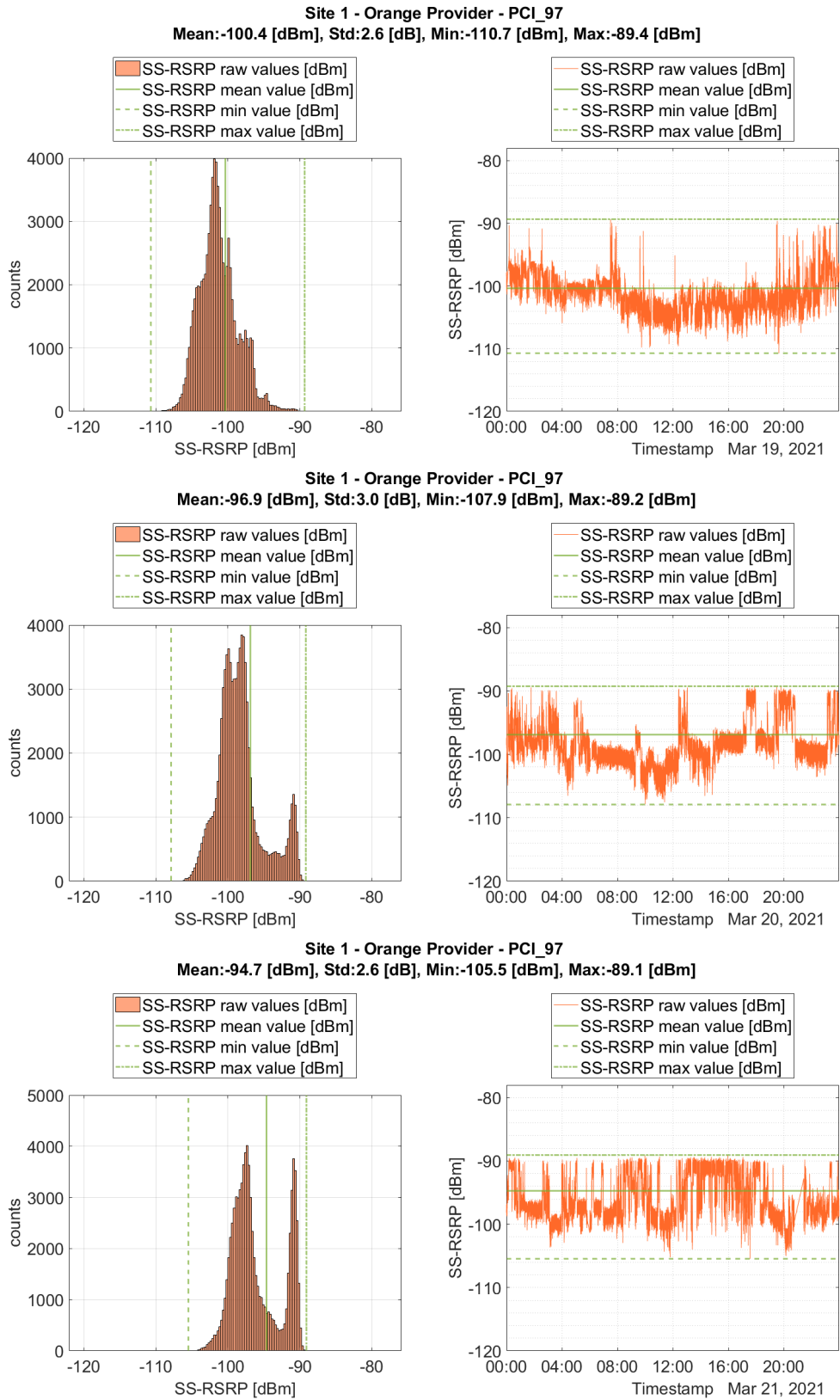


Figure 101: Site n.1 PCI 97 daily analysis.

Chapter 5 - 5G control signals: Stability analysis

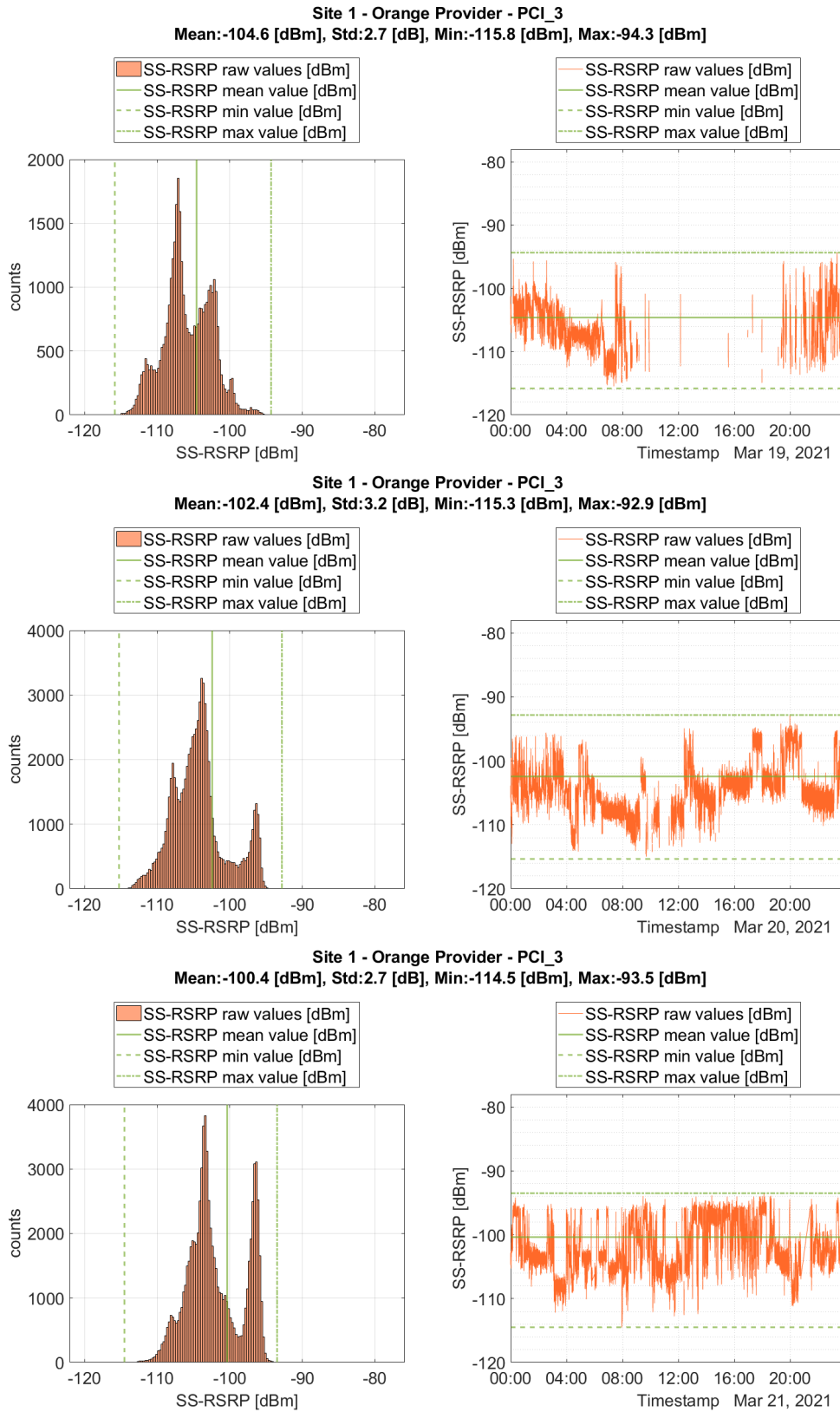


Figure 102: Site n.1 PCI 3 daily analysis.

Chapter 5 - 5G control signals: Stability analysis

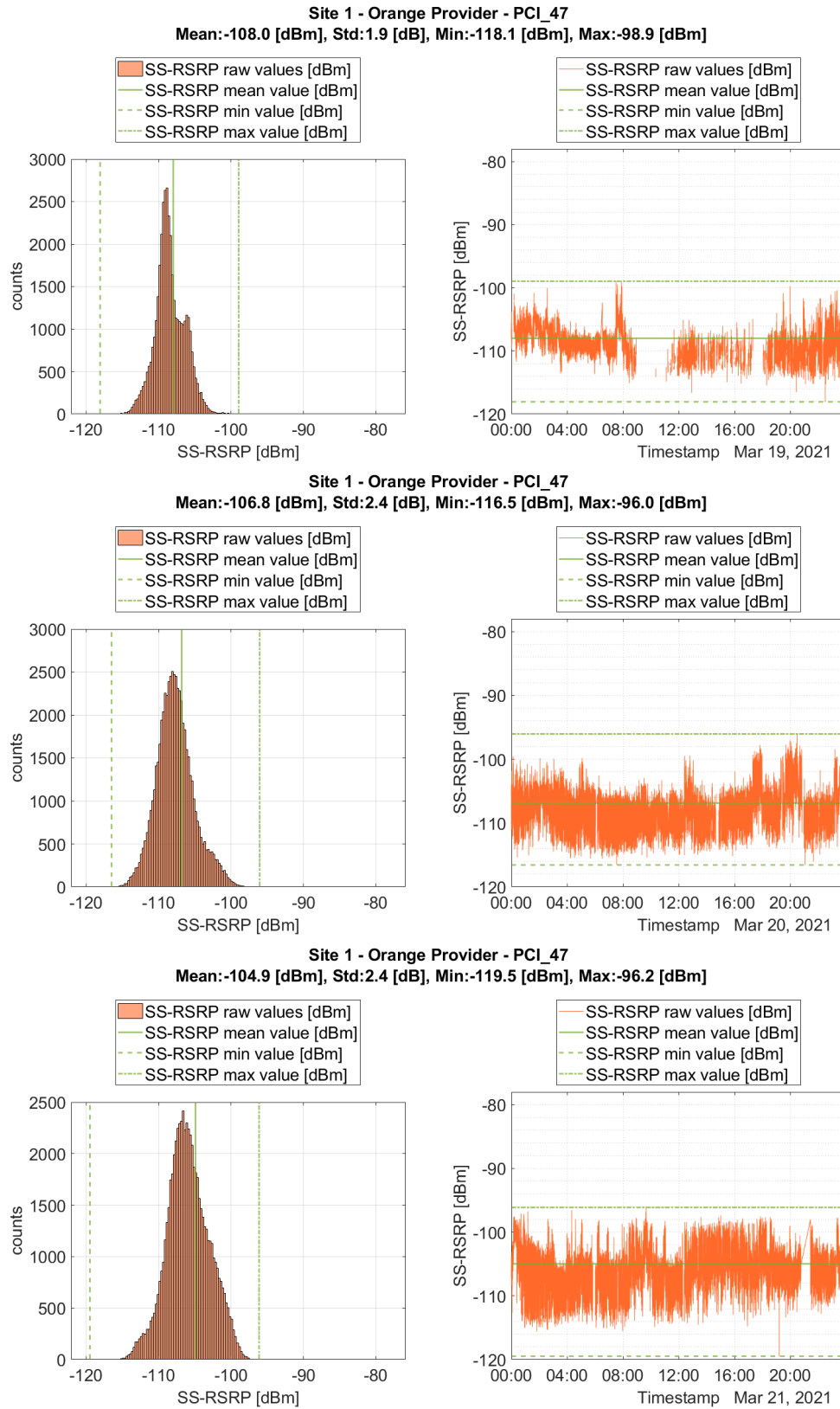


Figure 103: Site n.1 PCI 47 daily analysis.

Table 19 summarize Mean and Standard Deviation values obtained from the daily analysis. From daily standard deviation values it can be observed that variation around the mean level are roughly the same every days.

PCI	Provider	Mean [dBm]			Standard Deviation [dB]		
		19/03	20/03	21/03	19/03	20/03	21/03
61	Orange	-86,4	-84,5	-82,9	1,5	2,1	1,9
410	Orange	-95,3	-90,6	-88,7	2,9	2,5	2,2
97	Orange	-100,4	-96,9	-94,7	2,6	3,0	2,6
3	Orange	-104,6	-102,4	-100,4	2,7	3,2	2,7
47	Orange	-108,0	-106,8	-104,9	1,9	2,4	2,4

Table 19: Site n.1 Mean and Standard deviation from daily analysis.

The variation of the Mean between days can be characterized by its variation in terms of Standard deviation, as reported in the following table.

PCI	Provider	Standard Deviation of the daily Mean [dB]
61	Orange	1,4
410	Orange	2,1
97	Orange	2,0
3	Orange	1,7
47	Orange	1,4

Table 20: Site n.1 Standard Deviation of the daily Mean (only three days).

It must be noted that this results is an extremely preliminary results because it is based only on three samples available (only three days).

5.3.1.3 Six minutes interval data analysis

Six minutes interval is the averaging time for the whole-body exposure restriction in ICNIRP (1998) [5]. It is interesting to characterize the measured dataset using this time interval.

The upper part of Figure 104 shows the averaged SS-RSRP power level over six minutes non-overlapping intervals. The traces are more clear than previous representation due to the filtering effect of the mean operator. It is more evident the same trend on each signal. The lower part of Figure 104 shows the standard deviation of SS-RSRP power level over six minutes non-overlapping intervals. Also in this graph can be highlighted a strong similarity between traces.

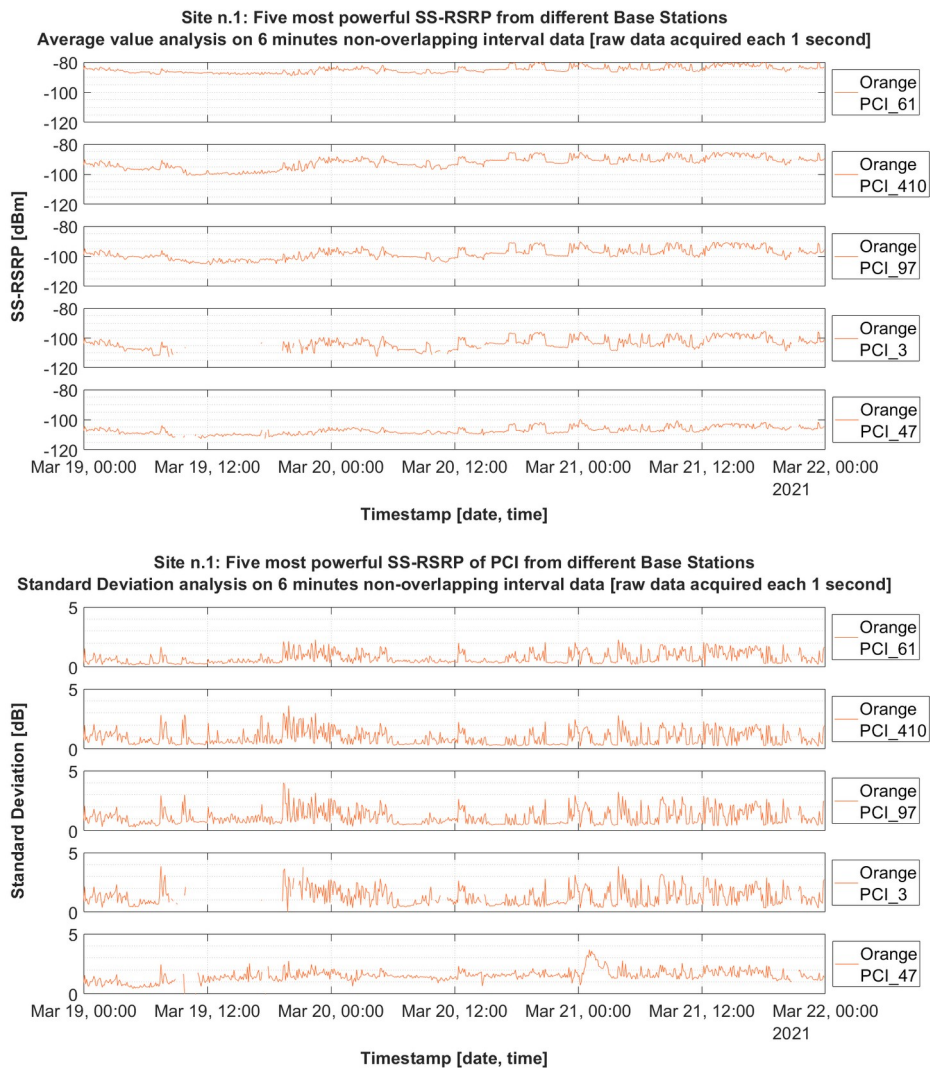


Figure 104: Site n.1 six minutes analysis, Mean and Standard Deviation versus date and time.

There are 720 intervals in the recorded data. Table 21 shows the maximum and minimum Mean value of the 720 received power six minutes intervals.

PCI	19/03/21		20/03/21		21/03/21	
	MinMean [dBm]	MaxMean [dBm]	MinMean [dBm]	MaxMean [dBm]	MinMean [dBm]	MaxMean [dBm]
61	-89,0	-82,4	-87,9	-79,7	-86,6	-79,4
410	-100,6	-88,4	-97,1	-85,5	-93,8	-85,4
97	-105,9	-94,1	-104,0	-91,0	-102,2	-90,4
3	-112,7	-99,4	-112,3	-96,1	-108,6	-95,7
47	-112,7	-103,8	-110,4	-101,9	-108,7	-99,8

Table 21: Site n.1 Maximum and Minimum Mean value of the 6 minutes intervals received power.

Table 22 shows the maximum and minimum Standard Deviation values of the 720 received power six minutes intervals.

PCI	19/03/21		20/03/21		21/03/21	
	MinSD [dB]	MaxSD [dB]	MinSD [dB]	MaxSD [dB]	MinSD [dB]	MaxSD [dB]
61	0,2	2,3	0,3	2,1	0,1	2,3
410	0,3	3,6	0,3	2,5	0,2	2,8
97	0,3	4,0	0,4	3,0	0,3	3,2
3	0,0	4,2	0,3	3,1	0,3	3,9
47	0,0	2,7	0,6	2,3	0,7	3,7

Table 22: Site n.1 Maximum and minimum Standard Deviation values of the 720 6 minutes intervals received power.

Observing results reported in Table 21, a not negligible variations between Mean Values from different intervals seems to be present. Table 23 reports the Standard Deviation of the six minutes intervals Mean.

PCI	Provider	Standard Deviation of the 6 minutes intervals Mean [dB]
61	Orange	2,0
410	Orange	2,6
97	Orange	2,9
3	Orange	2,8
47	Orange	2,1

Table 23: Site n.1 Standard Deviation of the 6 minutes intervals Mean.

5.3.1.4 Thirty minutes interval data analysis

The new whole-body exposure restriction in ICNIRP (2020) [6] has been change the averaging time from six to thirty minutes. It is interesting to characterize the measured dataset using this time interval.

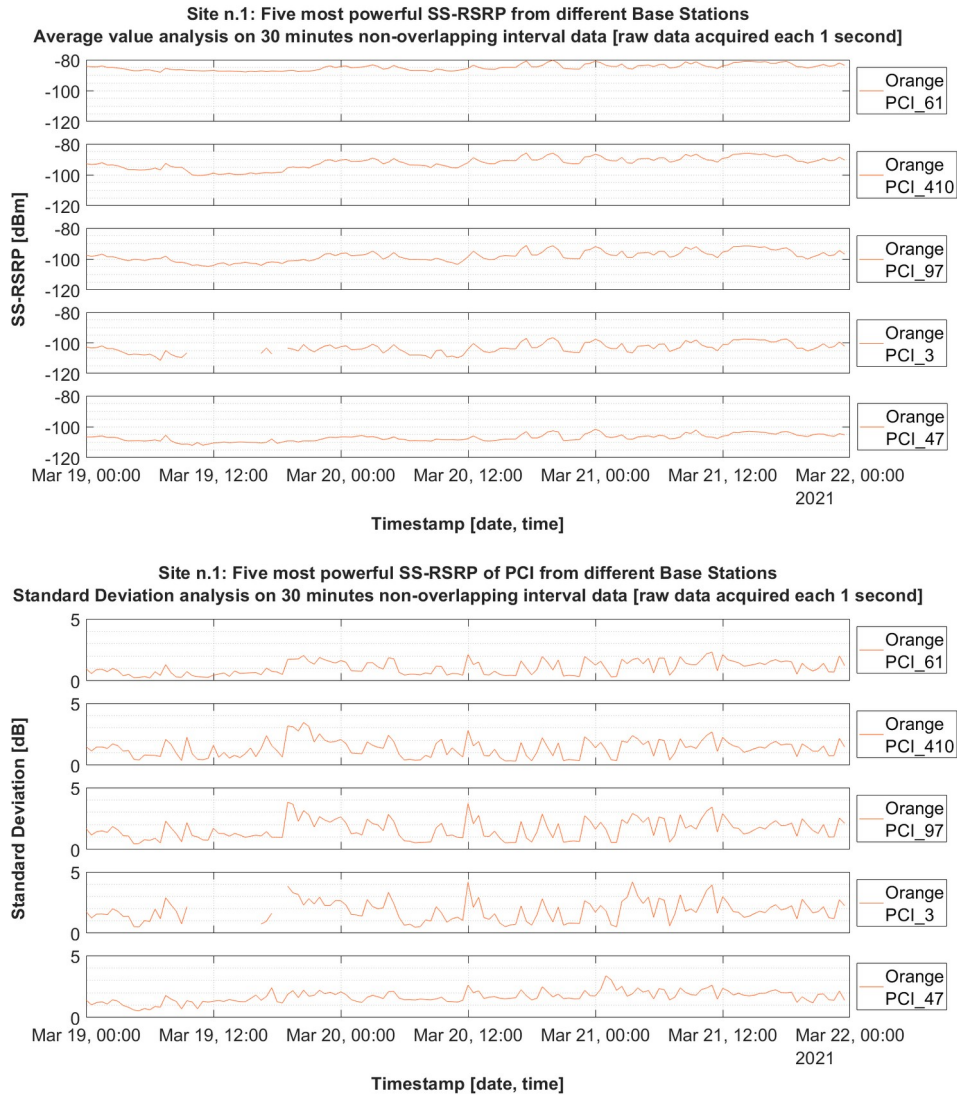


Figure 105: Site n.1 Thirty minutes analysis, Mean and Standard Deviation versus date and time.

The upper part of Figure 105 shows the averaged SS-RSRP power level over thirty minutes non-overlapping intervals. Also in this case, the traces are more clear than previous representation. It is more evident the same trend on each signal. The lower part of Figure 105 shows the standard deviation of SS-RSRP power level over thirty minutes non-overlapping intervals. Also in this graph can be highlighted a strong similarity between traces.

There are 144 intervals in the recorded data. Table 24 shows the maximum and minimum Mean value of the 144 received power 30 minutes intervals.

PCI	19/03/21		20/03/21		21/03/21	
	MinMean [dBm]	MaxMean [dBm]	MinMean [dBm]	MaxMean [dBm]	MinMean [dBm]	MaxMean [dBm]
61	-88,0	-84,0	-87,7	-80,3	-86,0	-80,9
410	-100,4	-90,2	-95,6	-85,8	-92,4	-86,1
97	-104,9	-96,5	-103,5	-91,3	-100,1	-91,5
3	-111,4	-101,1	-110,2	-96,5	-106,5	-97,4
47	-112,0	-105,5	-109,4	-102,6	-108,1	-101,5

Table 24: Site n.1 Maximum and Minimum Mean value of the 144 “30 minutes intervals” received power.

Table 25 shows the maximum and minimum Standard Deviation values of the 144 received power 30 minutes intervals.

PCI	19/03/21		20/03/21		21/03/21	
	MinSD [dB]	MaxSD [dB]	MinSD [dB]	MaxSD [dB]	MinSD [dB]	MaxSD [dB]
61	0,2	2,0	0,3	2,1	0,3	2,3
410	0,4	3,4	0,3	2,8	0,4	2,7
97	0,5	3,8	0,5	3,7	0,6	3,4
3	0,5	3,8	0,5	4,2	0,5	4,2
47	0,5	2,4	1,2	2,6	1,2	3,4

Table 25: Site n.1 Maximum and minimum Standard Deviation values of the 144 “30 minutes intervals” received power.

Observing results reported in Table 24, it seems to be a not negligible variations between Mean Values from different intervals. Table 26 reports the Standard Deviation of the six minutes intervals Mean.

PCI	Provider	Standard Deviation of the 30 minutes intervals Mean [dB]
61	Orange	1,8
410	Orange	2,4
97	Orange	2,6
3	Orange	2,5
47	Orange	2,0

Table 26: Site n.1 Standard Deviation of the 30 minutes intervals Mean.

5.3.2 Site n.2 measurement

As shown in 5.2.2.2, Site n.2 measurement were carried out in Frosinone, from 22/03/2021 to 01/04/2021 but the recorded continuous dataset is limited from 29/03/2021 00:00:00 to 31/03/2021 23:59:59. In this Scenario, the reference signals observed were coming from five base stations owned by four different Providers.

5.3.2.1 Complete data analysis

The following Figure 106 shows the date and time trend of the five most powerful SS-RSRP from PCI of different base stations. All traces are reported in the same x and y axis to facilitate the comparison. From a simple visual analysis of the different traces, It can be observed that the first two traces (PCI 415 and PCI 152) seem to be very variable, while the last three (PCI 391, 731, 399) seem to be very close to a reference value.

In the Site n.1 was observed that reference signals coming from same Provider has a similar behaviour. Focusing on Site n.2 trace PCI 152 and PCI 391 from Purple Provider, no similarity can be found among them.

When no power was detected by the Network Scanner, an empty value is reported on the graphs. During the measurement, the PCI 731 trace from Red Provider had two long signal absences where no power was detected.

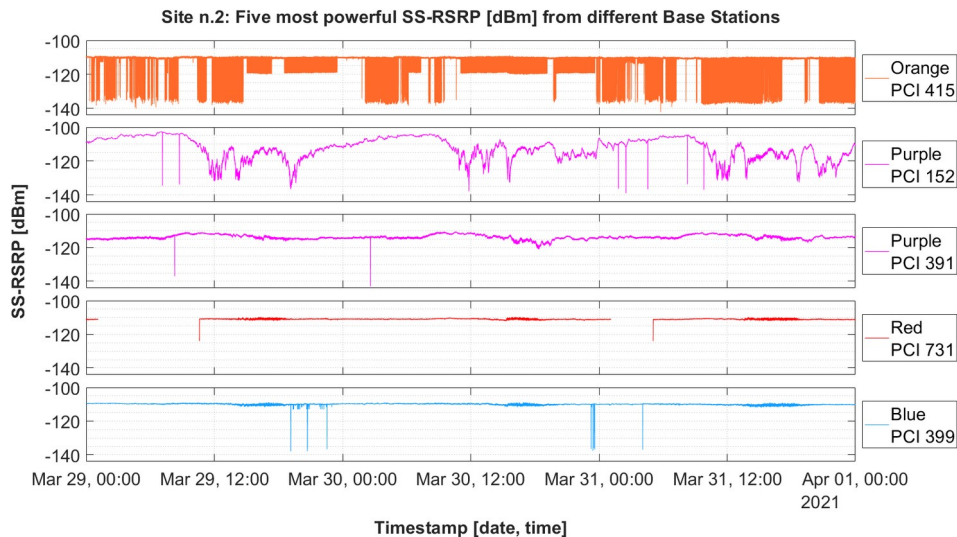


Figure 106: Site n.2 five most powerful SS-RSRP from different base stations versus date and time.

A first statistical characterization of the observed signals is reported in Table 27. Standard deviation values are more interesting than Mean values for the stability purpose.

<i>PCI</i>	<i>Provider</i>	<i>Mean [dBm]</i>	<i>Standard Deviation[dB]</i>
415	Orange	-111,3	1,9
152	Purple	-109,1	3,1
391	Purple	-113,5	1,2
731	Red	-110,9	0,3
399	Blue	-109,9	0,3

Table 27: Site n.2 first statistical characterization of the reference signal from 5G sources.

5.3.2.2 Daily data analysis

After the statistical characterization realized on all recorded data, a statistical characterization based on a daily subset of the recorded data is proposed.

Figure 107, Figure 108, Figure 109, Figure 110 and Figure 111 respectively show the statistical daily analysis conducted for the reference signals coming from PCI 415, 152, 391, 731 and 399.

Referring to the following figures, each figure is sub-divided into three rows. Each row represents a day. In each row there are two graphs. The rightmost graph represents the SS-RSRP power level versus time observed during the day as previous Figure 98. The leftmost graph represents a histogram of the power level observed during the day. In the x-axis of the histogram there are several power level bins, in the y-axis the counts of the occurrence of the respective power level bin. The histogram is an approximate representation of the distribution of numerical data.

All graphs are reported on the same x and y axis to facilitate the comparison between days of the same PCI and also between PCIs.

Chapter 5 - 5G control signals: Stability analysis

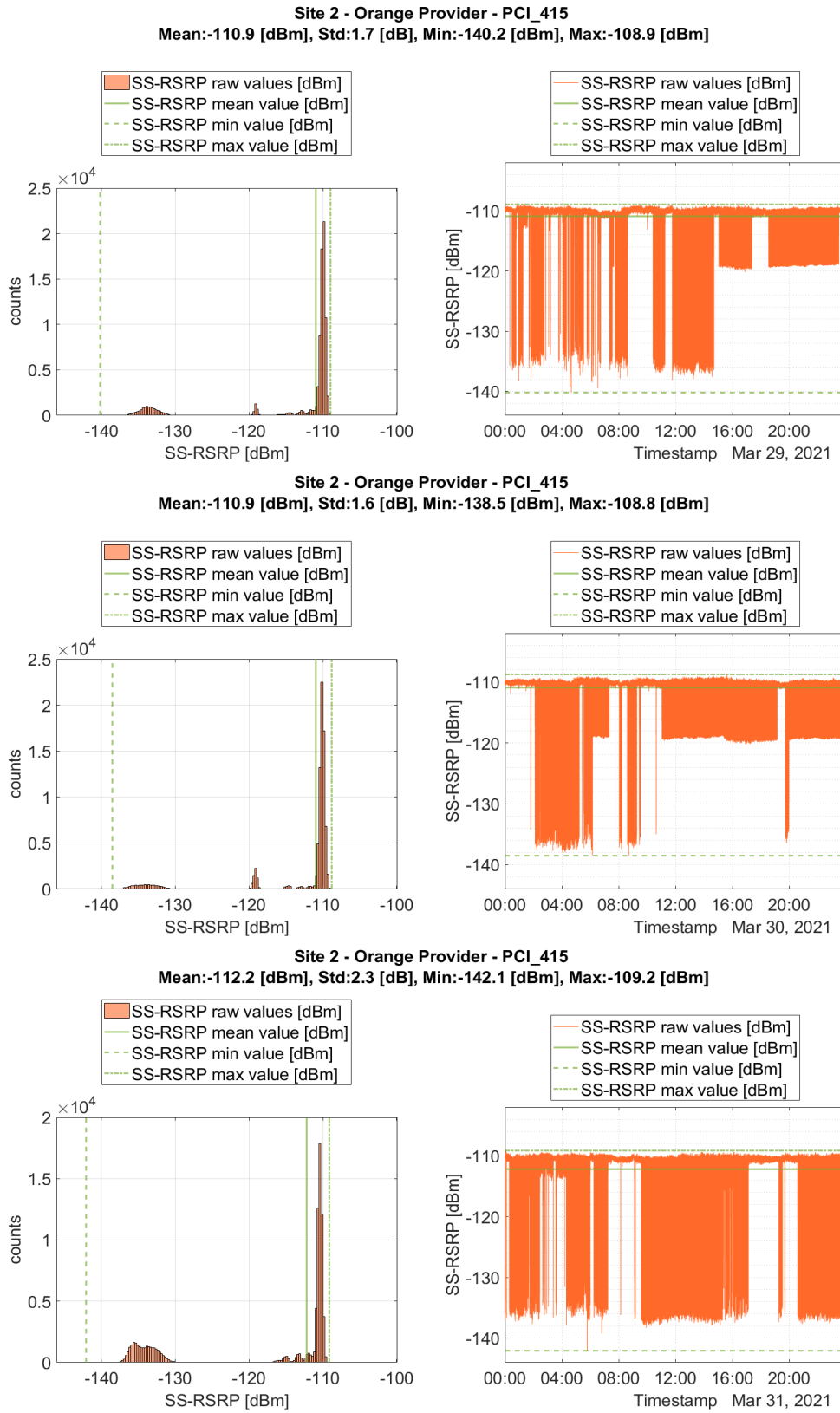


Figure 107: Site n.2 PCI 415 daily analysis.

Chapter 5 - 5G control signals: Stability analysis

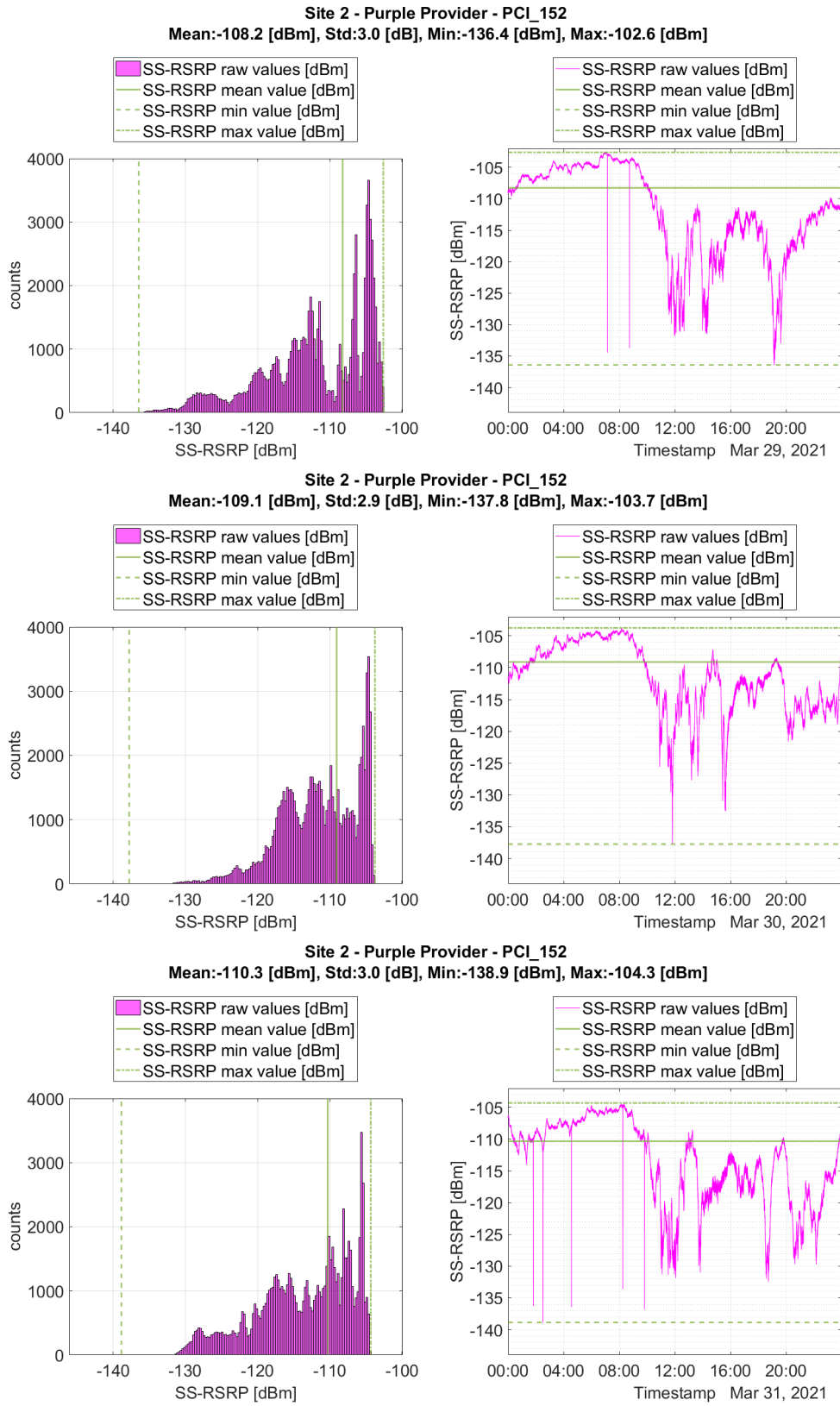


Figure 108: Site n.2 PCI 152 daily analysis.

Chapter 5 - 5G control signals: Stability analysis

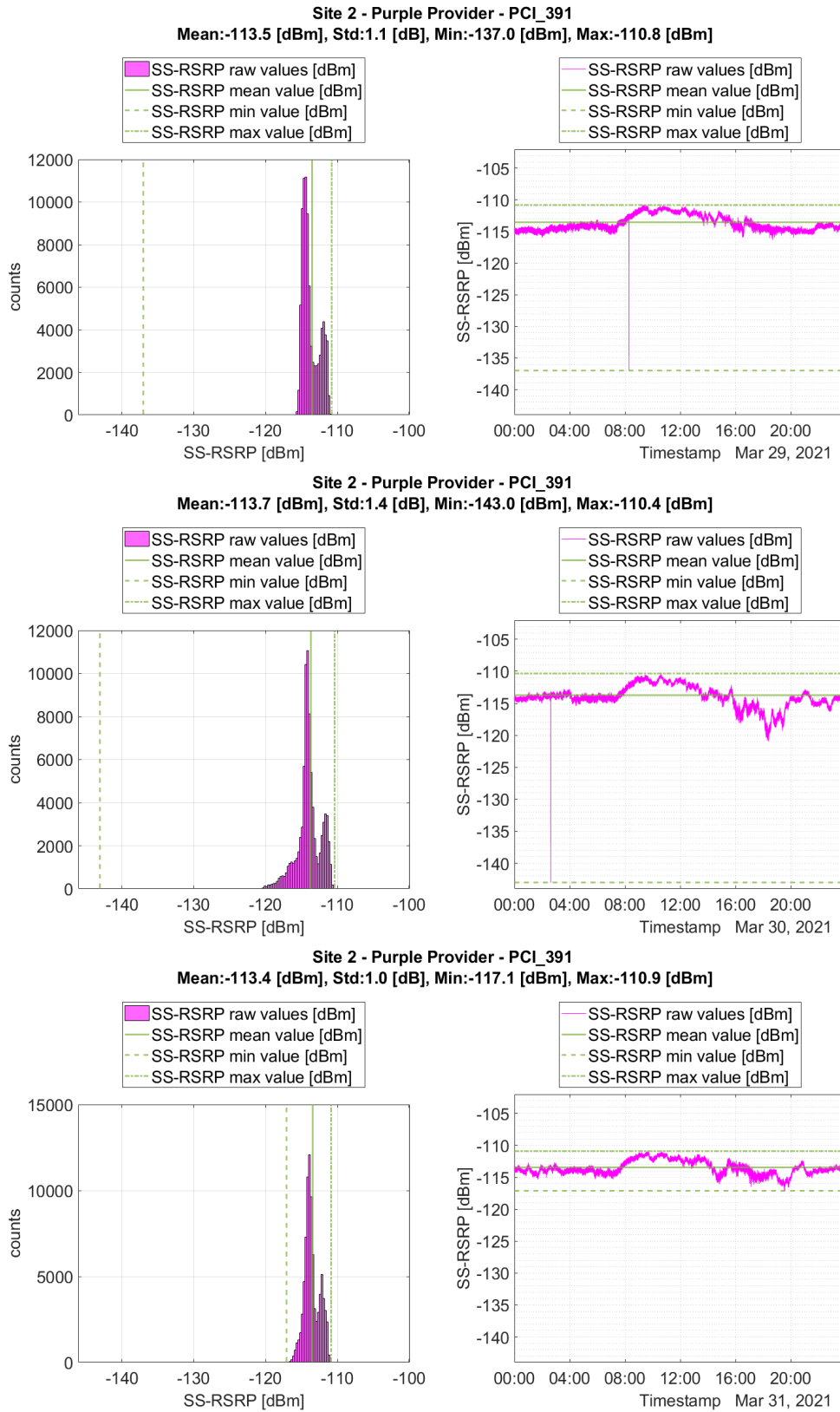


Figure 109: Site n.2 PCI 391 daily analysis.

Chapter 5 - 5G control signals: Stability analysis

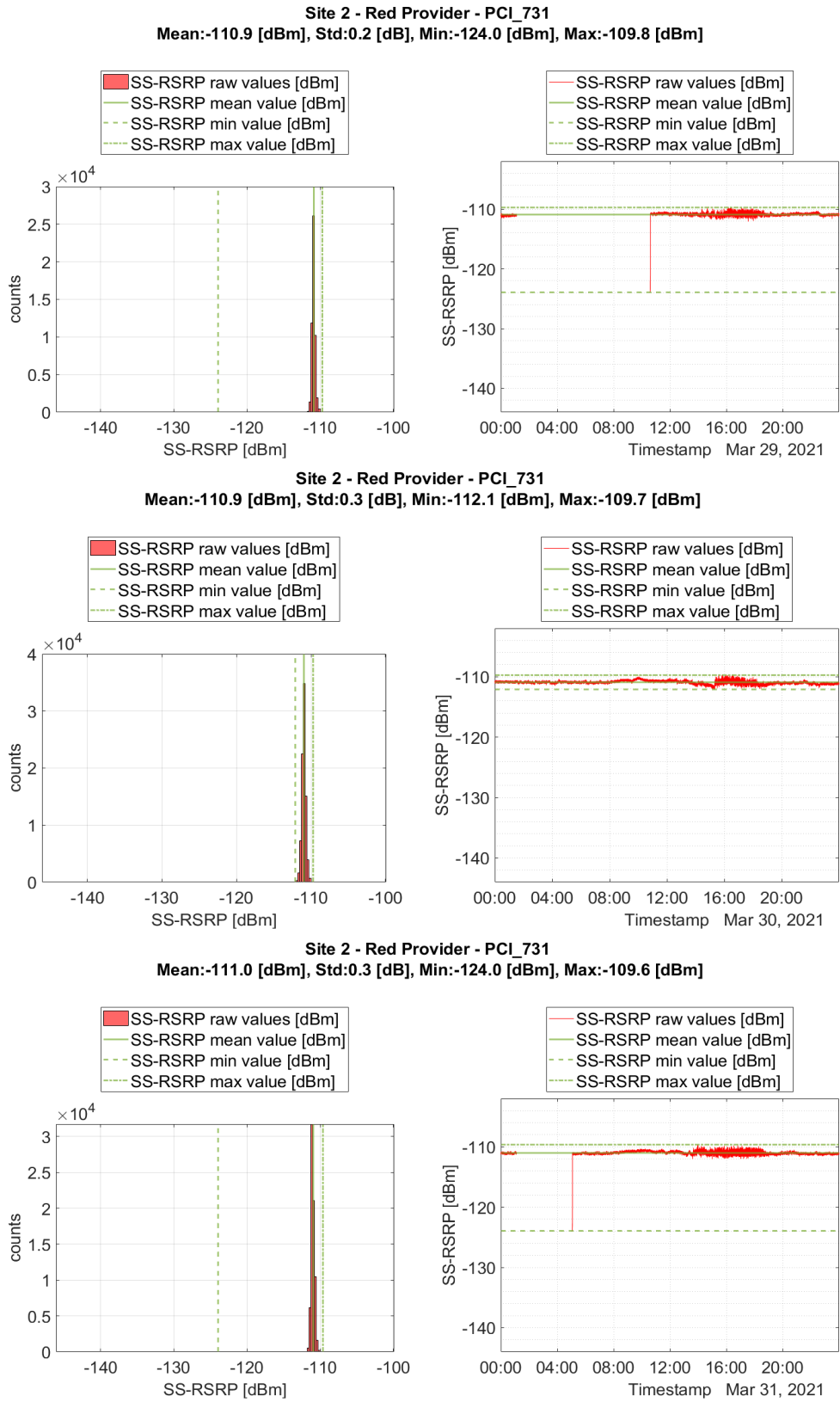


Figure 110: Site n.2 PCI 731 daily analysis.

Chapter 5 - 5G control signals: Stability analysis

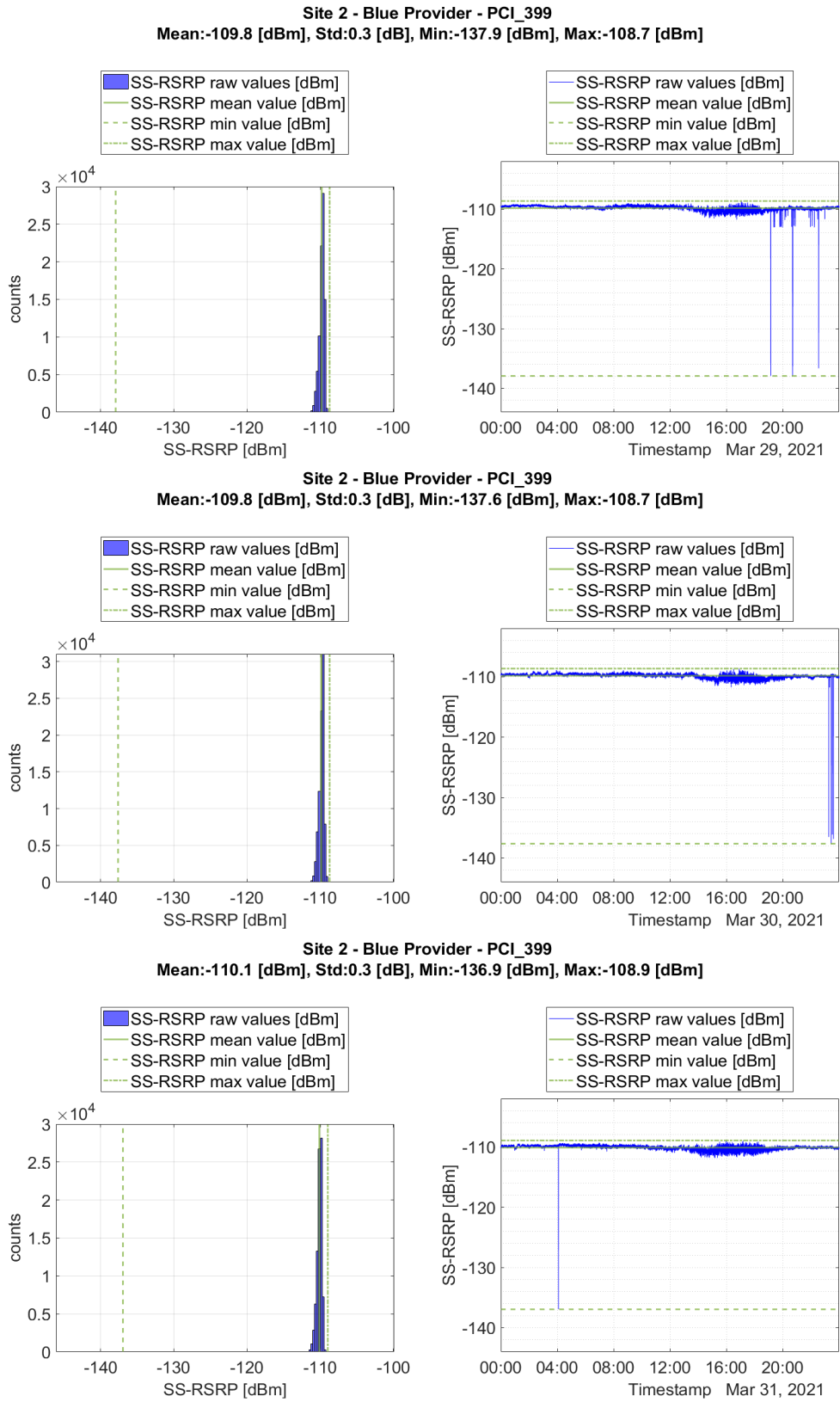


Figure 111: Site n.2 PCI 399 daily analysis.

Focusing on previous figures:

- PCI 415 can be associated to a Normal or Bimodal distributions, moreover the variability of the power levels is lower than expected from visual analysis of Figure 106;
- PCI 152 confirms its variability and its behaviour can be associate to a multimodal distributions;
- PCI 391 shows a bimodal distribution behaviour;
- PCI 731 and PCI 399 shows a Normal distribution behaviour with a low sigma.

Table 28 summarizes Mean and Standard Deviation values obtained from the daily analysis. From daily standard deviation values it can be observed that variation around the mean level are roughly the same every days.

PCI	Provider	Mean [dBm]			Standard Deviation [dB]		
		29/03	30/03	31/03	29/03	30/03	31/03
415	Orange	-110,9	-110,9	-112,2	1,7	1,6	2,3
152	Purple	-108,2	-109,1	-110,3	3,0	2,9	3,0
391	Purple	-113,5	-113,7	-113,4	1,1	1,4	1,0
731	Red	-110,9	-110,9	-111,0	0,2	0,3	0,3
399	Blue	-109,8	-109,8	-110,1	0,3	0,3	0,3

Table 28: Site n.2 Mean and Standard deviation from daily analysis.

The variation of the Mean between days can be characterized by its variation in terms of Standard deviation, as reported in Table 29.

PCI	Provider	Standard Deviation of the daily Mean [dB]
415	Orange	0,7
152	Purple	0,9
391	Purple	0,1
731	Red	0,1
399	Blue	0,2

Table 29: Site n.2 Standard Deviation of the daily Mean (only three days).

It must be noted that this results is an extremely preliminary results because it is based only on three samples available (only three days).

5.3.2.3 Six minutes interval data analysis

Six minutes interval is the averaging time for the whole-body exposure restriction in ICNIRP (1998) [5]. It is interesting to characterize the measured dataset using this time interval.

The upper part of Figure 112 shows the averaged SS-RSRP power level over six minutes non-overlapping intervals. The traces are more clear than previous representation. The lower part of Figure 112 shows the standard deviation of SS-RSRP power level over six minutes non-overlapping intervals.

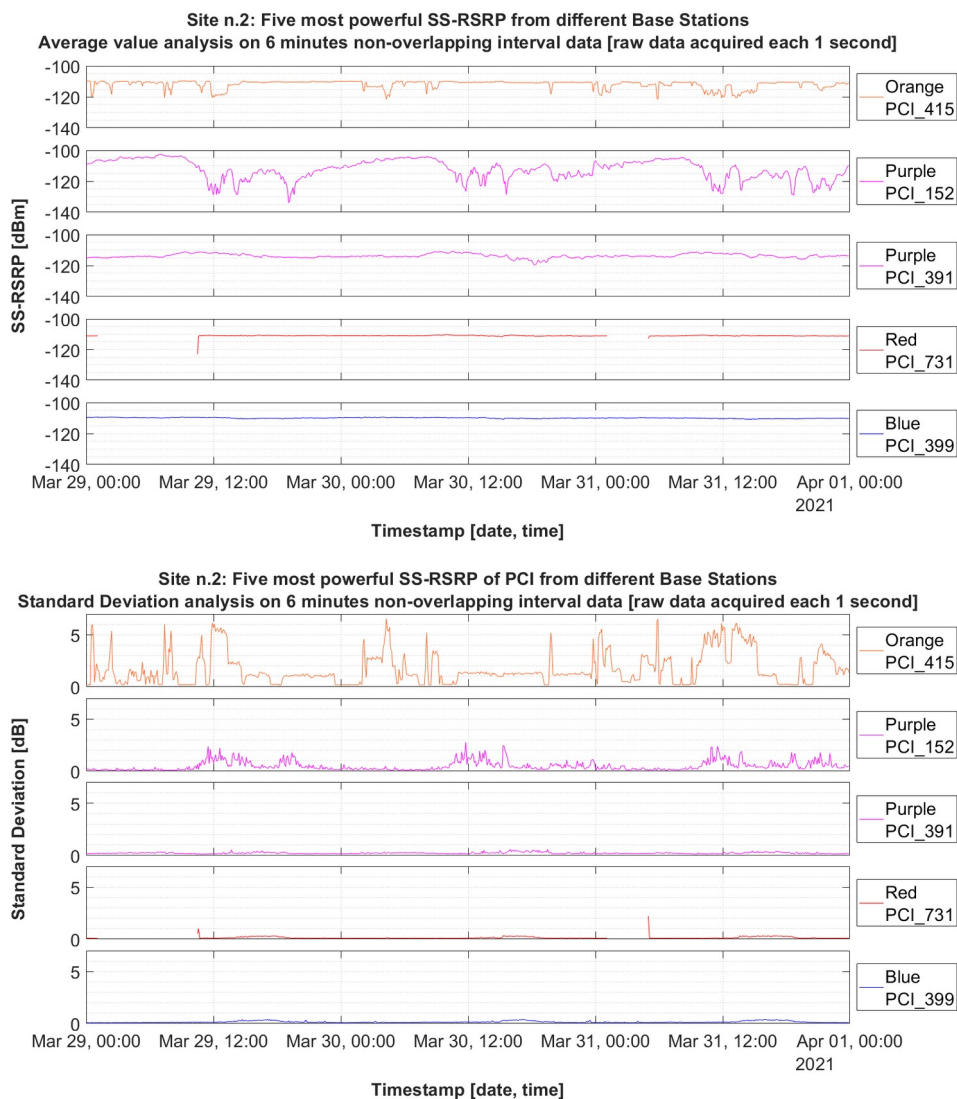


Figure 112: Site n.2 Six minutes analysis, Mean and Standard Deviation versus date and time.

There are 720 six minutes intervals in the recorded data. Table 21 shows the maximum and minimum Mean value of the 720 received power six minutes intervals.

PCI	29/03/21		30/03/21		31/03/21	
	MinMean [dBm]	MaxMean [dBm]	MinMean [dBm]	MaxMean [dBm]	MinMean [dBm]	MaxMean [dBm]
415	-120,6	-109,7	-121,7	-109,8	-121,5	-110,1
152	-134	-102,7	-128,8	-104,1	-129,1	-104,7
391	-115,2	-111,3	-119,8	-110,9	-116,2	-111,3
731	-122,9	-110,6	-111,7	-110,3	-112,8	-110,6
399	-110,6	-109,3	-110,7	-109,3	-110,8	-109,6

Table 30: Site n.2 Maximum and Minimum Mean values of the 6 minutes intervals received power.

Table 31 shows the maximum and minimum Standard Deviation values of the 720 received power six minutes intervals.

PCI	29/03/21		30/03/21		31/03/21	
	MinSD [dB]	MaxSD [dB]	MinSD [dB]	MaxSD [dB]	MinSD [dB]	MaxSD [dB]
415	0,2	6,2	0,2	6,6	0,2	6,5
152	0,0	2,4	0,1	2,8	0,1	2,4
391	0,1	0,5	0,1	0,6	0,1	0,4
731	0,1	1,0	0,1	0,3	0,1	2,2
399	0,1	0,4	0,1	0,4	0,1	0,4

Table 31: Site n.2 Maximum and minimum Standard Deviation values of the 720 6 minutes intervals received power.

Table 23 reports the Standard Deviation of the six minutes intervals Mean.

PCI	Provider	Standard Deviation of the 6 minutes intervals Mean [dB]
415	Orange	1,4
152	Purple	3,1
391	Purple	1,2
731	Red	0,3
399	Blue	0,3

Table 32: Site n.2 Standard Deviation of the 6 minutes intervals Mean.

5.3.2.4 Thirty minutes interval data analysis

The new whole-body exposure restriction in ICNIRP (2020) [6] has been changed the averaging time from six to thirty minutes. It is interestingly to characterize the measured dataset using this time interval.

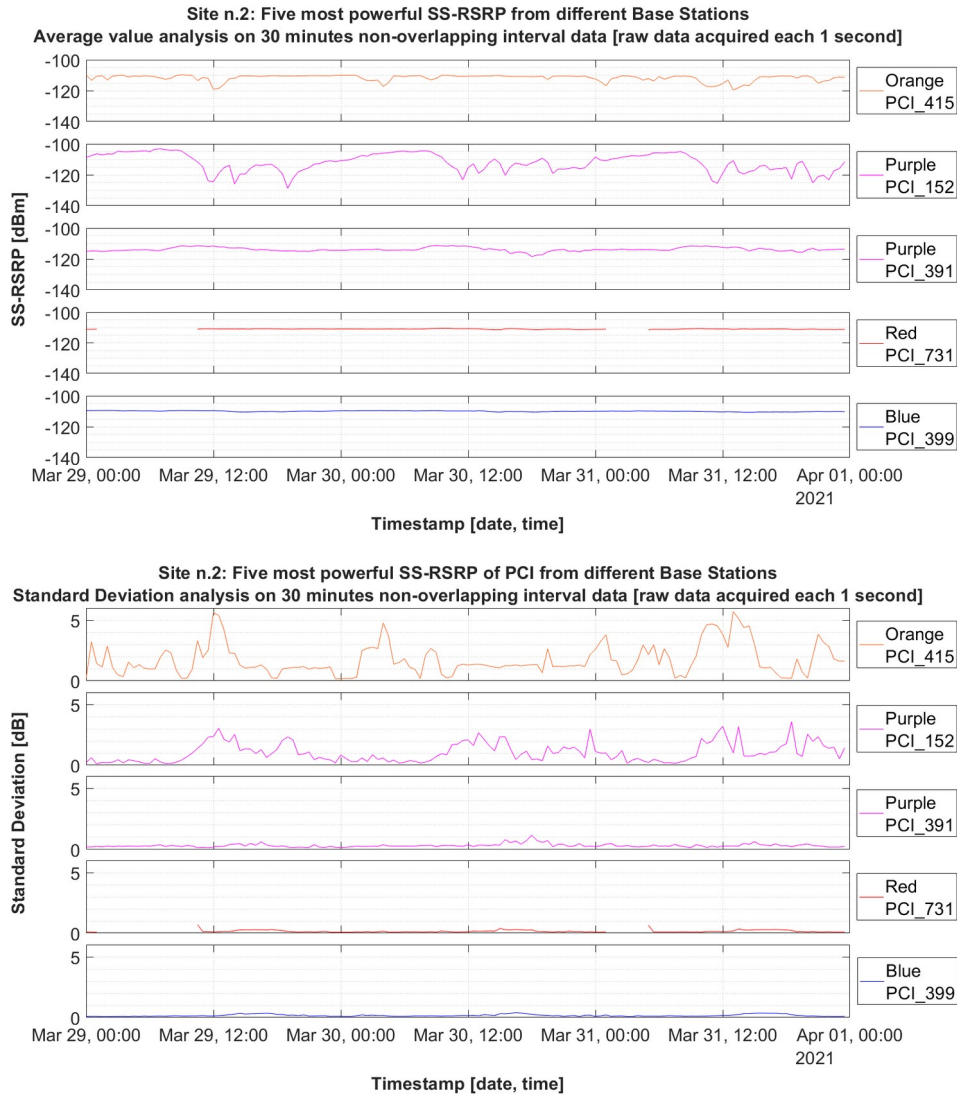


Table 33: Site n.2 Thirty minutes analysis, Mean and Standard Deviation versus date and time.

The upper part of Figure 105 shows the averaged SS-RSRP power level over thirty minutes non-overlapping intervals. The traces are more clear than previous representation. Lower part of Figure 105 shows the standard deviation of SS-RSRP power level over thirty minutes non-overlapping intervals. The flatness of PCI 391, PCI 731 and PCI 399 is more evident.

There are 144 intervals inside the recorded data. Table 24 shows the maximum and minimum Mean value of the 144 received power 30 minutes intervals.

PCI	29/03/21		30/03/21		31/03/21	
	MinMean [dBm]	MaxMean [dBm]	MinMean [dBm]	MaxMean [dBm]	MinMean [dBm]	MaxMean [dBm]
415	-119,1	-109,7	-117,2	-110,0	-119,6	-110,3
152	-128,7	-103,1	-123,3	-104,4	-125,4	-104,9
391	-115,0	-111,4	-118,4	-111,2	-115,7	-111,5
731	-111,1	-110,7	-111,4	-110,4	-111,3	-110,6
399	-110,4	-109,4	-110,5	-109,5	-110,7	-109,7

Table 34: Site n.2 Maximum and Minimum Mean value of the 144 “30 minutes intervals” received power.

Table 25 shows the maximum and minimum Standard Deviation values of the 144 received power 30 minutes intervals.

PCI	29/03/21		30/03/21		31/03/21	
	MinSD [dB]	MaxSD [dB]	MinSD [dB]	MaxSD [dB]	MinSD [dB]	MaxSD [dB]
415	0,2	5,6	0,2	4,8	0,2	5,7
152	0,1	3,0	0,2	3,0	0,1	3,6
391	0,1	0,6	0,2	1,2	0,2	0,6
731	0,1	0,7	0,1	0,4	0,1	0,6
399	0,1	0,4	0,1	0,4	0,1	0,4

Table 35: Site n.2 Maximum and minimum Standard Deviation values of the 144 “30 minutes intervals” received power.

Observing results reported in Table 24, it seems to be a not negligible variations between Mean Values from different intervals. Table 36 reports the Standard Deviation of the six minutes intervals Mean.

PCI	Provider	Standard Deviation of the 30 minutes intervals Mean [dB]
415	Orange	1,2
152	Purple	3,0
391	Purple	1,1
731	Red	0,2
399	Blue	0,3

Table 36: Site n.2 Standard Deviation of the 30 minutes intervals Mean.

5.4 Conclusion

In the previous paragraph several statistical analysis have been realized on measured dataset. In this paragraph the results will be summarized to give a general indication on signal stability.

Referring to following tables:

- SD [dB] represents the Standard Deviation calculated on the complete dataset recorded (about 259.200 samples for each PCI);
- Max SD1d [dB] represents the maximum of the daily Standard Deviation (about 86.400 samples for each PCI and for 3 intervals);
- SD1dm [dB] represents the Standard Deviation of the daily mean (3 samples for each PCI);
- Max SD6d [dB], represents the maximum of the daily Standard Deviation (about 360 samples for 720 intervals);
- SD6mm [dB] represents the Standard Deviation of the six minutes intervals (720 samples for each PCI);
- Max SD30d [dB], represents the maximum of the daily Standard Deviation (360 samples for each PCI and for each 144 intervals);
- SD30mm [dB] represent the Standard Deviation of the six minutes intervals (144 samples for each PCI).

Before to read the results several considerations must be taken into account:

- The field tests were carried out in an early stage of 5G deployment where 5G traffic is almost absent and installations could be operating in test mode;
- 5G DSS implementation is vendor-specific and measurements were carried out on signals coming from the same provider, that with a high probability means same vendor;
- Results are presented in the terms of maximum worst case.

5.4.1 Site n.1 stability results

Table 37 summarizes the Site n.1 stability analysis with information taken respectively from Table 18, Table 19, Table 20, Table 21, Table 22, Table 23, Table 24, Table 25 and Table 26.

PCI	SD [dB]	Max SD1d [dB]	SD1dm [dB]	Max SD6m [dB]	SD6mm [dB]	Max SD30m [dB]	SD30mm [dB]
61	2,2	2,1	1,4	2,3	2,0	2,3	1,8
410	2,9	2,9	2,1	3,6	2,6	3,4	2,4
97	3,2	3,0	2,0	4,0	2,9	3,8	2,6
3	3,1	3,2	1,7	4,2	2,8	4,2	2,5
47	2,5	2,4	1,4	3,7	2,1	3,4	2,0

Table 37: Site n.1 Standard Deviations summarization.

Considering the worst possible case applying the maximum operator on each column of Table 37 it is possible to obtain Table 38.

SD [dB]	Max SD1d [dB]	SD1dm [dB]	Max SD6m [dB]	SD6mm [dB]	Max SD30m [dB]	SD30mm [dB]
3,2	3,2	2,1	4,2	2,9	4,2	2,6

Table 38: Site n.1 Standard Deviations worst case summarization.

Analysing Table 38, it is possible to give an indication of the stability of a 5G DSS reference signal in terms of standard deviation in the worst possible case:

- The maximum standard deviation calculated on the complete trace of the raw data is 3,2 dB;
- The maximum standard deviation calculated on the raw data every day is 3,2 dB;
- The maximum standard deviation calculated on the daily mean values value is 2,1 dB;
- The maximum standard deviation calculated on the raw every 6 minutes is 4,2 dB;
- The maximum standard deviation calculated on the 6-minutes mean values is 2,9 dB;
- The maximum standard deviation calculated on the raw every 6 minutes is 4,2 dB;

- The maximum standard deviation calculated on the 30-minutes mean values is 2,6 dB.

Comparing the result with the typical uncertainty of the measurement chains this value is higher than expected.

5.4.2 Site n.2 stability results

Table 39 summarizes the Site n.2 stability analysis with information taken respectively from Table 27, Table 28, Table 29, Table 30, Table 31, Table 32, Table 33, Table 34, Table 35 and Table 36.

PCI	SD [dB]	Max SD1d [dB]	SD1dm [dB]	Max SD6m [dB]	SD6mm [dB]	Max SD30m [dB]	SD30mm [dB]
415	1,9	2,3	0,7	6,6	1,4	5,7	1,2
152	3,1	3,0	0,9	2,8	3,1	3,6	3,0
391	1,2	1,4	0,1	0,6	1,2	1,2	1,1
731	0,3	0,3	0,1	2,2	0,3	0,7	0,2
399	0,3	0,3	0,2	0,4	0,3	0,4	0,3

Table 39: Site n.2 Standard Deviations summarization.

Considering the worst possible case applying the maximum operator on each column of Table 39 it is possible to obtain Table 40.

SD [dB]	Max SD1d [dB]	SD1dm [dB]	Max SD6m [dB]	SD6mm [dB]	Max SD30m [dB]	SD30mm [dB]
3,1	3,0	0,9	6,6	3,1	5,7	3,0

Table 40: Site n.2 Standard Deviations worst case summarization.

Analysing Table 40, it is possible to give an indication of the stability of a 5G reference signal in terms of standard deviation in the maximum worst possible case. Also in this case comparing the result with the typical uncertainty of the measurement chains this value is a higher than expected.

Remarking that the field tests were carried out in an early stage of 5G deployment where 5G traffic is almost absent and installations could be operating in test mode. It is possible to exclude from the result the PCI 415 and PCI 152.

Considering only the PCI 391, PCI 731 and PCI 399, three of five observed signals from three different Providers, the maximum worst case is presented in Table 41.

<i>SD</i> [dB]	<i>Max</i> <i>SD1d</i> [dB]	<i>SD1dm</i> [dB]	<i>Max</i> <i>SD6m</i> [dB]	<i>SD6mm</i> [dB]	<i>Max</i> <i>SD30m</i> [dB]	<i>SD30mm</i> [dB]
1,2	1,4	0,2	2,2	1,2	1,2	1,1

Table 41: Site n.2 Standard Deviations worst case summarization, limited to PCI 391, PCI 731 and PCI 399

Considering Table 41, it is possible to give an indication of the stability of a 5G reference signal in terms of standard deviation in the maximum worst possible case:

- The maximum standard deviation calculated on the complete trace of the raw data is 1,2 dB;
- The maximum standard deviation calculated on the raw data every day is 1,4 dB;
- The maximum standard deviation calculated on the daily mean values value is 0,2 dB;
- The maximum standard deviation calculated on the raw every 6 minutes is 2,2 dB;
- The maximum standard deviation calculated on the 6-minutes mean values is 1,2 dB;
- The maximum standard deviation calculated on the raw every 6 minutes is 1,2 dB;
- The maximum standard deviation calculated on the 30-minutes mean values is 1,1 dB.

These values not only are comparable with typical uncertainty of the measurement chains but, in the majority of case, they are lower than level measurement uncertainty of the Network Scanner (Table 11).

This first raw result candidates the SS-RSRP of 5G signal as a good reference signal to be used in the process of extrapolation to maximum RF field strength for 5G systems.

6 Conclusion and further development

The scope of this thesis was the study of the stability of the 5G reference signals. Before to carry out measurement and the stability analysis an extensive background was acquired.

In the first chapter limits and measurement methods of electromagnetic fields (EMFs) were identified. The primary sources used to identify Limits were the ICNIRP guidelines. The primary sources used to identify Measurement Methods were IEC and CEI standards. Legal requirements established by National Governments are based on the identified limits and measurement methods are essential to assess the conformity of an installation with the legal requirements.

Among available Measurement Methods, the extrapolation to maximum power represents one of the most attractive measurement method. It enables to extrapolate the maximum possible output power emitted by a radio base station system (a time variant signal), measuring a time invariant component of the system (pilot, control or reference signal/channel). The extrapolation to maximum power is standardized for 2G, 3G, and 4G technologies, but is still under investigation for 5G technology. Standardization entities and scientific community are working on this matter.

In the second chapter the main characteristics of the 4G control signals have been presented. After that, the available methods for extrapolation to maximum power of 4G systems have been evaluated.

In the third chapter the main characteristics of the 5G control signals (i.e. SS/PBCH block) were presented. After an extensive research on available free scientific literature, four experimental extrapolation process were selected. Inside chapter three, the proposals were presented and compared. Although any proposal has its own approach, it was identified a common philosophy for the extrapolation process. The power measurement of a resource element inside the SS/PBCH block is a common step.

To complete the 5G systems overview, the fourth chapter introduced the Dynamic Spectrum Sharing feature. This feature enables the transmission of 5G signals inside 4G spectrum. Although DSS degrades the overall system performance of both 4G and 5G, this feature is and will be used by some operators to rapidly increase the coverage of 5G signals.

In the fifth chapter the experimental activities carried out during the thesis work were described.

Thanks to Rohde & Schwarz a last generation Network Scanner was available for about a month. After a first week to understand the main

functions of the instrument, two measurement campaigns were carried out. Some problems were encountered during the usage of the Network Scanner.

It was used for recording 5G signals in two locations, namely Site n.1 and Site n.2, for at least three consecutive days.

The experimental activities included also the practical installation of the measurement setup in Site n.2. The antenna was mounted on a small tower, the RF cable was placed and the electrical and network connections were realized. Site n.1 and Site n.2 setups were remote controlled thanks to the network connection and a remote control software. The experimental activities included also preliminary surveys and two drive tests to localize signal sources in Site n.2.

From recording the SS-RSRP values of five most powerful PCI were extracted. A python script was developed to adapt and merge extracted files. Several Matlab scripts were written for the stability analysis and for plotting the graphs. The results of the stability analysis were presented in the final paragraph of the fifth chapter.

Thanks to first raw results presented in chapter five, the SS-RSRP of 5G signal was identified as a good candidate to be used in the process of extrapolation to maximum RF field strength for 5G systems.

Concluding, this thesis work is part of the activities of Instrumentation and Measurement Team of the Department of Electrical and Information Engineering "Maurizio Scarano" of University of Cassino and Southern Lazio and it represents a first approach to 5G signals. Field tests were carried out in an early stage of 5G deployment where 5G traffic is almost absent. Moreover, the measurement were executed without the help of the Providers.

Future works may will use the recorded data:

- to perform more elaborated statistical analysis on SS-RSRP;
- to extract other informations related to SSB/PBCH block like SS-RSRQ, SINR to better understand the behaviour of the SS-RSRP.

Bibliography

- [1] 5GROWTH @5growth_eu, “The evolution of mobile wireless communication technology: from 1G to 5G.,” 24-Jun-2020. [Online]. Available: https://twitter.com/5growth_eu/status/1275700745795493889
- [2] M. Chiani, E. Paolini, and F. Callegati, “White Paper - Open issues and beyond 5G,” presented at the 5G Italy - The Global Meeting in Rome, CNR Piazza Aldo Moro Roma, 2018, p. 11 [Online]. Available: <https://www.5gitaly.eu/2018/wp-content/uploads/2019/01/5G-Italy-White-eBook-Beyond-5G.pdf>
- [3] Ericsson, “Ericsson Mobility Report Q2 Update September 2020,” p. 4, 2020.
- [4] R. Pawlak, P. Krawiec, and J. Zurek, “On Measuring Electromagnetic Fields in 5G Technology,” *IEEE Access*, vol. 7, pp. 29826–29835, 2019, doi: 10.1109/ACCESS.2019.2902481.
- [5] ICNIRP, “Guidelines on limiting exposure to non-ionizing radiation: a reference book based on the guidelines on limiting exposure to non-ionizing radiation and statements on special applications,” *Health Physics*, vol. 74, no. 4, pp. 494–522, 1998.
- [6] ICNIRP, “Guidelines for Limiting Exposure to Electromagnetic Fields (100 kHz to 300 GHz),” *Health Physics*, vol. 118, no. 5, 2020.
- [7] ICNIRP, “GUIDELINES FOR LIMITING EXPOSURE TO TIME-VARYING ELECTRIC AND MAGNETIC FIELDS (1 Hz TO 100 kHz),” *Health Physics*, vol. 99, no. 6, pp. 818–836, Dec. 2010, doi: 10.1097/HP.0b013e3181f06c86.
- [8] WHO, “World Health Organization. Radiofrequency fields; Public Consultation Document,” Geneva, 2014.
- [9] European Commission. Directorate General for Health and Consumers., *Opinion on potential health effects of exposure to electromagnetic fields (EMF)*. LU: Publications Office, 2015 [Online]. Available: <https://data.europa.eu/doi/10.2772/75635>. [Accessed: 24-Apr-2021]
- [10] SSM’s Scientific Council on Electromagnetic Fields, “2015:19 - Recent Research on EMF and Health Risk - Tenth report from SSM’s Scientific Council on Electromagnetic Fields,” p. 102, 2015.
- [11] SSM’s Scientific Council on Electromagnetic Fields, “2016:18 - Recent Research on EMF and Health Risk - Eleventh report from SSM’s Scientific Council on Electromagnetic Fields,” p. 115, 2016.
- [12] SSM’s Scientific Council on Electromagnetic Fields, “2018:09 - Recent Research on EMF and Health Risk - Twelfth report from SSM’s Scientific Council on Electromagnetic Fields,” 2018.
- [13] ACGIH, *2017 TLVs and BEIs: Based on the documentation of the threshold limit values for chemical substances and physical agents & biological exposure indices*. Cincinnati, OH, 2017 [Online]. Available: <http://www.acgih.org/forms/store/ProductFormPublic/2017-tlvs-and-beis>
- [14] A. M. J. van den Heuvel, B. J. Haberley, D. J. R. Hoyle, N. A. S. Taylor, and R. J. Croft, “The independent influences of heat strain and dehydration upon cognition.,” *Eur J Appl Physiol*, vol. 117, no. 5, pp. 1025–1037, May 2017, doi: 10.1007/s00421-017-3592-2.

- [15] A. Hirata, I. Laakso, T. Oizumi, R. Hanatani, K. H. Chan, and J. Wiart, "The relationship between specific absorption rate and temperature elevation in anatomically based human body models for plane wave exposure from 30 MHz to 6 GHz.," *Phys Med Biol*, vol. 58, no. 4, pp. 903–921, Feb. 2013, doi: 10.1088/0031-9155/58/4/903.
- [16] P. G. Weyand, B. R. Smith, and R. F. Sandell, "Assessing the metabolic cost of walking: the influence of baseline subtractions," *Annual International Conference of the IEEE Engineering in Medicine and Biology Society. IEEE Engineering in Medicine and Biology Society. Annual International Conference*, vol. 2009, p. 6878–6881, 2009, doi: 10.1109/iembs.2009.5333126.
- [17] L. P. J. Teunissen, A. Grabowski, and R. Kram, "Effects of independently altering body weight and body mass on the metabolic cost of running.," *J Exp Biol*, vol. 210, no. Pt 24, pp. 4418–4427, Dec. 2007, doi: 10.1242/jeb.004481.
- [18] K. Sasaki, M. Mizuno, K. Wake, and S. Watanabe, "Monte Carlo simulations of skin exposure to electromagnetic field from 10 GHz to 1 THz.," *Phys Med Biol*, vol. 62, no. 17, pp. 6993–7010, Aug. 2017, doi: 10.1088/1361-6560/aa81fc.
- [19] S. Kodera, A. Hirata, D. Funahashi, S. Watanabe, K. Jokela, and R. J. Croft, "Temperature Rise for Brief Radio-Frequency Exposure Below 6 GHz," *IEEE Access*, vol. 6, pp. 65737–65746, 2018, doi: 10.1109/ACCESS.2018.2878149.
- [20] ICNIRP, "Differences between the ICNIRP (2020) and previous guidelines." [Online]. Available: <https://www.icnirp.org/en/differences.html>. [Accessed: 27-Oct-2020]
- [21] "IEEE Standard for Safety Levels with Respect to Human Exposure to Electric, Magnetic, and Electromagnetic Fields, 0 Hz to 300 GHz - Redline," *IEEE Std C95.1-2019 (Revision of IEEE Std C95.1-2005/ Incorporates IEEE Std C95.1-2019/Cor 1-2019) - Redline*, pp. 1–679, Oct. 2019.
- [22] C.-K. Chou, "New IEEE EMF Exposure Safety Standard - Presentation," presented at the IEEE Oakland East Bay Life Member Affinity Group, Livermore, California, 2019, p. 47.
- [23] W. H. Bailey *et al.*, "Synopsis of IEEE Std C95.1TM-2019 'IEEE Standard for Safety Levels With Respect to Human Exposure to Electric, Magnetic, and Electromagnetic Fields, 0 Hz to 300 GHz,'" *IEEE Access*, vol. 7, pp. 171346–171356, 2019, doi: 10.1109/ACCESS.2019.2954823.
- [24] WHO, "The International EMF Project," *who.int*. [Online]. Available: <https://www.who.int/peh-emf/project/en/>. [Accessed: 11-Mar-2021]
- [25] RWTH Aachen University, "EMF-PORTAL," *EMF-PORTAL*. [Online]. Available: <https://www.emf-portal.org/en/>. [Accessed: 11-Mar-2021]
- [26] ITU-T, "ITU-T K.91 – Guide on electromagnetic fields and health." ITU-T, May-2020.
- [27] R. Nyberg and H. Lennart, "Scientists and doctors warn of potential serious health effects of 5G - EU 5G Appeal." 13-Nov-2017 [Online]. Available:

- http://www.stralskyddsstiftelsen.se/wp-content/uploads/2017/09/170913_scientist_5g_appeal_final_it.pdf
- [28] R. Nyberg and L. Hardell, “Scientists warn of potential serious health effects of 5G,” *5G APPEAL*. [Online]. Available: <http://www.5gappeal.eu/the-5g-appeal/>. [Accessed: 11-Mar-2021]
- [29] L. Hardell and M. Carlberg, “Mobile phone and cordless phone use and the risk for glioma - Analysis of pooled case-control studies in Sweden, 1997-2003 and 2007-2009.,” *Pathophysiology*, vol. 22, no. 1, pp. 1–13, Mar. 2015, doi: 10.1016/j.pathophys.2014.10.001.
- [30] National Toxicology Program (NTP), *NTP Technical Report on Toxicology and Carcinogenesis Studies In B6C3F1/N Mice Exposed to Whole-Body Radio Frequency Radiation at a Frequency (1,900 MHz) and Modulations (GSM and CDMA) Used by Cell Phones. (Draft)*, no. TR 595 (Draft). US, 2018, pp. 1–270 [Online]. Available: https://ntp.niehs.nih.gov/ntp/about_ntp/trpanel/2018/march/tr596peerdraft.pdf
- [31] National Toxicology Program (NTP), *NTP Technical Report on Toxicology and Carcinogenesis Studies In B6C3F1/N Mice Exposed to Whole-Body Radio Frequency Radiation at a Frequency (1,900 MHz) and Modulations (GSM and CDMA) Used by Cell Phones*, no. TR 596. US, 2018, pp. 1–260 [Online]. Available: https://ntp.niehs.nih.gov/ntp/htdocs/lt_rpts/tr596_508.pdf
- [32] Falcioni L *et al.*, “Report of final results regarding brain and heart tumors in Sprague-Dawley rats exposed from prenatal life until natural death to mobile phone radiofrequency field representative of a 1.8 GHz GSM base station environmental emission,” *Environ Res*, vol. 165, pp. 496–503, 2018, doi: 10.1016/j.envres.2018.01.037.
- [33] ICNIRP, “EPIDEMIOLOGIC EVIDENCE ON MOBILE PHONES AND TUMOR RISK: A REVIEW,” *EPIDEMIOLOGY*, vol. 20(5), pp. 639–652, 2009.
- [34] ICNIRP, “ICNIRP Note: Critical Evaluation of Two Radiofrequency Electromagnetic Field Animal Carcinogenicity Studies Published in 2018,” *Health Physics*, vol. 118, no. 5, pp. 525–532, May 2020, doi: 10.1097/HP.0000000000001137.
- [35] WHO, “Global Health Observatory data repository - Exposure limits for radio-frequency fields (public) Data by country,” *apps.who.int*, 31-May-2017. [Online]. Available: <https://apps.who.int/gho/data/node.main.EMFLIMITSPUBLICRADIOFREQUENCY?lang=en>. [Accessed: 10-Mar-2021]
- [36] European Communities, “1999/519/EC: Council Recommendation of 12 July 1999 on the limitation of exposure of the general public to electromagnetic fields (0 Hz to 300 GHz),” *OJ*, vol. L, no. 199, pp. 59–70, Jul. 1999.
- [37] Parlamento Italiano, “LEGGE 22 febbraio 2001 , n. 36: Legge quadro sulla protezione dalle esposizioni a campi elettrici, magnetici ed elettromagnetici.,” *Gazzetta Ufficiale*, vol. 55, Mar. 2001.
- [38] Presidenza del Consiglio dei Ministri, “DPCM 8 luglio 2003: Fissazione dei limiti di esposizione, dei valori di attenzione e degli obiettivi di qualità per la protezione della popolazione dalle esposizioni a campi elettrici, magnetici ed elettromagnetici generati a frequenze

- comprese tra 100 kHz e 300 GHz.,” *Gazzetta Ufficiale*, vol. 199, Aug. 2003.
- [39] Governo Italiano, “Decreto Legge 18 ottobre 2012, n. 179: Ulteriori misure urgenti per la crescita del Paese. (12G0201),” *Gazzetta Ufficiale*, vol. 245, Oct. 2012.
- [40] La Stampa, “Italy’s economic recovery plan unveiled,” *La Stampa*, 06-Oct-2020. [Online]. Available: <https://www.lastampa.it/esteri/la-stampa-in-english/2020/06/10/news/italy-s-economic-recovery-plan-unveiled-1.38951535>
- [41] European Parliament, “Directive 2013/35/EU of the European Parliament and of the Council of 26 June 2013 on the minimum health and safety requirements regarding the exposure of workers to the risks arising from physical agents (electromagnetic fields) (20th individual Directive within the meaning of Article 16(1) of Directive 89/391/EEC) and repealing Directive 2004/40/EC,” p. 21.
- [42] “Decreto Legislativo 1 agosto 2016 , n. 159: Attuazione della direttiva 2013/35/UE sulle disposizioni minime di sicurezza e di salute relative all’esposizione dei lavoratori ai rischi derivanti dagli agenti fisici (campi elettromagnetici) e che abroga la direttiva 2004/40/CE.,” *Gazzetta Ufficiale*, vol. 192, Aug. 2016.
- [43] IEC, “IEC 62232: Determination of RF field strength, power density and SAR in the vicinity of radiocommunication base stations for the purpose of evaluating human exposure.” Aug-2017.
- [44] Narda Safety Test Solutions, “MISURATORE DI CAMPI ELETTRICI E MAGNETICI NARDA 8053B - Catalogo sonde e accessori.” Narda Safety Test Solutions.
- [45] Consiglio regionale Calabria, “Corecom Calabria - Vigilanza inquinamento elettromagnetico.” [Online]. Available: http://corecom.consrc.it/hp2/contenuti/schedaPM.asp?PM=Bordo%20strada%20ad.za%20abitazioni&IDA=67&F_ANNO=2019&data=11/03/19. [Accessed: 24-Apr-2021]
- [46] Keysight Technologies, “N9322C Basic Spectrum Analyzer – Brochure,” p. 10.
- [47] Rohde & Schwarz, “LTE Over-The-Air Testing for Base Stations with R&S@FSH - Application Note.” [Online]. Available: https://scdn.rohde-schwarz.com/ur/pws/dl_downloads/dl_application/application_notes/1ef87/1EF87_1E.pdf
- [48] Keysight Technologies, “5G New Radio Modulation Analysis PathWave Vector Signal Analysis (89600 VSA),” p. 19.
- [49] IEC, “IEC TR 62669: Case studies supporting IEC 62232 – Determination of RF field strength, power density and SAR in the vicinity of radiocommunication base stations for the purpose of evaluating human exposure.” Apr-2019.
- [50] P. Joshi, M. Agrawal, B. Thors, D. Colombi, A. Kumar, and C. Tornevik, “Power Level Distributions of Radio Base Station Equipment and User Devices in a 3G Mobile Communication Network in India and the Impact on Assessments of Realistic RF EMF Exposure,” *IEEE Access*, vol. 3, pp. 1051–1059, 2015, doi: 10.1109/ACCESS.2015.2453056.

- [51] P. Joshi, B. Thors, D. Colombi, C. Tornevik, L. Larsson, and E. Larsson, "Realistic output power levels of multi-technology radio base stations and the implication on RF EMF exposure compliance assessments," presented at the The Joint Annual Meeting of The Bioelectromagnetics Society and the European BioElectromagnetics Association co-organized with the European COST EMF-MED Action BM1309, Ghent, Belgium, 2016.
- [52] ITU-R, "RECOMMENDATION ITU-R M.2012-4 - Detailed specifications of the terrestrial radio interfaces of International Mobile Telecommunications-Advanced (IMT-Advanced)," p. 227.
- [53] P. Panigrahi, "Is LTE 4G? What is difference between LTE and LTE Advanced?," *3glteinfo.com*, 23-Feb-2012. [Online]. Available: <http://www.3glteinfo.com/is-lte-4g-what-is-difference-between-lte-and-lte-advanced/>
- [54] 3GPP, "3GPP Release 8," *3gpp.org*, 2008. [Online]. Available: <https://www.3gpp.org/specifications/releases/72-release-8>
- [55] 3GPP, "3GPP Release 10," *3gpp.org*, 2011. [Online]. Available: <https://www.3gpp.org/specifications/releases/70-release-10>
- [56] 3GPP, "3GPP Release 13," *3gpp.org*, 2016. [Online]. Available: <https://www.3gpp.org/release-13>
- [57] Opensignal, "Opensignal map," *opensignal.com*. [Online]. Available: <https://www.opensignal.com/>. [Accessed: 28-Oct-2020]
- [58] C. Gessner, M. Roessler, and M. Kottkamp, "UMTS Long Term Evolution (LTE) - Technology Introduction: Application Note." Rohde & Schwarz, Jul-2012.
- [59] 3GPP, "3GPP TR 25.892; Feasibility Study for Orthogonal Frequency Division Multiplexing (OFDM) for UTRAN enhancement (Release 6)." Jun-2004.
- [60] ETSI, "ETSI TS 136 211 V16.2.0: LTE; Evolved Universal Terrestrial Radio Access (E-UTRA); Physical channels and modulation." ETSI, Sep-2020.
- [61] CEI, "CEI 211-7/E: Guide for the measurement and the evaluation of electromagnetic fields in the frequency range 10 kHz - 300 GHz, with reference to the human exposure Annex E: Measurement of the electromagnetic fields from Base Radio Station for mobile telecommunication systems (2G, 3G, 4G, 5G)." CEI, Nov-2019.
- [62] ITU-R, "IMT Vision – Framework and overall objectives of the future development of IMT for 2020 and beyond," p. 21.
- [63] Rohde & Schwarz, *5G New Radio: Fundamentals, procedures, testing aspects*. 2020 [Online]. Available: <https://gloris.rohde-schwarz.com/ebooks/5G>
- [64] ETSI, "ETSI TR 121 915 V15.0.0: Digital cellular telecommunications system (Phase 2+) (GSM); Universal Mobile Telecommunications System (UMTS); LTE; 5G; Release description; Release 15." ETSI, Oct-2019.
- [65] Ericsson, "5G deployment considerations." 2018 [Online]. Available: <https://www.ericsson.com/4a5daa/assets/local/reports-papers/5g/doc/5g-deployment-considerations.pdf>
- [66] European Round Table for Industry (ERT), "Assessment of 5G Deployment Status in Europe." European Round Table for Industry

- (ERT), Sep-2020 [Online]. Available: https://ert.eu/wp-content/uploads/2020/09/ERT-Assessment-of-5G-Deployment-Status-in-Europe_September-2020.pdf
- [67] F. Pujol, C. Manero, B. Carle, and S. Remis, “5G Observatory Quarterly Report 9 Up to September 2020,” p. 147, 2020.
- [68] Nperf, “5G coverage map worldwide,” *Nperf.com*. [Online]. Available: <https://www.nperf.com/en/map/5g>. [Accessed: 05-Nov-2020]
- [69] OOKLA, “OOKLA 5G MAP,” *Speedtest.net*. [Online]. Available: <https://www.speedtest.net/ookla-5g-map>. [Accessed: 05-Nov-2020]
- [70] Ericsson, “Ericsson Mobility Visualizer,” *ericsson.com*. [Online]. Available: <https://www.ericsson.com/en/mobility-report/mobility-visualizer>. [Accessed: 05-Nov-2020]
- [71] ETSI, “ETSI TS 138 211 V16.2.0: 5G; NR; Physical channels and modulation (3GPP TS 38.211 version 16.2.0 Release 16).” ETSI, Jul-2020.
- [72] ETSI, “ETSI TS 138 104 V16.4.0: 5G; NR; Base Station (BS) radio transmission and reception (3GPP TS 38.104 version 16.4.0 Release 16).” ETSI, Jul-2020.
- [73] ETSI, “ETSI TS 138 213 V16.2.0: 5G; NR; Physical layer procedures for control (3GPP TS 38.213 version 16.2.0 Release 16).” ETSI, Jul-2020.
- [74] ETSI, “ETSI TS 138 101-1 V16.4.0: 5G; NR; User Equipment (UE) radio transmission and reception; Part 1: Range 1 Standalone (3GPP TS 38.101-1 version 16.4.0 Release 16).” ETSI, Jul-2020.
- [75] ETSI, “ETSI TS 138 101-2 V16.4.0: 5G; NR; User Equipment (UE) radio transmission and reception; Part 2: Range 2 Standalone (3GPP TS 38.101-2 version 16.4.0 Release 16).” ETSI, Jul-2020.
- [76] D. Franci *et al.*, “An Experimental Investigation on the Impact of Duplexing and Beamforming Techniques in Field Measurements of 5G Signals,” *Electronics*, vol. 9, no. 2, 2020, doi: 10.3390/electronics9020223. [Online]. Available: <https://www.mdpi.com/2079-9292/9/2/223>
- [77] D. Franci *et al.*, “Experimental Procedure for Fifth Generation (5G) Electromagnetic Field (EMF) Measurement and Maximum Power Extrapolation for Human Exposure Assessment,” *Environments*, vol. 7, no. 3, p. 22, Mar. 2020, doi: 10.3390/environments7030022.
- [78] S. Adda *et al.*, “A Theoretical and Experimental Investigation on the Measurement of the Electromagnetic Field Level Radiated by 5G Base Stations,” *IEEE Access*, vol. 8, pp. 101448–101463, 2020, doi: 10.1109/ACCESS.2020.2998448.
- [79] METAS, “Technical Report: Measurement Method for 5G NR Base Stations up to 6 GHz - Version 2.1.” Federal Institute of Metrology METAS, 20-Apr-2020.
- [80] H. Keller, “On the Assessment of Human Exposure to Electromagnetic Fields Transmitted by 5G NR Base Stations;,” *Health Physics*, vol. 117, no. 5, pp. 541–545, Nov. 2019, doi: 10.1097/HP.0000000000001089.
- [81] S. Aerts *et al.*, “In-situ Measurement Methodology for the Assessment of 5G NR Massive MIMO Base Station Exposure at Sub-6

- GHz Frequencies,” *IEEE Access*, vol. 7, pp. 184658–184667, 2019, doi: 10.1109/ACCESS.2019.2961225.
- [82] 3GPP, “3GPP Release 15,” *3gpp.org*, 26-Apr-2019. [Online]. Available: <https://www.3gpp.org/release-15>
- [83] D. P. Malladi, “Key breakthroughs to drive a fast and smooth transition to 5G standalone,” <https://www.qualcomm.com/>, 19-Aug-2019. [Online]. Available: <https://www.qualcomm.com/news/onq/2019/08/19/key-breakthroughs-drive-fast-and-smooth-transition-5g-standalone>. [Accessed: 08-Apr-2021]
- [84] S. Maximov, C.-C. (Lewis) Yu, and M. A. El-saidny, “5G NR and 4G LTE Coexistence. A Comprehensive Deployment Guide to Dynamic Spectrum Sharing. White Paper.” MediaTek, Inc, 2020 [Online]. Available: <https://www.mediatek.com/blog/mediatek-whitepaper-dynamic-spectrum-sharing>
- [85] Keysight Technologies, “5G Dynamic Spectrum Sharing,” www.keysight.com. [Online]. Available: <https://www.keysight.com/it/en/cmp/2020/5g-dynamic-spectrum-sharing.html>. [Accessed: 18-Dec-2020]
- [86] Keysight Technologies, “5G Dynamic Spectrum Sharing - Course ID: E-KVO3W0,” *Keysight University*. [Online]. Available: <https://learn.keysight.com/learn/catalog>. [Accessed: 13-Apr-2021]
- [87] Rohde & Schwarz, “R&S®TSMA6 AUTONOMOUS MOBILE NETWORK SCANNER - Product Brochure Version 10.00.” [Online]. Available: https://scdn.rohde-schwarz.com/ur/pws/dl_downloads/dl_common_library/dl_brochures_and_datasheets/pdf_1/TSMA6_bro_en_5215-8241-12_v1000.pdf
- [88] Rohde & Schwarz, “R&S®ROMES4 DRIVE TEST SOFTWARE - Product Brochure Version 23.00.” [Online]. Available: https://scdn.rohde-schwarz.com/ur/pws/dl_downloads/dl_common_library/dl_brochures_and_datasheets/pdf_1/ROMES4_bro_en_5214-2062-12_v2300.pdf
- [89] Rohde & Schwarz, “Drive Test Software R&S®ROMES4 - Firmware/software version: 20.2 - Software Help.” .
- [90] Google, “Google Maps Street View online service.” [Online]. Available: <https://www.google.it/maps>. [Accessed: 23-Apr-2021]
- [91] CellMapper, “CellMapper.” [Online]. Available: <https://www.cellmapper.net/map>. [Accessed: 23-Apr-2021]
- [92] Google, “Google Earth Pro.” [Online]. Available: <https://www.google.it/intl/it/earth/>. [Accessed: 23-Apr-2021]
- [93] Google, “Use Viewshed to see a placemark’s surroundings,” support.google.com/. [Online]. Available: <https://support.google.com/earth/answer/3064261?hl=en>. [Accessed: 23-Apr-2021]
- [94] ETSI, “ETSI TS 138 215 V15.2.0: 5G; NR; Physical layer measurements (3GPP TS 38.215 version 15.2.0 Release 15).” ETSI, Jul-2018.